AD_____

Award Number: DAMD17-02-1-0706

TITLE: TARGET (Translational Approaches for the Reversal, Genetic Evaluation and Treatment) of Lung Cancer

PRINCIPAL INVESTIGATOR: Waun Ki Hong, M.D.
Fadlo R. Khuri, M.D.

CONTRACTING ORGANIZATION: The University of Texas
M.D. Anderson Cancer Center
Houston, Texas 77030

REPORT DATE: September 2004

TYPE OF REPORT: Annual

PREPARED FOR: U.S. Army Medical Research and Materiel Command
Fort Detrick, Maryland 21702-5012

REPORT DOCUMENTATION PAGE

Form Approved
OMB No. 074-0188

1. AGENCY USE ONLY (Leave blank)	2. REPORT DATE	3. REPORT TYPE AND DATES COVERED
	September 2004	Annual (1 Sep 2003 - 31 Aug 2004)

4. TITLE AND SUBTITLE
TARGET (Translational Approaches for the Reversal, Genetic Evaluation and Treatment) of Lung Cancer

5. FUNDING NUMBERS
DAMD17-02-1-0706

6. AUTHOR(S)
Waun Ki Hong, M.D.
Fadlo R. Khuri, M.D.

7. PERFORMING ORGANIZATION NAME(S) AND ADDRESS(ES)
The University of Texas M.D. Anderson Cancer Center
Houston, Texas 77030
E-Mail: whong@mdanderson.org

8. PERFORMING ORGANIZATION REPORT NUMBER

9. SPONSORING / MONITORING AGENCY NAME(S) AND ADDRESS(ES)
U.S. Army Medical Research and Materiel Command
Fort Detrick, Maryland 21702-5012

10. SPONSORING / MONITORING AGENCY REPORT NUMBER

11. SUPPLEMENTARY NOTES

12a. DISTRIBUTION / AVAILABILITY STATEMENT
Approved for Public Release; Distribution Unlimited

12b. DISTRIBUTION CODE

13. Abstract (Maximum 200 Words) (abstract should contain no proprietary or confidential information)

TARGET is focused on a series of projects designed to obtain data in the preclinical and clinical settings to help us further understand the epidemiology of lung cancer, the molecular biology, genetics and epigenetics of lung cancer in the context of tobacco-damaged aerodigestive tract tissue, and the anti-cancer activity of several promising new agents, and various treatment and drug delivery approaches in models of lung cancer and other aerodigestive tract tumors.

14. SUBJECT TERMS
lung cancer, genetic markers, molecular epidemiology

15. NUMBER OF PAGES
149

16. PRICE CODE

17. SECURITY CLASSIFICATION OF REPORT	18. SECURITY CLASSIFICATION OF THIS PAGE	19. SECURITY CLASSIFICATION OF ABSTRACT	20. LIMITATION OF ABSTRACT
Unclassified	Unclassified	Unclassified	Unlimited

TABLE OF CONTENTS

Introduction

Smoking is a major cause for several types of cancer, particularly lung cancer and cancers of the head and neck. Lung cancer is the leading cause of cancer death in both males and females in America, and is also the leading cause of cancer death worldwide. In America, it accounts for 28.5% of cancer deaths and 6.5% of all deaths. An estimated 173,700 Americans will develop lung cancer in 2004 and 160,440 will die from it. The vast majority (85%) of patients with lung cancer have non-small cell lung cancer (NSCLC) and across all stages of NSCLC, only 13.6% of males and 17.2% of women survive 5 years from diagnosis. More than 50% of cases are diagnosed at a late stage, for which the 5-year survival is only about 3%. While the death rate from head and neck cancer is not as high as from lung cancer, it also remains a major problem. Thus, to reduce lung cancer incidence and mortality, we believe that developing novel effective therapeutic strategies that target both current and former smokers who are at risk for development of cancer is vital to achieving tangible progress in patient care.

TARGET is focused on a series of complementary projects designed to obtain data in the preclinical and clinical settings to help us further understand the epidemiology of lung cancer, the molecular biology, genetics and epigenetics of lung cancer in the context of tobacco-damaged aerodigestive tract tissue, and the anti-cancer activity of several promising new agents, and various treatment and drug delivery approaches in models of lung cancer and other aerodigestive tract tumors.

TARGET addresses the following specific goals:

- develop an integrated approach to study genetic susceptibility markers related to DNA repair capacity in lung cancer using both surrogate tissue and target tissue
- study the genetic instability induced by tobacco-related carcinogenesis and the effects of chemoprevention on its reversal
- identify and characterize novel biomarkers for early diagnosis of lung cancer to aid better understanding of the development and progress of lung cancer
- study the process of the hypermethylation of the promoter regions of important pro-apoptotic genes such as the death-associated protein (DAP) kinase and the p16 gene, and establish the relationship with disease-specific and overall survival in completely resected, early-stage non-small cell lung cancer in order to develop an independent molecular prognostic model utilizing these important parameters
- evaluate the effects of a histone deacetylase inhibitor on non-small cell lung cancer cell lines by studying interactions with nuclear retinoid genes, such as RAR-β, and induction of apoptosis
- study the biological effects of the farnesyl transferase inhibitor SCH66336 on signal transduction and induction of apoptosis in aerodigestive tract cancer models
- better understand the global molecular changes in cellular responses and tumor suppressor gene FUS1 in order to elucidate its molecular mechanisms in lung cancer and thereby develop a gene replacement strategy using a FUS1-lipoplex in experimental mouse models of lung cancer
- develop perfluorocarbon-mediated gene transfer to allow repeated gene transfer through reduction and mechanical disruption of the humoral response
- develop and validate different anti-angiogenic therapeutic approaches in lung cancer utilizing both orthotopic and metastatic lung cancer models in mice and identify optimal combinations in sequences of anti-angiogenic agents while studying surrogate markers for their response

Project 1 Molecular Epidemiology of Lung Cancer

Principal Investigator: Margaret Spitz, M.D., M.P.H.

Specific Aim 1 Create a specimen and data resource
We will enroll (over two years) a consecutive series of 100 lung cancer cases of any histology, age, gender and ethnicity, undergoing thoracotomy for definitive therapy. These patients will have detailed epidemiologic risk assessments including tobacco exposure, dietary intake and family history. Blood samples, bronchial washings and bronchial biopsies will be obtained on each patient.

Update:
We have consented 59 cases since receiving DoD approval in May 2004. Forty-two of these patients have completed surgical resections to date. These patients are also enrolled in NCI protocol CPN 91-001, which allows for the collection of blood and sputum specimens from lung cancer cases and controls.

The UTMDACC IRB recently approved an amendment to Dr. Jonathan Kurie's chemoprevention study (ID00-230), which allows us to collect blood specimens and valuable risk information data from current and former smokers without lung cancer. These participants serve as Target controls, of which there are 21 scheduled in the month of August 2004.

Summary of Tissue Received

Tissue Type	# Rec'd
Tumor	42
Normal	42
Adjacent Bronchus	31
For Culture	19
Blood	44
Bronchial Brushes	41
Sputum	25

Demographics
Thirty-eight (64.5%) participants are female and 21 (35.5%) are male. Fifty-five participants are White (93%), 4 (6.7%) are Black, and 1 participant is Asian.

Specific Aim 2 Determine the genetic susceptibility profile in surrogate tissue.
We will perform a panel of genotypic (select polymorphisms in DNA repair genes) and functional (DNA repair capacity, mutagen sensitivity, and COMET) assays of genetic susceptibility on peripheral lymphocyte DNA from the 100 patients identified in Specific Aim 1.

Specific Aim 3 Determine the genetic susceptibility profile in target tissue
We will establish bronchial epithelial cell cultures from fresh tumor specimens at thoracotomy of the 100 lung cancer patients from Specific Aim 1 and perform, in parallel, phenotypic DNA repair capacity and mutagen challenge assays. We will compare, using FISH analyses, the rate of concordance of DNA deletions at 3p21.3 and 10q22 loci in cells obtained from bronchial washings and peripheral lymphocyte cultures of 50 patients.

Update for Aims 2 and 3:

We have genotyped for select polymorphisms in DNA repair genes and performed functional assays (DNA repair capacity, mutagen sensitivity, COMET, and telomere length) on peripheral lymphocyte DNA from the patients identified in Specific Aim 1.

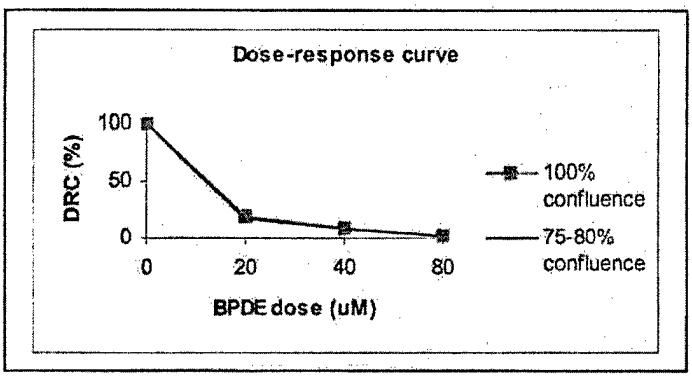

We have tested all functional assays on commercially available cells. For the DNA repair assay, we inoculated the frozen cells in 24-well culture plate and did transfection with BPDE-damaged luciferase plasmid into these passage 2 cells, and obtained a dose response curve for DNA repair capacity (DRC).

We have performed the following molecular cytogenetic and telomere length assays in lymphocyte cultures:

Assay	N (finished/total)
3p21	44/71
3p/cen	44/71
5p	28/71
10q	40/71
10q/cen	40/71
telomere length	52/71
BPDE sensitivity	53/71

We have performed FISH analyses for 3P and 10q for the samples indicated in the table below,.

Probe	TBB	NBB	TTP	NTP	TAB
3P	30	29	21	21	18
10q	26	26	17	17	9
Minna 3p	18	18	12	12	9
5p	1	1	14		

TBB: Tumor Bronchial Brush; NBB: Non-tumor Bronchial Brush; TTP: Tumor Touch Prep
NTP: Non-tumor Touch Prep: TAB: Adiacent Bronchus

Summary of FISH data

Variables	N	Mean(SD)	Range
cep3/3p-BB/NT(%Del)	43	2.56(1.84)	0.0 - 8.0
cep3/3p-BB/T(%Del)	44	6.30(4.03)	0.0 - 18.0
cep3/3p-TP/T(%Del)	37	20.19(10.92)	5.0 - 53.0
cep3/3p-TP/AB(%Del)	31	5.06(3.59)	0.0 - 16.0
cep3/3p-TP/NT(%Del)	35	4.80(3.36)	1.0 - 14.0
cep10/10q-BB/NT(%Del)	34	1.91(1.46)	0.0 - 6.0
cep10/10q-BB/T(%Del)	38	4.66(2.06)	2.0 - 11.0
cep10/10q-TP/T(%Del)	32	11.59(6.79)	4.0 - 27.0
cep10/10q-TP/AB(%Del)	18	4.94(3.39)	1.0 - 14.0
cep10/10q-TP/NT(%Del)	29	3.28(2.52)	0.0 - 9.0
cep3p-bpde(%Del) (lymphocytes)	42	2.23(0.62)	0.0 - 4.2
cep10q-bpde(%Del) (lymphocytes)	34	1.71(0.55)	0.6 - 3.2

The Table (Summary of FISH data) summarizes the actual values for the FISH studies in the bronchial brushes, touch preparations and lymphocyte cultures.

Specific Aim 4 Assess concordance of findings in paired samples

Update: We have also begun to evaluate correlations between data from lymphocytes, bronchial brushes and touch preparations.

There was no correlation overall between pack-years smoked and deletions in 3p in bronchial brushes from either the normal or tumor side. However, there is evidence of statistically significant correlations between 3p and 10q % deletions in bronchial brushes from tumor side (Fig.1), between 3p deletions in tumor touch prep with 10q touch prep (Fig. 2) and between 3p deletions in non-tumor touch preparations and pack years smoked (Fig. 3).

Figure 1

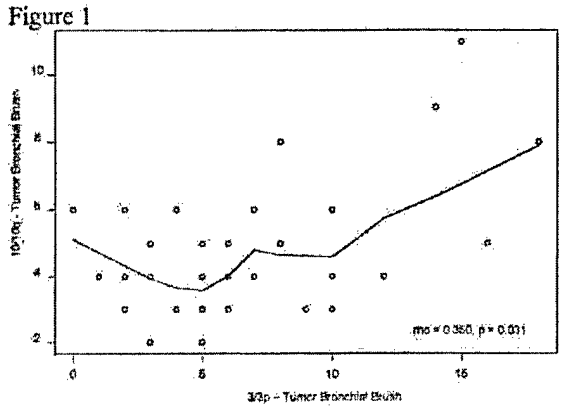

Figure 2

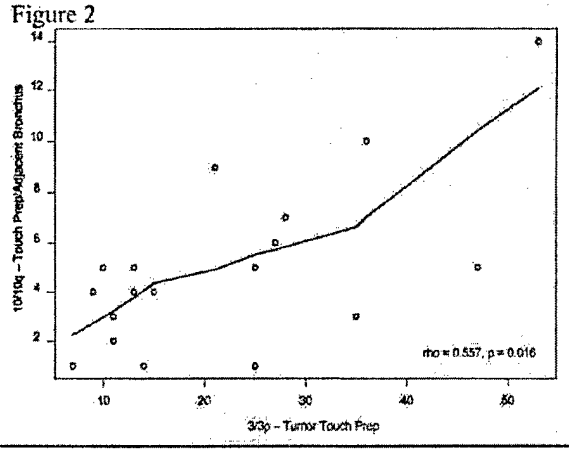

Figure 3

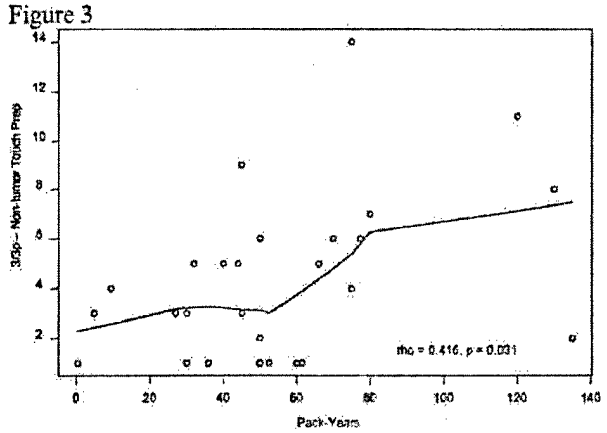

We have also received and processed 25 sputa and performed FISH on 9.

We have also looked at the correlation between telomere length and 3p aberrations in lymphocytes as well as in the target tissue. Telomere length in lymphocytes was significantly inversely associated with 3p aberrations in bronchial brushings from the tumor side (p=0.040) as well as with 3p aberrations in touch prep from tumor tissue (p=0.026). Telomere length in bronchial brushings on non-tumor bearing side was significantly inversely associated with 3p aberrations in touch prep from adjacent normal tissue (0.034). In addition, BPDE sensitivity in lymphocytes was significantly positively associated with 3p aberrations in lymphocytes (p=0.034) as well as with 3p aberrations in touch prep from tumor tissue (p=0.035) and from adjacent normal tissue (p=0.006).

Correlation of telomere length between lymphocytes and lung epithelial cell

	N	correlation coefficient	P value
lymphocytes/ brushing normal side	26	0.5226	0.0062
lymphocytes/ brushing tumor side	28	0.3546	0.0641
brushing normal/ brushing tumor side	26	0.6896	0.0001

Correlation of telomere length and BPDE sensitivity with 3p aberrations

telomere length	PBLs	BB tumor	BB normal	Touch prep tumor	Touch prep normal	Touch prep. adj.
LYMPHOCYTES						
corr. Coef	0.0369	-0.4874	-0.3293	-0.5225	-0.3055	-0.4889
P-value	0.8551	**0.0402**	0.1969	**0.0261**	0.2331	**0.0761**
BB normal						
corr. Coef	0.0135	-0.3041	0.1209	-0.3605	-0.3155	-0.5692
P-value	0.9491	0.2198	0.6439	0.1417	0.2174	**0.0336**
BB tumor						
corr. Coef	-0.0227	-0.2594	0.0572	-0.1594	-0.3205	-0.1321
P-value	0.9103	0.2986	0.8275	0.5276	0.2097	0.6525
BPDE-sensitivity						
corr. Coef	0.3238	-0.0678	-0.0079	0.343	0.0255	0.4792
P-value	**0.0341**	0.7078	0.9662	**0.035**	0.8844	**0.0064**

The key accomplishments are:

We have tested all functional assays on commercially available cells, and have started applying the assays to the tissue cultures set up by Dr. Koo. We have also begun to evaluate correlations between data from lymphocytes, bronchial brushes and touch preparations.

Project 2 Genetic Instability by Smoking Status

Principal Investigator: Walter Hittelman, Ph.D.

Specific Aim 2.1 Determine the optimal conditions for detecting clonal changes using inter-simple sequence repeat PCR (Inter-SSR PCR). Standardize and validate inter-SSR PCR for application to bronchial biopsy specimens

Our initial studies had suggested that fluorescence Inter-SSR PCR (FISSR-PCR) could be used to sensitively detect the presence of clonal outgrowths in small tissue specimens. The goal of this first Specific Aim was to improve the technology for use on tissue sections and to determine the sensitivity and reproducibility of this technique for detecting clonal and subclonal lung cell populations. In the prior Progress Report, we reported that we had optimized the conditions of FISSR-PCR for DNA fingerprinting and showed that the results were fairly reproducible in premalignant and malignant cell lines. We also showed, using the BEAS2B, 1799, 1198, and 1170I lung cell progression model, that the number of detectable clonal changes increased as cells stepwise progressed from an immortalized to a malignant stage of lung tumor development. We also showed that each of these cell populations contained multiple subclonal populations distinguishable by FISSR-PCR and that the degree of subclonal variation increased as the cell populations moved toward the tumor phenotype.

To determine the sensitivity of FISSR-PCR for detecting subclonal variants, we subcloned the BEAS2B line into monoclonal outgrowths. We then chose two clones that differed in two bands (Figure 1) and mixed their DNAs in different ratios prior to FISSR-PCR analysis. As shown in Figure 2, subclonal variants occupying 25% of the population could be detected by this approach.

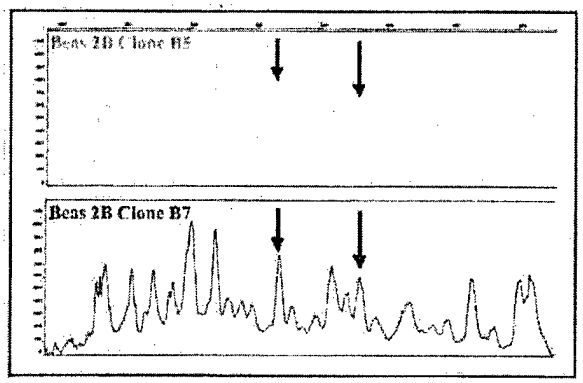

Figure 1. DNA fingerprints of two BEAS2B subclones with differing bands

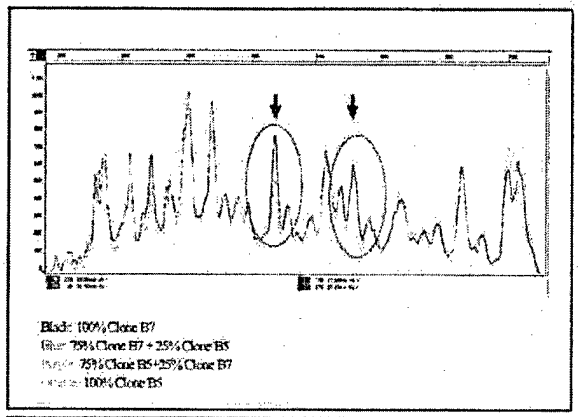

Figure 2: DNA fingerprints of mixtures of BEAS2B clones in different proportions.

To better estimate the sensitivity of this technique to detect the presence of smaller subclonal populations, we mixed two distinct 1170I subclonal populations in different proportions and determined the relative peak heights of the distinct peaks that distinguished the two populations (Figure 3). Plotting these results as a function of relative dilutions of the two lines (Figure 4), we estimated that a subclonal population could be detected by FISSR-PCR if it occupied around 20% of the total population.

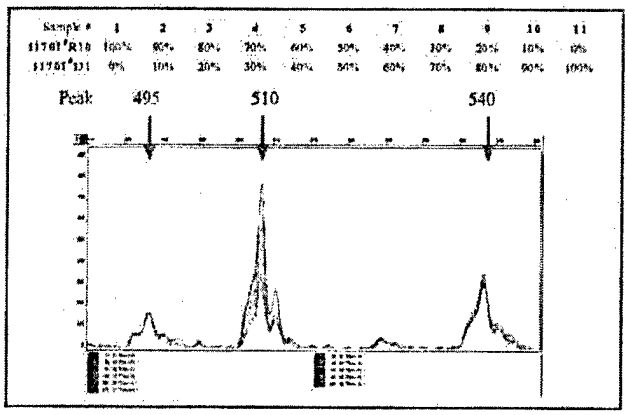

Figure 3. Mixing of two 1170l single cell clones in different ratios to simulate subclonal outgrowth

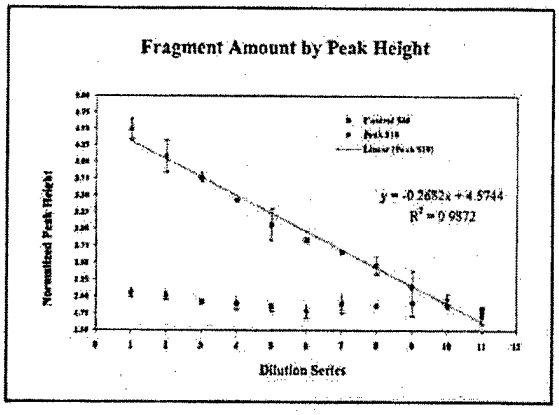

Figure 4. Quantification of relative peak heights following FISSR-PCR analysis of mixed 1170l subclonal populations

We next initiated studies to determine our ability to carry out FISSR-PCR on cells microdissected from paraffin embedded specimens. The first studies were carried out on cell culture pellets that have been formalin-fixed and embedded in paraffin. These studies suggested that the use of paraffin-embedded material limited our ability to carry out analyses on very small amounts of microdissected material due to limitations in DNA extraction from the paraffin-embedded material, limitations in the size of the PCR products to about 500 base pairs due to formalin-induced DNA cross links, and interference of detergent used in the DNA extraction with the fluorescence signal detection. We therefore decided to focus more on frozen tissue sections. To optimize the conditions for the FISSR-PCR reactions, we focused on three initial components of the analysis. First, in collaboration with Dr. Ignacio Wistuba, we compared the laser capture microdissection technique with needle dissection and found that both techniques were suitable. Second, we optimized the DNA extraction methodology from the frozen tissue material, with or without phenol extraction and ethanol precipitation and examined the effect of column purification of the DNA. Third, we optimized the PCR reaction by examining different PCR systems, including the effect of hot start PCR, different DNA polymerases, different PCR buffer systems, and different PCR temperatures.

To determine the feasibility for detecting subclonal changes in frozen lung tissue sections, in collaboration with Dr. Ignacio Wistuba, we obtained human lung samples from lung tumor resection cases and microdissected out multiple areas from the tumor specimens, including tumor, stromal, and apparently normal epithelial regions. For example, for human lung sample case 252, we microdissected eight regions from different parts of the resection specimen, including three tumor regions, four normal epithelial regions, and one stromal region (Figure 5) as well as a lymphocytic region.

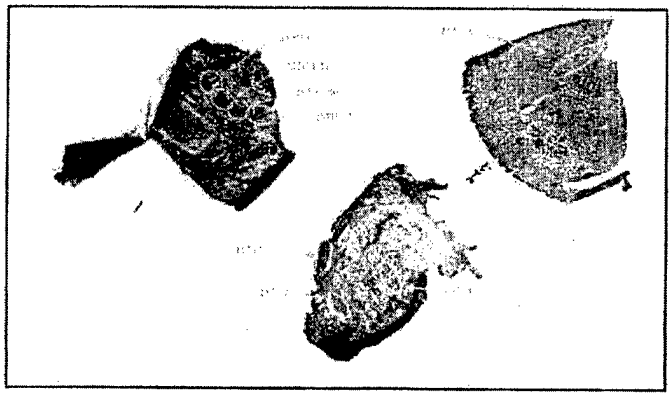

Figure 5. Illustration of areas microdissected from case 252.

Using the stroma as the tissue portion without clonal changes, we were able to detect three common band changes

distinct from the stroma in all three tumor regions examined, and two of the tumor regions showed an additional common band change. In this case, none of the apparently normal lung epithelial regions showed any band changes that were distinct from the stromal regions. The results of this case and two other cases examined in the same manner are summarized in Table 1.

Sample	Major bandChanges	Total changes
320N E1	31	0
320N E2	31	0
320N E3	31	0
320B E1	31	0
320B S1	31	0
320B S2	31	5
320T1	31	387g, 423g, 723L, 734g	4
320T2	31	179g, 275L, 368g, 387g, 423g.	5
399B S1	31	6
399B S2	31	8
399N E1	31	452L, 611L	2
399T	31	453L, 611L2, 723L	4

Table 1. Summary of DNA band changes for cases 252, 320, and 399.

Interestingly, in case 320, the two tumor regions showed 4 and 5 band changes, respectively, that were distinct from the stroma. However, while the two tumor regions showed two common band changes that were distinct from the stromal regions, they differed in the other apparent band changes. This suggested that while the two tumor regions may have derived from a common precursor clone, they evolved differently from the original clone (i.e., they would be called subclones of the tumor). None of the four normal epithelial regions showed any bands that were distinct from the stroma.

Case 399 illustrated a different kind of interesting observation. In this case, the tumor region showed four DNA bands that were distinct from the stromal regions. However, the apparently normal region showed two DNA band changes that were distinct from the stromal regions. Moreover, the two DNA band changes observed in the apparently normal epithelium were identical to two bands found in the tumor specimen, suggesting that some clonal changes developed prior to tumor development.

In the early part of these lung tumor studies, there was some concern about the quality of the frozen sections that were being used. More recent studies have focused on better-preserved tumor resection specimens. We compared the results of microdissecting approximately 1000 cells with that dissected from about 400 cells from different regions of the same tumor (Figure 6). As can be seen in Figure 2, under these conditions, differences in bands between the normal and tumor microdissected regions were still detectable when approximately 400 cells were analyzed. As shown in Table 2, using one of the normal epithelial regions as the standard for normal (no

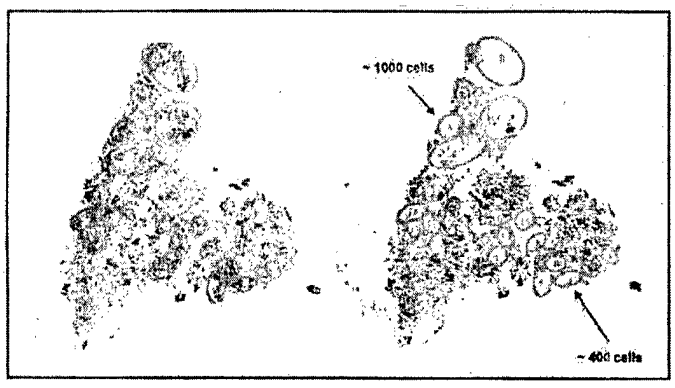

Figure 6. Identification of areas of microdissection of normal and tumor epithelium from case 268.

stroma or lymphocytes are analyzed in this case), the tumor specimens showed a high degree of subclonal variation, with anywhere from 3 to 9 band changes distinct from the "normal" epithelial control out of the 31 bands that were informative under these conditions. All the tumor regions showed two bands in common (i.e., 505 loss and 724 loss) suggesting that there was a common precursor clone. The finding that a specimen from apparently normal epithelium (N6) and a specimen from a region that did not appear fully malignant (T2N) also showed the band 724 loss suggests that this alteration occurred early in the field of tumorigenesis. Moreover, the normal epithelium also showed 1 to 2 band changes that were distinct from the region that served as the normal control. Interestingly, the fact that not all band changes detected in the histologically normal epithelium were identical suggests the presence of several clones in the normal epithelial field of the tumor.

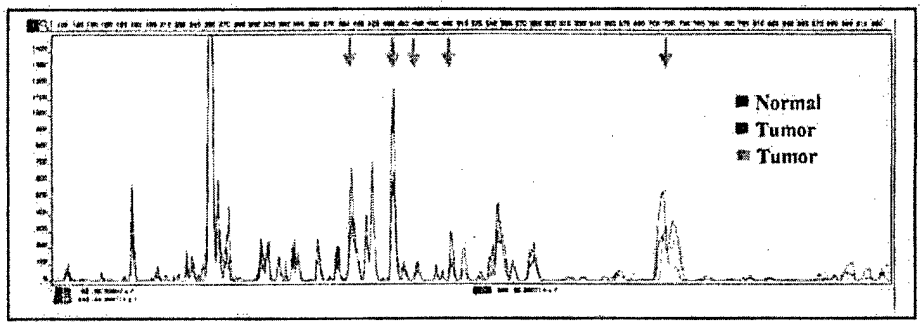

Figure 7. FISSR-PCR analysis of one normal and two tumor regions of case 268. Arrows denote location of band changes.

Major Band	Band Change										Total Changes
31							505L				1
31			385L								1
31			385L					554L			2
31											0
31		418G									1
31									724L		1
31	----										----
31		274G							724L		2
31		274G									1
31	175G	274G			423G		456G	505L	724L	736G	7
31					423G	445L	456G	505L	724L	736G	6
31					423G	445L	456G	505L	724L	736G	6
31					423G	445L	456G	505L	724L		5
31				418G		445L		505L	554L	724L 736G	6
31				418G	423G			505L	554L	724L 736G	6
31				418G	423G	445L		505L	554L	724L 736G	7
31				418G	423G			505L		724L 736G	5
31					423G	445L	456G	505L		724L 736G	6
31				418G	423G		456G	505L		724L 736G	6
31	175G			418G	423G	445L	456G	505L	554L	724L 736G	9
31				418G	423G	445L	456G	505L		724L 736G	7
31	175G			418G	423G	445L	456G	505L		724L 736G	8

Table 2. Summary of clonal band changes in microdissected regions of tumor and normal epithelium for case 268.

Similar type patterns have been observed in several other cases where tumors and their surrounding normal epithelium and stromal tissue have been compared using FISSR-PCR. In nearly all cases, we have found definite evidence for subclonal heterogeneity within the tumor regions, with more than three band changes from normal control found in all the tumor regions. Evidence for subclonal variation in normal appearing epithelium has been observed in some but not all cases. It will be important to increase the number of informative bands through multiplex FISSR-PCR analysis to increase the dynamic range of this assay in order to make it useful for detecting the degree of clonal outgrowth in normal appearing epithelium in lung tissues at risk.

Specific Aim 2.2 Determine whether smoking status influences changes in clonal frequency and determine whether chemopreventive intervention has differential impact on clonal outgrowths in current and former smokers

Once we have increased the number of primers used in the FISSR-PCR analysis to increase the dynamic range of the assay, we will apply the technique to bronchial biopsy specimens from current and former smokers. In our original research plan, we had hoped to utilize paraffin-embedded bronchial biopsy specimens where we had previously carried out chromosome in situ hybridization studies and had identified the frequency of clonal outgrowths by nearest neighbor statistics. Unfortunately, the studies carried out on this project suggest that the use of frozen tissue sections is more appropriate for FISSR-PCR studies. Therefore, it will be necessary to identify bronchial biopsy specimens that have been frozen, and we will need to carry out in situ hybridization analyses on parallel tissue sections to those where we will carry out FISSR-PCR studies in order to compare the relative sensitivity of the two technologies for assessing the degree of subclonal outgrowth in lung epithelium of current and former smokers.

The key accomplishments are:

We have adapted the fluorescence inter-simple sequence PCR technology to the analysis of normal epithelium in the field of lung tumors and have demonstrated the presence of subclonal outgrowths in this apparently normal epithelium. With multiplexing of FISSR-PCR, these results suggest that this technology may be useful for quantifying the level of subclonal outgrowths in normal lung tissue at cancer risk and will permit comparisons between the bronchial epithelium of current and former smokers.

Publications

Abstracts:

1. Lu T, and Hittelman WN. Quantitative fluorescence inter-simple sequence repeat CR (FISSR-PCR) for subclonal analysis of bronchial cell populations. Proc. AACR, 2004.

Articles:

1. Hittelman WN, Kurie JM, and Swisher S. Molecular Events in Lung Cancer and Implications for Prevention and Therapy. In: Anderson Associates Monograph on Lung Cancer. F Fossella, R Komaki, and J Putnam, Jr., (eds.) pp 280-298, 2003.

2. Lu T and Hittelman WN. Improvement and application of fluorescence inter-simple sequence repeat polymorphism chain reaction for the study of subclonal growths in lung epithelial cell populations. Chest 125 (Suppl. 5):110-111S, 2004.

Project 3 Epithelial Biomarkers of Lung Cancer: Evaluation of Airway Secretions to Study Lung Carcinogenesis

Principal Investigator: J. Peter Koo, Ph.D.

Specific Aim 1 Identify proteins whose secretion or release is different in squamous metaplastic tracheobronchial epithelial cells as compared to normal mucous epithelial cells

Phenotypes of the cultures of primary normal human tracheobronchial epithelial (NHTBE) cell are dependent on retinoic acid (RA) when the cultures are maintained in air-liquid interface (ALI) culture method. Cultures maintained in RA-sufficent media generate a fully-differentiated mucociliary bronchial epithelium mimicking *in vivo* tracheobronchial epithelium, in contrast the cultures become squamous metaplasia in RA-deficient media. To identify proteins whose secretion or release is different in squamous metaplastic tracheobronchial epithelial cells as compared to normal mucous epithelial cells, apical surface liquid (ASL) from the NHTBE cell cultures grown in RA-sufficient (mucous) or RA-deficient (squamous) media were collected by apical washing with PBS. Protein profiles of the ASL from the squamous metaplastic NHTBE cultures were analyzed by two dimensional polyacrylamide gel electrophoresis (2-D PAGE). Initial identification of protein spots on the 2-D PAGE was performed by matrix assisted laser desorption/ionization-time of flight-mass spectrometry (MALDI-TOF) and nanoelectrospray-tandem mass spectrometry (nES-MS/MS) analysis in collaboration with the Proteomics Core Facility in our institution.

We have optimized conditions for 2-D PAGE analysis using ASL from squamous and mucous NHTBE cells. Representatitve 2-D gel images were shown in Fig. 1. A total of 36 protein spots that represent greater level in the ASL from the squamous NHTBE cells selected for protein identification. The protein spots were isolated and digested in gel using trypsin and subjected for HPLC/mass spectrophotometry(MS)/MS analysis. In collaboration with Dr. Kobayashi's group, we have identified the proteins. Surprisingly, majority of the proteins found greater level in the ASF of squamous NHTBE cells were revealed as S100A8, s100A9, Annexin I, Annexin II, and squamous cell carcinoma antigen (SCCA). Interestingly, SCCA and Annexin I and II were detected as multiple protein spots with different molecular weight and pI (isoelectric point), suggesting that they appear to be present as post-translationally distinct forms. We are currently preparing a manuscript to report these findings.

Specific Aim 2 Identify and characterize abnormal proteins secreted by lung squamous cell carcinomas

To determine the proteins identified from the Specific Aim 1 (S100A8, s100A9, Annexin I, Annexin 2, and SCCA), are.

We also performed 2-D immuno blot analysis using antibodies specific to S100A8 and Annexin I to verify multiple spots of S100 A8 and Annexin I (Fig. 5.) Further characterization is underway to determine whether the proteins are post-translationally modified, alternative splice products, or simply products of degradation.

To test whether the proteins identified from the Specific Aim 1 (S100A8, s100A9, Annexin I, Annexin 2, and SCCA) are abnormally overexpressed in only premalignant squamous metaplasia or remain overexpressed in cancer cells, we initially performed 2-D Western blot analysis to determine the expression patterns of S100A8 and Annexin 1 in H292 and H1734 NSCLC cell lines. As shown in Fig. 2, S100A8 proteins were detected at two different sites in

H292 mucoepidermoid NSCLC cells. However, no immunoreactive spots were detected with S100A8 antibody in the whole cell lysates from H1734 adenocarcinoma cell lines. Annexin I was detected at the multiple spots with different MW and pI in both H292 and H1734 NSCLC cell lines. Further analysis with antibodies against S100A9, Annexin 2, and SCCA in several different NSCLC cell lines are underway.

While we are working on the identification of abnormal proteins expressed in squamous metaplastic NHTBE cells using a proteomics approach, we also applied a genomics approach. To identify global molecular changes in H292 cell lines, we compared gene expression of the H292 cells with that of NHTBE cells cultured in a three-dimensional organotypic culture system that maintains pseudostratified normal mucociliary phenotype recapitulating *in vivo* bronchial epithelium. Microarray analysis using Affymetrix U95Av2 chips revealed that 1683 genes were differentially expressed with a greater than 1.5-fold change in the H292 cells. Further oncological analysis of these differentially expressed genes indicated that the WNT, apoptosis, cell cycle pathways, and cell proliferation were significantly altered. The expression of selected genes and the concurrent alteration of the pathways were validated using quantitative real-time polymerase chain reaction (QRT-PCR) and fluorescence-activated cell sorting functional analysis. Western blot with several NSCLC cell lines confirmed that the expression of genes related to these pathways is commonly changed in the tested cell lines. These findings showed that NSCLC cells maintain their growth and survival with concurrent deregulation of WNT, apoptosis, and cell cycle pathways, which are commonly altered in many types of cancer cells, and the organotypically cultured NHTBE cells can be used as a counterpart to study molecular changes in tumor cells of bronchogenic epithelial origin. The data was summarized in Fig. 3. A manuscript was submitted for publication.

Specific Aim 3 Evaluate the efficacy of these differently-secreted proteins to serve as novel biomarkers using readily-accessible clinical specimens

This study is scheduled in Year 3.

Specific Aim 4 Establish primary bronchial epithelial cells in culture and evaluate the expression of candidate biomarkers in bronchial epithelium of lung cancer patients.

We proposed to investigate the expression and regulation of the biomarkers in bronchial epithelial cells in cultures and to address whether the molecular alterations are persistent during the development and differentiation of bronchial epithelium of the lung cancer patients. The source for epithelial cells is from bronchial biopsy tissues collected from 100 newly diagnosed, and previously untreated lung cancer patients who are undergoing surgery at M. D. Anderson Cancer Center, as described in Project 1 (PI: Margaret Spitz) of the TARGET program.

We have obtained 17 bronchial tissue specimens from surgically removed lung sections of 17 different patients. Bronchial epithelial cells from the 17 tissue specimens were successfully isolated and stored in liquid nitrogen for further studies proposed in the Specific Aim 4 and also distributed to Dr. Spitz's laboratory for their proposed studies in Project 1.

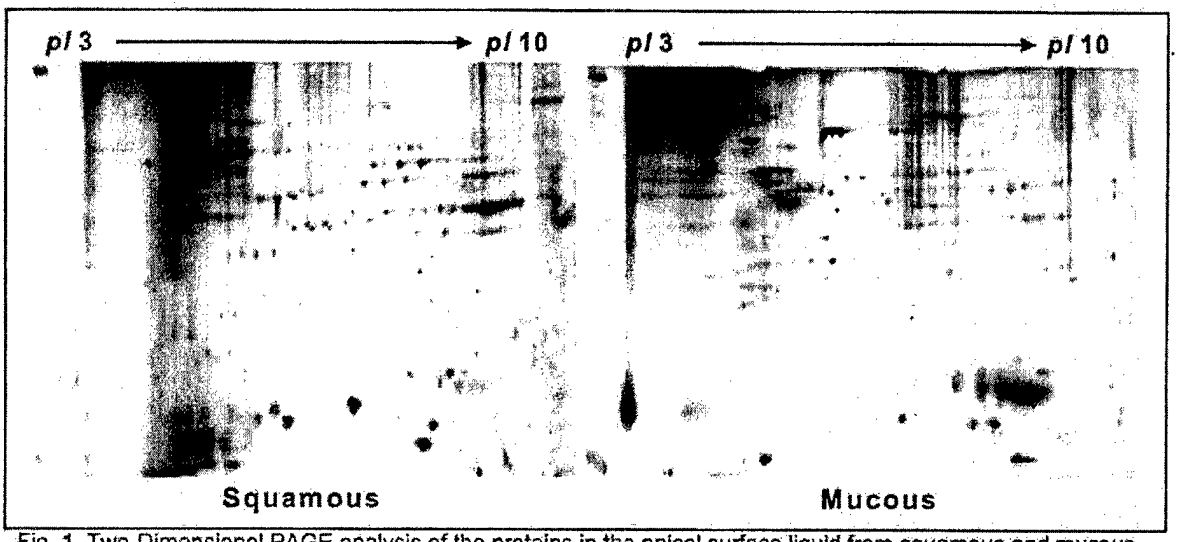

Fig. 1. Two-Dimensional PAGE analysis of the proteins in the apical surface liquid from squamous and mucous NHTBE cells.

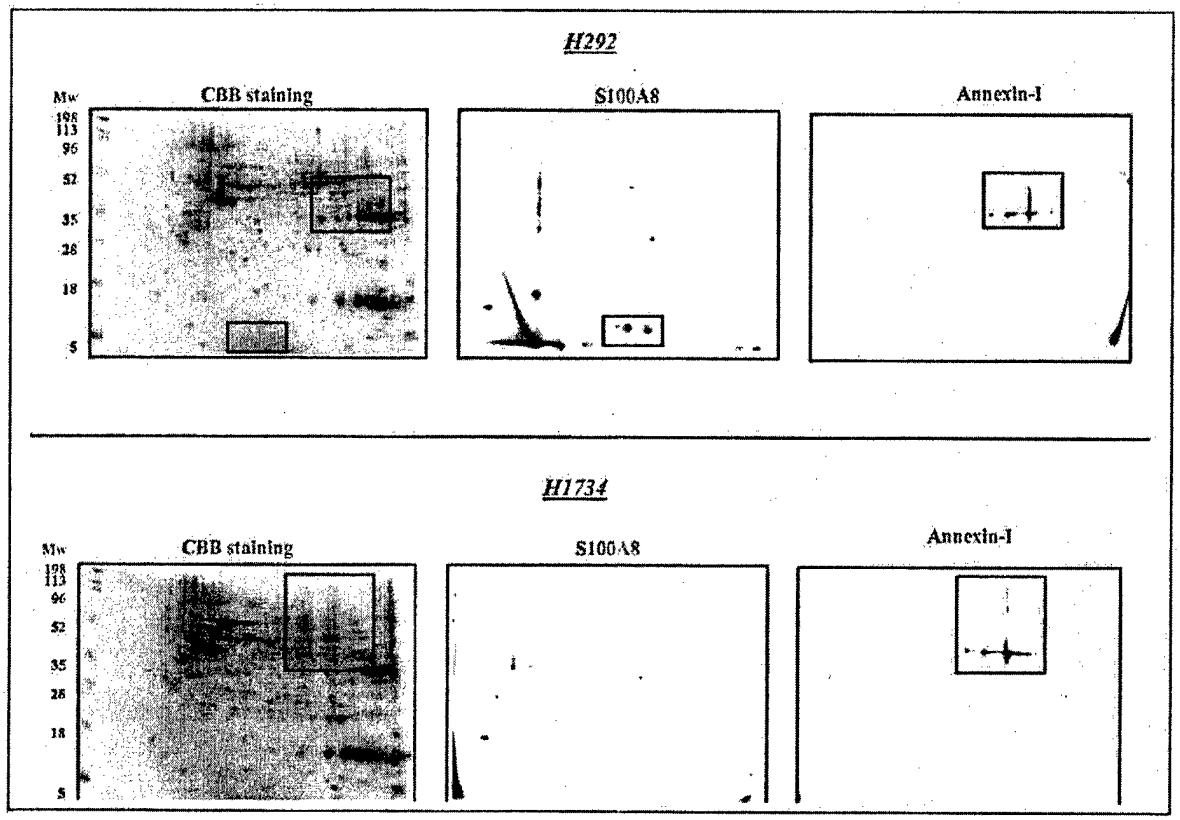

Fig. 2. Western blot analysis of S100A8 and Annexin I in H292 and H1734 cell lines.

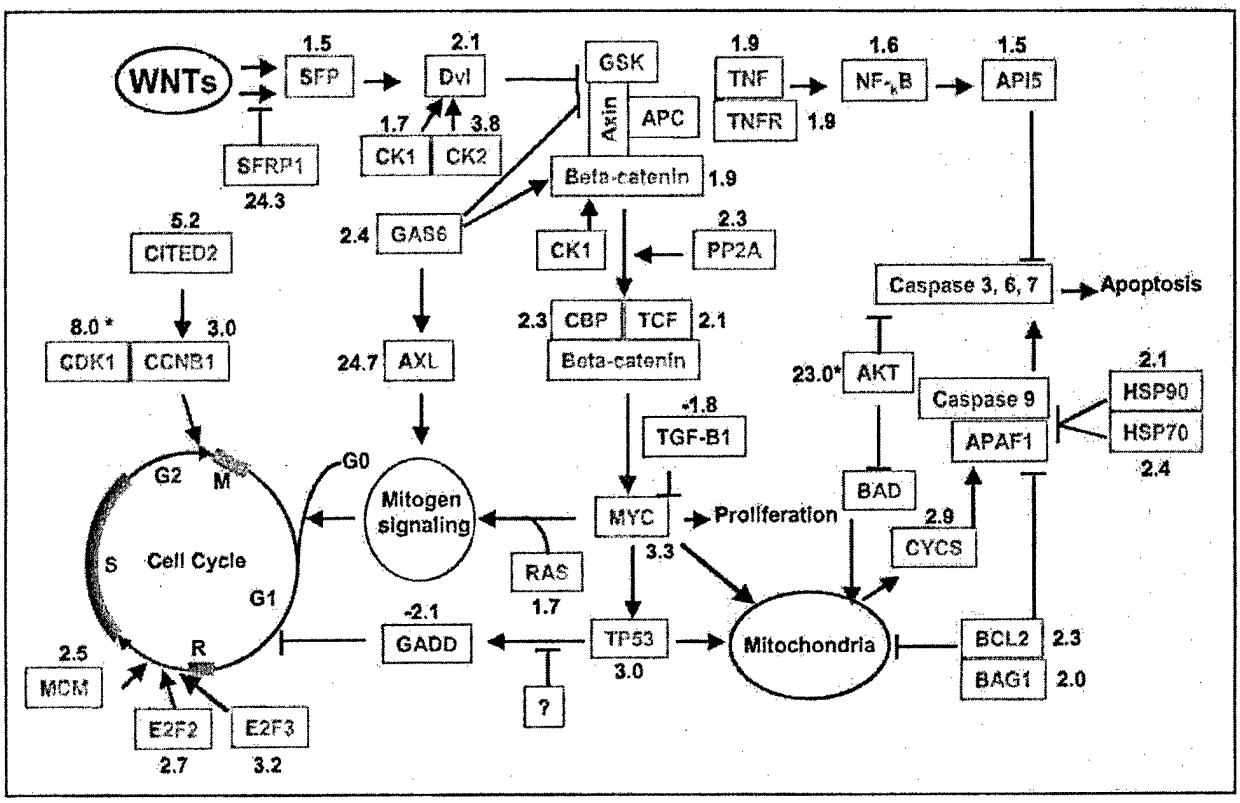

Fig. 3. Schema of genetically altered network in H292 cells. The network consists of three pathways, WNT, cell cycle, and apoptosis which includes mitochondria and TNF, and an event, proliferation. The genes in green had no change, the genes in red were upregulated, and the genes in blue were downregulated. The black numbers are the LBFC (details in Materials and Methods), which the numbers * were obtained from QRT-PCR results. DVL, human disheveled protein; CK1, casein kinase 1; CK2, casein kinase 2; GSK, glycogen synthase kinase 3 beta; PP2A, protein phosphatase 2A; CBP, CREB-binding protein; TCG, T-cell factor; TGF-B1, transforming growth factor-beta1; RAS, Ras; GADD, growth arrest and DNA-damage-inducible gene; E2F2, E2F transcription factor 2; MCM, minichromosome maintenance deficient; TNFR, TNF receptor, NF-κB, nuclear fctor-κB, HSP70, heat shock protein 70 kD; HSP90, heat shock protein 90 kD; APAF1, apoptotic protease activating factor 1; BAD, Bc1-XL/Bc1-2 associated death gene; BAG1, BCL2-associated athanogene 1.

The key accomplishments are:

Proteins secreted from abnormal squamous metaplastic bronchial epithelial cells, but not from normal mucous epithelial cells were identified using 2-dimensional PAGE and MALDI-TOF or HPLC/MS/MS spectrometry; They are squamous cell carcinoma antigens (SCCA), annexin I and II, S100A9, and S100A8.

All of the identified proteins present as multiple forms with different molecular weight and isoelectric point, suggesting that they were posttranslational modified or alternatively spliced products.

We found that genes in the WNT pathway, apoptosis, and cell cycle are concurrently deregulated in non-small cell lung cancer cells as compared to normal bronchial epithelial cells. Significant progress has been made identifying eligible subjects, procuring tumor tissue blocks, and performing biomarker assays. We expect to complete these aspects of the project, in addition to data analysis and manuscript preparation, within the 3-year funding period.

Project 4: Prognostic Role of Promoter Hypermethylation of Death-Associated Protein (DAP) Kinase and p16 Genes in Early-Stage Non-Small Cell Lung Cancer

Principal Investigator: Charles Lu, M.D.

Specific Aim 1 To examine the relationship between hypermethylation of the death-associated protein (DAP) kinase gene promoter and disease-free, disease-specific, and overall survival in completely resected, early-stage NSCLC.

Specific Aim 2 To examine the relationship between hypermethylation of the p16 gene promoter and disease-free, disease-specific, and overall survival in completely resected, early-stage NSCLC.

Specific Aim 3 To examine the relationship between hypermethylation of the p16 gene promoter and history of tobacco smoke exposure in early-stage NSCLC.

Specific Aim 4 To determine the independent prognostic significance of these two molecular biomarkers after adjusting for relevant clinicopathologic variables (T-stage, N-stage, age, gender, histology, type of surgery, performance status, weight loss, smoking status).

The specific goal of this research proposal is to determine the prognostic importance of promoter hypermethylation of selected candidate genes in patients with early-stage, resected NSCLC who have been followed as part of a clinical research database. This study will create a high-quality database that includes clinical information in addition to surgical pathology specimens.

Subjects in this study are identified from a clinical research database of patients who have undergone surgical resection by faculty members of the Department of Thoracic and Cardiovascular Surgery, The University of Texas M. D. Anderson Cancer Center. This database was established in 1997, and includes all patients who undergo thoracic surgical resection at M. D. Anderson Cancer Center. Detailed demographic, clinical, and pathologic data are recorded using standardized data collection forms. Follow-up clinical information is also collected at each clinic visit. Patients with completely resected NSCLC with pathologic stages I or II who do not receive post-operative adjuvant therapy (either chemotherapy or chest radiotherapy) are eligible for this protocol. The proposed sample size is 300 subjects.

A query of the Department of Thoracic Surgery clinical research database yielded an initial list of 559 patients who underwent surgery between January 1, 1997 and December 31, 2001. To date, the medical records of these 559 patients have been screened, and 362 (64.7%) eligible subjects have been identified. Our collaborator in the Department of Pathology (Dr. Ignacio Wistuba) has reviewed these screened patients to determine if sufficient surgical tissue samples (paraffin blocks) exist to perform the required hypermethylation assays. Two hundred eighty five paraffin blocks have been retrieved. Two hundred eighty two subjects have had DAP kinase and p16 promoter hypermethylation assays performed on their tumor specimens in the laboratory of Dr. Li Mao. In order to achieve our target sample size of 300 subjects, we will screen additional patients who underwent surgery in 2002.

Subjects with available tumor tissue have been entered into the study database. We are currently conducting a thorough review of the clinical data for these subjects (gender, age, tumor histology, preoperative clinical variables (performance status, weight loss, smoking status), and obtaining follow-up information (date of disease recurrence, date of death/last follow-up, development of second primary tumors).

The key accomplishments are:

Significant progress has been made identifying eligible subjects, procuring tumor tissue blocks, and performing biomarker assays. We expect to complete these aspects of the project, in addition to data analysis and manuscript preparation, within the 3-year funding period.

Project 5: An Epigenetic Approach to Lung Cancer Therapy

Principal Investigator: Reuben Lotan, Ph.D.

The objective of Project 5 is to examine the potential of using agents that modulate epigenetic events such as a histone deacetylase inhibitor (e.g., SAHA) and demethylating agent (e.g., 5-aza-2-deoxycytidine) and their combination for chemoprevention and therapy of lung and head and neck cancers.

During the past year we have made progress in Specific Aims 1 and 2 as well as the additional Specific Aim 5.

Specific Aim 1 We have extended our observation on the effects of the histone deacetylase inhibitor SAHA to premalignant lung bronchial epithelial cells and premalignant oral cavity epithelial cells. We found that the premalignant cells were sensitive and that their sensitivity was higher at low cell density than at high cell density. The cells were also very sensitive to the demethylating agent 5-aza-2-deoxycytidine. Normal cells were less affected by SAHA.

Specific Aim 2 We have gained a better understanding of the mechanism of action of SAHA. Specifically, using head and neck squamous cell carcinoma cells we found that SAHA induced apoptosis in head and neck cancer cells but not in normal oral epithelial cells and we have begun to understand the mechanism involved as described below:

SAHA induces apoptosis via the mitochondrial (intrinsic) pathway in HNSCC cells. Apoptosis can be initiated via the mitochondrial (intrinsic) pathway that functions through caspase-9, or via the death-receptor (extrinsic) pathway that acts through caspase-8. The release of cytochrome C from the mitochondria initiates caspase activation, thus triggering the important intrinsic apoptotic pathway frequently induced by cytotoxic agents. We next examined the effects of incubating 17B and 22B cells with 4 □M SAHA on several key aspects of apoptosis initiation via the intrinsic pathway, such as cytochrome C release, activation of caspases and cleavage of protein substrates. We found that SAHA triggered a rapid (within 3 hours) release of cytochrome C into the cytosol in 17B and 22B HNSCC cells. This was followed by activation of caspase-9 within 15 hours, as demonstrated by the decreased expression of procaspase-9 by Western blotting. Next, we observed a time-dependent activation of the effector caspase-3 within 15 hours, as demonstrated by decrease in procaspase-3 and appearance of the cleaved form of the caspase substrate PARP. We noted that low levels of cleaved PARP were present in untreated 22B cells, and that the levels of cleaved PARP increased after 3 hours in 22B cells, compared to within 15 hours in 17B cells. A higher level of spontaneous apoptosis occurring within the 22B cells could cause these findings. Taken together, these results demonstrate that SAHA targets the mitochondria and activates the intrinsic, cytochrome C-mediated apoptotic pathway in HNSCC cells.

Activation of the caspase cascade is required for SAHA-induced apoptosis. We examined the effect of SAHA on apoptosis induction in the presence of a caspase inhibitor to determine whether activation of the caspase cascade is necessary for SAHA to induce apoptosis in HNSCC cells. The pan-caspase inhibitor Z-VAD-FMK suppressed SAHA-induced apoptosis in 17B and 22B cells. This indicates that activation of the caspase cascade is required for SAHA to induce apoptosis in these HNSCC cell lines. However, the caspase-9 inhibitor only partially blocked the induction of apoptosis, indicating that alternative caspase cascades also play a role in SAHA-induced apoptosis. We therefore evaluated whether a caspase-8 inhibitor would also block apoptosis. The specific inhibitor of caspase-8 blocked the induction of apoptosis in

HNSCC cells by SAHA to greater extent than the caspase-9 inhibitor, and less than the pan-caspase inhibitor.

SAHA activates the death receptor (extrinsic) apoptosis pathway. The death receptor (extrinsic) apoptosis pathway involves binding of a ligand to one of the TNF family of death receptors, activation of caspase-8, followed by caspase-3 activation. However, the intrinsic and the extrinsic pathways are linked through the ability of caspase 8 to cleave BID, which in turn leads to cytochrome c release from the mitochondria. To explore whether incubation of HNSCC cells in SAHA would also activate the death receptor pathway, we evaluated the expression of Fas(CD95) and FasL(CD95L) before and after exposure to SAHA for various time periods. There was little if any expression of Fas and FasL in untreated 17B and 22B cells but after incubation with SAHA, there was a time-dependent increase in expression of both molecules. In contrast, untreated Leuk1 and gingival cells expressed both Fas and FasL, and SAHA did not increase the level of expression. In both HNSCC cell lines, the expression of Fas and FasL increased by 3 hours, but in the 17B cells, expression peaked at 15 hours, whereas in the 22B cells, expression was strongest at 24 hours. SAHA also activated caspase-8 and cleaved BID by 15 hours in both HNSCC cell lines, demonstrating activation of the extrinsic apoptosis pathway by this agent.

Inhibition of Fas activation blocks SAHA-induced apoptosis. Chemotherapeutic agents can trigger different pathways leading to apoptosis. To determine whether activation of Fas was required for SAHA to induce apoptosis, we incubated 17B and 22B cells with SAHA in the presence of soluble Fas to compete for FasL. Soluble Fas was able to block the induction of apoptosis in these cells by SAHA. This indicates that activation of Fas is required for SAHA to induce apoptosis in HNSCC cells.

Specific Aim 5 We have began to analyze the genes that are regulated by SAHA using an Affymetrix oligonucleotide micro array. The analysis involved treating the cells with SAHA and isolating the ribonucleic acid from which a complementary DNA was synthesized and used as a probe to hybridize to the commercial Affymetrix chips. The data are currently being analyzed by the bioinformatics experts in the Department of Biomathematics/Biostatistics.

The key accomplishments are:

- Establishing that premalignant epithelial cells of oral cavity and lung are sensitive to SAHA
- Discovery that SAHA inhibits the growth of cancer cells by G2 arrest and apoptosis induction
- Elucidation of the mechanism by which SAHA induces apoptosis as the increased expression of Fas (death receptor) and activation of the Fas ligand/Fas mediated apoptosis pathway

A manuscript describing the findings about the mechanism of apoptosis induction by SAHA has been written and will be submitted within one month for publication.

Project 6 The Role of the Farnesyl Transferase Inhibitor CH66336 in Treatment of Carcinoma of the Aerodigestive Tract

Principal Investigator: Fadlo Khuri, M.D.

Farnesyl transferase inhibitors (FTIs) are a new class of anticancer drugs whose mechanism of action is still incompletely understood. We were the first group to show evidence for clinical synergy between paclitaxel and lonafarnib in the clinic (1, 2).

Specific Aim 1 Evaluate the effects of SCH66336 on Ras downstream signaling events by evaluating its effect on downstream molecules such as Raf, Erk-1/2, Akt-2, and jun-terminal kinase (junk-1), assaying apoptosis and also examining SCH66336's effect on angiogenesis in both lung and head and neck squamous cell carcinoma cell lines

We investigated lonafarnib (SCH66336), an FTI, in head and neck squamous cell carcinoma (HNSCC) and non-small cell lung cancer (NSCLC) cell lines. Lonafarnib treatment inhibited cell growth by inducing G2/M phase arrest. In the head and neck cancer cell line, UMSCC38, p-Raf levels were decreased after lonafarnib treatment; however, Erk1/2 activity was not modulated. In contrast, Akt protein expression was decreased and over-expressed a constitutively active Akt, partially rescued the G2/M arrest, and increased cdc2 activity. Furthermore, we found no evidence of transcriptional regulation of Akt; rather, we detected a decrease in exogenous Akt protein level, replenished by MG132, a proteasome inhibitor. In conclusion, we have evidence for a novel mechanism of action of lonafarnib in which Akt protein is degraded through a ubiquitin-based mechanism, reducing Akt expression, decreasing cdc2 activity and leading to G2/M phase cell-growth arrest (3).

Although FTIs were originally designed to target Ras activation, many studies indicate that they may inhibit cell growth and induce apoptosis independent of Ras mutation status. Thus, their mechanisms of action remain largely unknown. The PI3 kinase-Akt pathway has been proposed to be a target for FTI's action, but its role in mediating FTI's biological effects is still controversial. We examined the effect of lonafarnib on the growth of a panel of 11 human non-small cell lung cancer (NSCLC) cell lines and the role of the Akt pathway in mediating its growth inhibitory effects (4). Lonafarnib was effective to inhibit the growth of NSCLC cell lines, particularly after a 5-day treatment, regardless of Ras mutation status. The IC50s for a 3-day and a 5-day treatment ranged from 2.1 to 9.8 μM and from 0.14 to 3.12 μM, respectively. Under normal culture condition (5% serum), lonafarnib induced apoptosis only in a few cell lines but G1 or G2/M arrest in most cell lines. However, cells underwent rapid apoptosis when exposed to lonafarnib in low serum (0.1%) culture medium. The majority of NSCLC cell lines expressed an undetectable level of active or phospho-Akt (p-Akt). Lonafarnib at up to 10 μM did not decrease either the Akt level or the p-Akt level in any of the tested cell lines, even after 48 h treatment. Unexpectedly, lonafarnib increased p-Akt level in one cell line, which, however, was as sensitive as the other cell lines to lonafarnib treatment and underwent G2/M arrest. The PI3 kinase inhibitor LY294002 at 10 μM decreased the p-Akt level but failed to induce apoptosis. It suppressed elevated p-Akt by 1 or 5 uM lonafarnib but failed to enhance the effect of lonafarnib on induction apoptosis. Although 10 μM LY294002 in combination with 10 μM lonafarnib did synergistically induce apoptosis, the p-Akt level remained increased. Therefore, we conclude that Akt is not likely to be a target for lonafarnib's effect on growth arrest and apoptosis induction in human NSCLC cells. This is further supported by our finding that addition of 0.15% bovine serum albumin (BSA), which approximately equals the protein amount in 5% serum,

prevented cells from apoptosis, which occurred in 0.1% serum medium. This result clearly indicates that low serum conditions enhance the effect of lonafarnib on induction of apoptosis by simply increasing its intracellular concentration due to less binding of lonafarnib to protein rather than inactivating PI3 kinase-Akt survival pathway.

Specific Aim 2 Evaluate the effects of SCH66336 on protein expression in both lung and head and neck cancer cell lines by identifying proteins whose expression is altered by treatment with SCH66336 and determining the role of these proteins as biomarkers and effectors of response to treatment with farnesyl transferase inhibitors

We also investigated the effect of lonafarnib on modulation of proteins in head and neck cancer. We found that several proteins are upregulated and others downregulated by FTI. To reveal novel mechanisms of FTI induced tumor growth inhibition or induction of apoptosis, we performed two-dimensional electrophoresis (2-DE) and mass spectrometry to identify differentially expressed proteins after lonafarnib treatment (5). We visualized over 500 proteins using colloidal coumassie blue staining. Thirty-five differentially expressed proteins were found compared to the protein expression profile of the untreated control. The identity of twenty-two of the 35 proteins was obtained through mass peptide fingerprinting. All of the proteins identified were unlikely to be direct substrates of farnesyl transferase because they lack a CAAX motif, and include (1) heat shock proteins, (2) receptors, (3) binding proteins, (4) enzymes, and (5) proteins with unknown properties. Further studies to identify their function and significance are ongoing at Emory University utilizing the Emory Proteomics Core facility, in collaboration with Dr. Jan Pohl, Director of the Proteomics Core at Emory University School of Medicine. We have just hired a postdoctoral fellow, Dr. Ludavic Lacroix, from Institute Gustave Roussy, Paris, France, with expertise in proteomics, to focus exclusively on Specific Aim 2 and pursue this Specific Aim to its conclusion.

Specific Aim 3 Evaluate the efficacy of SCH66336 as an inhibitor of growth and as an inducer of apoptosis in an orthotopic model of head and neck squamous cell carcinoma, where we can obtain serial tissue to evaluate changes in cell signaling, induction of apoptosis and inhibition of angiogenesis

This is ongoing with orthotopic mouse models of head and neck cancer in development, in collaboration with Dr. Dong M. Shin and Georgia Chen, both of whom have been recruited from the University of Pittsburgh. Drs. Shin and Chen have significant expertise in translational research in head and neck cancer, and are guiding our mouse models cancer program at the Winship Cancer Institute.

Specific Aim 4 Expand on our preliminary data to focus on the underlying mechanisms by which farnesyl transferase inhibitors induce apoptosis in combination with retinoids such as 4-HPR, or taxanes such as docetaxel or paclitaxel, in non-small cell lung cancer and squamous head and neck cancer cell lines

Farnesyl transferase inhibitors (FTIs) are anti-cancer agents developed to target oncogenic Ras proteins by inhibiting Ras farnesylation. FTIs synergize with the taxanes and other microtubule-stabilizing drugs, however, the mechanistic basis underlying this synergistic interaction remains elusive. Here we show that the FTI, lonafarnib (LNF), affects the microtubule cytoskeleton resulting in microtubule bundle formation, increased microtubule stabilization and acetylation, and suppression of microtubule dynamics. In addition, a similar microtubule-stabilization effect is observed in tumors resected from patients treated with LNF. Notably, treatment with the combination of low doses of LNF with taxol dramatically enhanced tubulin acetylation (a marker of microtubule stabilization) as compared to either drug alone. This synergistic effect correlated

with farnesyl transferase inhibition and was accompanied by a synergistic increase in mitotic arrest and cell death. Mechanistically, we show that the enhanced tubulin acetylation observed with the LNF/taxol combination is due to inhibition of the tubulin deacetylase HDAC6, both in cells and *in vitro*. This mechanism is further supported by data showing that the LNF/taxane combination is synergistic only in cells lines expressing wild-type HDAC6, but not a catalytic-mutant HDAC6, revealing that functional HDAC6 is required for the synergistic combination of LNF with taxanes. These observations were expanded to other classes of FTIs, by showing that a similar mechanism of synergy applies for other FTIs in combination with taxanes. Furthermore, tubacin, a specific HDAC6 inhibitor, synergistically enhanced tubulin acetylation in combination with taxol, mimicking the LNF/taxol effects. Taken together, these data suggest a cause-effect relationship between HDAC6 inhibition, enhanced tubulin acetylation and cell death, providing a molecular basis for FTI/taxane synergistic antiproliferative combination.

CONCLUSION: In summary, lonafarnib is active in inducing growth arrest and apoptosis in human NSCLC and HNSCC cells, through mechanisms independent of Ras mutation and Akt activation in NSCLC. This suggests a completely novel, Akt-independent mechanism of action for these compounds in lung cancer, unlike our previous data generated with head and neck cell lines.

Discoveries:

- Novel ras-dependent and independent effects of farnesyl transferase inhibitors uncovered
- Proteomic analysis of FTI treated cell lines detects several important classes of proteins that are upregulated or downregulated by this class of compounds
- Lonafarnib inhibits HDAC6 through a novel mechanism in several lung cancer cell lines. This may serve as an important target for development of trials targeting synergy between novel signal transduction inhibitors and tubulin targeting cytotoxics

Publications:

1. Khuri FR, Glisson BS, Kim ES, Meyers ML, Herbst RS, Thall PF, Munden RF, Statkevich YP, Bangert S, Thompson E, Cascino M, Shin DM, Papadimitrakopoulou V, Kurie JM, Kies MS, Lee JS, Fossella FV, Hong WK. Phase I study of farnesyl transferase inhibitor (FTI) SCH66336 with paclitaxel in solid tumors. *Clinical Cancer Research,* May 2004.
2. Kim ES, Kies MS, Fossella FV, Glisson BS, Zaknoen S, Baum CM, Summey C, Lu C, Papadimitrakopoulou V, Hong WK, Khuri FR. Phase II study of the farneslytransferase inhibitor (FTI) lonafarnib with paclitaxel in patients with taxane-refractory/resistant non-small cell lung cancer. In press, *Cancer,* 2004 .
3. Hassan KA, Lee H-Y, Kim E, Bishop WR, Kirschmeier P, Mao L, Khuri FR. A novel mechanism of farnesyltransferase inhibitor (SCH66336) arresting head and neck squamous cell carcinoma cells. *Proceedings of the American Association for Cancer Research*, 44, abstract #800, pp. 156, 2003.
4. Sun S-Y, Zhou Z, Wang R, Khuri FR. Akt is not a target for the growth inhibition and apoptosis induction by the farnesyltransferase inhibitor SCH66336 in human lung cancer cells. In press, *Cancer Biology and Therapy,* 2004.
5. Wu W, Hassan KH, Hong WK, Mao L, and Khuri FR. Proteomic identification of proteins associated with farnesyltransferase inhibitor treatment. *Proceedings of the American Association for Cancer Research*, 43, abstract #4667, pp. 943, 2002.

Project 7 Mechanisms and Therapeutic Applications of the Tumor Suppressor Gene *FUS1* in Lung Cancer

Co-Principal Investigator: Lin Ji, Ph.D.
Co-Principal Investigator: Rajagopal Ramesh, Ph.D.

Specific Aim 7.1 To determine the global molecular changes and cellular responses to FUS1-mediated tumor-suppressor activities in human NSCLC cells by high throughput gene and protein expression profiling.

We used DNA microarrays and ProteinChip arrays and an inducible-FUS1 expression system to determine the gene and protein expression patterns mediated by induction of *FUS1* in NSCLC cells at either a therapeutic or physiological level. The specific targets of FUS1 protein will be identified by comparison of the gene and protein expression profiles, and proteins of interest will be isolated. We are now using the technologies and protocols developed in this pilot study to FUS1-mediated gene and protein modulations in lung cancer cells. We have established FUS1-stable transfectants of NSCLC cell lines, which allow us to gene and protein expression changes mediated by FUS1 expression under physiological conditions. We have developed a novel two-dimensional liquid chromatography (2D-LC) method for the fractionation and separation of crude protein lysates and for protein profiling and identification using a

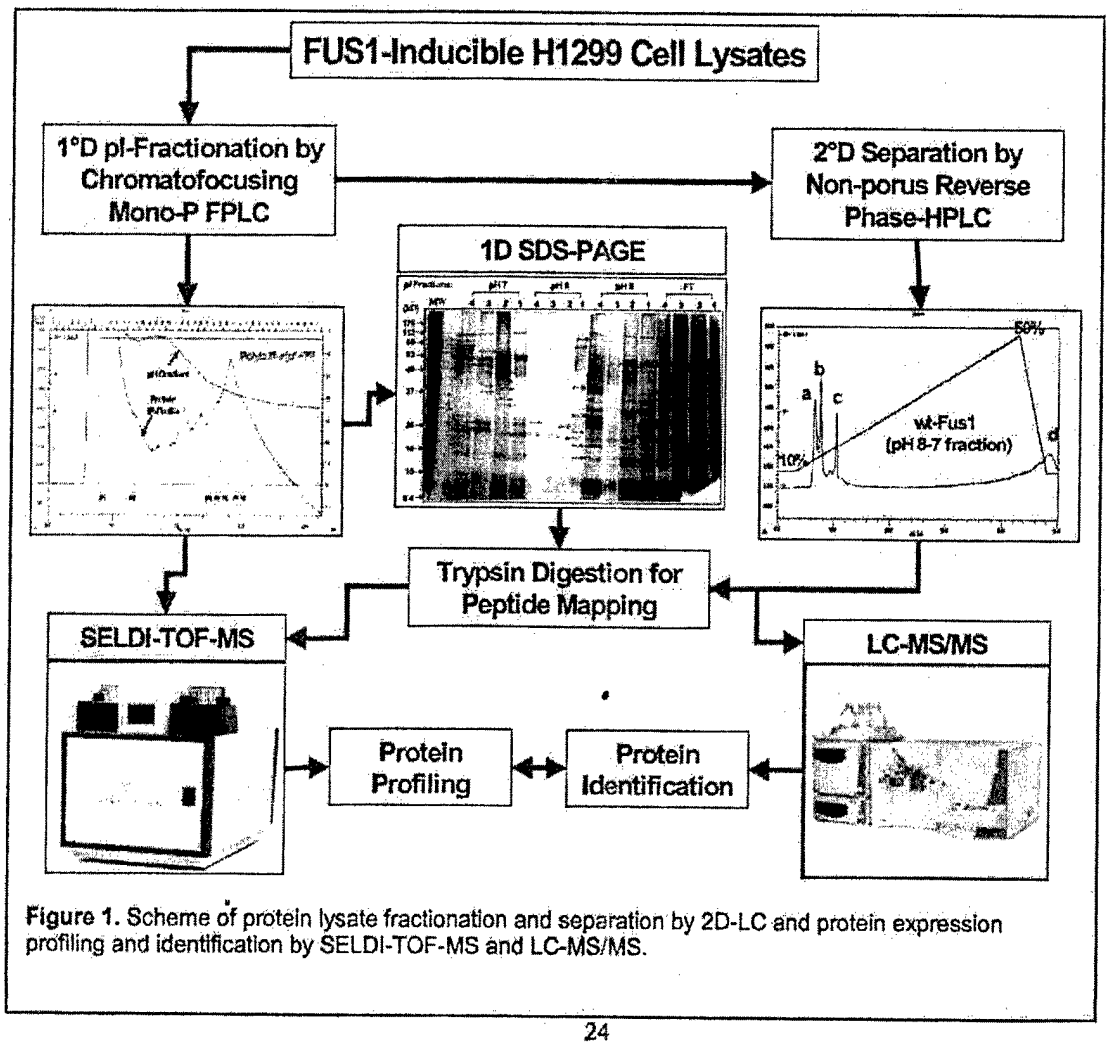

Figure 1. Scheme of protein lysate fractionation and separation by 2D-LC and protein expression profiling and identification by SELDI-TOF-MS and LC-MS/MS.

ProteinChip Array-based surface enhanced laser desorption/ionization time of flight mass spectrometry (SELDI-TOF-MS) (Fig. 1).

We have successfully applied this technology to perform a proteomic analysis for evaluating modulations of protein expression in FUS1-expressing tumor cells, compared with non-expressing controls. For the 1°D-LC, cell lysates were fractionated based on the pI values of proteins by FPLC with a chromafocusing Mono-P column. The pI-fractionated samples were either directly applied protein profiling on CM10 and Q10 ProteinChip arrays by SELDI-MS or subjected to the 2°D-LC, using a Non-porus reverse phase (NP-RP) colume by HPLC, for

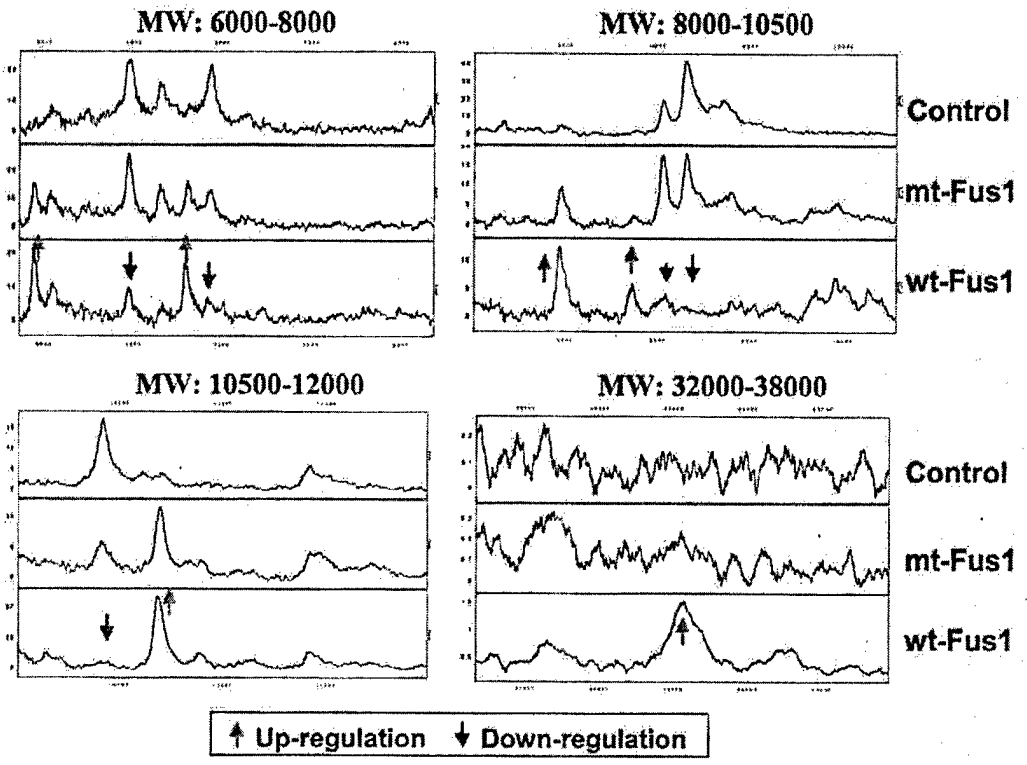

Figure 2. Differential protein expression in NSCLC H1299 cells upon induction of wild-type FUS1 (wt-FUS1) by comparison with those un-induced or functional deficient mutant FUS1 (mt-FUS1) expressing control cells.

further protein separation and identification. From protein expression profiles, we have been able to detect more than 50 protein peaks that represent the differentially expressed protein species in response to the activation of FUS1 protein in these lung cancer cells. Some examples of protein profiles are shown in figure 2. We are now in the process of identifying these FUS1-targeted cellular proteins and elucidating the FUS1-activated biological pathways as we planned in this study.

Specific Aim 7.2: To elucidate the molecular mechanism of FUS1 in lung cancer pathogenesis by determining the expression and subcellular localization of the FUS1 protein in human normal lung tissue and tumor samples at various stages of development.

We previously demonstrated that enforced expression of the wild-type (wt)-FUS1 in 3p21.3-deficient NSCLC cells significantly suppressed tumor cell growth by induction of apoptosis and

alteration of cell cycle kinetics in vitro and in vivo. However, the molecular mechanism and signaling pathway involved in FUS1-mediated apoptosis and its role in pathogenesis of lung cancer remain unknown. In this study we aimed to identify the potential cellular targets of Fus1 protein to gain insight into the mechanism of Fus1 function and to explore the clinic application of Fus1 as a molecular therapeutic agent for lung cancer. We found the inactivation of Fus1 products in majority of primary lung tumors by either loss of expression or deficiency of posttranslational myristoylation modification of Fus1 protein, as demonstrated by immuno-histochemical analysis on both paired lung cancer patient samples and lung cancer tissue micro-arrays and by Fus1-antibody capture analysis on a ProteinChip array with SELDI-TOF-MS in LCM-enriched lung cancer and non-involved cells, respectively. Using a ProteinChip array-based analysis of protein-protein interaction and peptide mapping, we discovered that Fus1 protein directly interacts with the apoptotic protease activation factor Apaf1 protein. This Fus1-Apaf1 interaction was further confirmed by Immuno-precipitation and immuno-blot analysis using either anti-Fus1 or anti-Apaf1 antibodies. We also observed that both the wt-Fus1 and a N-myristoylation-deficient mutant Fus1 (myr-mt-Fus1) protein but not the C-terminal-deletion (10-20 amino acids) mutants of Fus1 proteins could bind to Apaf-1 protein in H1299 transfectants. A computer-aided structural analysis predicted a PDZ domain in the C-termini of the both Fus1 and Apaf1 proteins, suggesting that the Fus1-Apaf-1 interaction might be mediated through these classic PDZ protein-protein interaction motifs. Using an immuno-fluorescence image analysis (IFIA) with Fus1 and Apaf1 antibodies, we detected the co-localization of the Apaf1 proteins with both the wt-Fus1 and myr-mt-Fus1 proteins with distinct subcellular patterns, with the wt-Fus1, co-localized in their typical mitochondria and ER membrane locations but, with the myr-mt-Fus1, which is deficient of membrane-attachment, appearing throughout the cytoplasm. Using IFIA, we also detected a Fus1-mediated inactivation of anti-apoptotic Bcl2 as well as binding with pro-apoptotic Cytochrome C on mitochondria membrane and releasing it into cytosol.

We also found that co-expression of wt-Fus1 and wt-p53 in NSCLC cells that are deficient in both proteins significantly enhanced the response of these cells to the DNA-damaging agents CDDP and ionizing radiation-induced apoptosis and growth inhibition. A detailed immuno-blot and quantitative real time RT-PCR analysis showed that the enhanced apoptosis induction and tumor cell growth inhibition might be caused by Fus1-mediated down-regulation of MDM2 protein, stabilization of p53 protein, and the resulting p53-upregulation of Apaf1 expression in response to DNA damage. These results suggest that Fus1 protein may function as a key mediator in Apaf1-mediated mitochondrial apoptosis pathway by recruiting and directing cytoplasmic Apaf1 protein to a critical cellular location and activating it in situ, and by upregulating activity of other proapoptotic effectors such as p53 and dowregulating anti-apoptotic mediators such as Bcl2 family proteins for the efficient induction of apoptosis.

Specific Aim 7.3 To quantitatively evaluate interactions of the *FUS1* gene with other 3p21.3 TSGs for their tumor-suppressing activities *in vitro* and *in vivo*.

In this study, we explored the capability of the wt-FUS1 gene product as a modulator of chemotherapeutic drugs for enhancing chemotherapeutic potency and overcoming drug resistance in lung cancer cells. We found that a transient expression of the wt-Fus1 protein in FUS1-expressing plasmid-transfected H1299 cells significantly enhanced the cisplatin-mediated inhibitory effect on tumor cell growth at a low dose (1mM) of cisplatin treatment. In addition, a stable expression of the wt-FUS1 gene, which is under the control of a ponasterone A-inducible promoter, reduced more than 30% of IC50 values of both cisplatin and paclitaxel treatments in H1299 cells, even at a low level of induced Fus1 expression. However, the maximum stable expression of a functionally deficient mutant Fus1 protein (mt-Fus1) in a similar inducible

system did not enhance the sensitivity of tumor cells to these drugs. Furthermore, a significant increase in apoptotic cell populations was detected in cells with the induced expression of the wt-Fus1 protein but not in those with induced expression of mt-Fus1, as shown by a FACS analysis with TUNEL reaction. These results suggest that the wt-Fus1 may play a critical role in modulating the sensitivity of tumor cells to the chemotherapeutic agents, especially to DNA damaging agents such as cisplatin and that a combination treatment with the FUS1-lipoplex-mediated molecular therapy and the cisplatin or taxane-based chemotherapy may be an efficient treatment strategy for lung cancer.

To determine whether exogenous expression of Fus1 gene in combination with p53 TSG has a synergistic tumor suppression activity, we coexpressed Fus1 and p53 genes by cotransfection in human non-small cell lung (NSCLC) cells and evaluated the combined effects of these two tumor suppressors on inhibition of NSCLC cell growth. We found that coexpression of p53 and wild-type Fus1 (wt-Fus1), but not its NH2-myristoylation site mutant (mut-Fus1), synergistically inhibited cell proliferation and induced apoptosis in human NSCLC cells. We also found that the combination expression of wt-Fus1 and p53 enhanced the sensitivities of NSCLC cells to g-radiation and cisplatin treatment. Furthermore, we found that the synergistic tumor suppression by Fus1 and p53 is implicated in Fus1-mediated augmentation of APAF-1 expression, accumulation of p53 protein, and inactivation of MDM2 in NSCLC cells. Our results therefore revealed a novel molecular mechanism involving Fus1-mediated tumor suppression function and its interaction with other cellular components in the pathways regulating p53 activity. Our findings showed that gene therapy by synergistic tumor suppressors such as Fus1 and p53 in combination with chemotherapy or radiotherapy may be an effective therapeutic strategy for NSCLC and other cancers.

Specific Aim 7.4: To determine the dose-limiting toxicity and biodistribution of the FUS1-lipoplex in a murine model and in a non-human primate model and to evaluate the therapeutic effect of the FUS1-lipoplex in local, solid tumors and experimental metastatic lung tumors.

Intratumoral Injection of FUS1-lipoplex suppresses human xenograft tumor growth. We tested the tumor suppressor function of *FUS1* gene *in vivo* by direct intratumoral injection of DOTAP:Chol-*FUS1* complex. Treatment of subcutaneous lung tumor xenograft (H1299, and A549) for a total of six doses with DOTAP:Chol-*FUS1* complex resulted in a significant suppression of tumor growth ($P = 0.005$ for H1299, and $P = 0.01$ for A549) compared to control

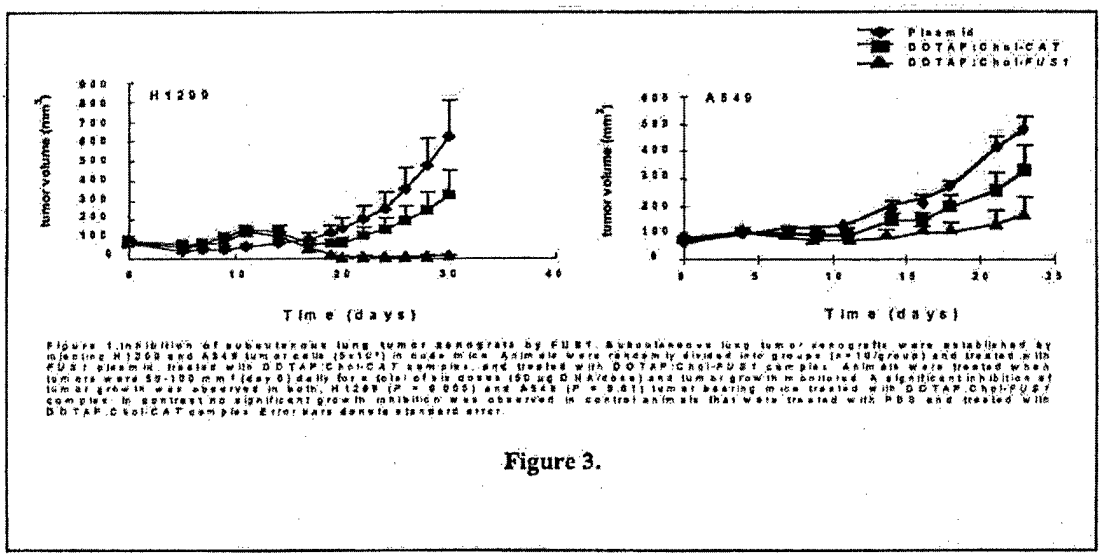

Figure 3.

animals that were treated with *FUS1* plasmid DNA, and treated with DOTAP:Chol-*CAT* complex (Figure 3; Ito et al., Cancer Gene Ther. In press).

That the tumor inhibition was due to FUS1 protein expression was demonstrated by immunohistochemical analysis. FUS1 protein expression was detected in the subcutaneous tumor tissues primarily localized to the cytoplasm as observed *in vitro* (data not shown). Expression was primarily observed in the tumor cells.

However, expression in other cells intermixed with tumor cells was also observed. The subtype of cells staining positive for FUS1 in the tumor was not determined. Furthermore, tumors treated with DOTAP:Chol-*FUS1* complex underwent significant apoptotic cell death as evidenced by TUNEL staining compared to tumors from those animals that were treated with plasmid DNA or DOTAP:Chol-*CAT* complex. (Figure 4; Ito et al., Cancer Gene Ther. In press). Induction of apoptotic cell death was observed in both H1299 and A549 tumors.

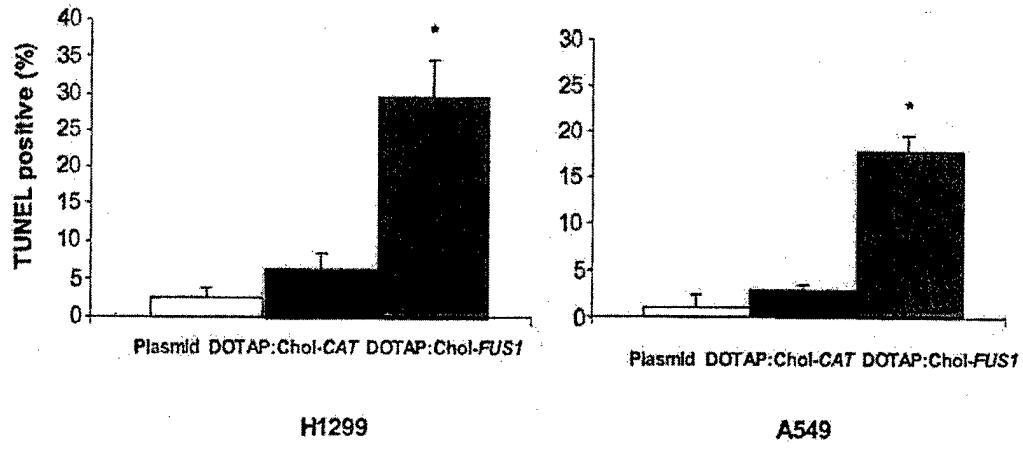

Figure 2. Induction of apoptosis in subcutanous tumors treated with DOTAP:Chol-*FUS1*. Subcutaneous lung tumor (H1299 and A549) xenografts that were treated with FUS1 plasmid, treated with DOTAP:Chol-*CAT* complex, and treated with DOTAP:Chol-*FUS1* complex were harvested and subjected to TUNEL staining. Animals were treated DOTAP:Chol-*FUS1* complex demonstrated 15-35% TUNEL positive staining of tumor tissues (33% for H1299, and 18% for A549; $P = 0.001$). In contrast no significant growth inhibition was observed in control animals that were treated with PBS and treated with DOTAP:Chol-*CAT* complex. Error bars denote standard error.

Figure 4.

Intravenous injection of DOTAP:Chol-*FUS1* complex inhibits experimental lung metastasis. To test the tumor suppressor activity of *FUS1* on experimental lung metastases, lung tumors were established by injecting A549 tumor cells via tail vein. Intravenous treatments of these lung tumor bearing animals with DOTAP:Chol-*FUS1* complex resulted in a significant inhibition ($P = 0.001$) of lung metastases compared to control animals that were treated with PBS, treated with *FUS1* plasmid DNA, treated with liposome alone, and treated with DOTAP:Chol.-*CAT* complex (Figure 5; Ito et al., Cancer Gene Ther. In press). Animals treated with DOTAP:Chol-*CAT* complex demonstrated some tumor inhibition. The ability of DOTAP:Chol-*CAT* complex treatments to demonstrate some antitumor activity is not surprising and is attributed to non-specific antitumor activity. However, tumor inhibition was not significant compared to animals treated with PBS, treated with *FUS1* plasmid DNA and treated with liposome. These results show that the therapeutic effect observed in lung tumor bearing animals when treated with DOTAP:Chol-wt*FUS1* is specific to wt*FUS1*.

Intravenous treatment of lung tumor bearing animals with DOTAP:Chol-*FUS1* complex prolongs animal survival. We next evaluated the effect of DOTAP:Chol-*FUS1* treatments on animal survival. Treatment of experimental A549 lung tumor bearing animals with DOTAP:Chol-*FUS1* complex resulted in a significant ($P = 0.01$) and prolonged survival (mean survival time = 80 days) (Figure 6; Ito et al., Cancer Gene Ther., in press). In contrast, no significant survival was observed of animals that were treated with PBS (mean = 47.8), treated with *FUS1* plasmid (mean = 51.6), treated with liposome (mean = 47.2), and treated with DOTAP:Chol-*CAT* complex (mean = 47.8). Furthermore, histopathological analysis of various organs demonstrated no significant treatment-related toxicity.

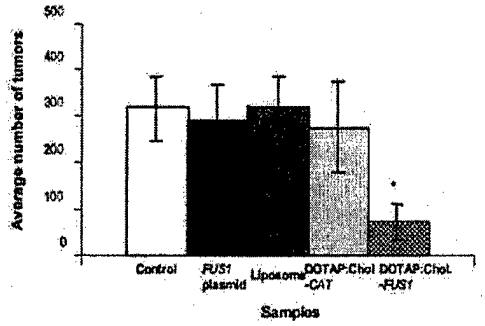

Figure 5. DOTAP:Chol-*FUS1* complex inhibits experimental lung metastasis. Experimental lung metastasis was established in nude mice by injecting A549 tumor cells (10⁶) via tail vein. Six-days later animals were divided randomly into groups (n=10/group) and treated with PBS, treated with plasmid DNA alone (10 μg), treated with liposome alone, treated with DOTAP:Chol-CAT complex, and treated with DOTAP:Chol-*FUS1* complex. Animals were treated daily for a total of six doses (10 μg DNA/dose) via tail vein. Three-weeks after the last treatment animals were euthanized, lungs were injected with India ink solution and harvested. Lungs were examined under a stereomicroscope and the number of tumor nodules counted. A significant ($P = 0.001$) reduction in the number of tumor nodules was observed in animals treated with DOTAP:Chol-*FUS1* complex compared to control animals. Error bars denote standard error.

Figure 5.

From the results of our preclinical studies, it is evident that FUS1 functions as an effective tumor suppressor gene which when delivered intratumorally or intravenously effectively inhibits primary and disseminated lung tumor growth. These exciting results indicate the feasibility of using FUS1 complexed with DOTAP:Chol-liposome for treatment of lung cancer in the clinic.

Although the therapeutic efficacy was demonstrated in nude mouse model, the toxicity of the DNA-liposome complex was not tested that is relevant to determine the dose-limiting toxicity. For this purpose we have initiated toxicity studies in mice (C3H) and in non-human primates (Cynomolgus monkeys; *Macaca fascicularis*). In this study, single dose and multiple dose-related toxicity will be studied. These studies are being conducted at the M. D. Anderson Veterinary Facility in Bastrop, TX. The toxicology studies are being carried out under conditions regulated by the FDA for IND filing. In our initial proposal we had proposed to use β̃gal DNA. However, since FUS1 gene will actually be tested in humans and not β-gal, we have changed our strategy and now plan to conduct toxicity studies using FUS1 gene. Preliminary toxicology results indicate an IC_{10} to be at 40μg of FUS1 DNA in mice. Although monkey studies showed no significant morbidity, the concentration of DNA inducing morbidity was similar to that in mice. The toxicology data is currently being documented for submission to the FDA. It is anticipated that the outcome of these studies will enable us to initiate a Phase-I/II clinical trial for lung cancer.

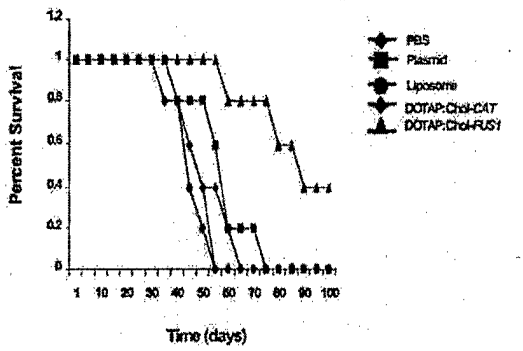

Figure 6. Treatment with DOTAP:Chol-*FUS1* complex increases animal survival. Experimental lung metastasis was established in nude mice by injecting A549 tumor cells. Six-days later animals were divided randomly into groups (n=5/group) and treated with PBS, treated with plasmid DNA alone (10 μg), treated with liposome alone, treated with DOTAP:Chol-CAT complex, and treated with DOTAP:Chol-*FUS1* complex. Animals were treated daily for a total of six doses (10 μg DNA/dose) via tail vein. Following the last treatment animals were monitored daily for morbidity and mortality. Survival was estimated by using the Kaplan-Meier and Wilcoxon signed-rank tests. Survival was significantly longer in animals treated with DOTAP-Chol-*FUS1* complex (mean survival time: 80 days; $P = 0.01$) compared to animals that were treated with PBS (mean survival time: 47.8 days), treated with plasmid DNA alone (mean survival time: 51.6 days) treated with liposome alone (mean survival time 47.2 days), and treated with DOTAP:Chol-CAT complex (mean survival time: 47.8 days).

Figure 6.

An additional study that we have undertaken as part of this proposal though is to develop strategies to overcome the DOTAP:Chol-DNA complex induced toxicity. Our studies and those of others have shown acute inflammatory response to be the primary source for toxicity. We are currently developing strategies using several anti-inflammatory drugs to suppress liposome-induced inflammation without affecting the transgene expression. One such drug that we have identified is the non-steroidal anti-inflammatory drug (NSAID), naproxen. *In vitro* and *in vivo* studies show that naproxen effectively inhibits liposome-induced inflammation without affecting

FUS1 transgene expression. In fact, an enhanced antitumor activity is observed suggesting that naproxen use can be beneficial. We are currently studying the mechanisms. The results of our preliminary studies are currently being written for submission to the journal "Nature Biotechnology" for publication.

The key accomplishments are:

- Studied molecular mechanisms of a novel tumor suppressor gene (TSG) FUS1, identified an apoptotic protease activating factor 1 (Apaf1) as the cellular target that directly interacts with Fus1 protein, and found that Fus1 protein functioned as a key mediator in Apaf1-mediated mitochondrial apoptosis pathway by recruiting and directing cytoplasmic Apaf1 protein to a critical cellular location and activating it in situ, and by upregulating activity of other pro-apoptotic effectors such as p53 and dowregulating anti-apoptotic mediators such as Bcl2 family proteins for the efficient induction of apoptosis
- Studied the effects of Fus1 in combination with other tumor suppressor genes such as p53 and chemotherapeutic agents such as cisplatin, taxel, protein tyrosine kinase inhibitors on tumor cell proliferation and apoptosis *in vitro* and *in vivo*. Our results suggest that co-expression of FUS1 and p53 could synergistically inhibit lung cancer cell growth and the wt-Fus1 may play a critical role in modulating the sensitivity of tumor cells to the chemotherapeutic agents, especially, to DNA damaging agent Cisplatin and protein tyrosin kinase inhibitor Gefitinib
- Demonstrated the selective and increased uptake of liposome-DNA complexes by tumor cells in the lung compared to surrounding normal tissues. A phenomenon shown for the first time. These findings were highlighted in the editorial section of the journal "Molecular Therapy". These findings allow us to utilize the inherent properties of the DOTAP:Chol-DNA liposome complexes
- Demonstrated that host-inflammatory response in tumor-bearing animals is reduced compared to normal animals, which is partly mediated by the production of IL-10 by tumor cells. Hence differences exist in the liposome-DNa complex induced toxicity. This forms a basis to conduct toxicity studies in tumor-bearing animals that is relevant to patients in the clinic
- Developed novel strategies to suppress liposome-DNA complex induced inflammatory response. This strategy is being planned for incorporation in the phase-I/II clinical trial.
- Demonstrated the therapeutic effect of FUS1 in xenograft tumor models.
- Toxicology studies are completed. Results are being compiled for submission to FDA.

Conclusion:

Our results point to an essential role of Fus1 in apoptotic pathway by directing the critical assembling of apoptosome for cells in response to carcinogenic stimulus such as DNA-damaging chemicals and gamma radiation. Our results also imply that a combination treatment with the FUS1-lipoplex-mediated molecular therapy and the cisplatin or taxane-based chemotherapy may be an efficient treatment strategy for lung cancer. Our results have also established the feasibility of using DOTAP:Chol-based liposomal gene delivery for systemic therapy of lung cancer. Furthermore, FUS1 has been shown to be an effective tumor suppressor. Toxicology studies have established the maximum tolerated dose and are being submitted for initiation of clinical trial. This will be the first systemic gene therapy-based therapy for lung cancer.

Related Publications (published and submitted) (2002-2003):

1. Uno F, Sasaki J, Nishizaki M, Carboni G, Xu K, Atkinson EN, Kondo M, Minna, JD, Roth JA, and Ji L. Myristoylation of the FUS1 protein required for tumorsuppression in human lung cancer cells. *Cancer Research* 64, 2969-2976, 2004.

2. Nishizaki M, Sasaki J, Fang B, Atkinson EN, Minna, JD, Roth J, and Ji L. Synergistic tumor suppression by coexpression of FHIT-mediated MDM2 inactivation and p53 stabilization in human NSCLC cells. *Cancer Research* 64 (16), 5632-5640, 2004.

3. Ito I, Began G, Mohiuddin I, Saeki T, Saito Y, Branch CD, Stephens LC, Yen N, Roth JA, Ramesh R. Increased uptake of liposomal-DNA complex by lung metastases following intravenous administration. *Molecular Therapy* 7(3): 409-418, 2003.

4. Ito I., Saeki T, Mohiuddin I, Saito Y, Varporclyan A, Branch C, Roth JA, and Ramesh R. Persistent transgene expression following intravenous administration of a liposomal complex: role of IL-10 mediated immune suppression. *Molecular Therapy* 9 (3): 318-327, 2004.

5. Ito I, Ji L, Gopalan B, Tanaka F, Saito Y, Branch CD, Xu K, Atkinson NE, L. Clifton Stephens, Minna JD, Roth JA, and Ramesh R. DOTAP:cholesterol liposome mediated delivery of the 3p gene FUS1 inhibits growth of human lung cancer in vivo. *Cancer Gene Therapy* 2004, (in press).

Published Abstracts and Presentations:

1. Uno F. Sasaki J, Nishizaki M, Carboni G, Xu K, Minna JD, Roth JA, and Ji L. Myristoylation of Fus1 protein is required for Fus1-mediated tumor suppressing activities in human lung cancer. American Association for Cancer Research (AACR), 94th Annual Meeting, Washington, District of Columbia, July 11-14, 2003. *Proceedings of the American Association for Cancer Research* 44:75, 2003.

2. Gopalan B, Ji L, Ito I, Saito Y, Branch CD, Xu Kai, Stephens C, Minna JD, Roth JA, and Ramesh R. The anti-inflammatory drug naproxen protects mice from lipoplex-mediated toxicity. American Association for Cancer Research (AACR), 94th Annual Meeting, Washington, District of Columbia, July 11-14, 2003. *Proceedings of the American Association for Cancer Research* 44:923, 2003.

3. Jiichiro Sasaki, Futoshi Uno, John D. Minna, Jack A. Roth, Lin Ji. Enhanced Sensitivity of Tumor Cells to Chemotherapeutic Agents by Activation of FUS1 Tumor Suppressor Gene in Lung Cancer Cells. *Proceedings of The 95th American Association for Cancer Research (AACR) Annual Meeting*, Orlando, FL, March 27-31, 2004.

4. Futoshi Uno, Jiichiro Sasaki, Gitanjali Jayachandran, Kai Xu, John D. Minna, Jack A. Roth, Lin Ji. Activation of Apoptotic Signaling Pathway by Direct Interaction between Tumor Suppressor Fus1 and Apaf-1 proteins in Lung Cancer Cells Back to Search. *Proceedings of The 95th American Association for Cancer Research (AACR) Annual Meeting*, Orlando, FL, March 27-31, 2004.

Patents:

1. Ji L, Roth JA, Detection of Expression and Posttranslational Modification of Fus1 Protein on ProteinChip Array by SELDI-TOF-MS. MDA04-107, 2004

2. Ji L, Fang B, Roth JA, Novel hTMC promoter and vectors for the Tumor-selective and high-efficient Expression of Cancer Therapeutic Genes, MDA04-109, 2004

3. Kundra V, Fang B, Ji L, Yang D, In Vivo Imaging of Gene Expression Targeting the Telomerase Promoter. MDA04-091, 2004

4. Ji L, Roth JA. Protamine-adenoviral vector complex-mediated gene therapy for cancers. PCT/US03/09152; U.S. Patent, US03-09152, U.S. Serial No. 60-366846. MDA01-025. 2001.

5. Ji L, Roth JA, Minna JD. and Lerman MI. Chromosome 3p21.3 genes as tumor suppressors. U.S. Patent, US-2004-0016006-A1; World Patent: WO 02/04511 A2

Project 8: Therapeutic Targeting of bcl-xl Expression in Non-Small Cell Lung Carcinoma

Principal Investigator: W. Roy Smythe, M.D.

Dr. Roy Smythe left M. D. Anderson in February 2004 to assume the prestigious position of Chairman, Department of Surgery, at Scott & White in Temple, TX. Scott & White is the clinical education site for The Texas A&M University System Health Science Center College of Medicine. Dr. Smythe's cutting-edge research at M. D. Anderson Cancer Center, to include his Department of Defense research, uniquely positioned him to be a top competitor for such a distinguished position.

The bcl-xl gene is a member of the bcl-2 family of genes that controls mitochondrial membrane potential and interacts with other members of this family to control apoptosis, or programmed cell death. When over-expressed, the bcl-xl protein leads to inhibition of apoptosis as well as decreases sensitivity to conventional treatments (i.e. chemotherapy and irradiation). Deceasing expression of this gene product by various means may conversely induce apoptosis in cancer cells and render them sensitive to more conventional available therapies. The following specific aims were proposed for this grant. Following each specific aim is a description of the work completed in this area.

Specific Aim 1 **Characterize the in vitro effects of bcl-xl ASO exposure on human NSCLC cells and evaluate such exposure as a prime for other pro-apoptotic therapies**

We have evaluated a panel of bcl-xl antisense oligonucleotides (ASO) on the human non-small cell carcinoma cell lines A549 and H1299. We have identified one particular construct (ISIS 15999) that can decrease cell viability in a lipid delivery system by 60%-90%. We have also demonstrated the ability of this in vitro treatment to increase the apoptotic (subg1 by FACS analysis) fraction of cells by more than 30%. This has also effectively sensitized these cell lines to cisplatin, with significant increases in both cell death and apoptosis over either monotherapy approach.

Due to a concern regarding the in vivo applicability of this approach, we have been evaluating an RNA silencing approach for down regulation of bcl-xl expression as well. Following sequence rules, we have designed and evaluated 5 separate siRNA double stranded constructs and have tested them on non-small cell lines in vitro. Two of these constructs were able to effectively decrease bcl-xl expression at both protein (Western blot) and mRNA (real-time PCR) levels. The most promising construct was utilized to develop a hairpin loop plasmid delivery system. Both the siRNA double stranded and plasmid constructs are able to induce apoptotic cell death in vitro. Notably, the bcl-xl siRNA plasmid construct delivered with a lipid delivery system can sensitize NSCLC cells to cisplatin and decrease the amount of cisplatin required to kill 50% of these cells (IC50) by a full log.

Specific Aim 2 **Develop an adenoviral vector capable of transferring an antisense bcl-xl gene construct**

A full length, rather than short segment, bcl-xl antisense adenoviral gene therapy vector (xl22) was developed (second generation replication deficient human type 5 construct). This has been characterized by sequencing as the intended sequence.

Specific Aim 3 **Characterize the in vitro effects of bcl-xl antisense adenoviral vector exposure on human NSCLC cells and evaluate such exposure as a prime for other pro-apoptotic therapies**

The xl22 vector was evaluated in vitro in NSCLC cells. This vector has been demonstrated to down regulate bcl-xl protein expression (Western Blot) and induce apoptotic cell death.

Specific Aim 4 **Characterize the therapeutic effects of bcl-xl antisense targeting with both ASO and adenoviral vectors in animal models of non-small cell lung carcinoma and evaluate such exposure as a prime for other pro-apoptotic therapies in vivo**

We have demonstrated the ability of ASO to decrease intraperitoneal tumor burden in a xenograft model of mesothelioma (identical bcl-2 family expression pattern) by 30%-40%. Likewise, we have demonstrated that the xl22 construct can decrease tumor burden by more than 60%. We have recently demonstrated the ability to transfer the backbone siRNA plasmid system with a reporter gene (E. Coli beta galactosidase) utilizing a dotap:cholesterol delivery method into in vivo intraperitoneal xenograft tumor.

Project 9: Improved Pulmonary Gene Delivery with Partial Liquid Ventilation for Treatment of Pulmonary Malignancies

Principal Investigator: Ara Vaporciyan, M.D.

Specific Aim 1 **To determine PFC's ability to diminish the immune response, both innate and the later cellular and humoral responses, to intratracheal administration of adenoviral vector.**

Task A: ***Evaluation of the innate immune and later cell mediated response at the cellular level***

During the initial period of this year we had continued to collect serum samples for the completion of this task as well as task B. Progressing concurrently with this work were the experiments outlined in Specific Aim 2. Based on the findings of Specific Aim 2 (see below), we elected to discontinue our efforts to define the immune response.

The hypothesis that PFC would allow repeated transfection was based on a significant body of literature, outlined in the background and significance of our grant, supporting the immune modulating properties of PFC. Specific Aim 1 was designed to elucidate the mechanism responsible for improved repeat gene transfer. The inability of PFC to allow repeated gene transfer (Specific Aim 2) forced us to reassess the importance of a detailed mechanistic analysis. The goal of the grant was to develop translational approaches for the treatment of lung cancer. A mechanistic study of PFC's immune effects did not appear to be appropriate in light of its inability to improve repeat transfection.

The budget allocated to the purchase of reagents necessary for the cytokine assays in tasks A and B will be returned to the PI of the TARGET grant for reallocation to other projects.

Task B: ***Evaluation of the innate immune and later cell mediated response at the molecular level***

See above.

Specific Aim 2: **To determine PFC's ability to enhance repeated gene transfer through reduction and mechanical disruption of the humoral response.**

Initial experiments examined the ability of PFC to enhance repeat gene delivery using adenoviral vectors 14 days after an initial viral transfection. On day 0, animals were transfected with 5×10^8 vp of adenovirus containing the β-galactosidase gene (B-gal). The control animals received the vector in 100μl of PBS while the PFC group received the same 100 μl followed by 3 ml PFC (10 ml/kg PFC). Both vector and PFC were delivered intratracheally. After 14 days the animals were anesthetized and the control animals received a similar dose of vector only, while the PFC group once again received vector and PFC. After 2 days the animals were sacrificed and β-gal expression determined. Unfortunately, the animals treated with PFC had a significantly diminished transfection compared to control animals.

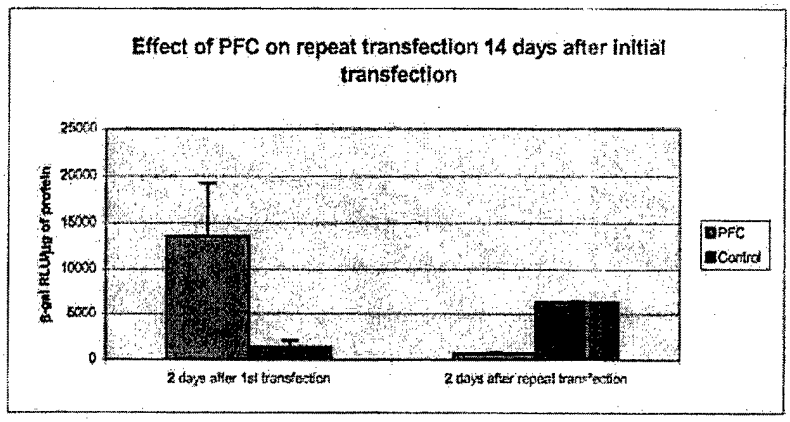

Figure 1

Surprisingly, the animals treated with vector alone had improved expression with repeat delivery compared to a single administration of vector (Figure 1).

One hypothesis for the poor transfection was interference due to residual PFC in the lung. Our earlier work in Specific Aim 1 had obtained expression data 14 days after transfection with and without PFC. Animals in the PFC group still had residual PFC within the lungs. This was discovered during homogenization of the lung since the PFC would appear as an immixable layer on top of the homogenized lung. The residual volume of PFC was small (< 500 µl or 15% of the initial volume) but it was hypothesized that this small amount could act as a barrier preventing the delivery of the vector to the alveolar compartment. Therefore, we repeated the experiments with a longer duration between repeat administrations.

These new experiments used the same conditions on day 0, however, the second administration of adenoviral was given on day 21 and the animals were harvested on day 23. Pilot experiments demonstrated < 250 µl of residual PFC (< 7.5% of the initial volume) by 21 days. Unfortunately, there was still no real transfection in the group treated with PFC compared to controls (Figure 2).

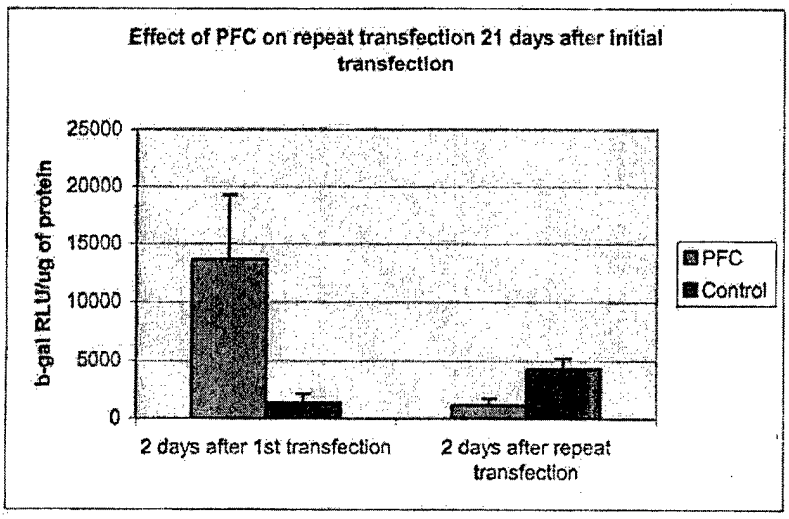

Figure 2

This was either caused by interference of adenoviral transfection by the small amount of residual PFC or due to an enhanced immune response generated by the high expression after the first transfection. To address the latte,r we began experiments using a less immunogenic vector. In collaboration with Dr. Ramesh (Project 7) we had preliminary *in vitro* data demonstrating improved gene transfer into A549 lung cancer cell lines using liposomes (DOTAP:cholesterol lipid formulation mixed with β-gal plasmid DNA) in the presence of PFC. This enhanced gene transfer coupled with the decreased immunogenic properties of liposomes prompted us to attempt *in vivo* pulmonary gene delivery using liposomes with PFC.

Our initial attempts with liposomes administered intratracheally, with or without PFC, resulted in 100% mortality within 10 minutes secondary to respiratory distress. Further work with various ratios of DOTAP and cholesterol revealed that the lethal agent was the cholesterol. A new lipid formulation consisting only of DOTAP and β-gal plasmid DNA was created and was able to be administered safely. However, at 1 and 2 days post administration there was no β-gal expression regardless of the presence or absence of PFC. We have discontinued work with liposomal vectors *in vivo*.

Specific Aim 3: **To determine PFC's ability to allow continued penetration of the pulmonary parenchyma in the setting of an animal model of severe emphysema.**

These experiments are scheduled for the second and third year of this project.

Specific Aim 4: **To determine the ability of PFC mediated gene transfer to effectively transduce a model of multifocal lung cancer.**

We have begun administering tumor cells to animals and generating a time course of tumor nodule growth within the lung. Our initial studies have identified microscopic tumor nodules at 14 days after intravenous injection of 10^6 rat fibrosarcoma cells. Examples of the tumor nodule are shown in figure 3. Based on their small size we have gone to 21 days after tumor injection

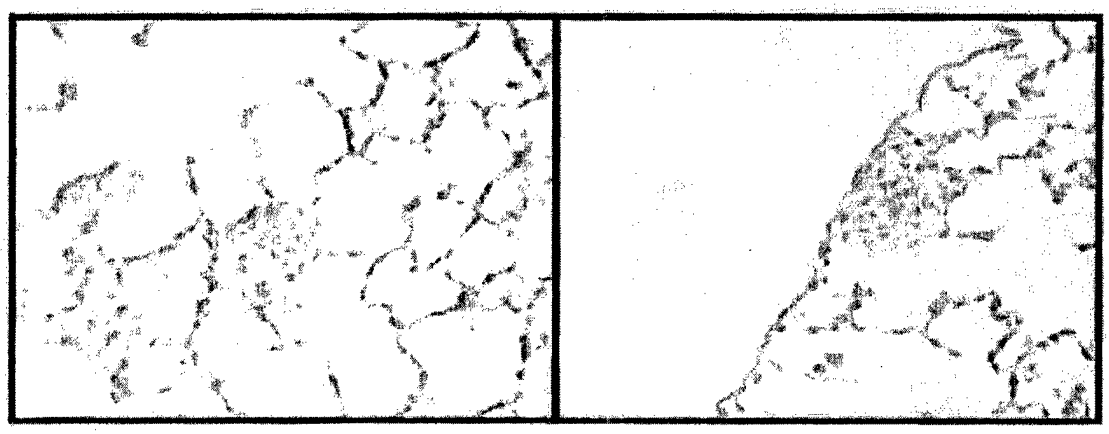

Figure 3

as the time point for attempted transfection. We have just initiated studies with adenoviral vector containing β-gal administered intratracheally with or without PFC in animals with pulmonary metastasis.

The key accomplishments are:

- Intratracheal administration of adenovirus allows transfection of the lung parenchyma only and is significantly increased when delivered in the presence of perfluorocarbon. Unfortunately, pulmonary transfection after repeated administration of adenovirus with perfluorocarbon intratracheally is not successful.
- We have explored DNA:Liposomal complexes with perfluorocarbon as well. Although *in vitro* studies were promising, any complex containing cholesterol given intrathecally was lethal and complexes without cholesterol were unable to transfect lung tissue when administrered intrathecally.
- An animal model of pulmonary metastasis in a immunocompetent rat has been developed and experiments testing the ability of perfluorocarbons to enhance tumor transfection is being investigated.

Project 10: Development of Novel Murine Models of Lung Cancer and Evaluation of Antiangiogenic Agents

Co-Principal Investigator: Michael O'Reilly, M.D.
Co-Principal Investigator: Roy Herbst, M.D., Ph.D.

The primary goal of our ongoing studies is to provide a rational basis for use of antiangiogenic agents with conventional and emerging modalities in the treatment of lung cancer. We have now developed and validated murine models of orthotopic and metastatic human lung cancer for testing the efficacy of antiangiogenic agents alone and in combination with cytotoxic chemotherapy. Experimental animal models of primary human non-small cell (H441 and PC14 adenocarcinoma and H226 squamous cell carcinoma) and small cell lung (NCI-H69, NCI-H187, and NCI-N417) cancer in mice are now in place to study the biology and therapy of human lung cancer. In these models, tumor cells injected (Figure 1) into the lung parenchyma of nude mice produce lung lesions and different tumors produced different patterns of spread. We recently published a paper (Onn et al, Clinical Cancer Research 9:5532-5539, 2003) describing our orthotopic model of non-small cell lung cancer and are preparing a manuscript describing the small cell lung cancer models.

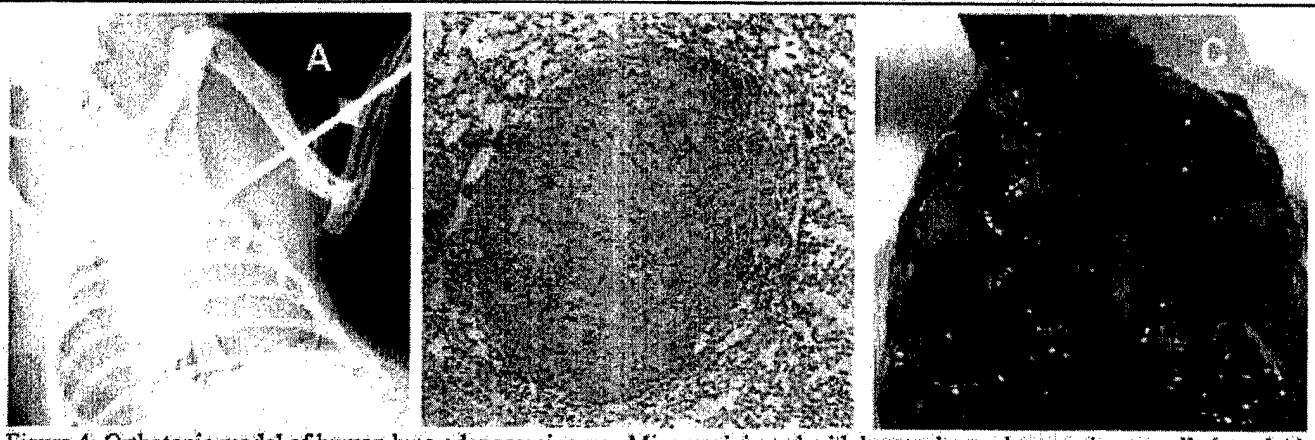

Figure 4: Orthotopic model of human lung adenocarcinoma. Mice are injected with human lung adenocarcinoma cells (panel A) and a solitary lesion (panel B) develops that subsequently spreads (panel C) throughout the thorax.

Our primary lung cancer models recapitulate the local and regional growth patterns seen in lung cancer patients, i.e. from a solitary nodule to a diffuse thoracic disease involving both lungs and the lymph nodes. However, lung cancer patients frequently succumb to metastatic disease. To address this we are now developing murine models of metastatic cancer to the brain and bone by injecting human non-small cell or small cell lung cancer into the brain (through the calvarium or by intracarotid injection) or bone (via intratibial injection). For human lung adenocarcinoma (PC14 and H441) we have now established cell lines that preferentially grow in the brain or bone and closely mimic metastatic patterns observed clinically in lung

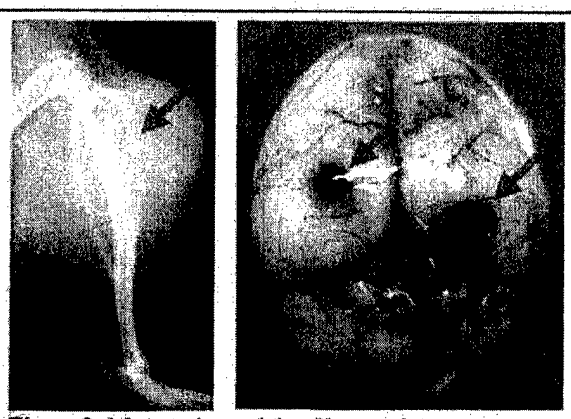

Figure 2: Metastatic models of human lung adenocarcinoma. Bone (left panel, arrow indicates a lytic lesion) or brain metastases (right panel, arrows indicate bilateral lesions) after intratibial (bone) or intracarotid (brain) injection of tumor cells.

cancer patients with metastatic disease to these sites (Figure 2).
Using our primary and metastatic lung cancer models we have completed studies of antiangiogenic therapy alone and in combination with chemotherapeutic agents. ZD6474 is an oral angiogenesis inhibitor that targets VEGFR2 and EGFR. For two different human lung adenocarcinomas (PC14and H441), oral therapy with ZD6474 resulted in the near complete suppression of malignant growth of established lung tumors (Figure 3) and prevented pleural effusion formation and inhibited chest wall invasion. In contrast, systemic weekly therapy with Taxol had little or no effect on lung cancer progression. These studies have provided preliminary data for a project on a PO1 grant application that we recently submitted and are currently in the process of revising for resubmission.

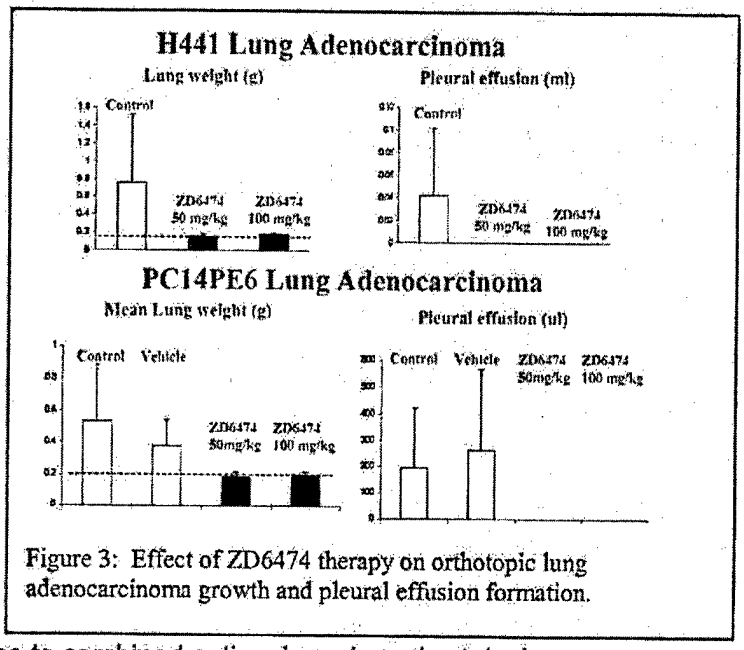

Figure 3: Effect of ZD6474 therapy on orthotopic lung adenocarcinoma growth and pleural effusion formation.

ZD6474 was also effective against lung adenocarcinoma in our brain and bone metastatic models. In our orthotopic lung and brain metastatic models (lung adenocarcinoma), the activity of ZD6474 was enhanced by combined therapy with Taxotere or Taxol. In contrast, in the bone metastatic model the activity of ZD6474 was antagonized by Taxol. These data suggest that organ microenvironment influences response to combined antiangiogenic and cytotoxic therapies. Our studies will allow for the rational design of clinical trials with antiangiogenic therapy when combined with chemotherapy. We have now initiated studies of different sequencing of antiangiogenic agents with chemotherapy for treatment of lung cancer to determine how to optimize combined modality therapy with these agents.

To assess the effects of ZD6474 antiangiogenic therapy of human lung cancer upon the tumor vasculature, we analyzed tumor tissue using immunofluorescence double staining for CD31/PECAM-1 (endothelial cells) and CD31/TUNEL (apoptotic cells). Endothelial cell apoptosis (Figure 4) preceded tumor cell apoptosis suggesting that effects on the vasculature may be a useful surrogate for conventional tumor response. In current and ongoing studies we are studying several different parameters using molecular analyses of tumor tissue for primary and metastatic lung cancer treated with antiangiogenic therapy alone and in combination with chemotherapy. These studies have direct clinical relevance given that surrogates for response to therapy with antiangiogenic and other biologically targeted therapies are needed in the clinic.

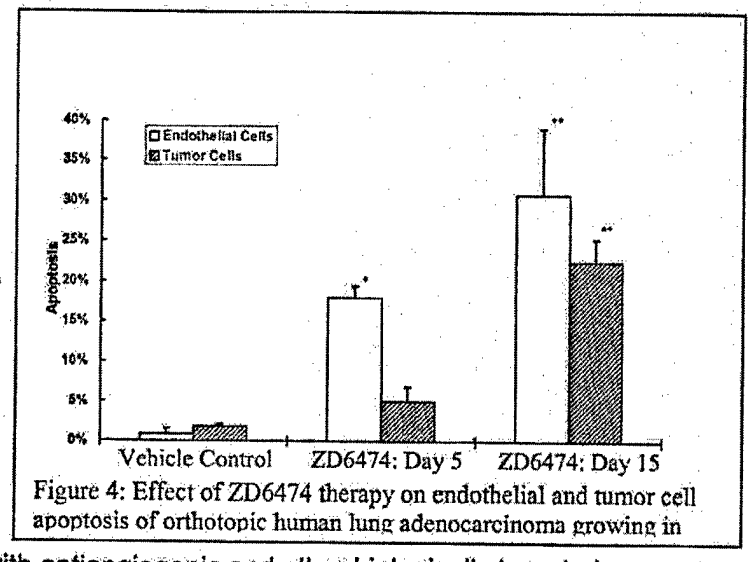

Figure 4: Effect of ZD6474 therapy on endothelial and tumor cell apoptosis of orthotopic human lung adenocarcinoma growing in

In summary, we have made substantial progress with Project 10 as follows.

1. Development and validation of primary and metastatic murine models of human lung cancer that closely mimic patterns of disease that are observed clinically.
2. Demonstration of efficacy of antiangiogenic therapies, as compared to conventional therapies, in primary and metastatic lung cancer models.
3. Combined modality treatment of primary and metastatic lung cancer with antiangiogenic therapy and cytotoxic chemotherapy.
4. Molecular and functional analyses of tumor tissue and tumor vasculature in lung cancer treated with antiangiogenic therapy and the development of potential surrogates for response to therapy.

Core B: Biostatistics & Data Management

Core Director: J. Jack Lee, Ph.D.
Core Co-Director: B. Nebiyou Bekele, Ph.D.

Core Goals:

- To provide the statistical design, sample size and power calculations for each project.
- To facilitate prospective data collection and quality control of data for the clinical trials, animal experiments, and basic science studies associated with the TARGET program.
- To provide all statistical data analysis including descriptive statistical analysis, hypothesis testing, estimation, modeling of prospectively generated data.
- To generate statistical reports for all projects.
- To collaborate and assist all project investigators in the publication of scientific results.

From the inception of the TARGET program, the Biostatistics and Data Management Core has worked actively with all the Projects in their research efforts, especially in the area of bio-statistical advice and consulting; in the initial design of studies; analysis of experimental results and development of a decision analytic model to assess the effect of prophylactic cranial irradiation for patients with small cell lung cancer.

In collaboration with Dr. Ruth Katz, we have analyzed various data sets relating to the relationship between deletions of the 3p and 10q genes and overall survival for patients with NSCLC. We have submitted 1 paper for publication with 3 papers in progress.

In collaboration with Dr. Charles Lu, we have analyzed factors potentially prognostic for overall survival in resected Stage I NSCLC patients. This paper has been submitted to JCO.

In collaboration with Lin Ji, we have analyzed the relationship between the expression of FUS1 protein in tumor tissue compared to normal tissue. We used the marginal homogeneity test to test for differences between the paired samples (Normal Vs. Tumor). The marginal homogeneity test, a generalization of McNemar's test, assesses the equality of categorical responses from two populations, where the data consist of paired, dependent categorical responses, one from each population. This research has been published in Cancer Research and Dr Bekele was acknowledged.

In Collaboration with Dr. Scott Cantor (a decision scientist) and Dr. Jin-Soo Lee (Director of the National Cancer Center of Korea) we have developed a decision analytic model to examine the effects of PCI on quality adjusted life years (QALYs). Utility assessments of the effects of PCI (and associated neurotoxicity) were elicited from Dr. Jin-Soo Lee (an expert in this field). Survival times for both the PCI group and the Non-PCI group were modeled using a log normal distribution which mimicked survival times reported in the literature. Quality adjusted survival time and expected QALYs are estimated for current survival rates and assuming the cure rate will increase in the future due to improved therapy and management of this disease. This research is in progress.

Publications

1. Uno F, Sasaki J, Nishizaki M, Carboni G, Xu K, Atkinson EN, Kondo M, Minna JD, Roth JA, Ji L "Myristoylation of the Fus1 Protein is Required for Tumor Suppression in Human Lung Cancer Cells" (Dr Bekele Acknowledged)

2. Barkan GA, Caraway NP, Jiang F, Zaidi TM, Fernandez R, Vaporcyin A, Morice R, Zhou X, Bekele BN, Katz RL. "Comparison of Molecular Abnormalities in Bronchial Brushings and Tumor Touch Preparations: The Potential Use of Fluorescence In Situ Hybridization (FISH) to Identify Predictive Markers in Early-Stage Lung Carcinomas" (Submitted)

3. Lu C, Soria JC, Tang X, Xu XC, Wang L, Mao L, Lotan R, Kemp B, Bekele BN, Feng L, Hong WK, Kurie FR. "Prognostic Factors in Resected Stage I Non-Small Cell Lung Cancer (NSCLC): A Multivariate Analysis of Six Molecular Markers" (Submitted)

KEY RESEARCH ACCOMPLISHMENTS

We have tested all functional assays on commercially available cells, and have started applying the assays to the tissue cultures set up by Dr. Koo. We have also begun to evaluate correlations between data from lymphocytes, bronchial brushes and touch preparations. We have adapted the fluorescence inter-simple sequence PCR technology to the analysis of normal epithelium in the field of lung tumors and have demonstrated the presence of subclonal outgrowths in this apparently normal epithelium. With multiplexing of FISSR-PCR, these results suggest that this technology may be useful for quantifying the level of subclonal outgrowths in normal lung tissue at cancer risk and will permit comparisons between the bronchial epithelium of current and former smokers.

Proteins secreted from abnormal squamous metaplastic bronchial epithelial cells, but not from normal mucous epithelial cells were identified using 2-dimensional PAGE and MALDI-TOF or HPLC/MS/MS spectrometry; They are squamous cell carcinoma antigens (SCCA), annexin I and II, S100A9, and S100A8.

All of the identified proteins present as multiple forms with different molecular weight and isoelectric point, suggesting that they were posttranslational modified or alternatively spliced products.

We found that genes in the WNT pathway, apoptosis, and cell cycle are concurrently deregulated in non-small cell lung cancer cells as compared to normal bronchial epithelial cells. Significant progress has been made identifying eligible subjects, procuring tumor tissue blocks, and performing biomarker assays. We expect to complete these aspects of the project, in addition to data analysis and manuscript preparation, within the 3-year funding period. Significant progress has been made identifying eligible subjects, procuring tumor tissue blocks, and performing biomarker assays. We expect to complete these aspects of the project, in addition to data analysis and manuscript preparation, within the 3-year funding period.

- Establishing that premalignant epithelial cells of oral cavity and lung are sensitive to SAHA
- Discovery that SAHA inhibits the growth of cancer cells by G2 arrest and apoptosis induction Elucidation of the mechanism by which SAHA induces apoptosis as the increased expression of Fas (death receptor) and activation of the Fas ligand/Fas mediated apoptosis pathway
- Novel ras-dependent and independent effects of farnesyl transferase inhibitors uncovered
- Proteomic analysis of FTI treated cell lines detects several important classes of proteins that Are upregulated or downregulated by this class of compounds
- Lonafarnib inhibits HDAC6 through a novel mechanism in several lung cancer cell lines. This may serve as an important target for development of trials targeting synergy between novel signal transduction inhibitors and tubulin targeting cytotoxics
- Studied molecular mechanisms of a novel tumor suppressor gene (TSG) FUS1, identified an apoptotic protease activating factor 1 (Apaf1) as the cellular target that directly interacts with Fus1 protein, and found that Fus1 protein functioned as a key mediator in Apaf1-mediated mitochondrial apoptosis pathway by recruiting and directing cytoplasmic Apaf1 protein to a critical cellular location and activating it in situ, and by upregulating activity of other pro-apoptotic effectors such as p53 and downregulating anti-apoptotic mediators such as Bcl2 family proteins for the efficient induction of apoptosis
- Studied the effects of Fus1 in combination with other tumor suppressor genes such as p53 and chemotherapeutic agents such as cisplatin, taxel, protein tyrosine kinase inhibitors on tumor cell proliferation and apoptosis *in vitro* and *in vivo*. Our results suggest that co-expression of FUS1 and p53 could synergistically inhibit lung cancer cell growth and the wt-

Fus1 may play a critical role in modulating the sensitivity of tumor cells to the chemotherapeutic agents, especially, to DNA damaging agent Cisplatin and protein tyrosin kinase inhibitor Gefitinib

- Demonstrated the selective and increased uptake of liposome-DNA complexes by tumor cells in the lung compared to surrounding normal tissues. A phenomenon shown for the first time. These findings were highlighted in the editorial section of the journal "Molecular Therapy". These findings allow us to utilize the inherent properties of the DOTAP:Chol-DNA liposome complexes
- Demonstrated that host-inflammatory response in tumor-bearing animals is reduced compared to normal animals, which is partly mediated by the production of IL-10 by tumor cells. Hence differences exist in the liposome-DNa complex induced toxicity. This forms a basis to conduct toxicity studies in tumor-bearing animals that is relevant to patients in the clinic
- Developed novel strategies to suppress liposome-DNA complex induced inflammatory response. This strategy is being planned for incorporation in the phase-I/II clinical trial.
- Demonstrated the therapeutic effect of FUS1 in xenograft tumor models.
- Toxicology studies are completed. Results are being compiled for submission to FDA.
- Intratracheal administration of adenovirus allows transfection of the lung parenchyma only and is significantly increased when delivered in the presence of perfluorocarbon. Unfortunately, pulmonary transfection after repeated administration of adenovirus with perfluorocarbon intratracheally is not successful.
- We have explored DNA:Liposomal complexes with perfluorocarbon as well. Although *in vitro* studies were promising, any complex containing cholesterol given intrathecally was lethal and complexes without cholesterol were unable to transfect lung tissue when administrered intrathecally.
- An animal model of pulmonary metastasis in a immunocompetent rat has been developed and experiments testing the ability of perfluorocarbons to enhance tumor transfection is being investigated.
- Development and validation of primary and metastatic murine models of human lung cancer that closely mimic patterns of disease that are observed clinically.
- Demonstration of efficacy of antiangiogenic therapies, as compared to conventional therapies, in primary and metastatic lung cancer models.
- Combined modality treatment of primary and metastatic lung cancer with antiangiogenic therapy and cytotoxic chemotherapy.
- Molecular and functional analyses of tumor tissue and tumor vasculature in lung cancer treated with antiangiogenic therapy and the development of potential surrogates for response to therapy.

REPORTABLE OUTCOMES

Abstracts:

1. Lu, T., and Hittelman, W. N. Quantitative fluorescence inter-simple sequence repeat CR (FISSR-PCR) for subclonal analysis of bronchial cell populations. Proc. AACR, 2004.
2. Hassan KA, Lee H-Y, Kim E, Bishop WR, Kirschmeier P, Mao L, Khuri FR. A novel mechanism of farnesyltransferase inhibitor (SCH66336) arresting head and neck squamous cell carcinoma cells. *Proceedings of the American Association for Cancer Research*, 44, abstract #800, pp. 156, 2003.
3. Uno F. Sasaki J, Nishizaki M, Carboni G, Xu K, Minna JD, Roth JA, and Ji L. Myristoylation of Fus1 protein is required for Fus1-mediated tumor suppressing activities in human lung cancer. American Association for Cancer Research (AACR), 94th Annual

Meeting, Washington, District of Columbia, July 11-14, 2003. Proc. Am. Assoc. Cancer Res., 44:75, 2003.
4. Gopalan B, Ji L, Ito I, Saito Y, Branch CD, Xu Kai, Stephens C, Minna JD, Roth JA, and Ramesh R. The anti-inflammatory drug naproxen protects mice from lipoplex-mediated toxicity. American Association for Cancer Research (AACR), 94th Annual Meeting, Washington, District of Columbia, July 11-14, 2003. Proc. Am. Assoc Cancer Res., 44:923, 2003.
5. Jiichiro Sasaki, Futoshi Uno, John D. Minna, Jack A. Roth, Lin Ji. Enhanced Sensitivity of Tumor Cells to Chemotherapeutic Agents by Activation of FUS1 Tumor Suppressor Gene in Lung Cancer Cells. Proceedings of The 95th American Association for Cancer Research (AACR) Annual Meeting, Orlando, FL, March 27-31, 2004.
6. Futoshi Uno, Jiichiro Sasaki, Gitanjali Jayachandran, Kai Xu, John D. Minna, Jack A. Roth, Lin Ji. Activation of Apoptotic Signaling Pathway by Direct Interaction between Tumor Suppressor Fus1 and Apaf-1 proteins in Lung Cancer Cells Back to Search. Proceedings of The 95th American Association for Cancer Research (AACR) Annual Meeting, Orlando, FL, March 27-31, 2004.

Articles:

1. Hittelman, W. N., Kurie, J. M., and Swisher, S. Molecular Events in Lung Cancer and Implications for Prevention and Therapy. In: Anderson Associates Monograph on Lung Cancer. F. Fosella, R. Komaki, and J. Putnam, Jr., (eds.) pp 280-298, 2003.
2. Lu, T. and Hittelman, W. N. Improvement and application of fluorescence inter-simple sequence repeat polymorphism chain reaction for the study of subclonal growths in lung epithelial cell populations. Chest 125 (Suppl. 5):110-111S, 2004.
3. Khuri FR, Glisson BS, Kim ES, Meyers ML, Herbst RS, Thall PF, Munden RF, Statkevich YP, Bangert S, Thompson E, Cascino M, Shin DM, Papadimitrakopoulou V, Kurie JM, Kies MS, Lee JS, Fossella FV, Hong WK. Phase I study of farnesyl transferase inhibitor (FTI) SCH66336 with paclitaxel in solid tumors. *Clinical Cancer Research,* May 2004.
4. Kim ES, Kies MS, Fossella FV, Glisson BS, Zaknoen S, Baum CM, Summey C, Lu C, Papadimitrakopoulou V, Hong WK, Khuri FR. Phase II study of the farneslytransferase inhibitor (FTI) lonafarnib with paclitaxel in patients with taxane-refractory/resistant non-small cell lung cancer. In press, *Cancer,* 2004 .
5. Sun S-Y, Zhou Z, Wang R, Khuri FR. Akt is not a target for the growth inhibition and apoptosis induction by the farnesyltransferase inhibitor SCH66336 in human lung cancer cells. In press, *Cancer Biology and Therapy,* 2004.
6. Uno F, Sasaki J, Nishizaki M, Carboni G, Xu K, Atkinson EN, Kondo M, Minna, JD. Roth JA, and Ji L. Myristoylation of the FUS1 protein required for tumorsuppression in human lung cancer cells. Cancer Res. 64, 2969-2976, 2004.
7. Nishizaki M, Sasaki J, Fang B, Atkinson EN, Minna, JD, Roth J, and Ji L. Synergistic tumor suppression by coexpression of FHIT-mediated MDM2 inactivation and p53 stabilization in human NSCLC cells. Cancer Research 64 (16), 5632-5640, 2004.
8. Ito I, Began G, Mohiuddin I, Saeki T, Saito Y, Branch CD, Stephens LC, Yen N, Roth JA, Ramesh R. Increased uptake of liposomal-DNA complex by lung metastases following intravenous administration. Mol. Ther. 7(3): 409-418, 2003.
9. Ito I., Saeki T, Mohiuddin I, Saito Y, Varporciyan A, Branch C, Roth JA, and Ramesh R. Persistent transgene expression following intravenous administration of a liposomal complex: role of IL-10 mediated immune suppression. Mol. Ther. 9 (3): 318-327, 2004.
10. Ito I, Ji L, Gopalan B, Tanaka F, Saito Y, Branch CD, Xu K, Atkinson NE, L. Clifton Stephens, Minna JD, Roth JA, and Ramesh R. DOTAP:cholesterol liposome mediated

delivery of the 3p gene FUS1 inhibits growth of human lung cancer in vivo. Cancer Gene Ther. 2004, (in press).
11. Onn A, Isobe T, Itasaka A, Wu W, O'Reilly M, Hong WK, Fidler IJ, Herbst RS. Development of an Orthotopic Model to Study the Biology and Therapy of Primary Human Lung Cancer in Nude Mice. Clin Can Res 9:5532-5539, 2003.

Patents:

1. Ji L, Roth JA, Detection of Expression and Posttranslational Modification of Fus1 Protein on ProteinChip Array by SELDI-TOF-MS. MDA04-107, 2004
2. Ji L, Fang B, Roth JA, Novel hTMC promoter and vectors for the Tumor-selective and high-efficient Expression of Cancer Therapeutic Genes, MDA04-109, 2004
3. Kundra V, Fang B, Ji L, Yang D, In Vivo Imaging of Gene Expression Targeting the Telomerase Promoter. MDA04-091, 2004
4. Ji L, Roth JA. Protamine-adenoviral vector complex-mediated gene therapy for cancers. PCT/US03/09152; U.S. Patent, US03-09152, U.S. Serial No. 60-366846. MDA01-025. 2001
5. Ji L, Roth JA, Minna JD. and Lerman MI. Chromosome 3p21.3 genes as tumor suppressors. U.S. Patent, US-2004-0016006-A1; World Patent: WO 02/04511 A2

CONCLUSIONS

Project 1: Preliminary analyses indicate that lymphocyte markers predict genetic events in bronchials brushings and tumor tissue.

Project 2: We have adapted the fluorescence inter-simple sequence PCR technology to the analysis of normal epithelium in the field of lung tumors and have demonstrated the presence of subclonal outgrowths in this apparently normal epithelium. With multiplexing of FISSR-PCR, these results suggest that this technology may be useful for quantifying the level of subclonal outgrowths in normal lung tissue at cancer risk and will permit comparisons between the bronchial epithelium of current and former smokers.

Project 3: Panel of proteins composed of SCCA, annexin I and II, S100A9, and S100A8 may be useful molecular markers for detection of early metaplastic changes of bronchial epithelium.

Project 4: No conclusions can be drawn at the present time.

Project 5: Our studies indicate that epigenetic mechanisms are mediating the growth and survival of head and neck and lung premalignant and malignant cells and that reversal of epigenetic changes by various agents in particular HDAC inhibitor and dememthylating agents can result in growth inhibition and apoptosis.

Project 6: Lonafarnib is active in inducing growth arrest and apoptosis in human NSCLC and HNSCC cells, through mechanisms independent of Ras mutation and Akt activation in NSCLC. This suggests a completely novel, Akt-independent mechanism of action for these compounds in lung cancer, unlike our previous data generated with head and neck cell lines.

Project 7: Our results point to an essential role of Fus1 in apoptotic pathway by directing the critical assembling of apoptosome for cells in response to carcinogenic stimulus such as DNA-damaging chemicals and gamma radiation. Our results also imply that a combination treatment with the FUS1-lipoplex-mediated molecular therapy and the cisplatin or taxane-based chemotherapy may be an efficient treatment strategy for lung cancer. Our results have also

established the feasibility of using DOTAP:Chol-based liposomal gene delivery for systemic therapy of lung cancer. Furthermore, FUS1 has been shown to be an effective tumor suppressor. Toxicology studies have established the maximum tolerated dose and are being submitted for initiation of clinical trial. This will be the first systemic gene therapy-based therapy for lung cancer.

Project 9: Transfection of lung parenchyma by intratracheal administration of adenovirus is enhanced using perfluorocarbon. Repeated intratracheal administration of adenovirus with perfluorocarbon does not result in repeated transfection. Conclusions regarding transfection of pulmonary metastasis are pending.

Project 10: Targeted vascular therapy against lung tumor endothelial cells represents a viable target for therapeutic intervention. Based on our data, clinical trials using these agents will soon be initiated.

APPENDIX

Back

Abstract Number: 2925

Quantitative fluorescence inter-simple sequence repeat PCR (FISSR-PCR) for subclonal analysis of bronchial cell populations

Tao Lu and Walter N. Hittelman. ***The Univ. of Texas MD Anderson Cancer Center, Houston, TX.***

Tumorigenesis is a process of cumulative clonal and subclonal cell expansion in a field of epithelial cells driven by genetic instability. Quantitative assessment of the frequency and complexity of clonality in pre-malignant tissues may therefore provide cancer risk information. Inter-Simple Sequence Repeat PCR (ISSR-PCR) is a DNA fingerprinting technology that has proven useful for quantifying clonal changes in human tumors. FISSR-PCR involves the same technology as ISSR-PCR except that fluorescence-dye labeled oligonucleotide primers are utilized and the PCR products are analyzed using the ABI 377 DNA Sequencer. We previously demonstrated that FISSR-PCR could distinguish clonal outgrowths of bronchial epithelial clones derived from single cells. The purpose of this study was to determine the sensitivity of FISSR-PCR to detect subclonal variation in populations of bronchial epithelial cells. To this end, DNA of single cell clones with gains and losses at known loci, previously isolated from lung epithelial Beas 2B and 1170I cell lines, were mixed together in different proportions at 10% increments to mimic cell populations with different degrees of subclonal variation. Following gel separation and fluorescence quantitation of size (i.e., migration) and relative amount (peak size) of the resultant PCR fragments, the DNA band profiles were aligned on the basis of the largest cluster of common bands. The scans derived from the various cell mixtures were then compared on the basis of normalized peak heights. For common peaks between variant cell populations, the standard deviation was found to be less than 10% of the absolute mean value (data from triplicates of 11 population mixture reactions). On the other hand, the relative peak height of known variant bands varied linearly with the relative ratio of cell mixtures (linear regression analysis, $R^2 > 0.98$). Based on these studies, a change in relative peak height of 20% was sufficient to detect the presence of a subclonal variant. This suggests that FISSR-PCR may provide a sensitive technique for quantifying clonal variation in bronchial epithelial cell populations and may prove useful for cancer risk assessment. Supported in part by DAMD17-02-1-0706, CA-68437, and CA70907.

Presenter: Tao Lu

Affiliation: The Univ. of Texas MD Anderson Cancer Center, Houston, TX; E-mail: tlu@mail.mdanderson.org

Regulated Gap Junction-Cytoskeletal Associations in Rat Alveolar Epithelial Cells*

Yihe Guo, PhD; Cara Martinez-Williams; and D. Eugene Rannels, PhD

(CHEST 2004; 125:110S)

Abbreviations: Cx = connexin; GJ = gap junction

Connexin 43 (Cx43) is a predominant gap junction (GJ) protein that is expressed by pulmonary alveolar epithelial cells, both *in situ* and in primary culture. Cx43 expression increases with culture time, as type II cell isolates assume a more type I cell-like phenotype. In these cell populations, Cx trafficking, assembly, and turnover are regulated by diverse pathways, including those that involve integrin-mediated cell-extracellular matrix interactions and/or elements of the cytoskeleton. Immunocytochemical double labeling demonstrates the association of microtubules with the cellular internalization of Cx43-positive GJ plaques. Antibodies against the α5 integrin subunit block cell-extracellular matrix interactions, with little effect on tubulin expression. In contrast, the inhibition of mitogen-activated protein kinase kinase by PD98059 reduces tubulin expression, based either on direct immunostaining or on Western blot analysis. To examine the association of microtubules with GJ plaques, *day* 3 cells were exposed with colchicine (0.5 to 24 h). The drug disassembled the microtubules within 60 min, whereas Western blot showed no change in tubulin abundance. Colchicine caused a parallel redistribution of immunopositive Cx43 from the plasma membrane to the cytosol. These data are consistent with the conclusion that in alveolar epithelial cells, the direct association of cytoskeletal proteins with GJs plays a role in the regulation of Cx43 expression and intracellular distribution via integrin-mediated signal transduction pathways.

*From the Department of Cellular & Molecular Physiology, The Pennsylvania State University College of Medicine, Hershey, PA.
This study was supported by grants HL64682, HL10358 from the National Institutes of Health, and AHA 0150244N from the American Heart Association.

Correspondence to: D. Eugene Rannels, PhD, Department of Cellular and Molecular Physiology (C4600D), The Pennsylvania State University College of Medicine (H166), 500 University Dr, Hershey, PA 17033-0850; e-mail: grannels@psu.edu

Improvement and Application of Fluorescence Inter-Simple Sequence Repeat Polymerase Chain Reaction for the Study of Subclonal Growths in Lung Epithelial Cell Populations*

Tao Lu, PhD; and Walter N. Hittelman, PhD

(CHEST 2004; 125:110S–111S)

Abbreviations: FISSR = fluorescent dye-labeled primers for the inter-simple sequence repeat; PCR = polymerase chain reaction

Chromosome *in situ* hybridization and loss of heterozygosity analyses on bronchial biopsy specimens of current and former smokers have demonstrated the presence of clonal and subclonal outgrowths throughout the exposed lung epithelium. Since high frequencies of clonal outgrowths have been detected in the normal/premalignant epithelium adjacent to lung tumors, it is postulated that the frequency of subclonal outgrowths may provide a risk marker for lung cancer development. We therefore examined a quantitative technique with sufficient dynamic range (*ie*, inter-simple sequence repeat polymerase chain reaction [PCR]) for its ability to detect subclonal outgrowths in lung epithelial cell populations.

To improve the reproducibility and quantitative aspects of this method, we used fluorescent dye-labeled primers for the inter-simple sequence repeat (FISSR)-PCR reaction, separated and quantified the PCR products on a sequencer (model ABI 377I), and analyzed the results using computer software (GeneScan; Foster City, CA). To test the reproducibility of the sequencer, aliquots of single FISSR-PCR reactions were run in separate lanes and were shown to give reproducible band patterns. To test the reproducibility of the FISSR-PCR reaction, we carried out triplicate reactions with the same DNA source and showed reproducible band patterns. To determine its sensitivity for detecting clonal evolution during lung tumorigenesis, we quantified the number of genetic alterations detected by FISSR-PCR in a bronchial epithelial cell progression model system consisting of four evolved lung cell lines, including large T-antigen immortalized normal human bronchial epithelial cells (BEAS-2B cells), grown *in vivo* (1799 cells), treated with cigarette smoke condensate (1198 cells), and evolved to cancer (1170I cells) [originally

*From the Department of Experimental Therapeutics, University of Texas MD Anderson Cancer Center, Houston, TX.
This research was supported in part by grants DAMD17–02-1–0706, CA-68437, and CA70907.

Correspondence to: Tao Lu, PhD, Department of Experimental Therapeutics, Box 19, University of Texas MD Anderson Cancer Center, 1515 Holcombe Blvd, Houston, TX 77030; e-mail: tlu@mdanderson.org

derived by Klein-Szanto et al[1]]. Using two groups of primers, we identified nine alterations between the BEAS2B and 1799 cells, 3 additional changes to the 1198 cells, and 4 additional changes to tumorigenic 1170I cells. To determine the ability to detect subclonal populations, we isolated single-cell clones from the BEAS2B and 1170I populations, and demonstrated the presence of distinct subclones. To determine the sensitivity of this technique for detecting subclones, we carried out mixing experiments of subclonal fractions, and demonstrated a quantitative relationship between relative peak height and subclonal fraction.

These results suggest that FISSR-PCR has promise for quantifying the extent of subclonal outgrowth in cell populations, and that it may prove useful in the assessment of lung cancer risk when applied to the analysis of the bronchial epithelium of current and former smokers.

REFERENCE

1 Klein-Szanto AJP, Iizasa T, Momiki S, Garcia-Plazzo I, Caamano J, Metcalf R, Welsh J, Harris CC. A tobacco-specific N-nitrosamine or cigarette smoke condensate causes neoplastic transformation of xenotransplanted human bronchial epithelial cells. Proc Natl Acad Sci U S A 1992; 89:6693–6697

Sprouty 2 Gene in Mouse Lung Tumorigenesis*

George Minowada, MD; and York E. Miller

(CHEST 2004; 125:111S)

Abbreviations: NSCLC = non-small cell lung cancer; *Spry* = *Sprouty*

Members of the *Sprouty* (*Spry*) gene family encode novel proteins that function as intracellular antagonists of the Ras signaling pathway. Loss of *Spry* function would be predicted to enhance Ras signaling.

Several mechanisms appear to increase Ras signaling in the most common type of human lung cancer, non-small cell lung cancer (NSCLC). Epidermal growth factor receptor members and/or one of their ligands are expressed in most NSCLCs. Similarly, fibroblast growth factor 2 is expressed in many NSCLCs, if not most. Alternatively, 15 to 20% of NSCLCs have activating mutations in the *KRAS* gene. It remains unclear what role Ras signaling may play in the pathogenesis of NSCLC, but at least one consequence appears to be increased proliferation. In a mouse model of lung cancer, the chemical carcinogen urethane causes activating mutations in *K-ras* and induces lung tumors. Thus, perturbations that would be predicted to enhance Ras signaling appear to play a key role in the pathogenesis of some types of NSCLC. Such perturbations also appear to be markers of a more biologically aggressive cancer since patients with these tumors do worse.

Of the four members of the *Spry* family of genes, *Spry* 2 is expressed in the lung epithelium, the cell type from which NSCLC arises. We hypothesized that the Ras signaling antagonist *Spry* 2, which is expressed in the lung epithelium, modulates susceptibility to and/or the biological behavior of lung cancer. To begin to test this hypothesis, we have compared urethane-induced lung tumor development in *Spry* 2 lung-specific overexpressing mice (13 mice) with their littermate controls (14 mice). Consistent with the hypothesis, the mean tumor multiplicity and diameter were lower in the overexpressor mice (13.5 vs 18.7 tumors per mouse, respectively; 0.78 vs 0.86 μm per tumor, respectively).

*From the University Hospitals of Cleveland, Case Western Reserve University; Denver VAMC; University of Colorado Health Sciences Center.

Correspondence to: George Minowada, MD, Division of Pulmonary and Critical Care Medicine, Case Western Reserve University School of Medicine, University Hospitals of Cleveland, 2109 Adelbert Rd, BRB 10th Floor, Rm 1025, Cleveland, OH 44106; e-mail: gxm45@pop.uky.edu

Gene Expression Patterns, Prognostic and Diagnostic Markers, and Lung Cancer Biology*

Naftali Kaminski, MD; and Meir Krupsky, MD

(CHEST 2004; 125:111S–115S)

Key words: array comparative genomic hybridization; early detection; microarrays; non-small cell lung cancer; surrogate markers

Lung cancer is a common malignancy and is the major determinant of overall cancer mortality in developed countries.[1] Extensive prospective epidemiologic data clearly have established cigarette smoking as the major cause of lung cancer.[2] Tragically, despite an impressive

*From the Dorothy P. & Richard P. Simmons Center for Interstitial Lung Disease (Dr. Kaminski), Pulmonary, Allergy and Critical Care Medicine, University of Pittsburgh Medical Center, Pittsburgh, PA; and the Institute of Respiratory Medicine and Physiology (Dr. Krupsky), Sheba Medical Center, Sheba, Israel.

Dr. Kaminski's work was partly supported by the Tel-Aviv Chapter of the Israel Lung Association.

Correspondence to: Naftali Kaminski, MD, Dorothy P. & Richard P. Simmons Center for Interstitial Lung Disease, Pulmonary, Allergy and Critical Care Medicine, University of Pittsburgh Medical Center, NW 628 MUH, 3459 5th Ave, Pittsburgh, PA 15261; e-mail- kaminskin@upmc.edu

cancerbiology & therapy

First ISI Impact Factor (2003) = 3.024

Title:
The Farnesyltransferase Inhibitor Lonafarnib Induces Growth Arrest or Apoptosis of Human Lung Ca without Downregulation of Akt

Author(s):
Shi-Yong Sun, Zhongmei Zhou, Ruoxiang Wang, Haian Fu and Fadlo R. Khuri

PDF Coming Soon Vol: 3 | Issue: 11 | november 2004 | pgs: NA | Research Paper

Abstract:

Farnesyltransferase inhibitors (FTIs) have been demonstrated to induce growth arrest or apoptosis independent of Ras mutation. Alternatively, Akt has been proposed as a potential target for the FTI This study investigated whether Lonafarnib was effective in inhibiting the growth of human non-sm cancer (NSCLC) cells and elucidated the role of Akt in mediating such growth inhibitory effects. Lon clinical achievable concentration ranges, was effective in inhibiting the growth of 10 NSCLC cell line particularly after a prolonged treatment, regardless of Ras mutational status. Lonafarnib arrested c at G1 or G2/M phase in the majority tested cell lines. However it induced apoptosis when cells were in a low serum (0.1%) medium. The majority of NSCLC cell lines expressed undetectable level of phosphorylated Akt (p-Akt). Lonafarnib at up to 10 μM did not decrease either total Akt level or p-A any of the tested cell lines, even after a 48 h treatment. Unexpectedly, Lonafarnib even increased p in one cell line, although it was as sensitive as others to Lonafarnib treatment and underwent G2/M Bovine serum albumin completely rescued cells from Lonafarnib-induced apoptosis in low serum me indicating that proteins rather than cytokines or growth factors in serum masks Lonafarnib's pro-ap effect. Therefore, we conclude that Lonafarnib is effective in inhibiting the growth of NSCLC cells eit growth arrest or induction of apoptosis without downregulation of Akt.

Phase I Study of the Farnesyltransferase Inhibitor Lonafarnib with Paclitaxel in Solid Tumors

Fadlo R. Khuri,[1] Bonnie S. Glisson,[2] Edward S. Kim,[2] Paul Statkevich,[3] Peter F. Thall,[2] Michael L. Meyers,[3] Roy S. Herbst,[2] Reginald F. Munden,[2] Craig Tendler,[3] Yali Zhu,[3] Sandra Bangert,[2] Elizabeth Thompson,[2] Charles Lu,[2] Xue-Mei Wang,[2] Dong M. Shin,[2] Merrill S. Kies,[2] Vali Papadimitrakopoulou,[2] Frank V. Fossella,[2] Paul Kirschmeier,[3] W. Robert Bishop,[3] and Waun Ki Hong[2]

[1]Winship Cancer Institute, Emory University, Atlanta, Georgia; [2]The University of Texas M. D. Anderson Cancer Center, Houston, Texas; and [3]Schering-Plough Research Institute, Kenilworth, New Jersey

ABSTRACT

Purpose: **To establish the maximum tolerated dose of lonafarnib, a novel farnesyltransferase inhibitor, in combination with paclitaxel in patients with solid tumors and to characterize the safety, tolerability, dose-limiting toxicity, and pharmacokinetics of this combination regimen.**

Experimental Design: **In a Phase I trial, lonafarnib was administered p.o., twice daily (b.i.d.) on continuously scheduled doses of 100 mg, 125 mg, and 150 mg in combination with i.v. paclitaxel at doses of 135 mg/m^2 or 175 mg/m^2 administered over 3 h on day 8 of every 21-day cycle. Plasma paclitaxel and lonafarnib concentrations were collected at selected time points from each patient.**

Results: **Twenty-four patients were enrolled; 21 patients were evaluable. The principal grade 3/4 toxicity was diarrhea (5 of 21 patients), which was most likely due to lonafarnib. dose-limiting toxicities included grade 3 hyperbilirubinemia at dose level 3 (100 mg b.i.d. lonafarnib and 175 mg/m^2 paclitaxel); grade 4 diarrhea and grade 3 peripheral neuropathy at dose level 3A (125 mg b.i.d. lonafarnib and 175 mg/m^2 paclitaxel); and grade 4 neutropenia with fever and grade 4 diarrhea at level 4 (150 mg b.i.d. lonafarnib and 175 mg/m^2 paclitaxel). The maximum tolerated dose established by the continual reassessment method was lonafarnib 100 mg b.i.d. and paclitaxel 175 mg/m^2. Paclitaxel appeared to have no effect on the pharmacokinetics of lonafarnib. The median duration of therapy was eight cycles, including seven cycles with paclitaxel. Six of 15 previously treated patients had a durable partial response, including 3 patients who had previous taxane therapy. Notably, two of five patients with taxane-resistant metastatic non-small cell lung cancer had partial responses.**

Conclusions: **When combined with paclitaxel, the recommended dose of lonafarnib for Phase II trials is 100 mg p.o. twice daily with 175 mg/m^2 of paclitaxel i.v. every 3 weeks. Additional studies of lonafarnib in combination regimens appear warranted, particularly in patients with non-small cell lung cancer.**

INTRODUCTION

Mutations of the *ras* family of oncogenes that result in unregulated cell proliferation are common in human cancers (1). The *ras* mutations have been implicated in the development of colorectal cancer and have been associated with shortened survival in several tumor types, including non-small cell lung cancer (NSCLC; Refs. 2–6). *Ras* genes encode a protein, p21, that is located on the inner surface of the plasma membrane (1, 7). The p21 protein has GTPase activity and participates in signal transduction. Activation of the ras oncoprotein requires prenylation, a process that is catalyzed by farnesyltransferase (8–12).

Farnesyltransferase inhibitors (FTIs) are a novel class of compounds that block this critical enzymatic step in the formation of active ras proteins (8–13). Lonafarnib (Sarasar; Schering-Plough Corporation, Kenilworth, NJ) is a tricyclic nonpeptidomimetic compound (Fig. 1) that is active against a variety of tumors *in vitro* and in animal models of cancer (14). The antitumor activity of lonafarnib and other FTIs is related to the inhibition of farnesylation, although controversy currently surrounds the exact farnesylated proteins that are the key targets of FTIs (15, 16). For example, Ashar *et al.* (17) and Crespo *et al.* (18) have shown that FTIs have important effects on cell cycle arrest. The data of Crespo *et al.* suggest a direct effect on spindle formation with resultant prometaphase accumulation of mitotic lung cancer cells. Ashar *et al.* also showed that CENP-E and CENP-F, two centromeric proteins preferentially expressed in mitotic cells, are direct substrates for FTIs, and that their prenylation is completely inhibited by lonafarnib (19).

Compelling data reported by Moasser *et al.* supplied the scientific underpinning for our present study (20). They showed that, in several cell lines initially resistant to paclitaxel, the addition of a FTI enhanced the sensitivity of those cell lines to paclitaxel. Subsequent preclinical studies have demonstrated synergistic effects with lonafarnib plus paclitaxel on a number of human cell lines *in vitro* (21, 22) and enhanced activity *in vivo* (22). In the NCI-H460 lung cancer xenograft model, inhi-

Received 10/15/03; revised 12/16/03; accepted 1/9/04.
Grant support: F. Khuri was supported by Schering-Plough Research Institute and DAMD 17-02-1-0706.
The costs of publication of this article were defrayed in part by the payment of page charges. This article must therefore be hereby marked *advertisement* in accordance with 18 U.S.C. Section 1734 solely to indicate this fact.
Requests for reprints: Fadlo R. Khuri, Winship Cancer Institute, Emory University, 1365 Clifton Road NE, Building C-3094, Atlanta, GA 30322. Phone: (404) 778-4250; Fax: (404) 778-5520; E-mail: fkhuri@emory.edu.

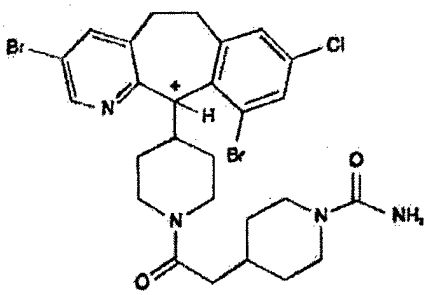

Fig. 1 Structure of lonafarnib {(11*R*)-4-[2-[4-(3,10-dibromo-8-chloro-6,11-digydro-5*H*-benzo[5,6] cyclohepta [1,2b]pyridin-11yl)-1-piperazinyl]-2-oxoethyl]-1-piperidinecarboxamide}.

bition of tumor growth was significantly greater with oral lonafarnib plus i.p. paclitaxel than with either agent alone (86% *versus* 52% and 61%, respectively; $P < 0.05$). Tumor growth inhibition on days 7 and 14 were 56 and 65% greater, respectively, with the combination than with paclitaxel alone. In line 69 wap-*ras*/F transgenic male mice, which develop paclitaxel-resistant mammary tumors at 6–9 weeks of age, oral lonafarnib significantly inhibited tumor growth ($P = 0.05$) and also sensitized the tumors to paclitaxel treatment, so that the combination of lonafarnib plus paclitaxel was more effective than lonafarnib alone ($P = 0.06$ for days 7 to 21; Refs. 22, 23). One proposed explanation for the synergistic activity is that treatment with FTI causes cells to accumulate in the G_2-M phase of the cell cycle in which paclitaxel is most effective (21, 24).

The main objectives of this trial were to establish the maximum tolerated dose (MTD) of lonafarnib, a novel FTI, in combination with paclitaxel in patients with solid tumors and to characterize the safety, tolerability, and dose-limiting toxic effects of this combination in patients with advanced solid malignancies. Furthermore, we particularly wanted to see whether durable responses could be achieved in a variety of taxane-sensitive tumors in patients previously treated with taxanes. Finally, we sought to characterize the pharmacokinetics of multiple-dose lonafarnib after its daily oral administration and of paclitaxel coadministered with daily lonafarnib.

PATIENTS AND METHODS

We sought to establish the MTD and the dose-limiting toxicity (DLT) of the lonafarnib/paclitaxel combination in adult patients with solid tumors. Previously treated patients and untreated patients were allowed to participate in the study. Eligibility criteria included a Karnofsky performance status of at least 70%, a histologically confirmed malignancy for which no curative treatment was available, measurable disease, and adequate hematological parameters [including a WBC count $\geq 3{,}000/mm^3$, an absolute neutrophil count of 1,500/μl ($\geq 1.5 \times 10^9$/liter), a platelet count $\geq 100 \times 10^9$/liter, and a hemoglobin level ≥ 10 g/dl]. Furthermore, patients were required to have adequate renal function, with a serum creatinine level ≤ 1.5 times the upper limit of normal or a measured 12-h creatinine clearance time of ≥ 50 ml/min/1.73 m^2. Also mandatory were normal hepatic function (baseline transaminase levels ≤ 3 times the upper limit of normal, bilirubin ≤ 2.0 mg/dl, and albumin ≥ 3.0 g/dl) and no manifestations of a malabsorption syndrome. All patients had to sign a written informed consent approved by the Institutional Review Board at the University of Texas M. D. Anderson Cancer Center. Patients taking agents that might alter the metabolism of lonafarnib via the CYP3A4 hepatic enzymatic system (such as azoles, macrolides, cyclosporin, systemic corticosteroids, estrogens, antiseizure drugs, rifampin, or isoniazid), or who had metastases to the brain were excluded from the study.

Patients received lonafarnib capsules p.o. twice daily (b.i.d.) with food as 50-mg, 75-mg, and 100-mg formulations in combination with paclitaxel administered i.v. every 3 weeks at 135 mg/m^2 or 175 mg/m^2 over 3 h (Fig. 2). Premedication consisted of 20 mg i.v. dexamethasone and 8 mg of i.v. ondansetron.

Statistical Methods. The dose-finding portion of the trial was conducted in a group of patients with a variety of different head and neck and lung cancers. The principal scientific goal was to determine a MTD, defined as the dose level at which the toxicity rate was closest to 20% and less than 33% with at least 33% of patients experiencing dose-limiting toxicities (DLT) at the next higher level. DLT was defined as the following: absolute neutrophil count < 500/μl for longer than 5 days or with fever ≥ 38.3°C; grade 4 thrombocytopenia (platelets < 25,000/μl) or anemia (Hb < 6.5 g/dl); grade 3–4 nausea/vomiting or grade 3 diarrhea despite optimal antiemetic or antidiarrheal treatment; or any other grade 3 treatment-related nonhematological toxicity; and treatment delay for toxicity lasting >2 weeks.

Associations between pairs of variables were assessed using the Fisher exact test, Kruskal-Wallis test, and Jonkheere-

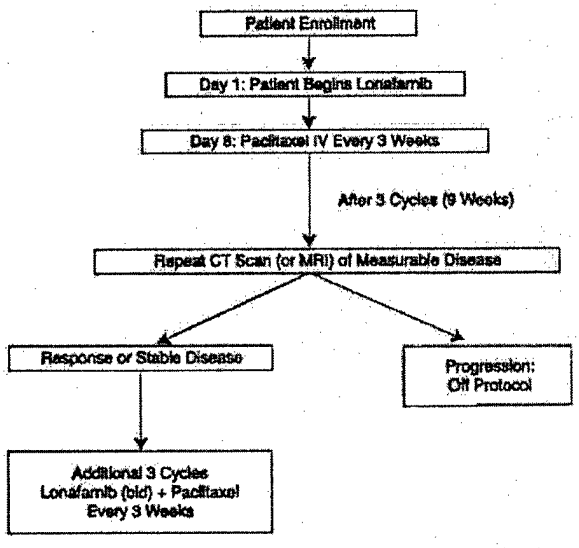

Fig. 2 Study design. Patients begin lonafarnib 1 week before receiving paclitaxel. Reevaluation occurs after every three cycles of treatment. If patients have responsive or stable disease, they proceed on study. If patients have progressive disease, they go off the study protocol. *CT*, computed tomography; *MRI*, magnetic resonance imaging.

Table 1 Number of patients and cycles by dose level of paclitaxel and lonafarnib in Phase I trial

Dose levels	Paclitaxel (mg/m²)	Lonafarnib (mg b.i.d.)	Cycles	No. of patients
1	135	50	0	0
2	135	100	1–9	3
			10–15	2
			16–32	1
3	175	100	1–3	9
			4–6	6
			7	5
			8	4
			9	2
			10–11	1
3A	175	125	1	5
			2–3	6
			4–6	5
			7–8	4
			9–10	3
			11–17	2
			18–24	1
4	175	150	1–2	4
			3–7	3
			8	2
			9–27	1

Terpstra test (25). Regression models of toxicity on the doses of paclitaxel and lonafarnib, and the indicator of prior chemotherapy, were fit using exact logistic regression (26, 27). Confidence intervals for probabilities of toxicity at particular dose and prior chemotherapy combinations were computed by repeating the exact logistic regression on 1000 bootstrap samples of the data. All of the computations were carried out using StatXact and SAS Proc Logistic.

Pharmacokinetic Methods. Plasma lonafarnib and paclitaxel concentrations were determined using validated liquid chromatography with tandem mass spectrometric detection and the high-performance liquid chromatography method, respectively. The lower limits of quantitation were 5.00 and 10.0 ng/ml plasma for lonafarnib and paclitaxel, respectively, and the linear ranges were 5.00–2500 ng/ml and 10.0–2500 ng/ml, respectively. The assay precision (% coefficient of variation) and accuracy (% Bias) were <11% and <10%, respectively, for lonafarnib, and <9% and <6%, respectively, for paclitaxel. Noninterference from the respective coadministered drug was demonstrated for both of the lonafarnib and paclitaxel methods.

Blood samples (~3 ml) for determination of plasma lonafarnib and paclitaxel concentrations were collected on day 1 of Cycle 1. Plasma was separated by centrifugation (4°C, ~3000 rpm for 15 min), then divided into two aliquots, and was stored frozen at −70°C until shipped to the analytical facility.

Individual plasma lonafarnib and paclitaxel concentrations were used for pharmacokinetic analysis using model-independent methods. The maximum plasma concentration (C_{max}) and time of maximum plasma concentration (T_{max}) were the observed values. The terminal phase rate constant (K) was calculated as the negative of the slope of the log-linear terminal portion of the plasma concentration-*versus*-time curve using linear regression. The terminal phase half-life, $t_{1/2}$, was calculated as $0.693/K$. The area under the plasma concentration-*versus*-time curve from time 0 to the time of final quantifiable sample ($AUC_{(tf)}$) and from time 0 to 12 h ($AUC_{(0-12\ h)}$) was calculated using the linear trapezoidal method. For paclitaxel, the $AUC_{(tf)}$ was extrapolated to infinity when appropriate as follows: $AUC_{(\infty)} = AUC_{(tf)} + C_{(tf)}/K$, where $C_{(tf)}$ is the estimated concentration determined from linear regression at time *tf*. Total body clearance, *CL/F* (lonafarnib) or *CL* (paclitaxel), was calculated by the following equation: CL/F = Dose/*AUC*. The apparent volume of distribution, *Vd/F* (lonafarnib) or *Vd* (paclitaxel), was calculated as: Vd/F = (Dose/*AUC*)/*K*.

For paclitaxel, the volume of distribution at steady state, *Vdss*, was estimated as total body clearance multiplied by mean residence time (*MRT*).

RESULTS

Twenty-four patients with a mean age of 58.3 years were enrolled on this Phase I study at the University of Texas M. D. Anderson Cancer Center, with the enrollment of new patients beginning on June 16, 1999, and continuing through March 30, 2000. Twenty-one patients actually received both paclitaxel and lonafarnib (Table 1). Patients were predominantly male (67%) and Caucasian (92%), with Karnofsky performance status of 90 to 100 (71%; Table 2). Slightly more than one-half of the patients had a primary diagnosis of NSCLC.

Toxicities. Among all of the dose levels, 92% of patients reported at least one toxicity at any grade and 54% of patients reported at least one grade 3/4 treatment-emergent nonhematological adverse event judged to be related to the study drugs. The most common treatment-related treatment-emergent nonhematological adverse events (including all grades) reported were gastrointestinal effects in 92% of patients (diarrhea 92%, nausea 79%, vomiting 50%, constipation 46%, stomatitis 38%, abdominal pain 29%); fatigue (88%), alopecia (83%), peripheral neuropathy (79%), arthralgia (71%), infections and infestations in 50% of patients (folliculitis 38%, oral candidiasis 13%, pneu-

Table 2 Patient demographics and disease characteristics

Subjects (*n*)	24
Age (yr)	
Median	59.5
Range	41–75
Sex	
Men	16 (67%)
Women	8 (33%)
Karnofsky performance status:	
Missing	1 (4%)
70–85	6 (25%)
90–100	17 (71%)
Histology	
NSCLC[a]	14 (58%)
Salivary	6 (25%)
HNSCC	4 (17%)
Prior chemotherapy (n = 21)	13
Prior taxane (n = 21)	9

[a] NSCLC, non-small cell lung cancer; HNSCC, head and neck squamous cell carcinoma.

Table 3 Number of patients with severe (grade 3) or life-threatening (grade 4) nonhematologic toxicities

Toxic effect	Dose level 2 (n = 3)		Dose level 3 (n = 9)		Dose level 3A (n = 5)		Dose level 4 (n = 4)	
	Grade 3	Grade 4	Grade 3	Grade 4	Grade 3	Grade 4	Grade 3	Grade 4
Bronchitis	0	0	0	0	1	0	0	0
Cardiac arrest	0	0	0	0	0	0	0	1
Chest wall pain	0	0	1	0	0	0	0	0
Diarrhea	0	0	2	0	1	1	2	0
Dysphagia	0	0	1	0	0	0	0	0
Dyspnea	0	0	0	0	1	0	0	0
Fatigue/weakness	0	0	0	0	0	0	2	0
Hyperglycemia	0	0	0	0	0	0	1	0
Neuropathy, peripheral	0	0	0	0	1	0	0	0
Fever	0	0	1	0	0	0	0	0
Infections (pneumonia)	0	0	0	0	1	0	0	0
Neoplasms, benign and malignant	0	0	1	0	0	0	0	0
Hyperbilirubinemia	0	0	1	0	0	0	0	0

Table 4 Number of patients with hematological toxicities by dose level during the treatment period

Toxic effect	Dose level 2			Dose level 3			Dose level 3A			Dose level 4		
	All	Gd[a] 3	Gd 4	All	Gd 3	Gd 4	All	Gd 3	Gd 4	All	Gd 3	Gd 4
Neutropenia	0	0	0	2	0	1	2	1	1	0	0	0
Leukopenia	1	1	0	4	1	1	3	1	0	1	1	0
Anemia	1	0	0	2	1	0	3	0	0	2	0	0

[a] Gd, grade.

monia 8%), respiratory system disorders (63%), anorexia (54%), rash (46%), weight decrease (29%); dizziness (25%); fever, blurred vision, liver and biliary system disorders, dehydration, myalgia, dry skin (21% each). All other adverse events occurred in fewer than 20% of patients. Grade 3 and grade 4 nonhematological toxicities by dose level are listed in Table 3.

Hematological toxicities occurred in 54% (13 of 24) of patients overall. Seven patients (29%) had grade 3/4 hematological toxicities. Table 4 shows that any grade and grade 3/4 anemia occurred in 34% (8 of 24) and 4% (1 of 24) of patients, respectively; any and grade 3/4 leukopenia occurred in 38% (9 of 24) and 21% (5 of 24) patients, respectively; and any and grade 3/4 neutropenia occurred in 17% (4 of 24) and 13% (3 of 24) of patients, respectively. Thrombocytopenia at any level was not observed in this study.

Both hematological and nonhematological toxic effects were generally mild and were neither more common nor more severe than those expected with paclitaxel. Patients had a median of one prior treatment with 13 of 22 evaluable patients having had prior chemotherapy including 9 who had a prior taxane (Table 2). Seven of the 9 patients previously treated with a taxane had disease progression on or within 3 months of taxane-based therapy, and 10 of 13 pretreated patients overall had progression of disease on or within 3 months of therapy.

Protocol-Defined DLTs. Overall, seven patients had DLTs as defined by protocol. No DLTs were seen at dose level 2. One patient at dose level 3 had grade 3 bilirubinemia. When the dose was escalated to level 4 (150 mg b.i.d. lonafarnib and 175 mg/m^2 paclitaxel) two of four patients had dose-limiting toxic effects in the first cycle (one grade 4 neutropenic fever, one grade 4 diarrhea). We then introduced dose level 3A (125 mg b.i.d. of lonafarnib, 175 mg/m^2 of paclitaxel) to determine whether an intermediate dose level would be tolerated. At this dose, two patients had grade 4 diarrhea in the first cycle. All of the DLTs were reversible on modification or cessation of treatment. On the basis of analysis of all available safety data, it has been determined that lonafarnib 100 mg b.i.d. and paclitaxel 175 mg/m^2 is appropriate for further evaluation in patients with NSCLC.

Table 5 Mean (percentage coefficient of variation) pharmacokinetic parameters of lonafarnib

Parameter	Dose level 2	Dose level 3	Dose level 3A	Dose level 4
C_{max}[a] (ng/ml)	760 (25)	960 (40)	1394 (35)	1267 (35)
Median T_{max} (h); range	5; 3–8	3; 0–10	8; 4–12	5; 3–6
AUC_{0-12h} (ng·h/ml)	5550 (51)	8789 (32)	12803 (36)	15443 (NA)
CL/F (ml/min)	364 (54)	207 (33)	181 (36)	165 (NA)
C_{min} (ng/ml)	286 (84)	524 (51)	883 (35)	1010 (47)

[a] C_{max}, maximum plasma concentration; T_{max}, time of maximum plasma concentration; AUC_{0-12h}, the area under the plasma concentration – *versus* – time curve from time 0 to 12 h; CL/F, total body clearance (lonafarnib); C_{min}, minimum plasma clearance.

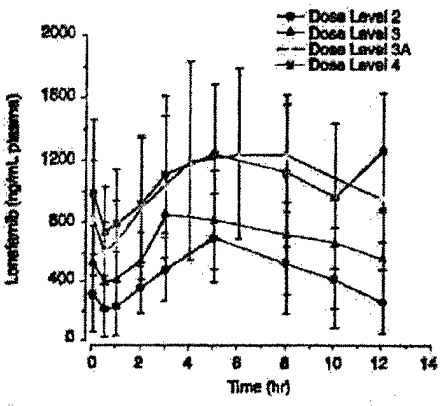

Fig. 3 Mean (±1 SD) plasma lonafarnib concentrations after multiple-dose oral administration of lonafarnib in combination with single-dose 3-h i.v. infusion of paclitaxel to patients with solid tumors.

Pharmacokinetics of Lonafarnib. Nineteen patients had samples collected for pharmacokinetic evaluations. Lonafarnib was slowly absorbed after oral administration with food. Median T_{max} ranged from 3 to 8 h (Table 5; Fig. 3). Half-life ($t_{1/2}$) could not be estimated in this study because of the lack of a definitive terminal phase in the plasma concentration-*versus*-time profiles after b.i.d. oral administration of lonafarnib with food (see Fig. 3). Mean plasma lonafarnib concentrations at 12 h after the dose were ~34–99% of the corresponding mean C_{max} values. The mean total body clearance ranged from 165 to 364 ml/min. The increases in lonafarnib *AUC* values were dose-related after oral administration of 100 mg, 125 mg, and 150 mg in combination with paclitaxel 175 mg/m^2. After administration of lonafarnib 100 mg with paclitaxel 175 mg/m^2, the mean lonafarnib C_{max} and *AUC* values were higher than those with paclitaxel 135 mg/m^2. However, given the variability of the data and sample size, the distribution of individual C_{max} and *AUC* values encompassed the same range, regardless of paclitaxel dose (Fig. 4). The C_{max} and *AUC* values obtained in this trial with lonafarnib 100 mg in combination with paclitaxel were similar to those obtained in previous Phase I trials in which lonafarnib 100 mg was administered alone (Table 6; Refs. 28–30). Thus, these observations suggest that a single dose of either 135 mg/m^2 or 175 mg/m^2 of paclitaxel did not affect the pharmacokinetics of lonafarnib.

Pharmacokinetics of Paclitaxel. Plasma paclitaxel concentrations (C_{max} and *AUC*) were similar among the dose groups for paclitaxel 175 mg/m^2 with lonafarnib 100 mg, 125 mg, and 150 mg (Table 7; Figs. 5 and 6). There appear to be no effects on paclitaxel pharmacokinetics at a dose of 175 mg/m^2 paclitaxel when the lonafarnib dose is increased from 100 mg to 150 mg. The relationships between dose and paclitaxel C_{max} or *AUC* values were disproportionate after the administration of paclitaxel 135 mg/m^2 and 175 mg/m^2 in combination with lonafarnib 100 mg; a 30% increase in paclitaxel dose resulted in an increase of ~74% in C_{max} and ~87% in *AUC*. This finding provided additional evidence for the nonlinear disposition for paclitaxel, as noted previously (31).

Plasma paclitaxel concentrations decreased rapidly immediately after cessation of the 3-h infusion, which was followed by a prolonged terminal phase (see Fig. 5). The mean terminal elimination $t_{1/2}$ of paclitaxel ranged from 12 to 19 h when blood samples were collected up to 48 h postdose for the first 17 patients. The mean $t_{1/2}$ was ~6 h when blood samples were collected up to 24 h postdose for patients 18–24 (see Table 7). The 6-h half-life was similar to that reported in the literature (31). The C_{max} and *AUC* values obtained in this study were similar to those previously reported when paclitaxel was given alone as a 3-h i.v. infusion (Table 8; Ref. 31).

Clinical Activity. The median number of treatment cycles on trial was eight, with a median of seven cycles containing paclitaxel. Activity was seen at the four dose levels studied (2, 3, 3A, and 4). Nine responses were durable, which we defined as a response detected at three or six cycles and confirmed at six or eight cycles, with median response duration of 6 months (range, 4–14 months). Most provocatively, we saw meaningful responses in three patients who had received prior taxane-based therapy, including two of five NSCLC patients who met the standard definition of taxane resistance (progression on or within 3 months

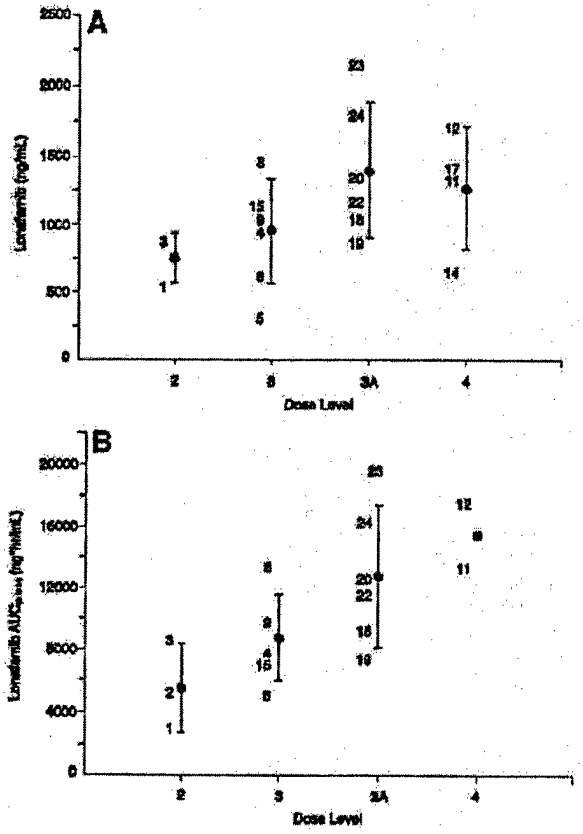

Fig. 4 Individual and mean (±1 SD) C_{max} (*A*) and $AUC_{0-12\ h}$ values (*B*) of lonafarnib after multiple-dose oral administration of lonafarnib in combination with single-dose 3-h i.v. infusion of paclitaxel to patients with solid tumors.

Table 6 Mean (coefficient of variation) pharmacokinetic parameters of lonafarnib after multiple-dose administration of lonafarnib 100 mg alone (previous Phase I studies) or in combination with paclitaxel (this study)

Study	Dose	*n*	C_{max}[a] (ng/ml)	AUC_{0-12} (ng·h/ml)
This study	100 + 135[b]	3	760 (25)	5550 (51)
This study	100 + 175[b]	8	960 (40)	8789[c] (32)
Eskens *et al.*[d]	100[e]	3	942 (58)	7299 (75)
Adjei *et al.*[f]	100	1	1680 (NA)	18295 (NA)
Hurwitz *et al.*[g]	100	2	784 (NA)	6221 (NA)

[a] C_{max}, maximum plasma concentration; AUC_{0-12}, the area under the plasma concentration - *versus* - time curve from time 0 to 12 h; NA, not appropriate (sample size < 3).
[b] Lonafarnib dose (mg) + paclitaxel dose (mg/m²).
[c] $n = 6$.
[d] Ref. 34.
[e] Lonafarnib alone dose (mg).
[f] Ref. 32.
[g] Ref. 33.

Table 7 Mean (percentage coefficient of variation) pharmacokinetic parameters of paclitaxel

Parameter	Dose level 2	Dose level 3	Dose level 3A	Dose level 4
C_{max}[a] (ng/ml)	1937 (19)	3368 (55)	4258 (43)	3515 (38)
AUC_{∞} (ng·h/ml)	9936 (7)	18563 (40)	17526 (38)	17634 (23)
$t_{1/2}$ (h)	18.6 (12)	13.3 (9)	5.62 (15)	12.1 (24)
CL (ml/min/m²)	227 (8)	182 (43)	183 (33)	171 (19)
Vd (liter/m²)	365 (7)	211 (47)	88.1 (35)	174 (9)
Vdss (liter/m²)	130 (16)	90.6 (54)	40.2 (47)	66.9 (12)

[a] C_{max}, maximum plasma concentration; AUC_{∞}, area under the plasma concentration - *versus* - time curve from time 0 to the final quantifiable sample extrapolated to infinity; $t_{1/2}$, terminal phase half-life; *CL*, total body clearance; *Vd*, volume of distributions; *Vdss*, the volume of distribution at steady state.

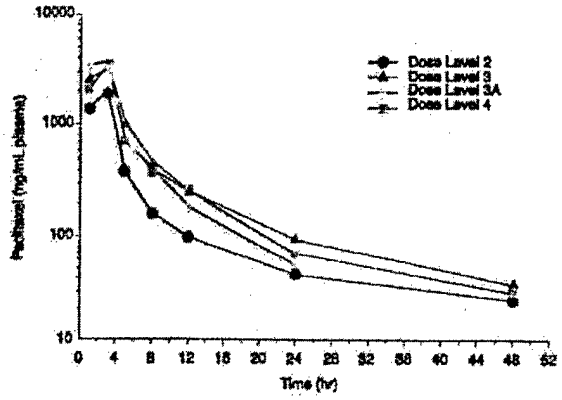

Fig. 5 Mean plasma paclitaxel concentrations after single-dose 3-h i.v. infusion of paclitaxel in combination with multiple-dose oral administration of lonafarnib to patients with solid tumors.

of taxane therapy). Only 4 of 21 patients had progressive disease by cycle 3, although all 21 patients had manifested disease progression within 3 months of study enrollment.

At the cycle-3 assessment interval, 7 patients demonstrated a partial response, 10 had minor responses or stable disease, and 4 had progressive disease (Table 9). Six of 7 responses were confirmed after six cycles. When total responses achieved on study were examined, 6 (50%) of the 12 patients with NSCLC achieved a partial response. In the setting of head and neck squamous cell carcinoma, two of the three patients had a partial response, and the one patient with a salivary gland tumor had prolonged disease stabilization and was treated for 30 cycles before disease progression. No significant associations were noted between response after three cycles or after six cycles and the dose of either lonafarnib ($P = 0.81$, $P = 0.70$, respectively) or paclitaxel ($P = 0.19$, $P = 0.32$, respectively).

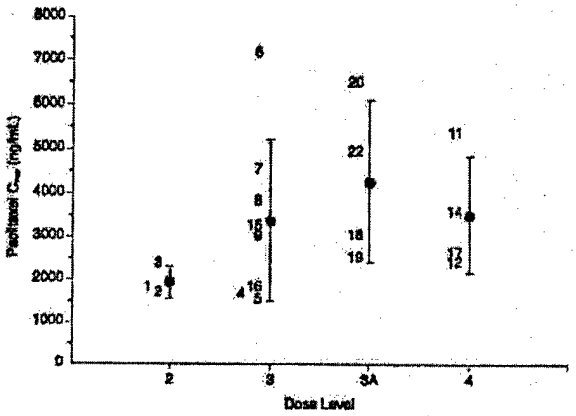

Fig. 6 Individual and mean (±1 SD) C_{max} values of paclitaxel after single-dose 3-h i.v. infusion of paclitaxel in combination with multiple-dose oral administration of lonafarnib to patients with solid tumors.

Table 8 Mean (coefficient of variation) pharmacokinetic parameters of paclitaxel after 3-h i.v. infusion of paclitaxel 135 mg/m² or 175 mg/m² in combination with multiple-dose lonafarnib 100 mg b.i.d., 125 mg b.i.d., or 150 mg b.i.d. (this study) or alone (previously reported study)

Dose	Study	*n*	C_{max} (ng/ml)	AUC_∞ (ng·h/ml)	*CL* (ml/min/m²)
135	This study	3	1937 (19)	9936 (7)	227 (8)
	Gianni *et al.*[a]	4	2818 (12)	9308 (10)	247 (9)
175	This study	16	3627 (46)	18309[c] (34)	179[c] (34)
	Gianni *et al.*[a]	3	5038 (15)	15797 (16)	190 (16)

[a] C_{max}, maximum plasma concentration; AUC_∞, area under the plasma concentration - *versus* - time curve from time 0 to the final quantifiable sample extrapolated to infinity; *CL*, total body clearance.
[b] Ref. 35.
[c] $n = 15$.

DISCUSSION

Other than the occasionally dose-limiting side effect of diarrhea, lonafarnib did not seem to contribute any significant side effects to those caused by paclitaxel. Patients with previous chemotherapy had a higher risk of toxicity. The substantial overlap of the eight 90% confidence intervals is due in large part to the small sample size ($n = 21$ evaluable patients). The only discernable trend with dose is an increase in the upper confidence limit with increasing total combined dose. Seven of the eight confidence intervals contain the targeted 30% toxicity rate. More precise estimates of the probability of toxicity would necessitate a larger sample size. The MTDs of lonafarnib and paclitaxel in this trial were lower than the doses recommended for either agent alone. The MTD of lonafarnib alone was determined to be 200 mg b.i.d. DLTs in studies of lonafarnib alone were generally similar to those seen in this trial and included reversible renal insufficiency (elevated creatinine levels), gastrointestinal symptoms (diarrhea, nausea, vomiting, anorexia), and hematological toxicities. Phase I studies of paclitaxel have demonstrated an MTD of 200 mg/m² for a single continuous infusion i.v. regimen. Myelosuppression and neurotoxicity are the primary DLTs of paclitaxel. Severe allergic reactions and skin rash associated with the vehicle (cremaphor EL) necessitate pretreatment with dexamethasone, diphenhydramine, and cimetidine or ranitidine.

No pharmacokinetic evidence was observed that either paclitaxel or lonafarnib enhanced the metabolism of the other agent. The pharmacokinetic values suggest that areas under the curve of both drugs were achieved in the active range. The target exposure for lonafarnib in clinical studies was to maintain a predose concentration in the range of 1–1.5 μM based on the concentration required to inhibit anchorage-independent growth of a series of human tumor cell lines.

We saw encouraging clinical activity in this Phase I study of combined paclitaxel and lonafarnib, confirming the preclinical activity previously reported for this combination (14, 20, 22, 32–34). Several Phase I studies of farnesyltransferase inhibitors have now been published (28–30, 35–39). Before this study, a total of two responses have been documented (one each with tipifarnib and lonafarnib) in previously treated patients with NSCLC (29, 36). The activity manifested with this protocol using fairly moderate doses of lonafarnib and paclitaxel is more

Table 9 Clinical activity of lonafarnib in combination with paclitaxel

After 3 Cycles	
Partial response	7 patients (3 previously treated with taxanes)
Minor response	3 patients
Stable disease	7 (4 previously treated with taxanes)
Progressive disease	4 (2 previously treated with taxanes)
Not assessed	3 (1 did not tolerate lonafarnib at 125 mg b.i.d.)
Median no. of total cycles on study:	8 (range, 2–30)
Median no. of paclitaxel courses on study:	7 (range, 2–30)
After 6 to 9 Cycles	
Partial response	8 patients (3 previously treated with taxanes)
Minor response	2 patients
Stable disease	6 (4 previously treated with taxanes)
Progressive disease	2 (2 previously treated with taxanes)
Not assessed	3
Median no. of total cycles on study:	8 (range, 2–30)
Median no. of paclitaxel courses on study:	7 (range, 2–30)
Any response by histology	
NSCLC[a]	12 patients (6 PR, 3 MR or StD, 3 PD)[b]
HNSCC	3 patients (2 PR, 1 StD)
Salivary	6 patients (1 PR, 4 StD, 1 PD)

[a] NSCLC, non-small cell lung cancer; PR, partial response; MR, minor response; StD, stable disease; PD, progressive disease; HNSCC, head and neck squamous cell carcinoma.
[b] Five patients (all NSCLC) were considered taxane-refractory/resistant. PRs were seen in 2 of 5 taxane-refractory/resistant NSCLC patients.

substantial. It is particularly heartening because little if any evidence exists to support the efficacy of paclitaxel as a second-line agent when administered as a 3-h infusion on a 3-week cycle (40–44).

The extent of disease stabilization that our trial revealed with this regimen was dramatic in an extensively pretreated heterogeneous patient population with progressive disease at the time of study enrollment. Recent evidence suggests that the stabilization of NSCLC may lead to clinically meaningful survival benefits.

In conclusion, this is the first reported clinical study of the combination of a taxane with a farnesyltransferase inhibitor in human solid tumors. Phase II trials of the combination as first-line and second-line therapy of stage III and IV NSCLC are ongoing to confirm or refute our data-driven hypothesis, namely, that lonafarnib may enhance taxane sensitivity and possibly overcome clinical taxane resistance in solid tumors.

ACKNOWLEDGMENTS

We thank Judie Wells for transcription and editing of the manuscript, Julie Starr for her expert editorial assistance, and Delores Curtis and Stephen Maxwell for bioanalytical support.

REFERENCES

1. Bos JL. ras oncogenes in human cancer: a review. Cancer Res 1989;49:4682–9. Erratum in: Cancer Res 1990;50:1352.

2. Slebos RJ, Kibbelaar RE, Dalesio O, et al. K-ras oncogene activation as a prognostic marker in adenocarcinoma of the lung. N Engl J Med 1990;323:561–5.

3. Rosell R, Li S, Skacel Z, et al. Prognostic impact of mutated K-ras in surgically resected non-small cell lung cancer patients. Oncogene 1993;8:2407–12.

4. Malats N, Porta M, Corominas JM, et al. Ki-ras mutations in exocrine pancreatic cancer: association with clinico-pathological characteristics and with tobacco and alcohol consumption. PANK-ras I Project Investigators. Int J Cancer 1997;70:661–7.

5. Sugio K, Molberg K, Albores-Saavedra J, et al. K-ras mutations and allelic loss at 5q and 18q in the development of human pancreatic cancers. Int J Pancreatol 1997;21:205–17.

6. Rall CJ, Yan YX, Graeme-Cook F, et al. Ki-ras and p53 mutations in pancreatic ductal adenocarcinoma. Pancreas 1996;12:10–7.

7. Bollag G, McCormick F. Regulators and effectors of ras proteins. Ann Rev Cell Dev Biol 1991;7:601–32.

8. Gibbs JB. Lipid modifications of proteins in the ras superfamily. In: Birnbaumer L, Dickey B, editors. GTPases in biology. New York: Springer-Verlag; 1993. p. 335–44.

9. Hancock JF, Magee AI, Childs JE, Marshall CJ. All ras proteins are polyisoprenylated but only some are palmitoylated. Cell 1989;57:1167–77.

10. Hancock JF, Paterson H, Marshall CJ. A polybasic domain or palmitoylation is required in addition to the CAAX motif to localize p21ras to the plasma membrane. Cell 1990;63:133–9.

11. Jackson JH, Cochrane CG, Bourne JR, et al. Farnesol modification of Kirsten-ras exon 4B protein is essential for transformation. Proc Natl Acad Sci USA 1990;87:3042–6.

12. Kato K, Cox AD, Hisaka MM, et al. Isoprenoid addition of Ras protein is the critical modification for its membrane association and transforming activity. Proc Natl Acad Sci USA 1992;89:6403–7.

13. Rowinsky EK, Windle JJ, Von Hoff DD. Ras protein farnesyltransferase: a strategic target for anticancer therapeutic development. J Clin Oncol 1999;17:3631–52.

14. Liu M, Bryant MS, Chen J, et al. Antitumor activity of SCH 66336, an orally bioavailable tricyclic inhibitor of farnesyl protein transferase, in human tumor xenograft models and wap-ras transgenic mice. Cancer Res 1998;58:4947–56.

15. Cox AD, Der CJ. Farnesyltransferase inhibitors and cancer treatment: targeting simply ras? Biochim Biophys Acta 1997;1333:F51–71.

16. Du W, Prendergast GC. Activation of the PI3′K-AKT pathway masks the proapoptotic effects of farnesyltransferase inhibitors. Cancer Res 1999;59:4208–12.

17. Ashar HR, James L, Gray K, et al. The farnesyl transferase inhibitor SCH 66336 induces a G(2) → M or G(1) pause in sensitive human tumor cell lines. Exp Cell Res 2001;262:17–27.

18. Crespo NC, Ohkanda J, Yen TJ, Hamilton AD, Sebti SM. The farnesyltransferase inhibitor, FTI-2153, blocks bipolar spindle formation and chromosome alignment and causes prometaphase accumulation during mitosis of human lung cancer cells. J Biol Chem 2001;276:16161–7.

19. Ashar HR, James L, Gray K, et al. Farnesyl transferase inhibitors block the farnesylation of CENP-E and CENP-F and alter the association of CENP-E with the microtubules. J Biol Chem 2000;275:30451–7.

20. Moasser MM, Sepp-Lorenzino L, Kohl NE, et al. Farnesyl transferase inhibitors cause enhanced mitotic sensitivity to Taxol and epothilones. Proc Natl Acad Sci USA 1998;95:1369–74.

21. Nielsen LL, Shi B, Hajian G, et al. Combination therapy with the farnesyl protein transferase inhibitor SCH66336 and SCH58500 (p53 adenovirus) in preclinical cancer models. Cancer Res 1999;59:5896–901.

22. Shi B, Yaremko B, Hajian G, et al. The farnesyl protein transferase inhibitor SCH66336 synergizes with taxanes in vitro and enhances their antitumor activity in vivo. Cancer Chemother Pharmacol 2000;46:387–93.

23. Porter GM, Armstrong L, Nielsen LL. Strategy for developing transgenic assays for screening antineoplastic drugs that affect tubulin polymerization. Lab Anim Sci 1995;45:145–50.

24. Donaldson KL, Goolsby GL, Wahl AF. Cytotoxicity of the anticancer agents cisplatin and Taxol during cell proliferation and the cell cycle. Int J Cancer 1994;57:847–55.

25. Hirji, KF. Exact distributions for polytomous data. J Am Stat Assoc 1992;87:487–92.

26. Mehta CR, Patel NR, Jajoo B. Exact logistic regression: theory, methods and software. Technical report. Cambridge, MA: Cytel Software Corporation; 1993.

27. Mehta CR, Patel NR, Senchaudhuri, P. Efficient Monte Carlo methods for conditional logistic regression. J Am Stat Assoc 2000;95:99–108.

28. Adjei AA, Erlichman C, Davis JN, et al. A Phase I trial of the farnesyl transferase inhibitor SCH66336: evidence for biological and clinical activity. Cancer Res 2000;60:1871–7.

29. Hurwitz HI, Colvin OM, Petros WP, et al. Phase I and pharmacokinetic study of SCH66336, a novel FPTI, using a 2-week on, 2-week off schedule [abstract]. Proc Am Soc Clin Oncol 1999;18:599.

30. Eskens F, Awada A, Cutler D, et al. Phase I and pharmacokinetic study of the oral farnesyl transferase inhibitor SCH 66336 given twice daily to patients with advanced solid tumors. J Clin Oncol 2001;19:1167–75.

31. Gianni L, Kearns CM, Giani A, et al. Nonlinear pharmacokinetics and metabolism of paclitaxel and its pharmacokinetic/pharmacodynamic relationships in humans. J Clin Oncol 1995;13:180–90.

32. Kohl NE, Omer CA, Conner MW, et al. Inhibition of farnesyltransferase induces regression of mammary and salivary carcinomas in ras transgenic mice. Nat Med 1995;1:792–97.

33. Sun J, Qian Y, Hamilton AD, Sebti SM. Ras CAAX peptidomimetic FTI276 selectively blocks tumor growth in nude mice of a human lung carcinoma with K-Ras mutation and p53 deletion. Cancer Res 1995;55:4243–7.

34. Prendergast GC, Davide JP, deSolms SJ, et al. Farnesyltransferase inhibition causes morphological reversion of ras-transformed cells by a complex mechanism that involves regulation of the actin cytoskeleton. Mol Cell Biol 1994;14:4193–202.

35. Zujewski J, Horak ID, Bol CJ, et al. Phase I and pharmacokinetic study of farnesyl protein transferase inhibitor R115777 in advanced cancer. J Clin Oncol 2000;18:927–41.

36. Schellens JHM, de Klerk G, Swart M, et al. Phase I and pharmacologic study with the novel farnesyltransferase inhibitor (FTI) R115777 [abstract]. Proc Am Assoc Cancer Res 1999;40:4780.

37. Soignet S, Yao S-L, Britten C, et al. Pharmacokinetics and pharmacodynamics of the farnesyl protein transferase inhibitor (L-778, 123) in solid tumors [abstract]. Proc Am Assoc Cancer Res 1999;40:3413.

38. Britten CD, Rowinsky E, Yao S-L, et al. The farnesyl protein transferase (FPTase) inhibitor L-78,123 in patients with solid cancers [abstract]. Proc Am Soc Clin Oncol 1999;18:597.

39. Hudes GR, Scholl J, Baab J, et al. Phase I clinical and pharmacokinetic trial of the farnesyltransferase inhibitor R115777 on a 21-day dosing schedule [abstract]. Proc Am Soc Clin Oncol 1999;18:601.

40. Huisman C, Smit EF, Giaccone G, Postmus PE. Second-line chemotherapy in relapsing or refractory non-small cell lung cancer: a review. J Clin Oncol 2000;18:3722–30.

41. Fossella FV, Lee JS, Shin DM, et al. Phase II study of docetaxel for advanced or metastatic platinum-refractory non-small cell lung cancer. J Clin Oncol 1995;13:645–51.

42. Gatzemeier U, von Pawel J, Gottfried M, et al. Phase III comparative study of high-dose cisplatin versus a combination of paclitaxel and cisplatin in patients with advanced non-small cell lung cancer. J Clin Oncol 2000;18:3390–9.

43. Socinski MA, Steagall A, Gillenwater H. Second-line chemotherapy with 96-hour infusional paclitaxel in refractory non-small cell lung cancer: report of a Phase II trial. Cancer Investig 1999;17:181–8.

44. Stewart DJ, Tomiak EM, Goss G, et al. Paclitaxel plus hydroxyurea as second-line therapy for non-small cell lung cancer. Lung Cancer 1996;15:115–23.

doi:10.1016/S1525-0016(03)00004-2

Increased Uptake of Liposomal–DNA Complexes by Lung Metastases Following Intravenous Administration

Isao Ito,[1] Gopalan Began,[1] Imran Mohiuddin,[1] Tomoyuki Saeki,[1] Yuji Saito,[1] Cynthia D. Branch,[1] Ara Vaporciyan,[1] L. Clifton Stephens,[2] Nancy Yen,[1] Jack A. Roth,[1] and Rajagopal Ramesh[1,*]

[1]*Department of Thoracic and Cardiovascular Surgery and* [2]*Department of Veterinary Medicine and Surgery, The University of Texas M. D. Anderson Cancer Center, Houston, Texas 77030*

**To whom correspondence and reprint requests should be addressed at the Department of Thoracic and Cardiovascular Surgery, The University of Texas M. D. Anderson Cancer Center, P.O. Box 445, 1515 Holcombe Boulevard, Houston, TX 77030. Fax: (713) 794-4901. E-mail: rameshi@mdanderson.org.*

We have investigated the effects of an improved liposomal formulation (extruded DOTAP: cholesterol (DOTAP:Chol)–DNA complex) on transgene expression in tumor cells and normal cells of murine and human origin both *in vitro* and *in vivo*. *In vitro*, transgene expression was significantly increased ($P = 0.01$) in human tumor cells compared to normal human cells. The increased transgene expression was due to increased uptake of the liposome–DNA complex by tumor cell phagocytosis. Furthermore, immunohistochemical analysis demonstrated a greater transgene expression in lung tumors than in surrounding normal tissues. Increased transgene expression due to enhanced uptake of the liposome–DNA complexes by tumor cells *in vivo* was also demonstrated using fluorescently labeled DOTAP:Chol liposomes. Finally, evaluation of lung tissue explants obtained from patients undergoing pulmonary resection demonstrated significantly higher ($P = 0.001$) transgene expression in tumor cells than in normal cells. Thus, we demonstrated that intravenous injection of DOTAP:Chol–DNA complex results in increased transgene expression in tumor and is due to increased phagocytosis of the complexes by tumor cells.

Key Words: liposome, gene therapy, phagocytosis, cancer, metastasis

Introduction

Progression of cancer is a multistep process in which the disease eventually becomes disseminated. Current treatments for disseminated tumors have had limited success because of treatment-related toxicity. A new alternative treatment strategy for cancer is gene therapy, which has shown promise in clinical trials [1–6]. This approach has, however, been limited to the treatment of locoregional disease because of the lack of a vector that can efficiently and selectively deliver genes systemically.

An alternative to adenoviral vectors is nonviral liposomal delivery systems that can be administered intravenously with limited vector-associated toxicity, resulting in higher transgene expression, especially in the lungs [7]. The development of efficient nonviral vectors that, when injected systemically, can selectively deliver therapeutic genes to tumors will provide novel therapeutic options for the treatment of cancer. Tumor targeting using tumor-specific promoters, attachment of ligands to the liposome surface, and pegylation of liposomes has been tested previously [8–16]. Although some degree of tumor targeting has been demonstrated using these targeted delivery systems, the level of transgene expression is often decreased. Recent studies have demonstrated that liposome–DNA complexes elicit an inflammatory response when injected systemically, resulting in suppression of transgene expression [17–22]. Furthermore, failure to achieve increased or sustained gene expression following repeated injections has been another major obstacle in the development of therapeutic applications of liposomes [18,23].

We recently showed that extruded cationic liposome (DOTAP:cholesterol, or DOTAP:Chol)–DNA complexes can achieve effective levels of transgene expression in tumor-bearing lungs and, when injected intravenously, can cure immunocompetent mice with disseminated experimental metastases, with minimal toxicity [24]. In the same study, we also showed that repeated daily injections resulted in a dose-dependent increase in transgene expression in tumor-bearing lungs. The unexpected curative potential of these complexes for disseminated disease and the apparent high levels of their expression in tumors raised an important question: were these effects due to

1525-0016/03 $30.00

increased expression of the transgene in tumor cells or due to increased uptake of the liposomes by tumor cells compared to surrounding normal cells?

In the study presented here, we demonstrate that intravenous injection of DOTAP:Chol liposome–DNA complexes *in vivo* results in significantly higher transgene expression in lung tumor cells than in normal cells and that this increased expression is due to increased uptake of these liposome–DNA complexes by tumor cells. Furthermore, transgene expression is demonstrated to be significantly higher in primary human lung tumor explants than in normal cells. Thus, utilizing the inherent property of tumor cells for increased liposomal–DNA complex uptake, effective delivery of therapeutic genes to the tumor can be achieved following systemic delivery.

Results

Cell Viability and Luciferase (*luc*) Gene Expression in Liposome–DNA Complex-Transfected Normal and Tumor Cells

We transfected normal human lung fibroblasts (WI38, MRC9), normal human bronchial epithelial cells (NHBE), human lung tumor cells (A549, H1299, H358, H322, and H460), murine fibroblasts (NIH/3T3, 10T1/2), and murine fibrosarcoma cells (UV2237m, K1735) all with DOTAP:Chol–*luc* DNA complex (Fig. 1). Determination of cell viability at 24 and 48 h after transfection demonstrated no significant toxicity in any of the cell lines tested (Fig. 1A). To determine whether differences existed in transgene expression between normal and tumor cells, we assayed transfected cells for *luc* activity. *luc* expression was 2 to 4 logs greater ($P = 0.01$) in human tumor cells compared to normal cells of human origin (Fig. 1B). However, *luc* expression in murine tumor cells was only 2- to 2 ½-fold greater compared to normal cells ($P = 0.04$; Fig. 1B).

In Vitro Uptake of Liposome–DNA Complex

Analysis of the liposome–DNA complex uptake in human tumor cells relative to normal human cells by fluorescence microscopy and flow cytometry revealed increased uptake in tumor cells compared to normal cells (Fig. 2). However, increased uptake of liposome–DNA complex was also observed in endothelial cells (HUVEC). The difference in the uptake of the liposome complex by these cells correlated with luciferase expression (Fig. 2)

Role of Phagocytic and Pinocytic Activity in the Uptake of Liposome–DNA Complex by Tumor Cells

We transfected tumor cells (H1299) with fluorescently labeled DOTAP:Chol–*luc* DNA complex (Figs. 3B and 3C) and positively charged 2-μm fluorescent latex microspheres (Fig. 3A) with or without cytochalasin B, an inhibitor of phagocytosis and pinocytosis, and observed them under a fluorescence microscope using a fluorescein or a rhodamine filter. Tumor cells transfected in the absence of cytochalasin B showed greater punctate fluorescence in the cytoplasm, indicating greater uptake of the liposome–DNA complex (Fig. 3B). In contrast, liposome–DNA complex uptake was blocked in cells transfected in the presence of the drug. Hoechst staining revealed presence of intact nucleus in the cells that were untreated or treated with cytochalasin B.

Uptake of Liposome–DNA Complex by Tumor Cells *In Vivo*

We injected UV2237m lung-tumor-bearing C3H/Ncr mice with fluorescently labeled DOTAP:Chol–*luc* DNA complex (50 μg DNA) via a tail vein. Animals receiving no treatment served as controls. We euthanized the animals at 24 h after injection, harvested their lungs, and prepared cryosections. Examination of tissue sections under fluorescence microscopy revealed intense fluorescence by tumor cells compared to surrounding normal cells (Fig. 4D). Minimal fluorescence was observed in controls (Fig. 4B). Further confirmation that the observed intense fluorescence was indeed from tumor cells was obtained by examining a hematoxylin-stained serial tissue section under bright-field microscopy (Figs. 4A and 4C)

To confirm further that the increased uptake of the liposome–DNA complex by tumor cells also resulted in increased transgene expression, we stained tissue sections for luciferase protein by immunohistochemical technique. Protein expression was greater in tumor cells (Fig. 4E) than in surrounding normal cells (Fig. 4H), indicating that tumor cells were the primary source of the observed *luc* expression. Furthermore, we observed *luc* expression to be higher in tumor-bearing lung tissue (Fig. 4E) than in the non-tumor-bearing lung tissue (Fig. 4G). A lung tissue section from a tumor-bearing animal receiving no treatment served as negative control (Fig. 4F). Additional controls included tissues stained with secondary antibody alone (Fig. 4I). Semiquantitative analysis demonstrated a significant ($P = 0.01$) increase in luciferase protein expression as indicated by the brown staining in the tumor tissue area compared to surrounding normal tissue area (Fig. 4J).

To confirm further that the observed result is not unique to UV2237m lung tumors, we performed similar experiments in nude mice bearing human A549 lung tumors. We injected the animals with DOTAP:Chol–*luc* DNA complex 2 or 3 weeks after tumor cell injection. The tumor load at 2 weeks is less and the tumors are small compared to tumor load and size at 3 weeks (data not shown). Immunohistochemical analysis of lung tissues 24 h after injection of liposome–DNA complex demonstrated increased luciferase expression ($P = 0.01$) in tu-

doi:10.1016/S1525-0016(03)00004-2

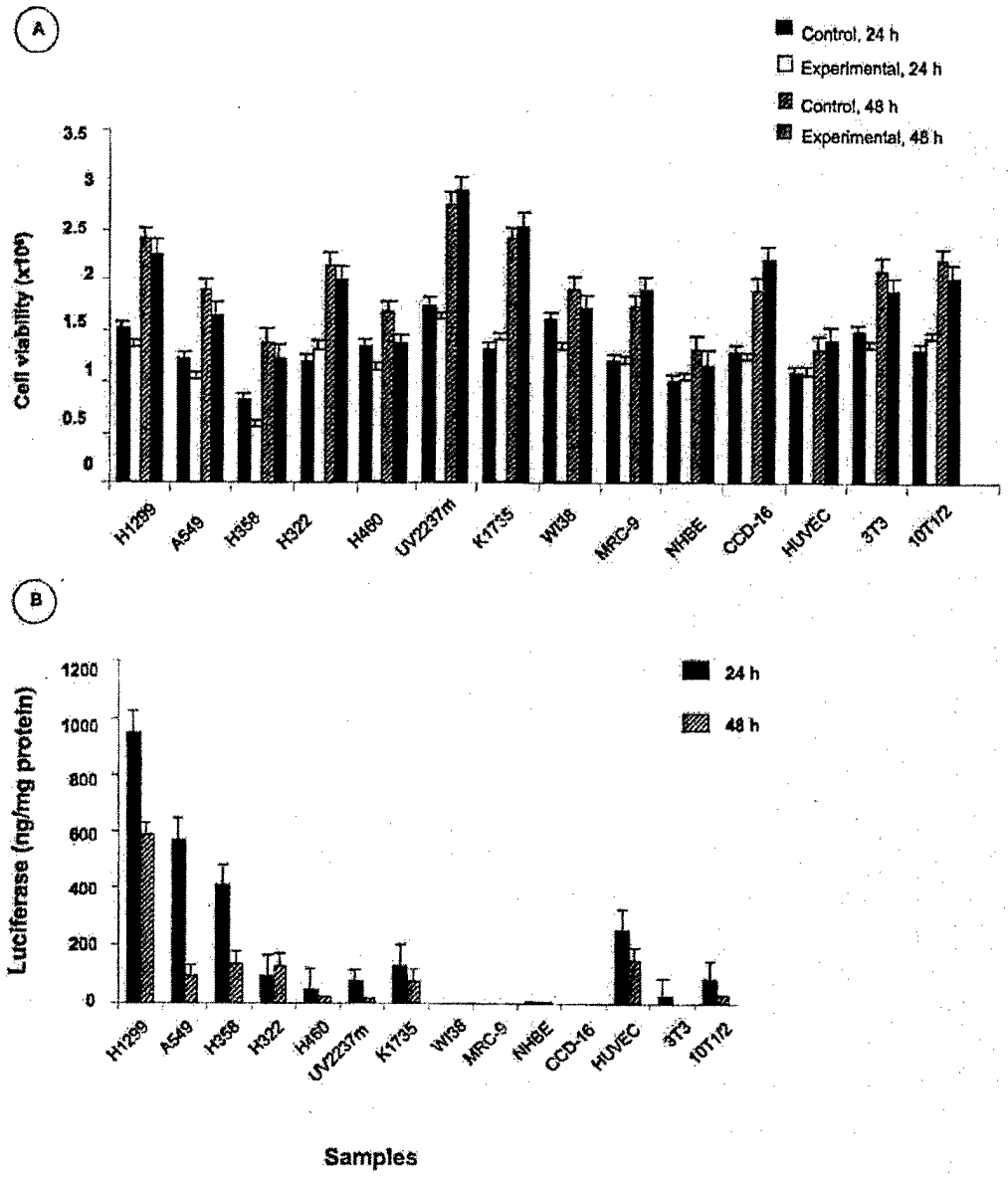

FIG. 1. Effect of liposome–DNA complex transfection on cell viability and *luc* expression in tumor cells and normal cells. Cells analyzed were human lung tumor cells (H1299, H358, H460, A549), normal lung fibroblast cells (WI38, CCD-16, MRC-9), normal bronchial epithelial cells (NHBE), human umbilical vein endothelial cells (HUVEC), murine fibroblasts (3T3, 10T1/2), and murine fibrosarcoma (UV2237m, K1735) cells. Cells (5×10^5) were either not transfected (control) or transfected with DOTAP:Chol–*luc* DNA complex and harvested at 24 and 48 h after transfection and analyzed for cell viability by trypan exclusion assay (A) and for *luc* activity using a luciferase assay kit (B). No significant toxicity was observed in transfected tumor and normal cells of both human and murine origin compared to untransfected control cells (A). *luc* expression was higher in both human tumor cells ($P = 0.01$) and murine tumor cells ($P = 0.04$) compared to normal cells (B). *luc* activity was expressed as nanograms per milligram of total protein. Each time point represents the mean of triplicate wells. Error bars represent standard errors.

mors compared to surrounding normal tissues (Figs. 5A and 5B). Furthermore, we observed increased luciferase expression in the tumor tissue in lungs that had small tumors and in lungs that had large tumors. These results indicate that increased uptake of liposome–DNA complex by tumor cells is not dependent on the tumor size or load.

doi:10.1016/S1525-0016(03)00004-2

Comparison of *luc* Expression in Alveolar Macrophages, Tumor-Bearing Lungs, and Non-Tumor-Bearing Lungs

We transfected alveolar macrophages isolated from UV2237m lung-tumor-bearing mice and non-tumor-bearing animals with DOTAP:Chol–*luc* complex and compared them to UV2237m tumor cells, which served as positive control. We determined *luc* expression 24 h after transfection. *luc* expression was significantly lower ($P = 0.0001$) in alveolar macrophages isolated from tumor-bearing animals than in alveolar macrophages from non-tumor-bearing animals (Fig. 6A). To eliminate the possibility that the difference in luciferase expression was due to cytotoxicity, cell viability assay was performed after transfection with DOTAP:Chol–*luc* DNA complex. No significant difference in cytotoxicity was observed between macrophages isolated from tumor-bearing animals and those isolated from non-tumor-bearing animals (Fig. 6B). Furthermore, analysis for luciferase expression in tumor-bearing and non-tumor-bearing lungs from which the alveolar macrophages were isolated demonstrated no significant difference in the expression levels (Fig. 6C). These results indicate that alveolar macrophages from lung-tumor-bearing animals are less transfectable than those from non-tumor-bearing animals.

In Vitro Comparison of *luc* Expression of Tumor Cells and Normal Cells Isolated from Primary Human Lung Tumor Explants

To determine whether differences in transgene expression also occurred in primary human lung tumor cells and normal cells, we obtained lung tissue explants from patients undergoing pulmonary resection for primary non-small-cell lung cancer. Tissue explants were confirmed as tumor or normal by histopathological analysis. Tumors were classified as poorly to moderately differentiated adenocarcinoma while normal pulmonary tissue comprised primarily fibroblasts. Cells isolated from normal and tumor tissue explants were transfected with DOTAP:Chol–*luc* DNA complex, and *luc* expression was determined 24 h after transfection. We observed significantly higher *luc* expression ($P = 0.001$) in tumor cells (2 ± 0.1 ng/mg protein) than in normal cells (0.06 ± 0.02 ng/mg protein), a finding consistent with those in established cultures of tumor and normal cells reported above.

Discussion

We recently demonstrated that very high levels of transgene expression can be achieved in tumor-bearing lungs when an extruded DOTAP:cholesterol–DNA complex is injected intravenously into both immunodeficient and immunocompetent animals and that this treatment has minimal toxicity [24]. In that study, repeated daily tail vein injections resulted in dose-dependent increases in transgene expression in lung-tumor-bearing animals and successfully cured one-third of mice with disseminated experimental metastases in a human xenograft model. The curative potential for disseminated disease and the apparent high levels of transgene expression in tumors were unexpected. One possibility for this observed therapeutic effect is that the uptake of liposome–DNA complexes by tumor cells and normal cells is the same, but tumor cells express the transgene more efficiently than normal cells. The second possibility is that the uptake of the complexes is increased in tumor cells over normal cells, which leads to higher expression levels of the transgene in the tumors. In the study presented here, we investigated the effects of the extruded DOTAP:Chol liposome–DNA complex on transgene expression in lung tumors and their surrounding normal tissues as well as the underlying mechanism both *in vitro* and *in vivo*.

Preliminary *in vitro* studies using tumor cells, normal fibroblasts, and endothelial cells of both murine and human origin demonstrated the DOTAP:Chol–*luc* DNA complex to be nontoxic to these cells. Analysis of these cells for transgene expression demonstrated increased *luc* expression in tumor cells over normal cells except endothelial cells. It is possible that the observed difference in transgene expression is due to differences in cellular proliferation rates between tumor and normal cells [30]. However, the differences observed in the present study cannot be attributed to cellular proliferation since the rate of proliferation of the different cell types used in the present study were similar except for NHBE and HUVEC (data not shown). The observed difference in transgene expression between tumor cells and normal cells might be due to any of several other known mechanisms, including differences in cell surface charge, phagocytic activity, endocytic activity, endosomal release, nuclear uptake, and transcriptional activity [31–36].

On the basis of these known differences, we studied the uptake of liposome–DNA complexes by normal and tumor cells using fluorescently labeled DOTAP:Chol liposome. Tumor cells had increased uptake of the liposome–DNA complexes over normal cells that correlated with increased luciferase activity. Surprisingly, endothelial cells also demonstrated increased uptake and expression. Since similar levels of luciferase activity were observed in tumor cells transfected with unlabeled DOTAP:Chol– and fluorescently labeled DOTAP:Chol–DNA complex, increased uptake cannot be attributed to the use of fluorescent lipid (data not shown). To identify the processes that mediate increased uptake of liposome–DNA complex by tumor cells, we examined surface charge using cationized ferritin, which attaches to the cell surface as a function of surface charge [37,38]. No significant difference was observed in the percentage binding of cationized ferritin to both tumor cells and NHBE and it did not correlate with the luciferase activity (data not shown). However, the increased uptake of liposome–DNA complex was observed

doi:10.1016/S1525-0016(03)00004-2

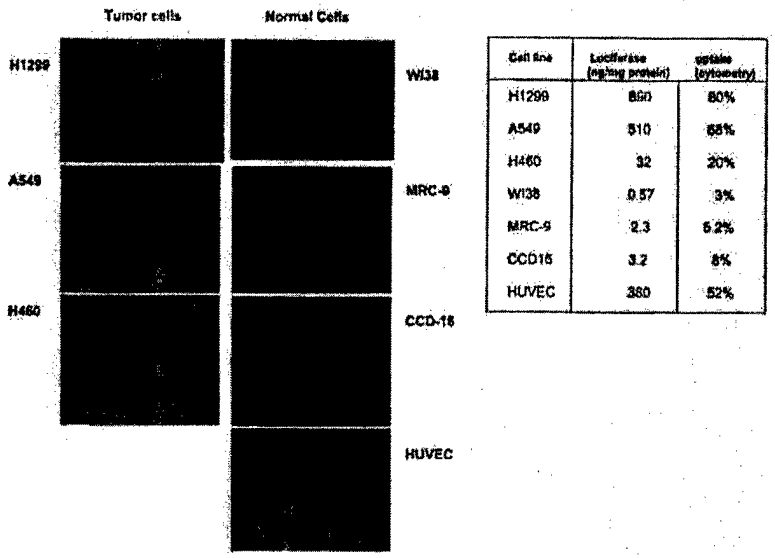

Cell line	Luciferase (ng/mg protein)	uptake (cytometry)
H1299	860	80%
A549	510	68%
H460	32	20%
WI38	0.57	3%
MRC-9	2.3	5.2%
CCD16	3.2	8%
HUVEC	380	52%

FIG. 2. Increased uptake of liposome–DNA complex by tumor cells. Tumor cells (H1299, A549, H460), normal cells (WI38, MRC-9, CCD-16), and endothelial cells (HUVEC) were transfected with fluorescently labeled DOTAP:Chol–DNA complex. Cells were analyzed for liposome–DNA complex uptake by fluorescence microscopy and flow cytometry and for luciferase expression by luminometer. Increased uptake was observed in tumor cells and in endothelial cells compared to normal cells. Increased uptake by tumor cells and HUVEC correlated with increased luciferase expression. Luciferase expression is expressed as nanograms per milligram of protein.

to be due to the phagocytic activity of the tumor cells since uptake was inhibited in the presence of cytochalasin B, an inhibitor of phagocytosis and pinocytosis. The ability of tumor cells to exhibit phagocytic activity is not surprising and is well documented [39]. However, greater phagocytic activity by tumor cells than by normal phagocytic and nonphagocytic cells treated with this liposome–DNA formulation has not been previously reported.

To explore further whether a similar phenomenon occurred *in vivo*, murine syngeneic lung-tumor-bearing animals were injected with the fluorescent liposome–DNA complex. They revealed increased uptake in the tumor cells compared to the surrounding normal cells. Furthermore, the increased uptake by tumors *in vivo* correlated with increased luciferase expression as demonstrated by immunohistochemical studies. Increased uptake of cationic liposome–DNA complexes by tumor cells *in vivo* following systemic delivery has been reported previously, consistent with the present report [40–43]. However, previous studies have attributed increased uptake of liposome–DNA complexes to leaky vasculature in the tumors. On the basis of our results, we believe that in addition to the presence of leaky vasculature in the tumors, increased phagocytic activity of the tumor cells is responsible for the observed increased uptake of DOTAP:Chol–DNA complex by tumor cells *in vivo*. Transgene expression in various other organs examined was very low (data not shown). Furthermore, real-time PCR analysis demonstrated low copy numbers of plasmid DNA in the liver, spleen, and ovaries compared to the lung (data not shown), suggesting that lung is the primary target for the intravenously injected DOTAP:Chol–DNA complex. This observation is in agreement with previously published reports [7,24]. However, in the presence of tumors in the

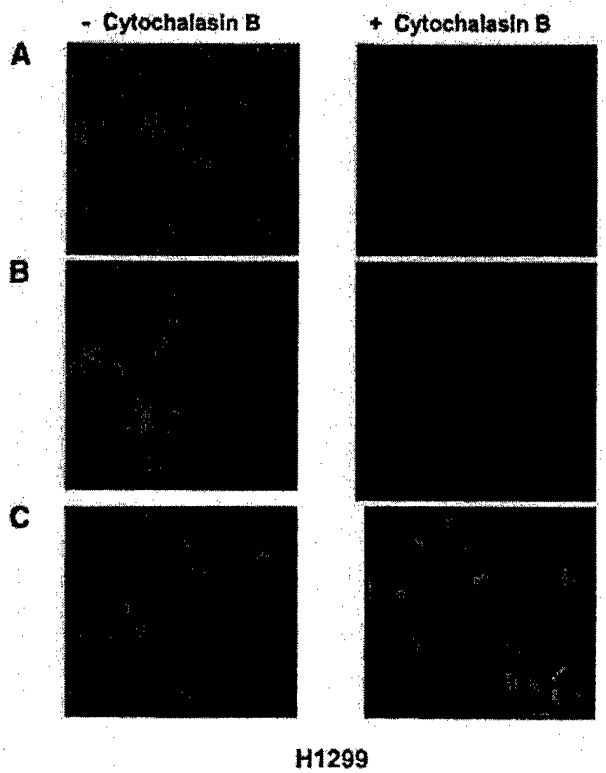

FIG. 3. Increased uptake of liposome–DNA complex by tumor cells is due to phagocytosis. Tumor cells (H1299) were transfected with 2 μm fluorescent microspheres (A) or fluorescently labeled DOTAP:Chol–*luc* DNA complex (B) in the presence or absence of cytochalasin B. Cytochalasin B, an inhibitor of phagocytosis, inhibited uptake of fluorescently labeled DOTAP:Chol–*luc* DNA complex by tumor cells (original magnification ×200). Hoechst staining of cells indicates intact nucleus (C).

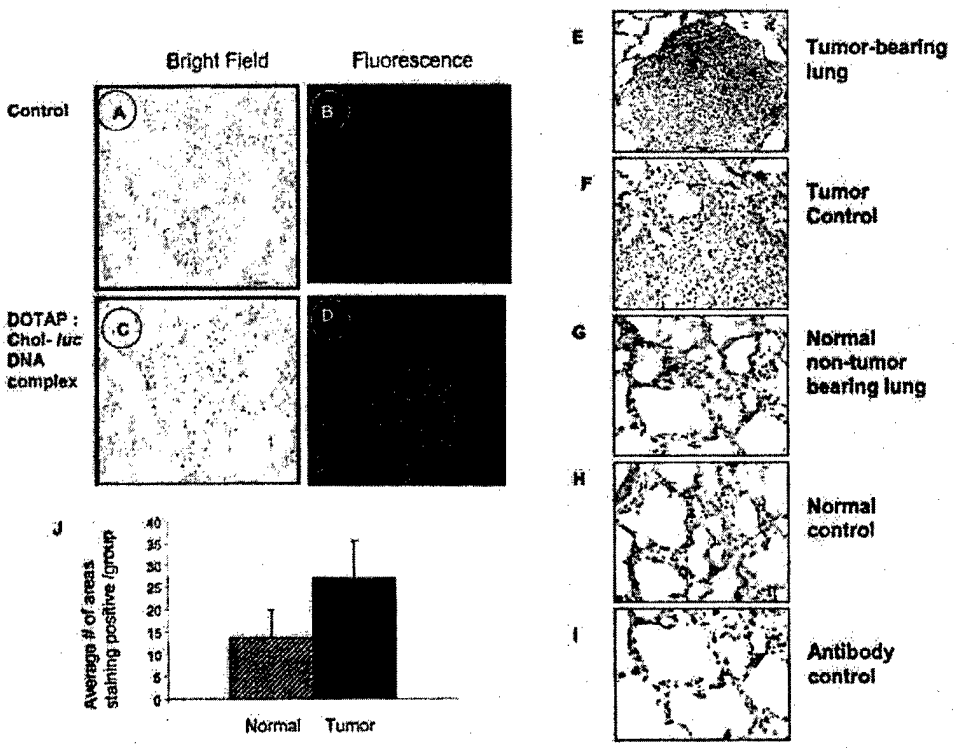

FIG. 4. Increased luciferase expression by lung tumors *in vivo* is due to increased uptake of liposome–DNA complex. UV2237m lung-tumor-bearing mice were injected with fluorescently labeled DOTAP:Chol–*luc* DNA complex via tail vein (C, D). Animals receiving no treatment served as controls (A, B). The animals were euthanized by CO_2 inhalation at 24 h after injection, and their lungs were isolated. Bright-field microscopy of hematoxylin-stained lung tissue sections revealed the presence of tumors in the lungs (A, C). Fluorescence microscopy of an unstained lung tissue section demonstrated greater fluorescence by tumor cells than by surrounding normal cells (D). Minimal fluorescence was observed in control tissue sections (B). Immunohistochemical analysis of lung tumor sections for luciferase protein demonstrated increased luciferase expression by tumors as indicated by the brown staining (E) compared to their surrounding normal tissue (H) and non-tumor-bearing lung tissue (G). Tumor-bearing lungs receiving no treatment (F) and tissue sections stained with no secondary antibody (I) served as controls (original magnification ×200). Arrows indicate cells staining positive for luciferase protein. Semiquantitative analysis of the areas staining positive indicated tumors staining more positively than surrounding normal tissues ($P = 0.01$) (J).

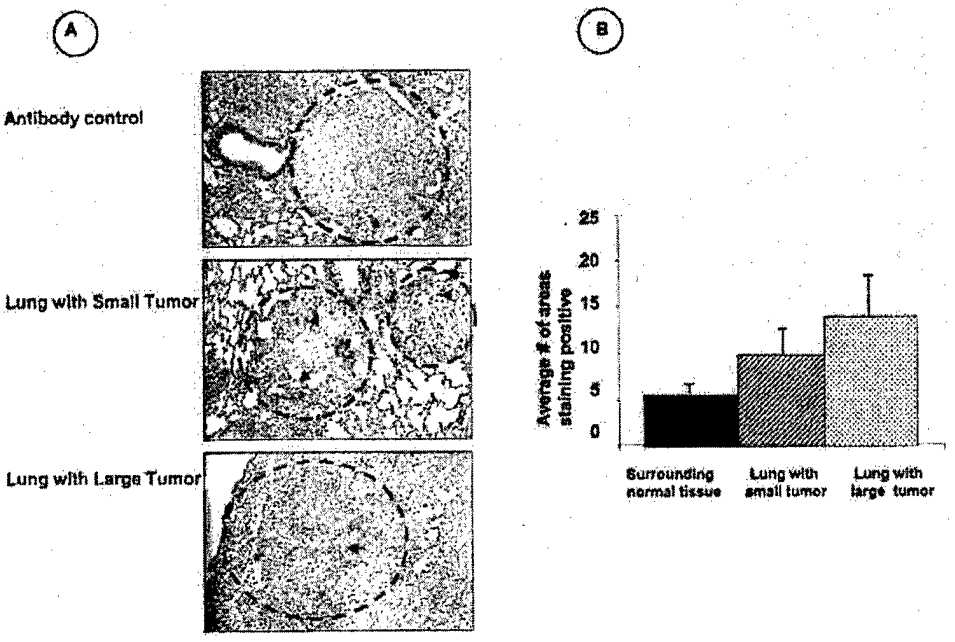

FIG. 5. Increased uptake of liposome–DNA complex by A549 lung tumors *in vivo*. Nude mice were injected with A549 lung tumor cells via tail vein. Animals were injected with DOTAP:Chol–*luc* DNA complex 2 weeks (small tumors) and 3 weeks (large tumors) after tumor cell inoculation. Tumor-bearing animals receiving no treatment served as controls. Immunohistochemical analysis of lungs harvested 24 h after treatment demonstrated higher *luc* expression ($P = 0.01$) in the tumors compared to surrounding normal tissues as indicated by the brown staining (A, B). Increased luciferase expression was observed in tumors that were small and in tumors that were large. Arrows indicate positive staining.

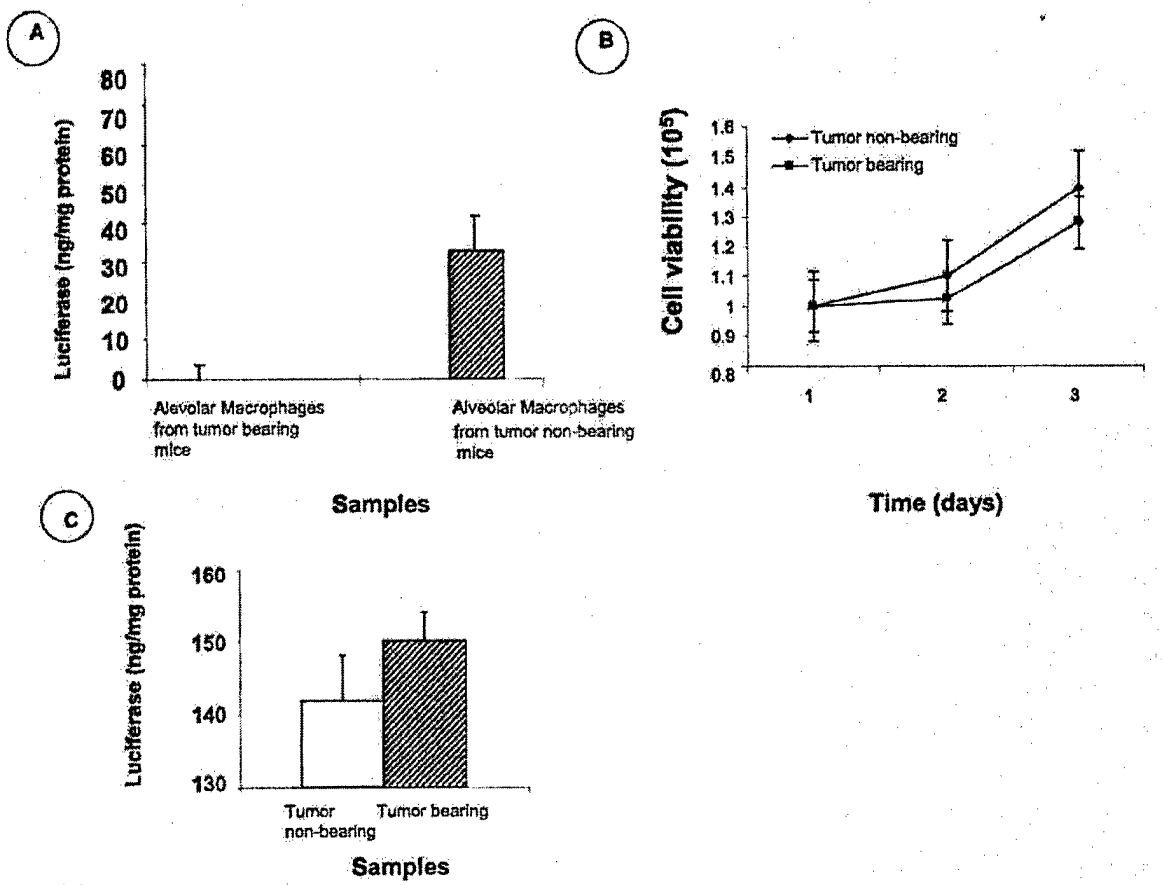

FIG. 6. Comparison of *luc* expression in alveolar macrophages isolated from tumor-bearing and non-tumor-bearing animals. Alveolar macrophages isolated from UV2237m lung-tumor-bearing and non-tumor-bearing animals were transfected with DOTAP:Chol–*luc* DNA complex and analyzed for *luc* expression 24 h after transfection. *luc* expression was significantly ($P = 0.001$) higher in macrophages isolated from non-tumor-bearing animals compared to those from tumor-bearing animals (A). Cell viability assay indicated no significant difference in proliferation between macrophages isolated from tumor-bearing animals and those isolated from non-tumor-bearing animals (B). Analysis of lungs for *luc* expression demonstrated no significant difference between tumor-bearing and non-tumor-bearing animals (C). *luc* activity was expressed as nanograms per milligram of total protein. Experiments were done in triplicate and bars denote standard errors.

lungs, increased uptake occurs in the tumors compared to the surrounding normal lung tissue. We next evaluated whether increased uptake of liposome–DNA complex is unique to murine tumors or is a generalized phenomenon that can observed with other tumors. Increased expression in human A549 lung tumors was observed compared to surrounding normal cells. Furthermore, the increased uptake of liposome–DNA complex was observed in lungs that had small tumors as well as in lungs that had large tumors, indicating that tumor size and number of tumors were not factors.

Additional evidence for increased uptake of the liposome–DNA complex by tumor cells was obtained from transmission electron microscope studies (data not shown). One argument that can be made from our *in vivo* results is that alveolar macrophages, which are also phagocytic, must phagocytose the injected complexes as efficiently as the tumor cells. Transfection of alveolar macrophages isolated from lung-tumor-bearing animals with DOTAP:Chol–*luc* DNA complex *in vitro* yielded significantly lower *luc* expression than transfection of macrophages from non-tumor-bearing animals. The findings presented in the present study contrast with previous reports demonstrating liposome–DNA complex to be a major target for macrophages and the reticuloendothelial system [44,45]. However, one major difference between our study and others is that we performed our experiments in tumor-bearing animals, while previously reported studies were based on experiments conducted in animals without tumors [44,45].

To test whether the pathophysiological state of the animal was important for normal functions of the macrophage, we conducted a separate but parallel set of experiments in which alveolar macrophages isolated from animals without tumors were transfected with DOTAP:Chol–*luc* DNA complex. *luc* expression was extremely significantly higher in macrophages from non-tumor-bearing compared to macrophages from tumor-bearing animals. One possibility for this difference is that the alveolar macrophages present in the tumor microenvironment are less phagocytic or are inactivated by factors produced by the tumor cells. Inactivation of macrophages in the tumor microenvironment has been previously demonstrated [46–48]. In fact alveolar macrophages from tumor-bearing animals were observed to be functionally inactive as indicated by stimulation assays (unpublished data).

Finally, increased uptake of liposome–DNA complex was demonstrated by transfecting primary tumor cells of poorly to moderately differentiated adenocarcinoma type and normal cells. Increased *luc* expression was observed in tumor cells compared to normal cells. The observation that tumor cells of poorly differentiated origin expressed *luc* at greater levels fits well with the findings of Matsui et al. [28], who showed that poorly differentiated airway epithelial cells phagocytose liposome–DNA complex more effectively, resulting in higher levels of transgene expression than in well-differentiated cells. Thus, transfection of primary tumor cells from tissue explants using DOTAP:Chol–DNA complex has been shown for the first time and supports our findings in established tumor cell lines.

Although the present study demonstrates that increased uptake of liposome–DNA complexes by tumor cells over surrounding normal cells is due to increased phagocytosis, it is also possible that other factors such as endosomal release, nuclear uptake, and increased transcription, may play a role. Further examination of these individual phenomena may help give a better understanding of the underlying differences between tumor and normal cells and in the development of an effective gene delivery vector. However, a note of caution is that the experimental metastases model used in the present study, although performed in such a way that the lung metastases are established, has limitations. It does not recapitulate the full sequence of events (from premalignancy to invasion and metastases) that primary tumors undergo. These cancer cells may undergo additional changes. Thus it may not be predictive of the responses of these tumors to a systemically delivered gene therapy agent. Therefore, the results of the present study, though relevant for lung cancer therapy, represent only an intermediate step on the path toward the development of a systemic gene transfer agent with broad utility.

Methods

Materials. All lipids (DOTAP, cholesterol) were purchased from Avanti Polar Lipids (Alabaster, AL). Fluorescent cholesterol analog 22-(*N*-(7-nitrobenz-2-oxa-1,3-diazol-4-yl)amino)-23,24-bisnor-5-cholen-3b-ol (fluoresterol) was purchased from Molecular Probes (Eugene, OR). RPMI 1640 medium, modified Eagle's medium (MEM), and fetal bovine serum (FBS) were purchased from GIBCO BRL Life Technologies (New York, NY). Polyclonal goat anti-human luciferase antibody was purchased from Promega Laboratories (Madison, WI).

Cell lines and animals. Human non-small-cell lung carcinoma (NSCLC) cell lines (A549, H1299, H460, H322, and H358) and normal human lung fibroblast cell lines (WI38, CCD16, and MRC-9) were obtained from American Type Culture Collection (ATCC; Rockville, MD) and maintained as per the supplier's recommendations. Human normal bronchial epithelial cells (NHBE) were obtained from Clonetics (Walkersville, MD) and maintained as recommended by the supplier. Murine fibrosarcoma cells (UV2237 and K1735) obtained from Dr. Isaiah Fidler, M. D. Anderson Cancer Center, and murine fibroblasts (NIH/3T3, and 10T1/2) purchased from ATCC were maintained in RPMI 1640 medium. Four- to six-week-old female C3H/Ncr mice (National Cancer Institute, Frederick, MD) and nude mice (Charles River Laboratory, Wilmington, DE) used in the study were maintained in a pathogen-free environment and handled according to institutional guidelines established for animal care and use.

Primary human lung cancer cells and normal epithelial cells were obtained from patients undergoing pulmonary resection. Tumor specimens were excised from surrounding normal epithelium and both normal parts and tumor parts were cut into smaller pieces. A pathologist used cytopathological and histopathological analysis to classify tissue specimens as tumor or normal. A total of five specimens from five individual patients were obtained. Tumor tissues from all five patients were histopathologically classified as poorly to moderately differentiated adenocarcinoma. Single-cell suspensions from tissues were prepared as previously described [25].

Purification of plasmids. The plasmid carrying the luciferase (*luc*) gene, under the control of the CMV40 promoter, was grown under ampicillin selection in the *Escherichia coli* host strain DH5α and purified by using an alkaline lysis method [7,26]. Endotoxin levels of purified plasmids were determined by using the chromogenic limulus amebocyte lysate kinetic assay kit (Kinetic-QCL; BioWhittaker, Walkersville, MD). The concentration and purity of the purified plasmid DNA were determined by $OD_{260/280}$ ratios.

Synthesis of liposomes and preparation of liposome–DNA complexes. Liposome (20 mM DOTAP:Chol) was synthesized and extruded through Whatman filters (Kent, UK) of decreasing sizes (1.0, 0.45, 0.2, and 0.1 nm) as previously described [7]. Fluorescently labeled DOTAP:Chol liposomes were synthesized using the same procedure except that cholesterol was replaced with a fluorescent cholesterol analog (fluoresterol) [27] and stored in the dark.

Particle size analysis. Freshly prepared liposome–DNA complexes were analyzed for mean particle size by using the N4 particle size analyzer (Coulter, Miami, FL). The mean particle sizes of the liposome–DNA complexes ranged between 300 and 325 nm.

In vitro transfection, cell viability, and luc gene expression. Human NSCLC cells, normal lung fibroblasts, NHBE cells, murine tumor cells (UV2237, K1735), and murine fibroblasts (NIH/3T3, 10T1/2), were seeded in six-well plates at 5×10^5 cells/well. The following day, cells were transfected with DOTAP:Chol–*luc* DNA complex (2.5 μg DNA) in serum-free medium for 3 h. Following transfection, cells were replenished with appropriate medium for each cell line containing 10% FBS, and incubation was continued. Cells were harvested at 24 and 48 h after transfection. Cell viability was determined by trypan blue exclusion assay and *luc* expression by using the luciferase assay kit (Promega) as previously described [24]. Luciferase expression was expressed as nanograms per milligram protein by comparing with recombinant luciferase protein. Cells that were not transfected served as controls.

In vitro uptake of liposome–DNA complex. Tumor cells and normal lung fibroblast cells were seeded in six-well plates at 5×10^5 cells/well. The following day, cells were transfected with fluorescently labeled DOTAP:Chol–*luc* DNA complex (2.5 μg DNA) in serum-free medium and analyzed after 3 h by fluorescence microscopy. Cells were analyzed for luciferase expression 24 h later, expressed as described above.

Phagocytic activity. H1299 tumor cells were seeded in six-well plates at 5×10^5 cells/well. The following day, cells were transfected with fluorescently labeled DOTAP:Chol–*luc* DNA complex (2.5 μg DNA) or positively charged 2-μm fluorescent microspheres (0.006%) (Molecular Probes, Eugene, Oregon) in serum-free medium in the absence or presence of 5 μg/ml cytochalasin B (Sigma Chemicals, St. Louis, MO) as previously described [28]. Three hours after transfection cells were stained with Hoechst 33348 and analyzed under fluorescence microscopy using a rhodamine, fluorescein, and UV filter.

Uptake and expression of DOTAP:Chol–luc DNA complex in vivo. UV2237 lung tumors were established in C3H mice by injecting 1×10^6 cells iv. Three weeks after tumor cell injection, uptake and expression of the liposome–DNA complex were determined using fluorescently labeled liposome–DNA complex. Animals were injected with fluorescent liposome–*luc* DNA complex (50 μg DNA) via a tail vein. At 24 h after treatment animals were euthanized, and their lungs were harvested and embedded in OCT medium for cryosectioning. Tissue sections (4 μm) were analyzed directly under fluorescence microscopy. Sections from non-tumor-bearing animals and untreated tumor-bearing animals served as controls.

In a separate set of experiments, A549 lung tumors were established in nude mice as previously described [24]. Briefly, A549 tumor cells (1×10^6) were injected into nude mice via the tail vein. Animals were injected with DOTAP:Chol–*luc* DNA complex at 2 weeks after tumor cell inoculation (low tumor load) or at 3 weeks (high tumor load) after inoculation. Animals were euthanized 24 h later and tumor-bearing lungs examined for luciferase protein expression by immunohistochemistry as described below.

Immunohistochemical analysis. Luciferase protein expression in the tissue sections was detected by immunohistochemical analysis as previously described [24] using a goat polyclonal luciferase antibody. Luc proteins were detected in tissues with DAB by enhancement using the avidin–biotin reaction ABC kit (Vector Laboratories, Burlingame, CA). The slides were then counterstained with hematoxylin and mounted with Aqua-Mount (Lerner Laboratories, Pittsburgh, PA). Controls included tissues with no primary antibody and only secondary antibody. The luciferase protein expression level in the tumor and the surrounding normal tissue was semiquantitatively determined by analysis image analysis using Optimas 6 software. Briefly, for each tissue section the total area staining positive as indicated by brown staining and the number of tumor areas staining positive was determined. The ratio of tumor area to total area of the tissue staining positive was then represented as percentage positive for tumor. A total of three samples comprising 15 sections for each group were analyzed in a blind fashion and represented as an average number for each sample.

luc expression in alveolar macrophages, normal lungs, and tumor-bearing lungs. UV2237 lung-tumor-bearing and non-tumor-bearing mice ($n = 15$) were injected with DOTAP:Chol–*luc* DNA complex (50 μg DNA) iv. Twenty-four hours later, animals were euthanized and alveolar macrophages from the lungs isolated as previously described [29]. Briefly, macrophages from bronchoalveolar lavage were collected and separated. More than 85% of the cell population was confirmed to be macrophages by a cytopathologist. The harvested macrophages were counted and plated into 6-well plates for luciferase expression (10^5 cells/well) and into 12-well plates for cell viability (1×10^4 cells/well). Plates were incubated overnight at 37°C in a 5% CO_2 incubator. Twenty-four hours later, macrophages were transfected either with naked *luc* plasmid DNA or with DOTAP:Chol–*luc* DNA complex (2.5 μg DNA). Twenty-four hours later cells were harvested and analyzed for viability by trypan blue exclusion assay or assayed for *luc* expression. *luc* expression was expressed as nanograms per milligram of protein. Experiments were performed in duplicate. Untransfected cells served as controls. In addition, the lungs harvested from tumor-bearing and non-tumor-bearing animals for isolating macrophages were analyzed for *luc* expression as described above.

luc expression in tumor cell explants. Primary cells isolated from normal and tumor tissue explants were plated at a density of 5×10^5 cells/well in six-well plates and transfected with DOTAP:Chol–*luc* DNA complex (2.5 μg DNA). Transfection and analysis for *luc* expression were performed as described above. Cells receiving no treatment served as controls.

Statistical analysis. The statistical significance of the experimental results was calculated using Student's *t* test and the Mann–Whitney test.

Acknowledgments

The authors thank C. Ralij Robinson, Debra Cameron, and Joyce M. Foud, Department of Pathology, for help in obtaining tissue specimens, and Peggy James for preparation of the manuscript. This work was supported in part by Public Health Service Grant P01CA78778-01A1 (J.A.R.), by the Specialized Program of Research Excellence (SPORE) in Lung Cancer (P50-CA70907) (J.A.R.), by the Texas Tobacco Settlement Fund, by the M. D. Anderson Cancer Center W. M. Keck Center for Cancer Gene Therapy, by Cancer Center Support (CORE) Grant CA 16672, by Career Development Award P50-CA70907-5 (R.R.), by a University of Texas M. D. Anderson Cancer Center Institutional Research Grant (R.R.), by a grant from the W. M. Keck Foundation Fund for Human Cancer Gene Prevention and Therapy (R.R.), by BESCT Lung Cancer Program Grant DAMD17-01-1-0689, by TARGET Lung Cancer Grant DAMD17-02-0706, by Texas Higher Education Coordinating Board ATP/ARP Grant 003657-0078-2001 (R.R.), and by a sponsored research agreement with Introgen Therapeutics, Inc.

RECEIVED FOR PUBLICATION JUNE 7, 2001; ACCEPTED JANUARY 2, 2003.

References

1. Swisher, S. G., *et al.* (1999). Adenoviral mediated p53 gene transfer in advanced non-small cell lung cancer. *J. Natl. Cancer Inst.* **91**: 763–771.
2. Roth, J. A., *et al.* (1996). Retrovirus-mediated wild-type *p53* gene transfer to tumors of patients with lung cancer. *Nat. Med.* **2**: 985–991.
3. Clayman, G. L., *et al.* (1998). Adenovirus-mediated *p53* gene transfer in patients with advanced recurrent head and neck squamous cell carcinoma. *J. Clin. Oncol.* **16**: 2221–2232.
4. Nabel, G. J., *et al.* (1993). Direct gene transfer with DNA–liposome complexes in melanoma: expression, biologic activity, and lack of toxicity in humans. *Proc. Natl. Acad. Sci. USA* **90**: 11307–11311.
5. Hung, M. C., Wang, S. C., and Hortobagyi, G. (1999). Targeted HER-2/neu-overexpressing cancer cells with transcriptional repressor genes delivered by cationic liposome). In *Non Viral Vectors for Gene Therapy* (L. Huang, M. C. Hung, and E. Wagner, Eds.), pp. 357–377. Academic Press, San Diego.
6. Nemunaitis, J., *et al.* (2000). Adenovirus-mediated p53 gene transfer in sequence with cisplatin to tumors of patients with non-small-cell lung cancer. *J. Clin Oncol.* **18**: 609–622.
7. Templeton, N. S., *et al.* (1997). Improved DNA: liposome complexes for increased systemic delivery and gene expression. *Nat. Biotechnol.* **15**: 647–652.
8. Kurane, S., *et al.* (1998). Targeted gene transfer of adenocarcinoma using a combination of tumor-specific antibody and tissue-specific promoter. *Jpn. J. Cancer Res.* **89**: 1212–1219.
9. Kunitomi, M., *et al.* (2000). Selective inhibition of hepatoma cells using diphtheria toxin A under the control of the promoter/enhancer region of the human alpha-fetoprotein gene. *Jpn. J. Cancer Res.* **91**: 343–350.
10. Chen, J., *et al.* (1998). Targeted in vivo delivery of therapeutic gene into experimental squamous cell carcinomas using anti-epidermal growth factor receptor antibody: immunogene approach. *Hum. Gene Ther.* **9**: 2673–2681.
11. Park, J. W., *et al.* (1995). Development of anti-p185HER2 immuno-liposomes for cancer therapy. *Proc. Natl. Acad. Sci. USA* **92**: 1327–1331.
12. Hara, T., *et al.* (1995). Receptor mediated transfer of pSV2CAT DNA to mouse liver cells using asialofetuin-labeled liposome. *Gene Ther.* **2**: 784–788.
13. Lee, R. J., and Huang, L. (1996). Folate-targeted, anionic liposome-entrapped polylysine-condensed DNA for tumor cell-specific gene transfer. *J. Biol. Chem.* **271**: 8481–8487.
14. Xu, L., Pirollo, K. F., and Chang, E. H. (1997). Transferrin-liposome-mediated p53 sensitization of squamous cell carcinoma of the head and neck to radiation in vitro. *Hum. Gene Ther.* **8**: 467–475.
15. Woodle, M. C., *et al.* (1992). Versatility of lipid compositions showing prolonged circulation with sterically stabilized liposomes. *Biochim. Biophys. Acta* **1105**: 193–200.

16. Harrington, K. J., *et al.* (2001). Effective targeting of solid tumors in patients with locally advanced cancers by radiolabeled pegylated liposomes. *Clin. Cancer Res.* **7**: 243–254.
17. Li, S., *et al.* (1998). Characterization of cationic lipid–protamine–DNA (LPD) complexes for intravenous gene delivery. *Gene Ther.* **5**: 930–997.
18. Li, S., *et al.* (1999). Effect of immune response on gene transfer to the lung via systemic administration of cationic lipidic vectors. *Am. J. Physiol.* **276**: L796–L804.
19. Freimark, B. D., *et al.* (1998). Cationic lipids enhance cytokine and cell influx levels in the lung following administration of plasmid–cationic lipid complexes. *J. Immunol.* **160**: 4580–4586.
20. Tan, Y., *et al.* (1999). The inhibitory role of CpG immunostimulatory motifs in cationic lipid vector mediated transgene expression in vivo. *Hum. Gene Ther.* **10**: 2153–2161.
21. Dow, S. W., *et al.* (1999). Lipid–DNA complexes induce potent activation of innate immune responses and antitumor activity when administered intravenously. *J. Immunol.* **163**: 1552–1561.
22. Qin, L., *et al.* (1997). Promoter attenuation in gene therapy: interferon-gamma and tumor necrosis factor alpha inhibit transgene expression. *Hum. Gene Ther.* **8**: 2019–2029.
23. Song, Y. K., *et al.* (1997). Characterization of cationic liposome-mediated gene transfer in vivo by intravenous administration. *Hum. Gene Ther.* **8**: 1585–1594.
24. Ramesh, R., *et al.* (2001). Successful treatment of primary and disseminated human lung cancers by systemic delivery of tumor suppressor genes using an improved liposome vector. *Mol. Ther.* **3**: 337–350. doi:10.1006/mthe.2001.0266.
25. Slocum, H. K., *et al.* (1981). Characterization of cells obtained by mechanical and enzymatic means from human melanoma, sarcoma and lung tumors. *Cancer Res.* **41**: 1428–1434.
26. Caenler, K. M. L., *et al.* (1999). Fetal gene transfer by transuterine injection of cationic liposome–DNA complexes. *Nat. Biotechnol.* **17**: 1188–1192.
27. Sparrow, C. P., *et al.* (1999). A fluorescent cholesterol analog traces cholesterol absorption in hamsters and is essential *in vivo* and *in vitro*. *J. Lipid Res.* **40**: 1747–1757.
28. Matsui, H., Johnson, L. G., Randell, S. H., and Boucher, R. C. (1997). Loss of binding and entry of liposome–DNA complexes decreases transfection efficiency in differentiated airway epithelial cells. *J. Biol. Chem.* **272**: 1117–1126.
29. Moxley, M. A., Baird, T. L., and Corbett, J. A. (2000). Adoptive transfer of acute lung injury. *Am. J. Physiol. Lung Cell Mol. Physiol.* **279**: 985–993.
30. Takeshita, S., *et al.* (1994). Increased gene expression after liposome-mediated arterial gene transfer associated with intimal smooth muscle cell proliferation. In vitro and in vivo findings in a rabbit model of vascular injury. *J. Clin. Invest.* **93**: 652–661.
31. Schramlova, J., *et al.* (1997). Electron microscopic demonstration of the interaction of liposomes and cells in vitro. *Folia Biol.* **43**: 161–167.
32. Mallery, S. R., *et al.* (2000). Controlled-release of doxorubicin from poly(lactide-co-glycolide) microspheres significantly enhances cytotoxicity against cultured AIDS-related Kaposi's sarcoma cells. *Anticancer Res.* **20**: 2817–2825.
33. Friend, D. S., Papahadjopoulos, D., and Debs, R. J. (1996). Endocytosis and intracellular processing accompanying transfection mediated by cationic liposome. *Biochim. Biophys. Acta* **1278**: 41–50.
34. Chu, Q., *et al.* (1999). Binding and uptake of cationic lipid: DNA complexes by polarized airway epithelial cells. *Hum. Gene Ther.* **10**: 25–36.
35. Barry, M. E., *et al.* (1999). Role of endogenous endonucleases and tissue site in transfection and CpG-mediated immune activation after naked DNA injection. *Hum. Gene Ther.* **10**: 2461–2480.
36. Zabner, J., *et al.* (1995). Cellular and molecular barriers to gene transfer by a cationic lipid. *J. Biol. Chem.* **270**: 18997–19007.
37. King, C. A., and Preston, T. M. (1977). Fluoresceinated cationised ferritin as a membrane probe for anionic sites at the cell surface. *FEBS Lett.* **73**: 59–63.
38. Williams, M. C. (1984). Endocytosis in alveolar type II cells: effect of charge and size of tracers. *Proc. Natl. Acad. Sci. USA* **81**: 6054–6058.
39. Ryser, H., Caulfield, J. B., and Aub, J. C. (1962). Studies on protein uptake by isolated tumor cells. *J. Cell Biol.* **14**: 255–268.
40. Anwer, K., *et al.* (2000). Cationic lipid-based delivery system for systemic cancer gene therapy. *Cancer Gene Ther.* **7**: 1156–1164.
41. Thurston, G., *et al.* (1998). Cationic liposomes target angiogenic endothelial cells in tumors and chronic inflammation in mice. *J. Clin. Invest.* **101**: 1401–1413.
42. Elmslie, R., Thamm, D., MacEwen, G., and Dow, S. (2001). Inhibition of tumor angiogenesis by systemic gene delivery in dogs with soft tissue sarcomas. *Proc. Am. Assoc. Cancer Res.* **42**: 704 [Abstract].
43. Liu, Y., *et al.* (1999). Systemic gene delivery expands the repertoire of effective anti-angiogenic agents. *J. Biol. Chem.* **274**: 13338–13344.
44. McLean, J. W., Thurston, G., and McDonald, D. M. (1999). Sites of uptake and expression of cationic liposome/DNA complexes injected intravenously). In *Non Viral Vectors for Gene Therapy* (L. Huang, M. C. Hung, and E. Wagner, Eds.), pp. 119–135. Academic Press, San Diego.
45. Liu, Y., *et al.* (1997). Factors influencing the efficiency of cationic liposome-mediated intravenous gene delivery. *Nat. Biotechnol.* **15**: 167–173.
46. Sotomayor, E. M., *et al.* (1991). Role of tumor-derived cytokines on the immune system of mice bearing a mammary adenocarcinoma. *J. Immunol.* **147**: 2816–2823.
47. Lopez, D. M., *et al.* (1996). Cytokine production by lymphoreticular cells from mammary tumor bearing mice: the role of tumor derived factors. *Anticancer Res.* **16**: 3923–3930.
48. Sotomayor, E. M., *et al.* (1993). Impaired activation of tumoricidal function in macrophages from mammary tumor bearers: the role of IFN-γ. *Int. J. Oncol.* **3**: 719–727.

Article

doi:10.1016/j.ymthe.2004.01.007

Persistent Transgene Expression Following Intravenous Administration of a Liposomal Complex: Role of Interleukin-10-Mediated Immune Suppression

Isao Ito,* Tomoyuki Saeki,† Imran Mohuiddin, Yuji Saito,†
Cynthia D. Branch, Ara Vaporciyan, Jack A. Roth, and Rajagopal Ramesh‡

Department of Thoracic and Cardiovascular Surgery, The University of Texas M. D. Anderson Cancer Center, Houston, TX 77030, USA

*Current address: Department of Surgery, Tokai University School of Medicine, Oolso Hospital, Kanagawa, Japan.
†Current address: Department of Surgery, Jikei University School of Medicine, Tokyo, Japan.

‡To whom correspondence and reprint requests should be addressed at the Department of Thoracic and Cardiovascular Surgery, The University of Texas M. D. Anderson Cancer Center, 1515 Holcombe Boulevard, Box 445, Houston, TX 77030, USA. Fax: (713) 794-4901. E-mail: rramesh@mdanderson.org.

Studies conducted in non-tumor-bearing, immunocompetent mice have shown that intravenous administration of liposome–DNA complex elicits an inflammatory response that results in a failure to sustain adequate transgene expression. In the present study, however, we investigated the effects of a cationic liposomal DOTAP:cholesterol (DOTAP:Chol)–DNA complex on cytokine production and transgene expression in both experimental lung tumor-bearing (TB) mice and non-tumor-bearing (NTB) syngeneic mice and nude mice. Intravenous injection of DOTAP:Chol–luciferase (*luc*) DNA complex resulted in tumor necrosis factor-α levels that were 50% lower and interleukin-10 levels that were 50–60% higher in TB mice than in NTB mice. Furthermore, a significant increase in luc expression ($P = 0.001$) that persisted for 7 days was observed in TB mice. In contrast, luc expression decreased significantly from day 1 to day 2 in NTB mice. Also, luc expression was two- to threefold higher in TB mice that were given multiple injections of DOTAP:Chol-*luc* complex than in mice who received a single injection. In contrast, luc expression was significantly suppressed following multiple injections in NTB mice ($P = 0.01$). Further analysis revealed IL-10 protein expression by the tumor cells in TB mice. Injection of anti-IL-10 antibody in TB mice resulted in a significant decrease in luc expression ($P = 0.01$) compared with that in mice injected with a control antibody. Based on these findings, we conclude that transgene expression persists in TB mice and is partly mediated by IL-10. Additionally, multiple injections of liposome–DNA complex can increase transgene expression in TB mice. These findings have clinical applications in the treatment of cancer.

Key Words: gene therapy, liposome, IL-10, cancer, cytokines, inflammation, lung, gene expression

Introduction

The development of efficient nonviral vectors that can deliver therapeutic genes when injected systemically will provide novel therapeutic options for the treatment of disseminated cancers. However, recent studies have demonstrated that liposomal vectors elicit an inflammatory response when injected systemically resulting in toxicity [1–7]. Induction of inflammatory responses due to the presence of immunostimulatory CpG sequences in plasmid DNA has been reported previously [8–12]. Associated with the inflammatory response is the production of proinflammatory cytokines (tumor necrosis factor- (TNF-α), interleukin-1 (IL-1), IL-6), which in turn have been shown to inhibit transgene expression [9,13]. Failure to achieve sustained transgene expression following repeated injections has also been attributed to the production of these proinflammatory cytokines [13]. Furthermore, a 3- to 4-day interval between injections was shown to be necessary to achieve sustained gene expression [14]. This need for injections at intervals has

1525-0016/$30.00

been attributed to the cells' "refractory" state [14]. Thus, the inability to increase transgene expression following repeated injections has been a major obstacle in the development of therapeutic applications of liposomes. Likewise, reducing the number of CpG sequences in the plasmid DNA has been shown to reduce the inflammatory response and increase transgene expression [15]. These results, however, were obtained from studies of non-tumor-bearing (NTB), immunocompetent animals.

In contrast to these reports, we recently demonstrated effective gene transfer to experimental lung tumors in mice following intravenous injections of extruded DOTAP:cholesterol (DOTAP:Chol)–DNA:liposome complex [16]. In that study, although animals were treated with repeated injections, the relative effectiveness of multiple treatments was not studied. However, the major difference between the results of our study and those of others is that we conducted experiments in tumor-bearing (TB) animals, while others studied NTB animals. It is therefore possible that the pathophysiological condition of the animal may influence transgene expression following intravenous administration of the liposome:DNA complex.

Several preclinical and clinical studies have demonstrated functional alterations of immune cells (macrophages, neutrophils, and T cells) resulting in immune suppression in lung cancer [17–21]. These alterations have been attributed to several factors, including the production of immunosuppressive factors by tumor cells [22–25] and alterations in the immune cell receptors [26]. On the basis of these reports, we speculated that TB and NTB animals might respond differently to liposome:DNA complexes administered intravenously.

In the present study, we investigated the effects of intravenous administration of DOTAP:Chol–DNA complex on the cytokine profile and transgene expression of lung TB and NTB immunocompetent mice and nude mice.

RESULTS

Cytokine Expression Following Intravenous Injection of DOTAP:Chol–luciferase (*luc*) DNA Complex

Prior to the start of the experiment, we established lung tumors by injecting 1×10^6 UV2237m or A549 cells intravenously via the tail vein into female C3H and nude mice, respectively. Ten to fifteen days after injection of tumor cells, we treated the animals with DOTAP:Chol-*luc* complex. Note that at this time the tumors are well established in the lungs and can be detected histologically (data not shown). Animals receiving no treatment served as controls. In a separate but parallel set of experiments, NTB animals were also untreated or treated with DOTAP:Chol-*luc* complex.

We analyzed serum samples from NTB and lung TB C3H mice injected with DOTAP:Chol-*luc* DNA complex for cytokine levels at regular time intervals. TNF-α, IL-1α, interferon-γ (IFN-γ), and IL-10 were produced by TB and NTB mice, with maximum peak levels observed in both groups at 2 h for TNF-α and at 6 h for IFN-γ (Fig. 1A). We observed maximum levels of IL-10 expression at 12 and 24 h in both groups. However, TNF-α levels were 50% lower in TB mice than in NTB mice. In contrast, IL-10 levels were 50–60% higher in TB mice (Fig. 1A). The expression of cytokines was time dependent over the 24-h postinjection period. IL-1α levels did not differ significantly in animals from the two groups. Cytokine levels except those of IL-1α were not detected in control animals that were not treated, were treated with naked plasmid DNA, or were treated with an empty liposome (data not shown).

To examine whether a similar phenomenon occurred in other tumor models we also determined serum cytokine levels in A549 lung TB nude mice and compared them to NTB nude mice (Fig. 1B). Both TB and NTB nude mice produced TNF-α, IL-1α, IFN-γ, and IL-10. The time courses for production of these cytokines were identical to those observed in C3H mice described above, with maximum production occurring at 2 h for TNF-α and at 6 h for IFN-γ. Similarly, we observed maximum levels of IL-10 expression at 12 and 24 h in TB and NTB mice. However, the levels of the cytokine produced in nude mice differed from the levels produced in C3H mice (Figs. 1A and 1B). Furthermore, TNF-α levels were moderately reduced in TB nude mice compared to NTB mice. The difference in the reduction of TNF-α levels in TB C3H mice and TB nude mice can be attributed to strain difference. However, other possibilities may exist and need additional investigation. In TB C3H mice we observed a significant increase in IL-1α at 12 h compared to NTB mice. This increase in IL-1α levels is not clear and needs additional investigation. These results demonstrate that increased IL-10 is produced in TB mice compared to NTB mice following injection of DOTAP:Chol–DNA complex.

Transgene Expression Persists in Tumor-Bearing Mice Following a Single Intravenous Injection of DOTAP:Chol-*luc* DNA Complex

To determine transgene expression *in vivo*, we injected lung TB and NTB C3H mice intravenously via the tail vein with DOTAP:Chol-*luc* DNA complex and removed their lungs at different times and analyzed them for luc activity. We observed luc expression in both TB and NTB mice, with maximal gene expression occurring 24 h after treatment in both groups (Fig. 2A). However, luc expression in NTB mice had decreased by 48 h after treatment and reached baseline levels by 72 h; luc expression remained at baseline through day 7. In contrast, levels of luc activity remained significantly higher than baseline ($P = 0.01$) in TB animals through

doi:10.1016/j.ymthe.2004.01.007

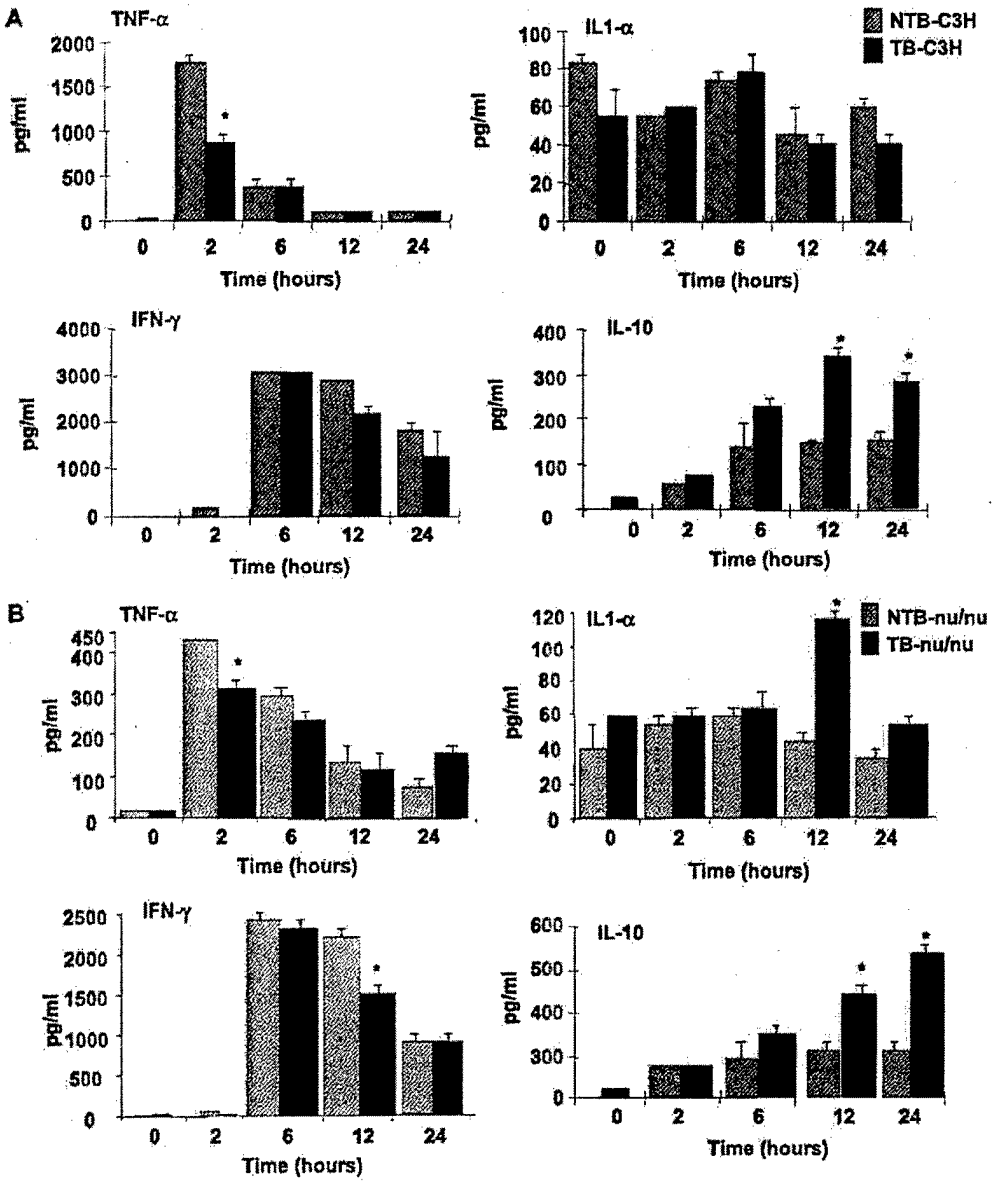

FIG. 1. Cytokine profile following systemic injection of DOTAP:Chol-*luc* DNA complex. Serum was collected from lung TB and NTB mice at 0, 2, 6, 12, and 24 h after injection of DOTAP:Chol-*luc* DNA complex (50 μg) and was assayed for cytokines (TNF-α, IL-1α, IFN-γ, IL-10) using ELISA. Untreated TB and NTB animals served as controls from each group. (A) Cytokine profile in UV2337m TB and NTB mice. (B) Cytokine profile in A549 lung TB and NTB mice. Data represent the average cytokine levels in four animals per group per time point.

day 7. However, a trend in decline (50%) of luc expression was observed on day 7 compared to day 1 in TB animals.

We performed an analysis of transgene expression in A549 lung TB and NTB nude mice. We observed increased luc expression at 24 h in both groups after treatment (Fig. 2B). However, significant levels of luc expression persisted in TB mice until day 7 compared to NTB mice. Although luc expression in NTB mice did not reach baseline levels as observed in C3H mice, luc expression was significantly reduced by day 3 compared to day 1. These results demonstrate that persistent trans-

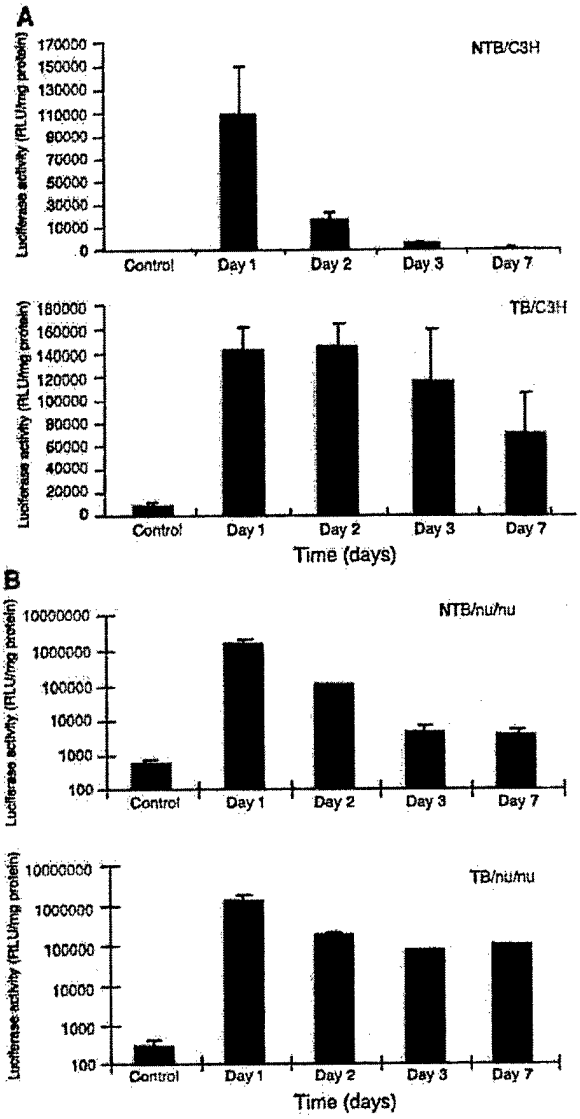

FIG. 2. Persistent transgene expression occurs in TB animals. (A) UV2237M TB and NTB C3H mice and (B) A549 TB and NTB nude mice were injected with DOTAP:Chol-*luc* DNA complex via the tail vein. Their lungs were resected on days 1, 2, 3, and 7 after treatment and analyzed for luc expression. Luc activity is expressed as relative light units (RLU) per milligram of total protein. Each time point represents the average luc activity in four animals. Bars represent standard deviation.

gene expression occurs in TB mice compared to NTB mice.

Repeated Injections of DOTAP:Chol-*luc* DNA Complex Result in Increased Transgene Expression

We next evaluated the effects of repeated injections on transgene expression in both lung TB and NTB C3H mice and nude mice. We injected the animals via the tail vein with the DOTAP:Chol-*luc* DNA complex either one time or daily for 3 consecutive days. We analyzed lungs for luc activity 48 h after injection. In C3H mice luc expression was observed in both TB and NTB mice. In TB C3H mice, however, luc expression was twofold greater ($P = 0.001$) in mice treated three times than in mice treated once (Fig. 3A). In contrast, NTB mice treated three times expressed significantly lower levels of luc than did those treated only once ($P = 0.01$). Similarly, analysis of luc expression in TB nude mice and NTB nude mice demonstrated expression of luc expression (Fig. 3B). TB nude mice that received three treatments demonstrated threefold increase in luc expression compared to mice treated once ($P = 0.001$). In contrast, NTB mice that received three treatments showed decreased luc expression compared to mice receiving a single treatment. Thus, expression of luc in TB mice receiving multiple treatments was higher than in TB mice receiving a single treatment. Furthermore, luc expression in TB mice receiving multiple treatments was higher than in NTB mice that received multiple treatments. These results demonstrate that repeated injections of DOTAP:Chol–DNA complex in TB mice results in increased transgene expression and are in agreement with our previous results [16].

Lung Tumor Cells Express IL-10

To determine whether tumor cells contributed to the production of IL-10, we stained lungs from UV2237m TB and NTB mice for murine IL-10. TB lungs, especially tumor cells, stained intensely for IL-10 (Fig. 4). We also observed staining of infiltrating lymphocytes in the lung tumor sections. In contrast, NTB lung cells showed very little IL-10 expression. We also observed IL-10 protein expression in human lung tumor cell lines and in clinical specimens from patients diagnosed with lung cancer (data not shown). To determine further the levels of IL-10 produced by UV2237m tumor cells, we analyzed cell culture supernatants for IL-10 production by ELISA. The level of IL-10 produced by murine tumor cells was approximately 30 pg/ml (data not shown). These results demonstrate that tumor cells in addition to lymphocytes produce IL-10.

Alveolar Macrophages from Lung TB Mice Are Less Responsive to Stimulation

Since we had observed IL-10 production by lung TB mice, we examined the suppressive effects of IL-10 on alveolar macrophages by macrophage activation assay. We plated alveolar macrophages isolated from lung TB and NTB C3H mice in 96-well plates and stimulated them with phorbol myristic acetate (PMA). We measured stimulation of macrophages by addition of 2′,7′-dicholorofluorescein diacetate. Macrophages from NTB mice showed significantly more activation ($P = 0.001$) than those from TB mice (Fig. 5A). Furthermore, a significant reduction

doi:10.1016/j.ymthe.2004.01.007

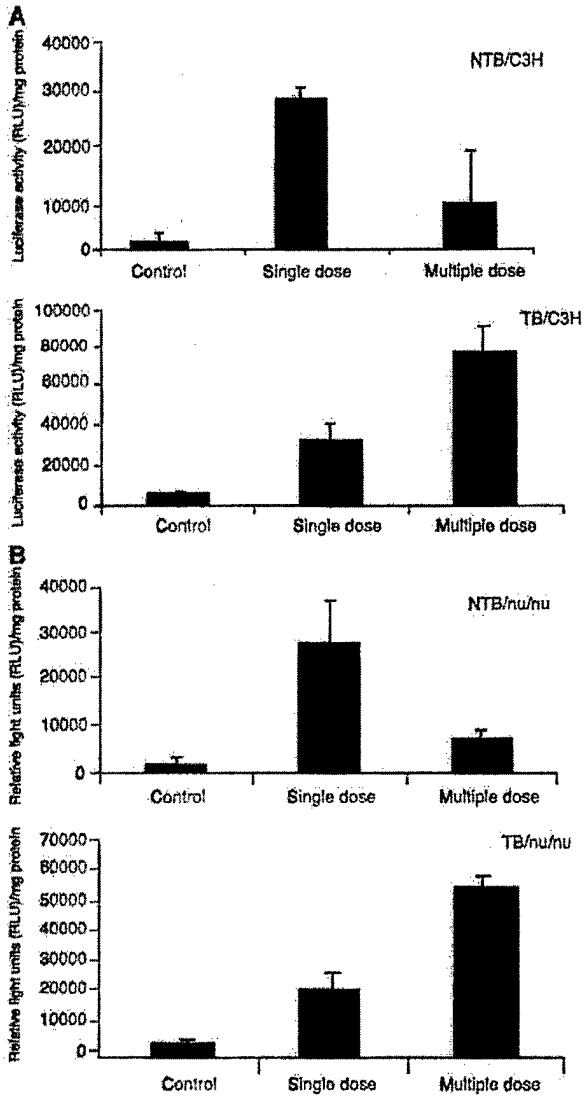

FIG. 3. Multiple treatments resulted in increased transgene expression. TB and NTB C3H or nude mice injected either once or three times with DOTAP:Chol-*luc* DNA complex (50 μg DNA/dose) via a tail vein were assayed for luc activity. (A) A twofold increase in luc activity was observed in TB C3H mice receiving three treatments compared with those receiving one treatment. In contrast, luc activity in NTB C3H mice receiving three treatments was significantly lower that in those receiving one treatment. (B) Luc activity in TB nude mice receiving three treatments showed two- to threefold increase in luc expression compared with those receiving one treatment. In contrast, luc activity in NTB nude mice receiving three treatments was significantly lower than in those receiving one treatment. Luc activity is expressed as RLU per milligram of total protein. Bars represent standard deviation.

($P = 0.01$) in TNF-α production by alveolar macrophages from TB mice was observed when the macrophages were treated with LPS (Fig. 5B). In contrast, macrophages from NTB animals produced higher levels of TNF-α when treated with LPS.

Neutralization of IL-10 in TB Animals Results in Decreased Transgene Expression

To determine the effects of IL-10 on transgene expression *in vivo*, we injected TB animals with a mouse IL-10 neutralizing antibody 24 h prior to injection of DOTAP:-Chol-*luc* DNA complex. Analysis of the lungs 48 h after liposome–DNA complex injection showed a significant reduction in luc expression ($P \leq 0.01$) compared with that in TB animals that were not treated with the neutralizing IL-10 antibody (DOTAP:Chol-*luc* complex

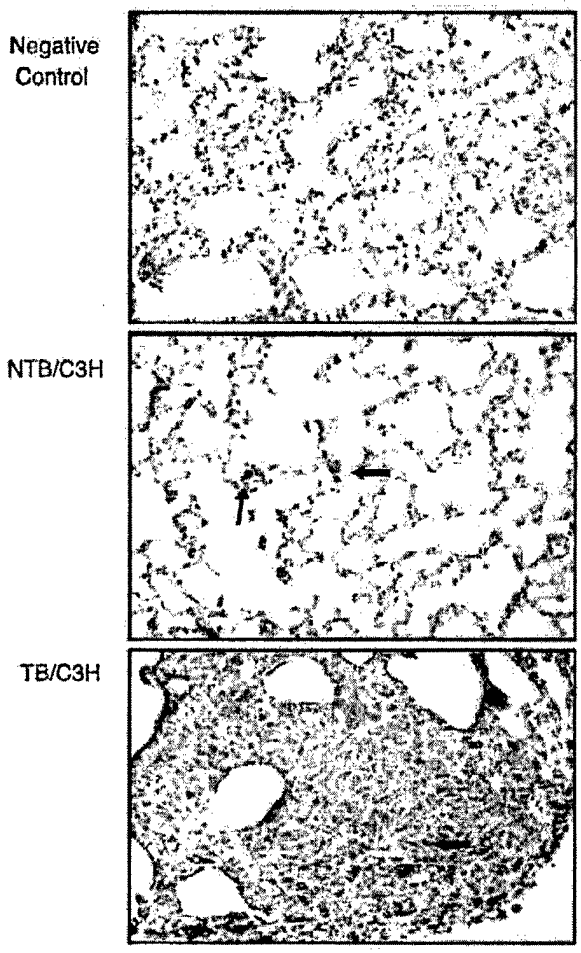

FIG. 4. UV2237M tumor cells produce IL-10. UV2237m TB and NTB lung tissue sections were immunohistochemically stained for mouse IL-10. IL-10 was detected in lung tissue sections as indicated by the intense brown cytoplasmic staining. Staining for IL-10 in NTB lung tissue sections was weak. Tissue sections stained only with secondary antibody served as negative controls. Arrows indicate cells staining positive for IL-10.

only) and in animals that were treated with a control isotypic antibody (Fig. 6). Luc expression was also significantly lower in animals that received the control IgG antibody than in animals that did not receive any antibody treatment, indicating nonspecific inhibition of gene expression.

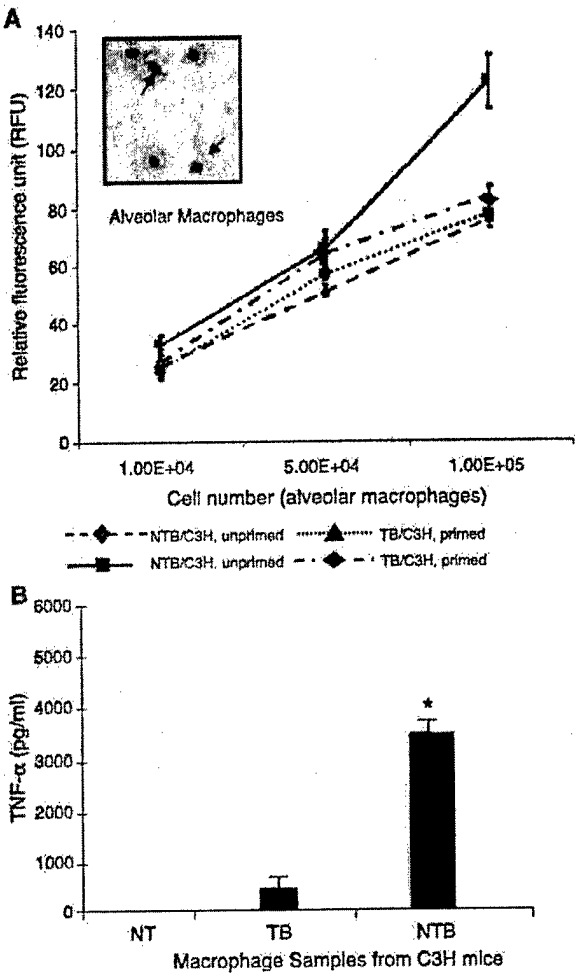

FIG. 5. Alveolar macrophages (AM) from TB mice are less responsive to PMA stimulation. (A) Alveolar macrophages from TB and TNB C3H mice were plated in 96-well plates at various cell densities and incubated overnight at 37°C. Cells were exposed to PMA (1 μg/ml) for 1 h. After 1 h, 2′,7′ dichlorofluorescein diacetate was added and incubated for 30 min. Macrophage stimulation was detected by measuring the fluorescence intensity at 530 nm in a spectrofluorometer. AM from TNB animals responded to PMA stimulation significantly compared to those from TB animals. AM not exposed to PMA served as controls. Values shown are the means of quadruplicate wells. Bars represent standard error. (B) Alveolar macrophages from TB and TNB C3H mice were treated with LPS (1 μg/ml) for 24 h and the culture medium was assayed for murine TNF-α. A significant amount of TNF-α protein was detectable in the medium from AM harvested from NTB mice compared to that from TB mice. AM not exposed to LPS served as negative control (NT). Positive control included was provided in the kit. Data are represented as the means of quadruplicate wells. Bars represent standard error.

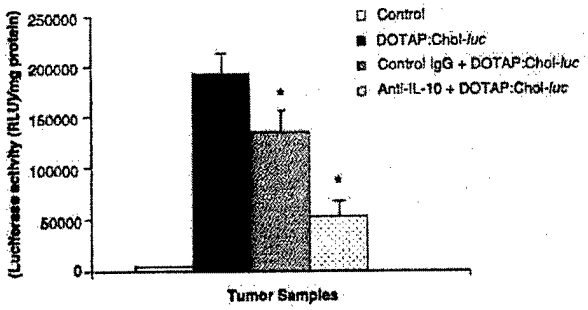

FIG. 6. Neutralization of IL-10 in TB mice results in decreased transgene expression. Lung tumors were established in C3H mice by injecting UV2237m cells (1×10^6 cells/well) via the tail vein. Three weeks later, animals were divided into three groups and treated as follows: group 1 received no treatment, group 2 received an intraperitoneal (ip) injection of isotypic control IgG antibody (20 μg), and group 3 received an ip injection of neutralizing anti-IL-10 antibody (20 μg). Twenty-four hours later, animals from all three groups were treated with DOTAP:Chol-*luc* DNA complex via the tail vein. Animals that did not receive any treatment served as negative controls. Animals were euthanized 48 h after injection, and their lungs were removed and analyzed for luc activity. Luc expression was significantly less in animals from group 3 than in those from groups 1 and 2. A significant reduction in luc activity was also observed in group 2 compared with group 1, indicating nonspecific inhibition. Luc activity is expressed as RLU per milligram of total protein. Bars represent standard error.

DISCUSSION

The present study demonstrated for the first time that transgene expression persists in TB animals but not in NTB animals. Although persistent transgene expression was demonstrated in TB animals *in vivo*, the cell types that primarily express the transgene were not investigated in the present study. However, we have recently demonstrated that tumor cells primarily express the transgene at higher levels compared to surrounding normal tissues, both *in vitro* and *in vivo* [27]. Based on our previous observation we can speculate that persistent transgene expression primarily occurs in tumor cells. However, expression can also persist in other cell types that are present within the tumor microenvironment.

The underlying mechanism for the prolonged transgene expression was next examined. It is possible that inflammatory cytokines (TNF-α, IL-1α), which have been previously shown to inhibit transgene expression, may be altered in TB animals or that the immune cells (macrophages, neutrophils, T cells) that produce the inflammatory cytokines are functionally altered in TB animals [17–25]. To understand the mechanism involved, we measured cytokine expression levels in TB and NTB animals after intravenous administration of a liposome–DNA complex. TNF-α, IL-1α, IFN-γ, and IL-10 expression was observed in both TB animals and NTB animals.

doi:10.1016/j.ymthe.2004.01.007

However, TNF-α levels were 50% lower in TB animals. The role of TNF-α as a proinflammatory cytokine and its primary source, alveolar macrophages, are well known [26,28]. It appears that the alveolar macrophages may be functionally suppressed by soluble factors released by the *in situ* tumor [29,30]. As a result, production of TNF-α and other cytokines triggered by TNF-α may also be reduced, thereby allowing persistent transgene expression. The observation that IL-10 levels were higher in TB animals supports this hypothesis. The inhibitory effects of IL-10 on macrophages and TNF-α production are well documented [29–34]. Similarly, IL-10 expression by tumor cells has been previously demonstrated [35–39]. Based on these reports we next determined the source of IL-10. Immunohistochemical analysis of TB lung tissue sections demonstrated intense cytoplasmic staining for IL-10 in UV2237m tumor cells. Additionally, *in vitro* assay demonstrated IL-10 production by tumor cells albeit at low levels. The difference in *in vitro* and *in vivo* IL-10 levels can be due to several reasons that include difference in tumor cell number, cell type (tumor cells, epithelial cells, mononuclear cells, etc.), and *in situ* tumor conditions. In support of this are the findings that IL-10 staining was also observed in infiltrating lymphocytes. Additionally, IL-10 expression was also observed in the surrounding normal tissues that comprised fibroblast and epithelial cells. In contrast, IL-10 expression was observed to be minimal in NTB lung tissue sections.

IL-10 is a Th_2-type cytokine that acts as an immunosuppressor under a variety of conditions and is primarily produced by macrophages and T cells [36,37]. Production of IL-10 and its effects on immune cells have been shown in a variety of human cancers [39–43]. In fact, it has been shown that IL-10 production by tumor cells suppresses the immune functions of macrophages and T cells, thereby promoting tumor growth [44–49]. Furthermore, when present in the tumor microenvironment, macrophages can produce IL-10 in an autocrine fashion, resulting in functional inactivation [36,37]. Based on these findings, we examined the effect of exogenous IL-10 on transgene expression in alveolar macrophages from TB and NTB animals, as well as the effect of PMA on macrophage stimulation as a measure of function. Transgene expression was significantly higher in alveolar macrophages from NTB animals compared with those from TB animals. However, in the presence of IL-10, transgene expression was significantly suppressed in macrophages from NTB animals (data not shown). This observation suggests two possibilities: the transgene expression was transcriptionally suppressed or the macrophages were functionally inactivated, resulting in a decreased inflammatory response. We believe that functional inactivation is a more likely mechanism since alveolar macrophages from TB animals, when exposed to PMA, were not stimulated. In contrast, macrophages from NTB animals, when exposed to PMA, were observed to undergo significant stimulation. Furthermore, a reduction in TNF-α production was observed in alveolar macrophages from TB animals compared with those from NTB animals.

The difference in the alveolar macrophage function may partly explain the observed increase in transgene expression in TB mice receiving repeated treatments compared to NTB mice. Although persistent and increased transgene expression has been demonstrated in TB mice it is not clear whether this is a local effect or a systemic effect. Preliminary studies from our laboratory indicate that this is primarily a local effect that is influenced by the tumor microenvironment. Analysis of transgene expression in mice bearing subcutaneous tumors demonstrated an increase in transgene expression over time when the mice were injected with a single dose of DOTAP:Chol-*luc* DNA complex. However, analysis of the normal tumor-free lungs from these subcutaneous tumor-bearing mice demonstrated a decrease in transgene expression over time (data not shown). We are currently conducting additional studies in the laboratory to delineate the local versus systemic effect.

Finally, the effect of IL-10 on transgene expression was demonstrated by *in vivo* neutralization experiments conducted in TB animals. Treating animals with a neutralizing anti-IL-10 antibody prior to injection of the liposome–DNA complex resulted in an approximately 50% reduction in luc expression compared with animals that did not receive the neutralizing antibody and animals that received an isotypic control antibody. These results indicate that blocking IL-10 activity might restore the inflammatory response, thereby resulting in decreased transgene expression levels. Based on these results, we would like to propose the following hypothesis: Tumor cells in addition to infiltrating inflammatory cells produce IL-10, which acts in an autocrine fashion to promote its growth and produce more IL-10 and in paracrine fashion to suppress the functions of immune cells (macrophages, monocytes, T cells) present in the tumor microenvironment or stimulate them to produce more IL-10 (Fig. 7). Intravenous injection of liposome–DNA complex in TB animals thus results in a diminished inflammatory response, resulting in persistent and enhanced transgene expression following repeated multiple treatments and in therapeutic effect. A note of caution in that apart from IL-10 other immunosuppressive factors produced by the tumor cells may also play a role in the observed persistent transgene expression. We are currently investigating these possibilities in the laboratory.

In conclusion, this study demonstrates for the first time that a diminished inflammatory response, partly mediated by IL-10, leads to persistent gene expression in lung TB animals.. This phenomenon allows multiple treatments, resulting in enhanced transgene expression and therapeutic efficacy. Thus, repeated delivery of ther-

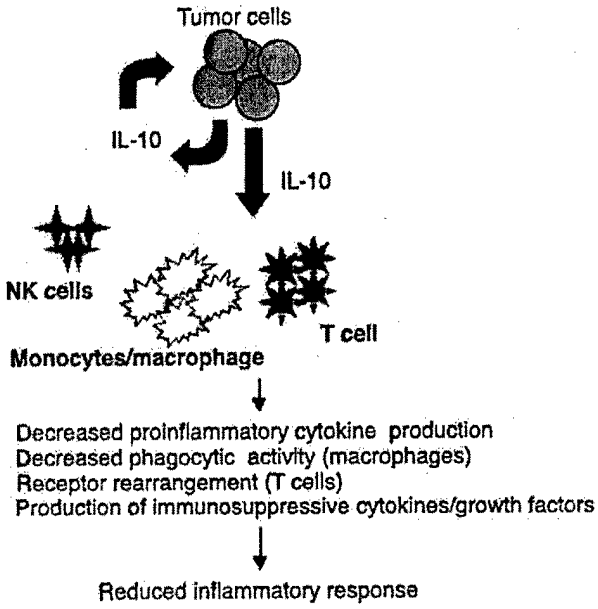

FIG. 7. Schematic representation of IL-10 production by tumor cells and its effects on immune cells and inflammatory response. Tumor cells produce IL-10, which acts in an autocrine manner to promote growth and production of more IL-10 and in a paracrine fashion to suppress the functions of immune cells (macrophages, T cells) present in the tumor milieu by decreasing phagocytic activity and proinflammatory cytokine production (IL-1, TNF-α, IL-6) and rearranging receptors. Intravenous injection of liposome–DNA complex in TB animals thus results in a diminished inflammatory response, resulting in persistent and enhanced transgene expression after repeated treatments and in a therapeutic effect.

apeutic genes encapsulated in a liposome is feasible for lung cancer treatment.

MATERIALS AND METHODS

Materials. All lipids (DOTAP, cholesterol) were purchased from Avanti Polar Lipids (Alabaster, AL, USA). RPMI 1640 medium and fetal bovine serum were purchased from Invitrogen (New York, NY, USA). Polyclonal goat anti-human IL-10 antibody and anti-mouse IL-10 monoclonal antibody were obtained from Pharmingen (San Diego, CA, USA). Anti-IL-10 neutralizing antibody was purchased from Biosource International (Camarillo, CA, USA) and isotypic IgG antibody was purchased from Sigma Chemicals (St. Louis, MO, USA).

Cell lines and animals. Murine fibrosarcoma cells (UV2237) obtained from Dr. Isaiah Fidler, M. D. Anderson Cancer Center, were maintained in RPMI 1640 medium. Human A549 lung cancer cells were obtained from American Tissue Culture Collection (Rockville, MD, USA) and maintained in Hams/F12 medium. Cells were regularly passaged and tested for the presence of mycoplasma. Four- to six-week-old female C3H/Ncr mice (National Cancer Institute, Frederick, MD, USA) and athymic nude mice (Charles River Laboratories, Wilmington, DE, USA) used in the study were maintained in a pathogen-free environment and handled according to institutional guidelines established for animal care and use.

Purification of plasmids. Growth and purification of plasmids used in the study have been described previously [16].

Synthesis, preparation, and particle size analysis of liposome:DNA complexes. The synthesis of 20 mM DOTAP:Chol, the preparation of liposome:DNA complexes, and the determination of mean particle sizes in freshly prepared liposome:DNA complexes have been described previously [16,50].

Cytokine profiles in TB and NTB mice. Experimental lung tumors were established by injecting 1×10^6 UV2237m and A549 tumor cells into C3H/Ncr mice and nude mice, respectively. Tumor cells were injected via the tail vein. Ten to fifteen days after tumor cell injection animals were given a single intravenous injection of DOTAP:Chol-*luc* DNA complex (50 μg DNA) via the tail vein. Cytokine profiles were determined in these lung TB mice and compared with those in NTB mice after treatment. Serum samples were collected from the animals at 0, 2, 6, 12, and 24 h after injection; the samples were stored at −80°C and analyzed for cytokines using murine cytokine ELISA kits (R&D Systems, Inc., Minneapolis, MN, USA). Assays were performed in quadruplicate according to the manufacturer's guidelines.

Luciferase expression in TB and NTB animals. Lung TB and NTB C3H mice and nude mice were injected with a single dose of DOTAP:Chol-*luc* DNA:liposome complex (50 μg DNA) via the tail vein. On days 1, 2, 3, and 7 after injection, the animals were euthanized using CO_2 inhalation, and their lungs were resected. The lungs were snap-frozen in liquid nitrogen and analyzed for luc expression as described previously [50]. Luc was expressed as relative light units (RLU) per milligram of protein. Four animals were analyzed at each of the time points. The experiments were performed twice, and the results reported were the average means of the two experiments.

In vivo luc expression following single and multiple treatments with DOTAP:Chol-luc DNA complex. UV2237m lung TB ($n = 15$) and NTB ($n = 15$) C3H mice and A549 lung TB ($n = 15$) and NTB ($n = 15$) nude mice were divided into three groups each. Five TB and five NTB mice were treated with intravenous injections of DOTAP:Chol-*luc* DNA complex once, and five more from each group were treated daily for 3 days. Five TB mice and five NTB mice did not receive any treatment and served as controls. The mice were euthanized by CO_2 inhalation 48 h after treatment, and their lungs were resected. Total protein was extracted from the lung tissues by homogenizing the tissue in lysis buffer and assaying for luc activity as described above (RLU/mg of protein). Each experiment was performed at least three times and the results reported were the means of the three experiments.

Immunohistochemical analysis. UV2237m lung tumors removed from C3H/Ncr mice were fixed in 10% buffered formalin before being embedded in paraffin and cut into 4-μm sections. Sections were stained for murine IL-10 expression as previously described [16]. Briefly, tissue sections were treated with 0.3% H_2O_2 in methanol for 30 min to block endogenous peroxidase activity and subsequently incubated with normal goat serum for 30 min at room temperature. Following incubation, slides were treated with goat polyclonal anti-IL-10 antibody for 60 min. After 30 min more of incubation with an appropriate secondary antibody (provided with the ABC kit; Vector Laboratories, Burlingame, CA, USA), IL-10 protein was detected in tissues using diaminobenzidine enhanced with the avidin–biotin reaction ABC kit. The slides were then counterstained with hematoxylin and mounted with Aqua-Mount (Lerner Laboratories, Pittsburgh, PA, USA).

Alveolar macrophage activation assay. Alveolar macrophages from TB and NTB C3H mice were acquired as previously described [27,51]. Briefly, the mice were euthanized using CO_2 inhalation, and an incision was made in the region of the trachea. Once the trachea was exposed, a 21-gauge needle was inserted, and 10 ml of sterile Hanks' balanced salt solution (HBSS) was infused into the lungs with a 10-ml syringe. After the lungs were flushed with HBSS, the remaining liquid was aspirated into a sterile Falcon centrifuge tube placed on ice. The procedure was repeated three to four times. Cells were centrifuged at 1000 rpm for 10 min, washed

doi:10.1016/j.ymthe.2004.01.007

thrice, and seeded in six-well plates. An aliquot of the cell preparation was subjected to cytopathological analysis, and more than 90% of the cells were identified as macrophages. Alveolar macrophages thus isolated were used for activation assay. Briefly, alveolar macrophages from TB and NTB C3H mice were plated in 96-well plates at varying cell densities (1×10^4, 5×10^4, and 5×10^5 cells/well) and incubated overnight at 37°C. The next day, PMA was added (1 μg/ml) to the wells and incubated. One hour after incubation with PMA, 2′,7′-dicholorofluorescein diacetate (DCFH-DA; Sigma Chemicals) was added to the wells. DCFH-DA is a substrate that is converted into a fluorescent 2′,7′-dicholorofluorescein product by intracellular oxidants produced by alveolar macrophages [52]. The amount of fluorescence produced is directly proportional to the macrophage response (activation) to PMA. This test is routinely used to measure alveolar macrophage response to various stress inducers [53,54]. Plates were incubated in the dark for 30 min, after which the plates were read in a spectrofluorometer at 485 nm excitation and 530 nm emissions. Values were obtained, and the results reported were the average of quadruplicates for each sample.

In a separate but parallel set of experiments, alveolar macrophages from TB and NTB C3H mice were plated in 96-well plates and incubated overnight. The next day, cells were treated with LPS (1 μg/ml; Sigma Chemicals) and culture supernatants assayed for TNF-α production using a murine TNF-α ELISA kit (R&D Systems). Untreated cells served as negative controls. Positive control was provided in the kit.

In vivo neutralization experiments with anti-IL-10 antibody. UV2237m lung TB C3H mice ($n = 15$) were divided into three groups and treated as follows: group 1 ($n = 5$) received no treatment, group 2 ($n = 5$) received a single intraperitoneal injection of control isotypic IgG antibody (20 μg); and group 3 ($n = 5$) received a single intraperitoneal injection of murine anti-IL-10 neutralizing antibody (20 μg). Twenty-four hours later, mice from all three groups were injected with DOTAP:Chol-*luc* DNA complex (50 μg DNA) via the tail vein. An additional group of animals ($n = 5$) that did not receive any treatment served as negative control for these experiments. The mice were euthanized 48 h after treatment with DOTAP:Chol-*luc*, and their lungs were resected and analyzed for luc activity as described above. Experiments were performed twice and results reported were the averages of two separate experiments.

Statistical analysis. The statistical significance of the experimental results was calculated using ANOVA. A P value <0.05 was considered significant.

Acknowledgments

The authors thank Dawn Chalaire for editorial assistance and Alma Vega for preparation of the manuscript. This work was supported in part by the Texas Higher Education Coordinating Board, ATP/ARP Grant 003657-0078-2001 (R.R.); by a Career Development Award from The University of Texas M. D. Anderson Cancer Center, SPORE in Lung Cancer P50-CA70907-5 (R.R.); by Public Health Service Grant P01CA78778-01A1 (J.A.R.); by the Texas Tobacco Settlement Fund; by the BESCT Lung Cancer Program, Grant DAMD17-01-1-0689 (Project 3); by TARGET Lung Cancer Grant DAMD17-02-1-0706 (Project 7); by an Institutional Research Grant (R.R.); by a Grant from the W. M. Keck Foundation (R.R.); by Cancer Center Support (CORE) Grant CA16672; and by a sponsored research agreement with Introgen Therapeutics, Inc.

RECEIVED FOR PUBLICATION MAY 26, 2003; ACCEPTED JANUARY 9, 2004.

References

1. Whitmore, M., *et al.* (1999). LPD lipopolyplex initiates a potent cytokine response and inhibits tumor growth. *Gene Ther.* **6:** 1867–1875.
2. Huang, L., and Li, S. (1997). Liposomal gene delivery—a complex package. *Nat. Biotechnol.* **15:** 620–621.
3. Li, S., *et al.* (1999). Effect of immune response on gene transfer to the lung via systemic administration of cationic lipidic vectors. *Am. J. Physiol.* **276:** L796–L804.
4. Freimark, B. D., *et al.* (1998). Cationic lipids enhance cytokine and cell influx levels in the lung following administration of plasmid–cationic lipid complexes. *J. Immunol.* **160:** 4580–4586.
5. Whitmore, M., *et al.* (1999). LPD lipopolyplex initiates a potent cytokine response and inhibits tumor growth. *Gene Ther.* **6:** 1867–1875.
6. Daw, S. W., *et al.* (1999). Lipid–DNA complexes induce potent activation of innate immune responses and antitumor activity when administered intravenously. *J. Immunol.* **163:** 1552–1561.
7. Scheule, R. K. J., *et al.* (1997). Basis of pulmonary toxicity associated with cationic lipid-mediated gene transfer to the mammalian lung. *Hum. Gene Ther.* **8:** 689–707.
8. Tousignant, J. D., *et al.* (2003). DNA sequences in cationic lipid:pDNA-mediated systemic toxicities. *Hum. Gene Ther.* **14:** 203–214.
9. Tan, Y., *et al.* (1999). The inhibitory role of CpG immunostimulatory motifs in cationic lipid vector mediated transgene expression in vivo. *Hum. Gene Ther.* **10:** 2153–2161.
10. Yew, N. S., *et al.* (2000). Reduced inflammatory response to plasmid DNA vectors by elimination and inhibition of immunostimulatory CpG motifs. *Mol. Ther.* **1:** 255–262.
11. Schwartz, D. A., *et al.* (1997). Cpg motifs in bacterial DNA cause inflammation in the lower respiratory tract. *J. Clin. Invest.* **100:** 68–73.
12. McLachlan, G., *et al.* (2000). Bacterial DNA is implicated in the inflammatory response to delivery of DNA/DOTAP to mouse lungs. *Gene Ther.* **7:** 384–392.
13. Qin, L., *et al.* (1997). Promoter attenuation in gene therapy: Interferon-gamma and tumor necrosis factor alpha inhibit transgene expression. *Hum. Gene Ther.* **8:** 2019–2029.
14. Li, S., *et al.* (1998). Characterization of cationic lipid–protamine–DNA (LPD) complexes for intravenous gene delivery. *Gene Ther.* **5:** 930–997.
15. Yew, N. S., *et al.* (2002). Cpg-depleted plasmid DNA vectors with enhanced safety and long-term gene expression *in vivo*. *Mol. Ther.* **5:** 731–738.
16. Ramesh, R., *et al.* (2001). Successful treatment of primary and disseminated human lung cancers by systemic delivery of tumor suppressor genes using an improved liposome vector. *Mol. Ther.* **3:** 337–350.
17. Kuda, T., Yasumoto, K., Yano, T., Nakahashi, H., Sugimachi, K., and Nomoto, K. (1987). Role of antitumor activity of alveolar macrophages in lung cancer patients. *Cancer Res.* **47:** 2199–2202.
18. Sotomayor, E. M., *et al.* (1993). Impaired activation of tumoricidal function in macrophages from mammary tumor bearers: the role of IFN-γ. *Int. J. Oncol.* **3:** 719–727.
19. Sotomayor, E. M., *et al.* (1995). Decreased macrophage mediated cytotoxicity in mammary tumor bearing mice is related to alterations in nitric oxide production and/or release. *Int. J. Cancer* **60:** 660–667.
20. Mazzoccoli, G., *et al.* (1999). Lymphocyte subpopulations anomalies in lung cancer patients and relationship to the stage of disease. *In Vivo* **13:** 205–209.
21. Koutsami, M. K., Gorgoulis, V. G., Kastrinakis, N. G., Asimacopoulos, P. J., and Kittas, C. (2002). Prognostic factors in non-small cell lung carcinoma. *Anticancer Res.* **22:** 347–374.
22. Solomayor, E. M., *et al.* (1991). Role of tumor-derived cytokines on the immune system of mice bearing a mammary adenocarcinoma. *J. Immunol.* **147:** 2816–2823.
23. Lopez, D. M., *et al.* (1996). Cytokine production by lymphoreticular cells from mammary tumor bearing mice: the role of tumor-derived factors. *Anticancer Res.* **16:** 3923–3930.
24. Lopez, D. M., *et al.* (1991). Modulation of the immune system by mammary tumor derived factors. *Cancer Invest.* **9:** 643–653.
25. Ghosh, P., *et al.* (1995). Gradual loss of T-helper 1 populations in spleen of mice during progressive tumor growth. *J. Natl. Cancer Inst.* **87:** 1478–1483.
26. Beutler, B., and Cerami, A. (1989). The biology of cachectin/TNF-α as primary mediator of host response. *Annu. Rev. Immunol.* **7:** 625.
27. Ito, I., *et al.* (2003). Increased uptake of liposomal–DNA complexes by lung metastases following intravenous administration. *Mol. Ther.* **7:** 409–418.
28. Vassali, P. (1992). The pathophysiology of tumor necrosis factor. *Annu. Rev. Immunol.* **10:** 411.
29. Fiorentino, D. F., Zlotnik, A., Mossman, T., Howard, M., and O'Garra, A. (1991). IL-10 inhibits cytokine production by activated macrophages. *J. Immunol.* **147:** 3815.
30. Alleva, D. G., Burger, C. J., and Elgert, K. D. (1994). Tumor-induced regulation of suppressor macrophage nitric oxide and TNF-α production: role of tumor-derived IL-10, TGF-β, and prostaglandin E_2. *J. Immunol.* **153:** 1674.
31. Kambayashi, T., Alexander, H. R., Fong, M., and Strassman, G. (1995). Potential involvement of IL-10 in suppressing tumor-associated macrophages. *J. Immunol.* **154:** 3383–3390.
32. Bogdan, C. Y., Vodovotz, Y., and Nathan, C. (1991). Macrophage deactivation by interleukin-10. *J. Exp. Med.* **174:** 1549.
33. de Waal Malefyt, R., Abrams, J., Bennet, B., Figdor, C., and deVries, J. E. (1991). Interleukin-10 inhibits cytokine synthesis by human monocytes: an autoregulatory role for IL-10 production by monocytes. *J. Exp. Med.* **174:** 1209.
34. Strassman, G., Koota, V., Finkelman, F., Fong, M., and Kambayashi, T. (1994). Evidence for the involvement of interleukin 10 in the differential deactivation of murine peritoneal macrophages by prostaglandin E2. *J. Exp. Med.* **180:** 2365.
35. Castl, G. A., *et al.* (1993). Interleukin 10 production by human carcinoma cell lines and its relation to interleukin 6 expression. *Int. J. Cancer.* **55:** 96.
36. Howard, M., and O'Garra, A. (1992). Biological properties of interleukin 10. *Immunol. Today* **13:** 198.

37. Moore, K. W., *et al.* (1993). Interleukin-10. *Annu. Rev. Immunol.* **11:** 165–190.
38. Loercher, A. E., *et al.* (1999). Identification of an IL-10 producing HLA DR negative monocyte subset in the malignant ascites of patients with ovarian carcinoma that inhibits cytokine protein expression and proliferation of autologous T cells. *J. Immunol.* **163:** 6251–6260.
39. Gotlieb, W. H., *et al.* (1992). Presence of interleukin-10 (IL-10) in the ascites of patients with ovarian and other intra-abdominal cancers. *Cytokine* **4:** 385–390.
40. de Waal Malefyt, R., *et al.* (1991). IL-10 and viral IL-10 strongly reduce antigen-specific human T cell proliferation by diminishing the antigen-presenting capacity of monocytes via downregulation of class II MHC expression. *J. Exp. Med.* **174:** 915–924.
41. Fiorentino, D. F., *et al.* (1991). IL-10 acts on the antigen-presenting cells to inhibit cytokine production by Th1 cells. *J. Immunol.* **146:** 3444–3451.
42. Ding, L., and Shevach, E. M. (1992). IL-10 inhibits mitogen-induced T cell proliferation by selectively inhibiting macrophage costimulatory function. *J. Immunol.* **148:** 3133–3139.
43. Bogdan, C., Vodovotz, Y., and Nathan, C. (1991). Macrophage deactivation by interleukin-10. *J. Exp. Med.* **174:** 1549–1555.
44. Armstrong, L., Jordan, N., and Miller, A. (1996). Interleukin-10 (IL-10) regulation of tumor necrosis factor alpha (TNF-alpha) from human alveolar macrophages and peripheral blood monocytes. *Thorax* **51:** 143–149.
45. Ralph, P., *et al.* (1992). IL-10, T lymphocyte inhibitor of human blood cell production of IL-1 and tumor necrosis factor. *J. Immunol.* **148:** 808–814.
46. de Waal Malefyt, R., Yssel, H., and de Vries, J. E. (1993). Direct effects of IL-10 on subsets of human CD4$^+$ T cell clones and resting T cells. *J. Immunol.* **150:** 4754–4765.
47. Yue, F. Y., *et al.* (1997). Interleukin-10 is a growth factor for human melanoma cells and downregulates HLA class-I, HLA class-II and ICAM-1 molecules. *Int. J. Cancer* **71:** 630–637.
48. Lu, Z. Y., *et al.* (1995). Interleukin-10 is a proliferation factor but not differentiation factor for human myeloma cells. *Blood* **85:** 2521–2527.
49. Masood, R., *et al.* (1995). Interleukin-10 is an autocrine growth factor for acquired immunodeficiency syndrome-related B-cell lymphoma. *Blood* **85:** 3423–3430.
50. Templeton, N. S., *et al.* (1997). Improved DNA:liposome complexes for increased systemic delivery and gene expression. *Nat. Biotechnol.* **15:** 647–652.
51. Moxley, M. A., Baird, T. L., and Corbett, J. A. (2000). Adoptive transfer of acute lung injury. *Am. J. Physiol. Lung Cell Mol. Physiol.* **279:** 985–993.
52. Wan, X. S., Zhou, Z., and Kennedy, A. R. (2003). Adaptation of the dichlorofluorescein assay for detection of radiation-induced oxidative stress in cultured cells. *Radiat. Res.* **160:** 622–630.
53. Goldsmith, C. A., Imrich, A., Danaee, H., Ning, Y. Y., and Kobzik, L. (1998). Analysis of air pollution particulate-mediated oxidant stress in alveolar macrophages. *J. Toxicol. Environ. Health A* **54:** 529–545.
54. Tsai, J. J., Kao, M. H., and Han, S. H. (1999). The respiratory burst activity of activated eosinophils in atopic asthmatics. *Int. Arch. Allergy Immunol.* **119:** 38–44.

[CANCER RESEARCH 64, 2969–2976, May 1, 2004]

Advances in Brief

Myristoylation of the Fus1 Protein Is Required for Tumor Suppression in Human Lung Cancer Cells

Futoshi Uno,[1] Jiichiro Sasaki,[1] Masahiko Nishizaki,[1] Giovanni Carboni,[1] Kai Xu,[1] Edward N. Atkinson,[2] Masashi Kondo,[3] John D. Minna,[3] Jack A. Roth,[1] and Lin Ji[1]

[1]Section of Thoracic Molecular Oncology, Department of Thoracic and Cardiovascular Surgery, and [2]Department of Biomathematics, The University of Texas M. D. Anderson Cancer Center, Houston, Texas; [3]Department of Internal Medicine and Pharmacology, Hamon Center for Therapeutic Oncology Research, The University of Texas Southwestern Medical Center, Dallas, Texas

Abstract

***FUS1* is a novel tumor suppressor gene identified in the human chromosome 3p21.3 region that is deleted in many cancers. Using surface-enhanced laser desorption/ionization mass spectrometric analysis on an anti-Fus1-antibody-capture ProteinChip array, we identified wild-type Fus1 as an N-myristoylated protein. N-myristoylation is a protein modification process in which a 14-carbon myristoyl group is cotranslationally and covalently added to the NH_2-terminal glycine residue of the nascent polypeptide. Loss of expression or a defect of myristoylation of the Fus1 protein was observed in human primary lung cancer and cancer cell lines. A myristoylation-deficient mutant of the Fus1 protein abrogated its ability to inhibit tumor cell-induced clonogenicity *in vitro*, to induce apoptosis in lung tumor cells, and to suppress the growth of tumor xenografts and lung metastases *in vivo* and rendered it susceptible to rapid proteasome-dependent degradation. Our results show that myristoylation is required for Fus1-mediated tumor-suppressing activity and suggest a novel mechanism for the inactivation of tumor suppressors in lung cancer and a role for deficient posttranslational modification in tumor suppressor-gene-mediated carcinogenesis.**

Introduction

Tumor suppressor genes (TSGs) play a major role in the pathogenesis of human lung and other cancers. Lung cancer cells harbor mutations and deletions in multiple known oncogenes and TSGs; however, genetic alterations and allelic losses on the short arm of chromosome 3 are among the most frequent and earliest cancer abnormalities detected in the pathogenesis of lung cancers and have been shown to occur in 96% of non-small cell lung cancers (NSCLCs) and in 78% of preneoplastic lung lesions (1). The frequent and early loss of heterozygosity and the overlapping homozygous deletions observed in the 3p21.3 region in lung and breast cancers suggest a critical role of one or more 3p21.3 genes as "gatekeepers" in the molecular pathogenesis of these cancers (2, 3).

The novel *FUS1* TSG is one of the candidate TSGs that have been identified in a 120-kb homozygous deletion region in human chromosome 3p21.3 (2, 4, 5). The cloned cDNA of *FUS1* (GenBank accession no. AF055479) is 333 bp in length and encodes a protein of 110 amino acid residues (Fig. 1*A*). However, the *FUS1* gene does not show homology with any known genes and proteins in databases. We have previously demonstrated that exogenous expression of the wild-type (wt) *FUS1* by plasmid- or adenoviral vector-mediated gene transfer significantly inhibits tumor cell growth, induces apoptosis, and alters cell cycle kinetics in 3p21.3-deficient NSCLC cells *in vitro* and efficiently suppresses tumor growth and inhibits tumor progression and metastases in various human lung cancer xenograft mouse models (4–6). However, the mechanisms involved in the inactivation of the *FUS1* gene in primary human cancers and in *FUS1*-mediated tumor suppression remain unknown. On the basis of our findings reported here, we hypothesize that loss of expression, haploinsufficiency, and deficiency of posttranslational modification of Fus1 protein may lead to loss of its tumor-suppression function and play an important role in lung cancer development.

Materials and Methods

Cell Lines and Cell Culture. The human NSCLC cell lines A549, NCI-H1299, NCI-H358, NCI-H226, NCI-H322, and NCI-H460, with various 3p21.3 and *p53* gene status as described previously (7, 8), and a normal human lung fibroblast cell line, WI-38, were used for *in vitro* and *in vivo* experiments. The A549 line was maintained in Ham's F12 medium supplemented with 10% FCS. The H1299, H358, H226, H322, and H460 lines were maintained in RPMI 1640 supplemented with 10% FCS and 5% glutamine. Normal fibroblast WI-38 cells were cultured in MEM supplemented with 10% FCS and 5% glutamine.

Tumor Cell-Induced Clonogenicity Assay. To analyze the effect of myristoylation of Fus1 protein on tumor cell-derived clonogenicity *in vitro*, we transfected H1299 cells (1×10^6) with various *FUS1*-expressing and control plasmid vector DNAs, using FUGEN 6 *in vitro* transfection reagent (Roche Molecular Biochemicals, Indianapolis, IN). Four μg of each test plasmid DNA were cotransfected with 1 μg of the neomycin-resistant gene-containing pcDNA3.1 vector (Invitrogen, Carlsbad, CA); the pcDNA3.1 (1 μg) vector alone and the pcDNA3.1 plus wt-p53 plasmid were used as negative and positive controls, respectively. Twenty-four h after transfection, cells were harvested, stained with trypan blue, and counted. Five thousand cells were replated on a 100-mm tissue culture dish in triplicate and grown in 5% fetal-bovine-serum-supplemented RPMI 1640 containing 400 μg/ml G418 for 2–3 weeks. The numbers of G418-resistant colonies were counted after staining with Crystal Violet.

Immunohistochemical Analysis. Samples of human lung tumor and parallel normal tissues were obtained from patients with informed consent through the Lung SPORE program at the University of Texas Southwestern Medical Center and at the M. D. Anderson Cancer Center. Expression of the Fus1 protein in tissue samples was analyzed by immunohistochemical staining with anti-Fus1 peptide polyclonal antibodies and a VECTASTAIN Elite ABC kit (Vector Laboratories Inc., Burlingame, CA). Briefly, the rabbit anti-Fus1 polyclonal antibodies used for immunohistochemical staining, raised against a synthetic oligopeptide derived from NH_2-terminal amino acid sequence of Fus1 protein, were affinity-purified by use of custom immunochemistry ser-

Received 11/26/03; revised 2/23/04; accepted 3/3/04.

Grant support: Partially supported by grants from the National Cancer Institute, the NIH (Grants SPORE CA70970 and CA71618); a W. M. Keck Gene Therapy Cancer Development grant (L. Ji); grants from the Department of Defense BESCT (Grant DAMD17-01-1-0689) and TARGET (Grant DAMD17-02-1-0706) Lung Cancer Programs; gifts to the M. D. Anderson Cancer Center Division of Surgery Core Laboratory Facility from Tenneco and Exxon; the M. D. Anderson Cancer Center Support Core Grant (CA16672); a grant from the Tobacco Settlement Funds as appropriated by the Texas State Legislature; and a sponsored research agreement with Introgen Therapeutics, Inc. (SR93-004-1).

The costs of publication of this article were defrayed in part by the payment of page charges. This article must therefore be hereby marked *advertisement* in accordance with 18 U.S.C. Section 1734 solely to indicate this fact.

Note: F. Uno, J. Saski, and M. Nishizaki contributed equally to this work.

Requests for reprints: Lin Ji, Department of Thoracic and Cardiovascular Surgery, Box 445, The University of Texas M. D. Anderson Cancer Center, 1515 Holcombe Boulevard, Houston, TX 77030. Phone: (713) 745-4530; Fax: (713) 794-4901; E-mail: lji@mdanderson.org.

vices provided by Bethyl Laboratories, Inc. (Montgomery, TX). The formalin-fixed, paraffin-embedded tissue sections were incubated with horseradish peroxidase-conjugated rabbit anti-Fus1 antibodies (0.1–2.0 μg/ml in PBS-BSA), and immunostaining was performed with the VECTASTAIN Elite ABC kit according to manufacturer's instruction. Subsequently, the sections were counterstained with Harries hematoxylin. Samples were examined under a microscope, and immunohistochemical images were recorded with an equipped digital camera.

Laser-Capture Microdissection (LCM) and Protein Preparation for Surface-Enhanced Laser Desorption/Ionization Mass Spectrometry (SELDI-MS) Analysis. Frozen tissue sections were rapidly removed from −80°C storage and immersed in or flooded with 70% alcohol for ~1 min, followed by H&E staining. The tumor cells and adjacent normal cells were precisely identified by microscopic examination. LCM was performed with the PixCell LCM microscope (Arcturus Engineering, Mountain View, CA). Approximately 500-1000 microdissected cells were then transferred to a thermoplastic film mounted on optically transparent LCM caps and incubated with 50 μl of protein lysis buffer containing 1% NP40, 0.5% sodium deoxycholate, 0.1% SDS, 1% DTT, and 1× complete protease inhibitors (Roche Biochemicals) in PBS on ice for 15 min. Cell samples were sonicated in a Transsonic 700/H sonication water bath (Lab-Line Instruments, Melrose Park, IL) at 4°C for 3 min, and protein lysate was cleared by centrifugation for 5 min at 13,000 rpm at 4°C. The protein lysates were either used immediately or stored at −80°C.

Antibody-Capture ProteinChip Array (ACPA) with SELDI-MS. The endogenous or exogenous wt-Fus1 or mutant Fus1 proteins were captured with affinity-purified rabbit Fus1 polyclonal antibodies from cultured cells or LCM-separated and enriched human primary lung tumor and noninvolved normal cells. Five μl (~10 μg) of protein lysate were spotted on a Fus1 antibody-coated preactivated surface (PS20) ProteinChip array and analyzed by SELDI-MS in the presence of CHCA matrix solution; both internal and external standards were used for mass/charge (*m/z*) calibration (Ciphergen Biosystems, Fremont CA). ACPA and SELDI-time-of-flight (TOF)-MS analysis were performed according to the manufacturer's instructions and procedures described in detail elsewhere (9–11).

Animal Studies. All animals were maintained and animal experiments were performed under NIH and institutional guidelines established for the Animal Core Facility at the University of Texas M. D. Anderson Cancer Center. Procedures for H1299 s.c. tumor inoculations in *nu/nu* mice have been described previously (8). When tumors reached an average of ~0.5 cm in diameter (~2 weeks after tumor inoculation), *N*-[1-(2,3-dioleoyloxyl)propyl]-*N,N,N*-trimethylammoniummethyl sulfate–cholesterol-complexed wt-*FUS1* or myristoylation-mutant (myr-mt)-*FUS1* plasmid vectors (*FUS1* lipoplex) were injected into the tumors three times within a week at a dose of 25 μg of plasmid DNA and 10 nmol liposome/tumor in 100 μl of 5% dextrose in water. PBS and *LacZ* were used as mock and negative controls, respectively. Tumor sizes were measured twice a week, and tumor volume was calculated using the equation $V\ (mm^3) = a \times b^2/2$, where a is the largest diameter and b is the smallest dimension.

To evaluate the effect of systemic administration of *FUS1* lipoplex on development of A549 experimental lung metastases in nude mice, we injected various lipoplexes every 2 days (three times/day) i.v. into all animals at a dose of 25 μg of plasmid DNA and 10 nmol of liposome each in 100 μl of 5% dextrose in water per animal. Each treatment group consisted of 10 animals. Lungs were harvested 2 weeks after the last injection, and metastatic colonies on the surfaces of lung were stained with Indian ink. Tumor colonies on lung surfaces were counted under a dissecting microscope without knowledge of the treatment groups, and the lung tissues were sectioned for further pathological and immunohistochemical analysis and for *in situ* apoptosis analysis with terminal deoxynucleotidyl transferase (Tdt)-mediated nick end labeling (TUNEL) staining (Roche Biochemical.)

Results

Loss of Expression of Fus1 Protein in Primary Lung Cancer and Cancer Cell Lines. In a previous study, we examined 40 primary lung cancers and found that mutation of the *FUS1* gene was infrequent and that there were only a few nonsense mutations and a COOH-terminal deletion mutation that arose from aberrant mRNA splicing (Fig. 1*A*; Ref. 5). In addition, we found no evidence for *FUS1* promoter region methylation (data not shown). *FUS1* expression has been detected in various normal human tissues, including brain, heart, pancreas, prostate, kidney, and lung, based on quantification of expressed sequence tags in Unigene clusters, as summarized in GeneCards[4] by the Crown Human Genomics Center and Yeda Research and Development Co. Ltd. (Rehovot, Israel). Although endogenous Fus1 protein expression could be detected in normal human bronchial epithelial cells and fibroblast cells (WI-38) by immunoblot analysis and *FUS1* mRNA transcription could be seen on Northern blots of RNAs prepared from lung cancer cell lines, we could not detect endogenous Fus1 protein in these lung cancer cell lines on immunoblots using the affinity-purified, anti-Fus1 peptide antibodies we developed (Fig. 1*B*). In addition, we performed immunohistochemical staining on a set of paired normal lung and lung cancer tissue sections (Fig. 1, *C–J*). We found that normal lung epithelial cells express Fus1 (Fig. 1, *D–F*) but that many lung cancers (15 of 20; >70%; Fig. 1, *H–J*) did not. We also found that even in those tumor samples with Fus1-positive staining, the staining was not uniformly detectable in all tumor cells (Fig. 1*G*). On the basis of both the lung-cancer-growth-suppressing properties of the Fus1 protein *in vitro* and in animal models and the observed loss of protein expression in primary tumors and tumor-derived cell lines, we hypothesized that *FUS1* would have to act as a TSG in a haploinsufficient manner (because most primary lung cancers experienced allelic loss in this 3p21.3 region; Ref. 12) and that both loss of expression and deficient posttranslational modification of Fus1 protein might lead to loss of its tumor suppression function and to lung cancer development.

Identification of Myristoyl Modification of Fus1 Protein. To test this hypothesis, we first performed computer-based homologous structure modeling and functional domain prediction of Fus1 protein to assess its biochemical and biophysical properties and to obtain possible leads to its biological function (Fig. 1*A*). The secondary protein structure prediction indicated that the wt-Fus1 protein is a highly hydrophobic protein with extensive helix-coil domain structures lacking transmembrane elements (Fig. 1*A*). The functional domains of Fus1 protein were predicted by use of a motif-based profile scanning program (13) and showed a potential myristoylation site at the NH_2 terminus, a protein kinase A interaction site, an A kinase-anchoring protein interaction (protein/protein) site, and a PDZ class II domain (Fig. 1*A*). From these analytical comparisons of Fus1 protein structure and function, we predict that Fus1 is a myristoylated member of the novel cAMP-dependent protein kinase A and A kinase-anchoring protein families, which are associated with many cellular processes, including transcription, signal transduction, metabolism, ion channel regulation, cell cycle progression, and apoptosis (14, 15).

To verify myristoylation of the Fus1 protein, we constructed a plasmid vector expressing either the wt-*FUS1* or a myristoylation-site-deficient mutant (myr-mt-*FUS1*) in which the predicted myristoylation site of glycine (G_2) was replaced with an alanine (A_2; Fig. 1*A*) by site-directed mutagenesis. A double-mutant (dmt-*FUS1*) in the COOH-terminal region, in which two highly hydrophobic isoleucine residues (I_{87} and I_{91}) were replaced with two neutral and rigid-conformation-promoting proline residues (P_{87} and P_{91}; Fig. 1*A*), was also constructed as another control to confirm the biological significance and specificity of the myristoylation-deficient mutation of Fus1 protein. The wt-Fus1- and mutant-Fus1-expressing plasmid vectors were used to transfect Fus1-deficient human NSCLC NCI-H1299 cells. The expression and posttranslational modification status of these wt and mutant Fus1 proteins were analyzed by SELDI-TOF-MS on an

[4] http://bioinfo.weizmann.ac.il/cards-bin/carddisp?FUS1.

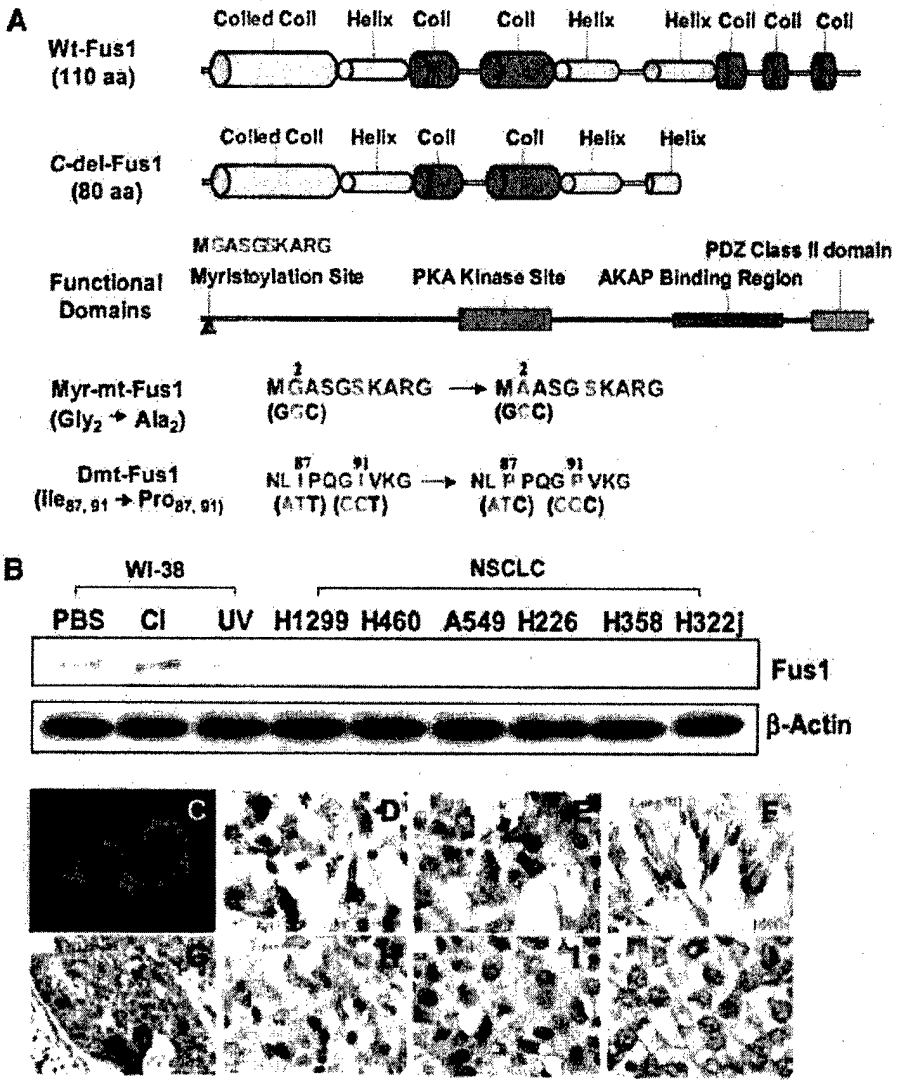

Fig. 1. Predicted secondary structure and functional domains of Fus1 protein and its expression in normal lung and primary lung tumors and tumor-derived cell lines. *A*, predicted secondary structure and functional domains of wild-type (wt)-Fus1 and C-del-Fus1. The predicted functional elements and domains, including a potential myristoylation site, protein kinase A (*PKA*) targeting site, A kinase-anchoring protein (*AKAP*) interface, and a PDZ class II domain are indicated. Mutant *myr-mt-Fus1*, in which the codon GGC for Gly_2 was changed to GCC for Ala_2, and double-mutant *Dmt-Fus1*, in which codon ATT for Ile_{87} and ATC for Ile_{91} were changed to CCT for Pro_{87} and CCC for Pro_{91}, respectively, were constructed by site-directed mutagenesis. *C-del-Fus1* is a tumor-related COOH-terminal deletion mutant derived by abnormal mRNA splicing. *B*, immunoblot analysis of endogenous Fus1 protein expression in normal lung fibroblast WI-38 cells grown in PBS under conditions of contact inhibition (*CI*) or after exposure of the cells to UV irradiation (100 joules for 5 min) and in non-small cell lung cancer (*NSCLC*) cells. The same blots were also probed for β-actin to ensure equal loading. *C–J*, immunofluorescence image analysis in wt-*FUS1*-transfected H1299 cells with FITC-conjugated rabbit anti-Fus1 antibodies (*C*) and immunohistochemical analysis of Fus1 protein expression in normal lung cells (*D* and *E*), bronchial epithelial cells (*F*), and primary lung tumor cells (*G–J*) in formalin-fixed, paraffin-embedded tissue samples. wt-Fus1 has a typical mitochondria/endoplasmic reticulum membrane localization in cytoplasm (*C*). Expression of Fus1 was detected in cytoplasm in normal lung (*D* and *E*) and bronchial epithelia (*F*). Fus1 expression was also detected in some tumor cells in one primary NSCLC (*G*) but was undetectable in other primary NSCLC cell lines (*H–J*) when we used rabbit anti-Fus1 polyclonal antibodies at a 1:2000 dilution. Magnifications: ×400 (*G*); ×1000 (*D–F*, *H–J*).

anti-Fus1 ACPA (Ciphergen Biosystems, Fremont, CA; Fig. 2*A*). The expressed Fus1 proteins in transfected H1299 cells were specifically captured on the protein chip and detected in the SELDI-TOF-MS spectra (Fig. 2*A*), but no protein peaks at corresponding mass positions were detected in the spectra with an anti-101F6 (a protein with encoding gene colocated in 3p21.3 region with *FUS1*) antibody-coated chip as a nonspecific control (Fig. 2*B*). The wt-Fus1 protein was identified as a myristoylated protein based on the detected mass of the captured wt-Fus1 protein (Fig. 2*A*), which showed a protein peak with a *m/z* ratio of 12,174 ± 6.25 Da compared with the predicted mass of 12,072.98 Da for the nonmyristoylated wt-Fus1 or 12,174.2 Da for the myristoyl-Fus1 protein. The myristoylation-deficient mutant (12,024.6 Da) and the COOH-terminal deletion mutant (8,783.5 Da) of Fus1 protein were also captured and detected on the protein array by SELDI-MS by comparing them with their calculated masses (Fig. 2*A*). No captured Fus1 proteins were detected in either the untransfected or p*LacZ*-transduced cells (Fig. 2*A*). On the basis of the 232-Da mass shift between the detected myristoylated Fus1 (12,174 Da) and the predicted nonmyristoylated Fus1 protein (11,942 Da; without the first methionine residue because the methionine residue is removed during myristoylation), we predict that the Fus1 protein is acylated at the G_2 with a 14-carbon myristate ($C_{14}H_{28}O_2$; 228.4 Da). The myristoylation of Fus1 protein was also confirmed by immunoblot analysis and immunoprecipitation analysis of the ^{14}C-myristate-labeled and acylated Fus1 protein in the p*FUS1*-transfected cells (Fig. 2*S*).

Defect of Myristoylation of Fus1 Protein in Primary Lung Cancer. Because mutation of *FUS1* is infrequent and no evidence has been found for methylation or mutation of the *FUS1* promoter region in lung cancers, other factors, such as haploinsufficiency, low expression, abnormal products arising from aberrant mRNA splicing, and posttranslational modification of Fus1, may play important roles in lung tumorigenesis (2, 3). We used ACPA analysis with SELDI-TOF-MS to evaluate the protein expression and myristoylation status in primary lung tumor and uninvolved normal lung tissue samples. Molecular analysis of tumors and their precursor lesions requires the isolation of specific cell subpopulations (normal, preneoplastic, and tumors) from a composite background of multiple cell types in tumor tissue biopsies. This was accomplished with LCM technology (16). To evaluate Fus1 protein expression and posttranslational modifications in human lung tumors and noninvolved tissues, we used LCM combined with appropriate tissue preparation methods to separate and enrich tumor or noninvolved normal cells, and the resulting separated cell populations (~500–1000 cells) were used for the Fus1-specific

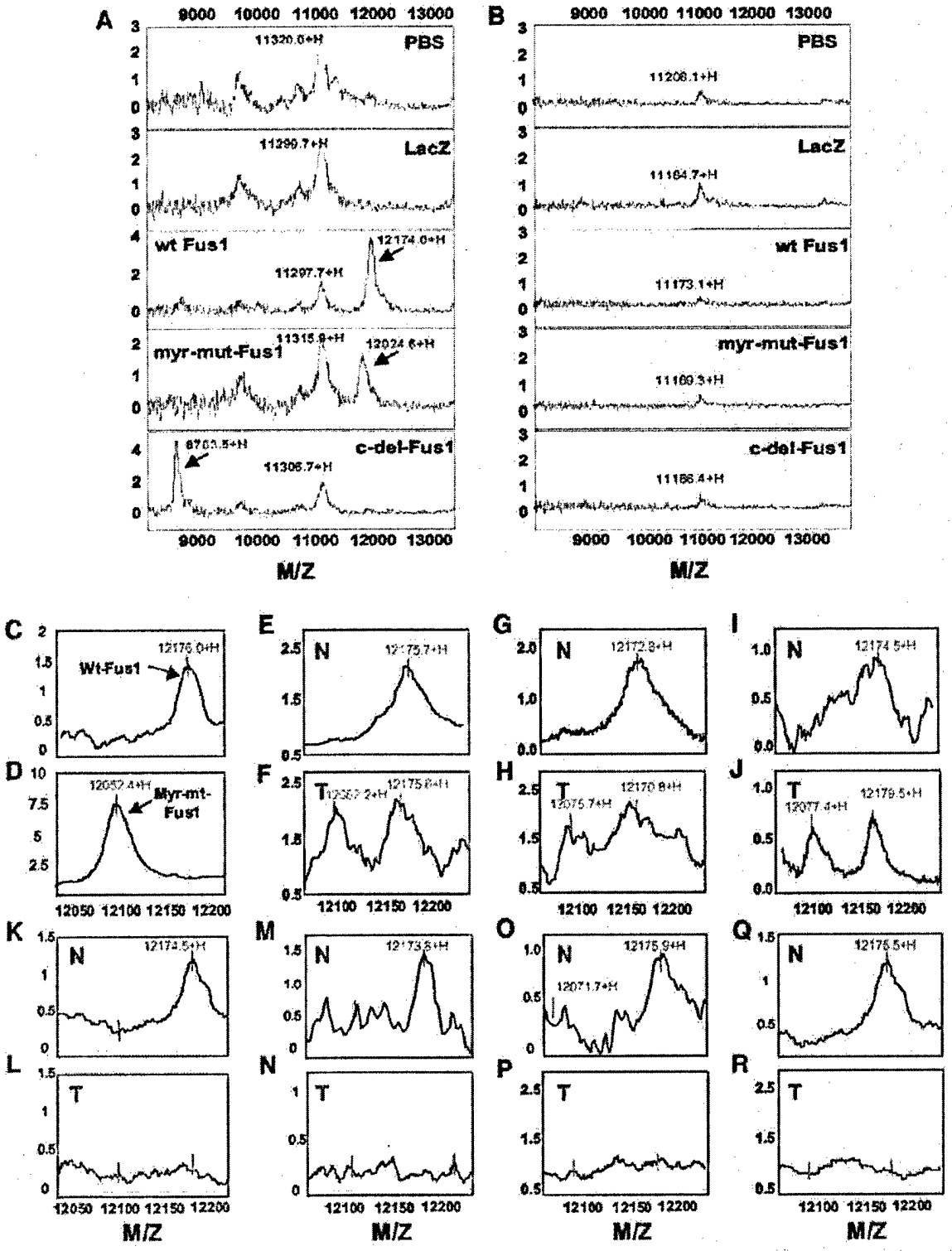

Fig. 2. Detection of myristoylation of Fus1 protein by surface-enhanced laser desorption/ionization time-of-flight mass spectrometric analysis on an anti-Fus1 antibody-capture ProteinChip array (ACPA). *A*, detection of Fus1 proteins captured on the anti-Fus1 antibody-coated preactivated surface (PS20) chip in wild-type (*wt FUS1*) or myristoylated mutant-*FUS1* (*myr-mut-Fus1*)-containing plasmid-transfected H1299 cells. The myristoylated Fus1 proteins are detected as a peak with a mass of 12,174 Da, and the nonmyristoylated Fus1 (*myr-mut-Fus1*) is detected with a mass of 12,024 Da compared with the calculated masses of 12,174 Da for the myristoylated wt-Fus1 and 12,025 Da for the myr-mut-Fus1, respectively. No corresponding proteins were detected in either PBS mock or *LacZ* control cells. B, ACPA assay with PS20 chips coated with nonspecific antibodies (anti-101F6). No Fus1 proteins were detected in these mass spectra when the same protein lysates as in *A* were applied. *C–R*, detection of status of Fus1 protein expression and posttranslational modification in laser-capture microdissection-enriched human primary lung tumor (*T*) and adjacent noninvolved normal (*N*) cells, shown as representative pairs (pair *E* and *F* through pair *Q* and *R*) from 15 tissue samples tested by ACPA assay as described in *B*. The protein lysates prepared from wild-type *FUS1* (*Wt-FUS1*)- (*C*) or myristoylated mutant-*FUS1* (*Myr-mt-FUS1*)-transfected (*D*) H1299 cells were used as positive controls. A single peak of myristoylated wt-Fus1 protein with a mass of 12,174 ± 5.2 Da was detected in normal cells, whereas two peaks, one with a mass of 12,174 Da, corresponding to the mass expected for the myristoylated wt-Fus1 protein, and another with a mass of 12,075 ± 8.5 Da, corresponding to the mass of the nonmyristoylated wt-Fus1 protein, were detected in tumor cells. In some tumors, these peaks were not detected. *S*, Western blot (*WB*) and

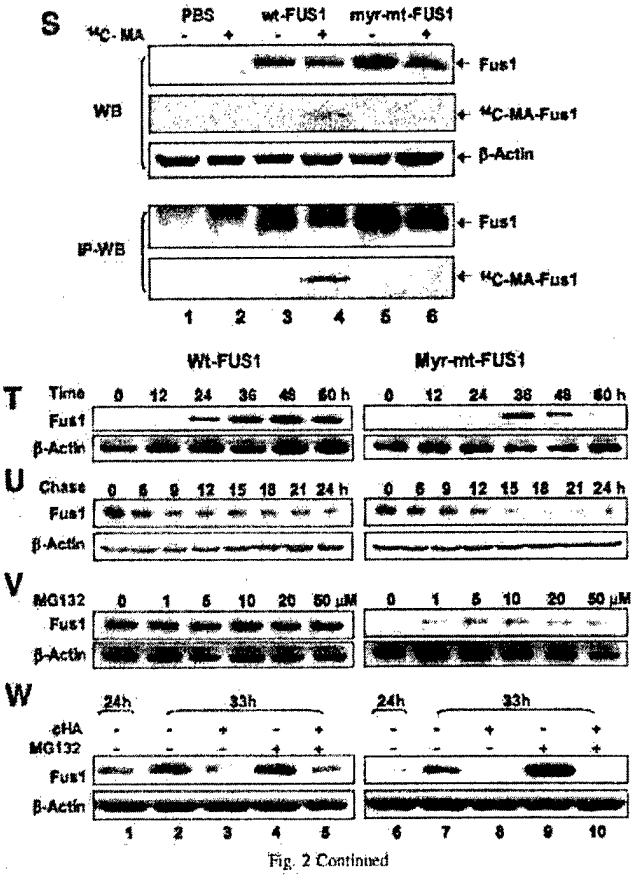

Fig. 2 Continued

ACPA analysis by SELDI-TOF-MS. We found that only myristoylated protein species could be detected in normal cells (13 of 15; $P = 0.0003$, nonparametric 2 × 2 contingency table: McNemar's χ^2 test) but that both the nonmyristoylated and myristoylated Fus1 protein were detected in tumor cells (5 of 15 samples; $P = 0.0442$) as indicated by detection of a peak corresponding to the Fus1 protein mass on the mass spectra (Fig. 2, *C–R*). In some tumor samples (7 of 15 samples; $P = 0.0030$), neither form of the Fus1 proteins could be captured (Fig. 2, *I*, *N*, *P*, and *R*), consistent with the results of the immunohistochemical analyses for these tumor and normal tissue samples. The remaining three samples tested were unresolvable because of the ambiguous spectra (spectra not shown). The difference in the observed Fus1 protein myristoylation status between the normal and the tumor cell populations was significant as indicated by a nonparametric McNemar marginal homogeneity test for the equality of categorical responses from two paired and dependent populations ($P < 0.001$).

Proteasome-Dependent Degradation of Nonmyristoylated Fus1 Protein. To explore the possible mechanism(s) for the involvement of the nonmyristoylated (or demyristoylated) Fus1 protein and the loss of its expression in primary lung cancer, we evaluated the stability of the exogenously expressed wt-Fus1 and myr-mt-Fus1 proteins in H1299 cells. We found that the duration of transient expression of myr-mt-Fus1 protein was much shorter than that of wt-Fus1. Myr-mt-Fus1 protein expression peaked at 36 h posttransfection and was almost undetectable after 60 h, whereas the wt-Fus1 protein was expressed at high levels beyond 60 h posttransfection (Fig. 2*T*). The half-life of the myr-mt-Fus1 protein was shorter than that of wt-Fus1 (~6 h for the former and 12 h for the later), as shown by pulse-chase of protein synthesis after treatment with the protein synthesis inhibitor cycloheximide (Fig. 2*U*). These results suggest that nonmyristoylated Fus1 protein may be degraded more rapidly than the myristoylated form. We therefore investigated the effect of the proteasome inhibitor (17) MG132 on degradation of Fus1 proteins. We found that the nonmyristoylated Fus1 protein levels increased in myr-mt-*FUS1*-transfected H1299 cells treated with various concentrations of MG132 (Fig. 2*V*). The MG132-induced recovery of the myr-mt-Fus1 protein could be detected at a very low level (1 μM; Fig. 2*V*) and was independent of protein synthesis, as demonstrated by significant protein accumulation on treatment with 10 μM of MG132 in the presence or absence of the protein synthesis inhibitor cycloheximide (Fig. 2*W*), with no effect shown on wt-Fus1 protein under the same experimental conditions (Fig. 2*W*). These results suggest that myristoylation may stabilize Fus1 protein and that demyristoylation may lead to rapid degradation of Fus1 protein through a proteasome-dependent pathway.

Disrupted Subcellular Localization of Myristoylation-Deficient Mutant of Fus1 Protein. One potential function of protein myristoylation is the facilitation of efficient interactions with cell membranes necessary for correct subcellular localization (18–20). We therefore analyzed the subcellular localization of myristoylation-positive wt-Fus1 and the myristoylation-deficient mt-Fus1 proteins in plasmid-transfected H1299 cells by immunofluorescence image analysis using FITC-conjugated anti-Fus1 antibodies (Fig. 3*3*, *A–D*). The myr-mt-Fus1 protein lost its characteristic intracellular membrane localization (Fig. 3, *C* and *D*), suggesting a critical role for myristoylation in the cellular localization of Fus1 protein.

Myristoylation Is Required for Fus1-Mediated Tumor-Suppressing Activities *in Vitro* and *in Vivo*. To evaluate the biological role of myristoylation in Fus1 protein-mediated tumor suppression, we compared the clonogenicity of the wt-Fus1- and myr-mt-Fus1-expressing H1299 cells *in vitro* (Fig. 3, *G* and *H*). The exogenous expression of both the *FUS1* genes and proteins in these H1299 transfectants was confirmed by reverse transcription-PCR (Fig. 3*E*) and by Western blot (Fig. 3*F*) analysis, respectively. Significant inhibition of clonogenicity was observed in myristoylated wt-Fus1-expressing H1299 cells, but no significant growth inhibition was observed in myr-mt-Fus1-expressing cells compared with the Fus1-nonexpressing controls (Fig. 3, *G* and *H*). The COOH-terminal double mutation of Fus1 (dmt-Fus1), which was theoretically expected to severely alter the hydrophobic and conformational properties in this region of Fus1 protein, was still able to significantly inhibit clonogenicity, similar to the effect of wt-Fus1 (Fig. 3, *G* and *H*).

We evaluated the effects of wt-Fus1 and myr-mt-Fus1 protein expression on tumor growth in H1299 s.c. tumor xenografts in *nu/nu*

Immunoprecipitation Western blot (*IP-WB*) analyses for verification of myristoylation of Fus1 proteins in H1299 transfectants. H1299 cells were transfected with either wild-type FUS1 (*wt-FUS1*) or myristoylation-deficient mutant-FUS1 (*myr-mt-FUS1*) plasmid vectors for 48 h and then incubated with ^{14}C-labeled myristic acid (*MA*; American Radiolabeled Chemicals, St. Louis, MO) in a final concentration of 5 μCi/ml for 90 min. Crude protein lysate (80 μg) was loaded in each lane for WB, and 1–2 mg of protein lysate with 1–2 μg of anti-Fus1 antibodies were used for IP. *T* and *U*, effect of myristoylation on Fus1 protein synthesis and stability by WB analysis during a 60-h time course posttransfection (*T*) and with a 3-h-interval pulse chase after treatment with 50 μM of protein synthesis inhibitor cycloheximide (*cHA*; *U*) in wild-type-*FUS1* (*Wt-FUS1*) (*left panels*) or myristoylation-deficient mutant-*FUS1* (*Myr-mt-FUS1*)-transfected (*right panels*) H1299 cells. *V* and *W*, effect of proteasome inhibitor MG132 on demyristoylation-induced degradation of Fus1 proteins. H1299 cells were transfected with wt-*FUS1* or myr-mt-*FUS1* plasmid DNAs for 24 h and then treated with DMSO (*Lane 0*) and various concentrations (1–50 μM) of MG132 (*V*), or were treated with 10 μM MG132 in the presence (+) or absence (−) of 50 μM cycloheximide (*W*). Expression of Fus1 proteins was analyzed by WB with anti-Fus1 antibodies. These experiments were carried at least twice with duplicates for each.

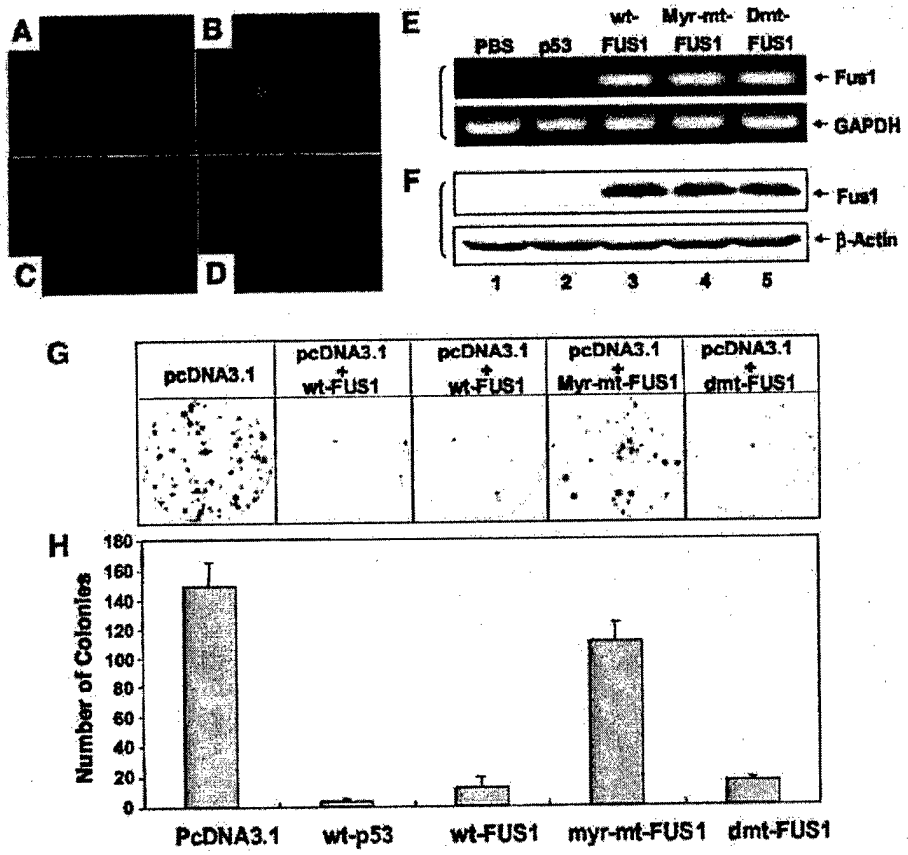

Fig. 3. Effects of myristoylation on Fus1 protein subcellular localization and Fus1-mediated tumor-suppressing activity *in vitro*. *A–D*, immunofluorescence image analysis of Fus1 protein expression and subcellular localization. H1299 cells were transfected with either wild-type Fus1-expressing (*A* and *B*) or myristoylation-deficient mutant-Fus1-expressing (*C* and *D*) plasmid vectors. Fus1 proteins were probed with FITC-conjugated anti-Fus1 antibody (*green*), and the nucleus was stained with Hoechst dye (*blue*; Sigma Chemical Co., St. Louis, MO). *E* and *F*, expression of *Fus1* genes and proteins in H1299 transfectants were verified by reverse transcription-PCR (*E*) and by Western blot analysis (*F*). *wt-FUS1*, wild-type Fus1; *Myr-mt-FUS1*, myristoylation-deficient mutant-Fus1; *Dmt-FUS1*, double-mutant Fus1; *GAPDH*, glyceraldehyde-3-phosphate dehydrogenase. *G* and *H*, effect of myristoylation of Fus1 protein on tumor cell-derived clonogenicity *in vitro*. H1299 cells (1×10^5) were transfected with plasmid DNAs *in vitro*. The wild-type (*wt-FUS1*), myristoylation-deficient mutant (*Myr-mt-FUS1*), or hydrophilic double mutant (*dmt-FUS1*) of Fus1-expressing plasmids were cotransfected with the neomycin-resistant gene-containing pcDNA3.1 vector; the pcDNA3.1 vector alone and the pcDNA3.1 plus wt-p53 plasmid were used as negative and positive controls, respectively. The numbers of G418-resistant colonies were counted after staining with Crystal Violet (*G*), and the quantitative analysis is shown in *H*. The experiments were repeated at least three times. The *bars* represent the SD, and the differences between the pcDNA3.1 vector alone and each testing construct was analyzed statistically by two-tailed Student's *t* test. $P \leq 0.05$ is considered significant.

mice by intratumoral injection of *N*-[1-(2.3-dioleoyloxyl)propyl]-*N,N,N*-trimethylammoniummethyl sulfate–cholesterol complexed with either wt-*FUS1* or myr-mt-*FUS1*-expressing plasmid DNAs (*FUS1* lipoplexes; Ref. 21) along with PBS as a mock control and *LacZ* plasmid vector as a negative control (Fig. 4*A*). The human NSCLC xenograft model, DNA lipoplex preparation, and treatment procedures were as described previously (4, 6, 21). Tumor growth was recorded from the first injection until 31 days after the last injection. Tumor volumes were normalized by calculating the percentage increase in tumor volume after treatment relative to volume at the beginning of treatment in each group. All of the tumors treated with wt-*FUS1* showed significantly suppressed growth ($P < 0.001$) compared with mouse groups treated with PBS or p*LacZ* controls (Fig. 4*A*). However, the tumor-suppressing activity of the myristoylation-deficient mutant (myr-mt-*FUS1*) of Fus1 protein was significantly reduced compared with wt-Fus1 ($P < 0.001$), although it retained a small inhibitory effect compared with the PBS and p*LacZ* controls (Fig. 4*A*).

We also evaluated the effect of the myristoylation of Fus1 protein on development of lung metastases, using the human NSCLC A549 xenograft metastasis mouse model by systemic (i.v.) administration of the wt-*FUS1* or myr-mt-*FUS1* lipoplexes compared with PBS, p*LacZ*, and the lung cancer-originated COOH-terminal deletion mutant of wt-*FUS1* and dmt-*FUS1* plasmid vector controls (4, 6). The development of A549 pulmonary metastases was significantly inhibited ($P < 0.001$), and the numbers of metastatic tumor colonies found on the surfaces of lungs from mice inoculated with A549 cells were reduced >85% in animals treated with wt-*FUS1* compared with those in control treatment groups (Fig. 4*B*). However, no significant reduction ($P < 0.003$) of metastasis formation was observed in animals treated with myr-mt-*FUS1*. The formation of metastases was significantly reduced ($P < 0.001$) in animals treated with dmt-*FUS1* compared with those controls treated with either PBS or *LacZ*, but the inhibitory effect was weaker than that observed in the wt-*FUS1*-treated group (Fig. 4*B*). The size of any remaining metastatic tumor nodules, as shown in H&E-stained sections of mouse lung tissues (Fig. 4*C*), was reduced in animals treated with wt-*FUS1* but not in those treated with myr-mt-*FUS1*, compared with either PBS or *LacZ*-treated controls. We analyzed the induction of apoptosis in these Fus1-expressing tumor cells by *in situ* apoptosis analysis with FITC-dUTP-labeled TUNEL staining (Roche Biochemicals; Fig. 4, *D–J*). Induction of apoptosis was detected in the wt-Fus1-expressing tumors (Fig. 4*E*) but not in myr-mt-Fus1-expressing (Fig. 4*F*) or PBS-treated (Fig. 4*D*) tumors, providing direct evidence for the need for both Fus1 expression and myristoylation in Fus1-mediated tumor suppression and apoptosis *in vivo*.

Discussion

Our studies present the first evidence supporting the biological importance of myristoyl modification of a TSG product and warrant further study of the role of the expression and posttranslational modification of Fus1 protein in the pathogenesis of lung and other human cancers. The N-myristoyl modification of proteins is achieved by a cotranslational linkage of myristic acid via an amide bond to the NH_2-terminal glycine residues of a variety of cellular and viral proteins in eukaryotic cells (22). Covalent modification of proteins by fatty acids such as myristate and palmitate is now a widely recognized form of protein modification, and ~100 proteins are known to be myristoylated (18, 20). N-Myristoyl proteins play essential roles in

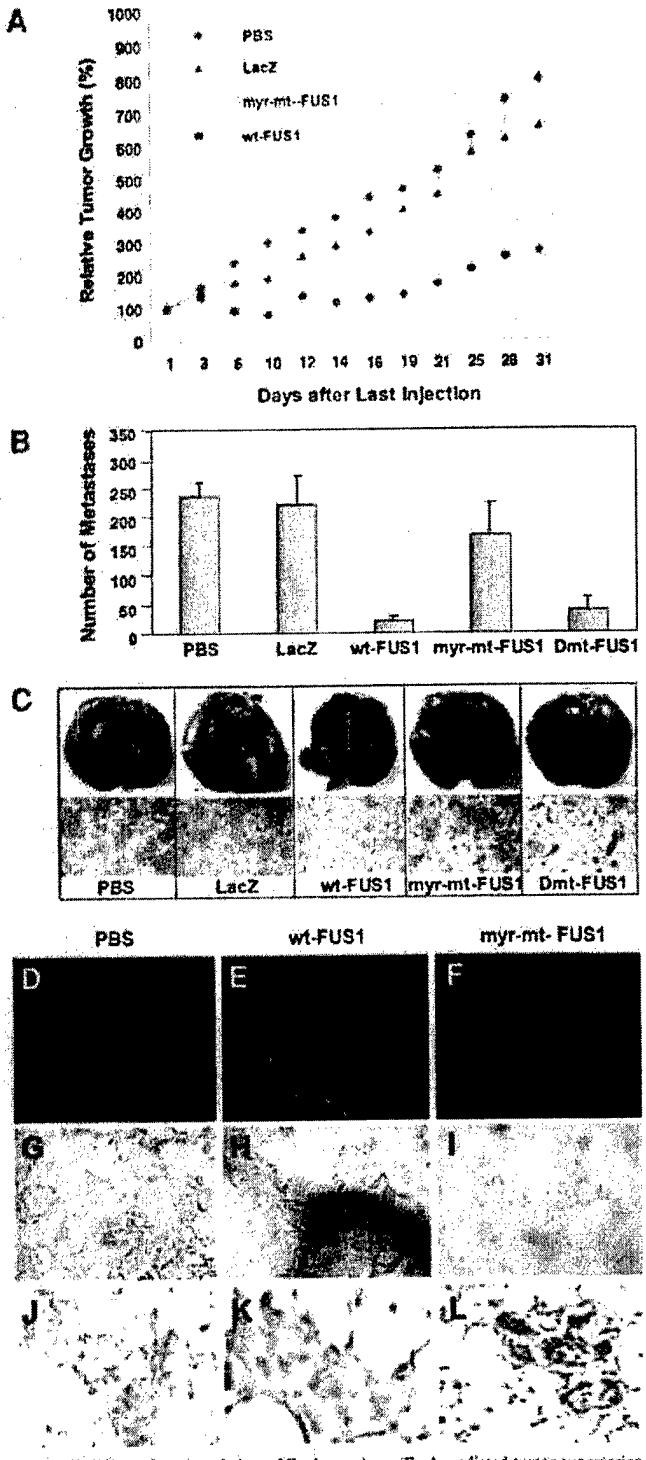

Fig. 4. Effect of myristoylation of Fus1 protein on Fus1-mediated tumor-suppressing activity *in vivo*. *A*, effect on H1299 human tumor xenograft growth in nude mice. Human non-small cell lung cancer H1299 cells were inoculated s.c. in nude mice. When the tumor reached 5–10 mm in diameter (2 weeks after tumor inoculation), *N*-[1-(2,3-dioleoyloxyl)propyl]-*N,N,N*-trimethylammoniummethyl sulfate-cholesterol-complexed wild-type *FUS1* (*wt-FUS1*) or myristoylation-deficient *FUS1* (*myr-mt-FUS1*) plasmid vectors (*FUS1* lipoplex) was injected into the tumors three times within 1 week. PBS and *LacZ* were used as mock and negative controls, respectively. Results are reported as the mean ± SD for 5–10 mice in each treatment group. Tumor volumes were normalized by the percentage increase of tumor sizes after treatment relative to those at the beginning of the treatment in each group. The mean tumor volumes ± SE (*bars*) from these experiments are shown. ANOVA was performed to determine statistical significance between each treatment group, using Statistica software (StatSoft Inc., Tulsa, OK), and $P \leq 0.05$ was considered significant. *B*, effect of systemic administration of *FUS1* lipoplex on development of A549 experimental lung metastases in nude mice. All animals received i.v. injections of various lipoplexes every 2 days (three times) at a dose of 25 μg of plasmid DNA and 10 nmol of liposome each in 100 μl of 5% dextrose in water per animal; PBS alone was used as a mock control and *LacZ* as a negative control. Each treatment group consisted of 10 animals. Lungs were harvested 2 weeks after the last injection, and metastatic colonies on the surfaces of lung were counted without knowledge of the treatment groups. *Bars* represent SE. A nonparametric *t* test (Wald–Wolfowitz runs test) was performed to determine the statistical significance between each treatment group, using Statistica software (StatSoft Inc.), and $P \leq 0.05$ was considered significant. Significant inhibition of metastasis development was observed in mice treated with wild-type *FUS1* (*wt-FUS1*; $P < 0.001$) and double-mutant-*FUS1* (*Dmt-FUS1*; $P < 0.001$) compared with mice treated with PBS or *LacZ*, but there was no significant inhibition in mice treated with myristoylation-deficient *FUS1* (*myr-mt-FUS1*; $P = 0.892$). The representative India ink-stained lungs and H&E-stained formalin-fixed, paraffin-embedded tissue sections in each treatment group are shown in *C*. The *white spots* on the lung surfaces indicate the metastatic tumor colonies. *D–I*, induction of apoptosis by wt-Fus1 expression *in vivo*. The A549 experimental metastasis tumor-bearing mice were treated with Fus1 lipoplexes three times within 1 week at the same dose as in *B*. Forty-eight h after the last treatment, animals were killed, and the lungs were harvested and freshly frozen. Induction of apoptosis was analyzed using an *in situ* apoptosis detection kit with FITC-dUTP-labeled terminal deoxynucleotidyl transferase (Tdt)-mediated nick end labeling reaction (Roche Biochemicals), and florescence images were examined under a fluorescence microscope and recorded with an equipped digital camera (*D–F*). Tumor morphology is shown in photographs *G–I*, taken at the same positions as above *D–F* under a regular optical light source. The hematoxylin-stained tissues from the same samples but in different sections were shown in photographs *J–L*.

diverse biological functions, such as regulating cellular structure, directing protein intracellular localization, mediating protein-protein and protein-substrate interactions, and regulating calcium and ion channel activities 18–20, 22). The requirement for myristoylation of the viral p60src protein to mediate its transforming and oncogenic properties demonstrated the biological importance of this hydrophobic myristoyl moiety (23). Recent genetic, biochemical, and cell-biological studies have provided insight into the molecular mechanisms of the regulation of protein myristoylation and explored strategies for modulating this process *in vivo* for therapeutic applications (18–20, 22). Our present evidence that primary lung cancers are deficient for myristoylation of Fus1 protein and that myristoylation is required for Fus1-mediated tumor suppressor activity *in vitro* and *in vivo* also indicates the cancer-preventive and therapeutic potential of positively regulating or reactivating myristoylation for Fus1.

Although the mechanism of demyristoylation is not known, demyristoylation of the myristoylated alanine-rich C-kinase substrate, as shown by electrospray mass spectrometry analyses of the myristoylated and demyristoylated forms of myristoylated alanine-rich C-kinase substrate proteins, has been found in brain (24), and the reduced expression of myristoylated alanine-rich C-kinase substrate has been reported in various cell lines after oncogenic or chemical transformation and in melanoma cells compared with normal choroidal melanocytes (25). The existence of a nonmyristoylated pool of a G protein α subunit (Gpa1p) in yeast has also been reported, and myristoylated Gpa1p is required for specific targeting of the protein to the plasma membrane; however, it is not clear how the nonmyristoylated proteins are generated and maintained (20, 26). Because point mutations of *FUS1* are infrequent, no mutation has been identified in its myristoylation site, and no evidence of epigenetic DNA methylation has been found in the *FUS1* promoter region in lung cancers, the observed reduced or lost expression and the deficient myristoylation of the Fus1 proteins in primary lung tumor cells and tumor-derived cell lines probably results from a deregulated myristoylation process or the accelerated proteasome-dependent degradation of demyristoylated Fus1 proteins.

Because most lung cancers experience allelic loss in this 3p21.3 region, haploinsufficiency may play a critical role in inactivation of Fus1 protein in lung cancer (3). In a diploid organism, each gene exists in two copies, in contrast to haploids, in which each cell contains a single copy of the genome. When one of the alleles is mutated or deleted, there is an ~50% reduction in the level of proteins

synthesized. Generally, the haploinsufficiency occurs when the level of proteins synthesized falls below a threshold level and is insufficient for the onset of some desired biological activity, leading to specific types of diseases or pathological changes. In our case, the haplotype in the 3p21.3 region where the *FUS1* gene is located may lead to a reduction or loss of FUS1 protein synthesis and deficiency of myristoylation, thus inactivating FUS1 and leading to the development of lung cancer. The importance of TSG haploinsufficiency in tumor cell biology has recently drawn increasing attention, and it may have profound effects on gene transcription, protein expression, posttranslational modification, stability, and does-dependent activity of TSGs because of the resulting decreased genomic stability, unbalanced chromosomal spatial symmetry, increased susceptibility to stochastic delays of gene initiation, altered transcriptional and translational stoichiometry, and interrupted gene expression (27–33). Although point mutations are rarely found in 3p21.3 genes in lung and other cancers, the accumulating evidence strongly argues that the extensive genomic changes (gains or losses of genetic material) collectively known as aneuploidy, which occurs frequently in lung cancer, particularly in adenocarcinoma, may collaborate with intragenic mutations during tumorigenesis and that changes in gene dosage may be modulated by the presence of adjacent genes with antagonistic activities, such as growth promotion and inhibition, a condition referred to as classic linkage disequilibrium (34). These observations raise the possibility that aneuploidy in chromosome 3; mutations of some critical checkpoint genes, such as *p53*, *Rb*, or *Ras*; and inactivation of the adjacent gatekeeper genes, such as *PTPRG*, *FHIT*, or *VHL* in the 3p region may influence the transcription, translation, and posttranslational processing of loss of heterozygosity-associated 3p21.3 genes such as *FUS1* to permit emergence of protumorigenic gene dosage changes or gene product inactivation that may facilitate early tumor development, inhibit cell proliferation, and induce apoptosis.

Our findings point to an essential role for protein myristoylation in human cancer pathogenesis and warrant further studies of alternative mechanisms involved in the inactivation of novel TSGs. Our results also suggest that it may be possible to prevent and delay tumorigenesis by neutralizing the effects of 3p haploinsufficiency before progression of premalignant lesions to invasive cancer and to suppress tumor growth by inducing apoptosis and altering cell cycle processes after tumor onset through wt-*FUS1* gene transfer.

Acknowledgments

We thank Dr. Sandra Hofmann at the University of Texas Southwestern Medical Center, Dallas for critical review of the manuscript; Drs. Nebiyou Bekele and Michael Gilcrease at M. D. Anderson Cancer Center for performing McNemar statistical analyses and for pathological evaluation of immunohistochemically stained human tissue sections, respectively; and Dr. Charlotte Clarke from Ciphergen Biosystems, Inc., for technical assistance with the SELDI-TOF-MS technology.

References

1. Lerman MI, Glenn GM, Daniel L, et al. A new polymorphic probe on chromosome 3p: lambda LIB28-77 (D3S169E). Nucleic Acids Res 1990;18:205.
2. Lerman MI, Minna JD. The 630-kb lung cancer homozygous deletion region on human chromosome 3p21.3: identification and evaluation of the resident candidate tumor suppressor genes. The International Lung Cancer Chromosome 3p21.3 Tumor Suppressor Gene Consortium. Cancer Res 2000;60:6116–33.
3. Zabarovsky ER, Lerman MI, Minna JD. Tumor suppressor genes on chromosome 3p involved in the pathogenesis of lung and other cancers. Oncogene 2002;21:6915–35.
4. Ji L, Nishizaki M, Gao B, et al. Expression of several genes in the human chromosome 3p21.3 homozygous deletion region by an adenovirus vector results in tumor suppressor activities in vitro and in vivo. Cancer Res 2002;62:2715–20.
5. Kondo M, Ji L, Kamibayashi C, et al. Overexpression of candidate tumor suppressor gene FUS1 isolated from the 3p21.3 homozygous deletion region leads to G_1 arrest and growth inhibition of lung cancer cells. Oncogene 2001;20:6258–62.
6. Ramesh R, Saeki T, Templeton NS, et al. Successful treatment of primary and disseminated human lung cancers by systemic delivery of tumor suppressor genes using an improved liposome vector. Mol Ther 2001;3:337–50.
7. Fondon JW, Mele GM, Brezinschek RI, et al. Computerized polymorphic marker identification: experimental validation and a predicted human polymorphism catalog. Proc Natl Acad Sci USA 1998;95:7514–9.
8. Ji L, Fang B, Yen N, Fong K, Minna JD, Roth JA. Induction of apoptosis and inhibition of tumorigenicity and tumor growth by adenovirus vector-mediated fragile histidine triad (FHIT) gene overexpression. Cancer Res 1999;59:3333–9.
9. Cai H, Wang Y, McCarthy D, et al. BACE1 is the major beta-secretase for generation of Aβ peptides by neurons. Nat Neurosci 2001;4:233–4.
10. Davies H, Lomas L, Austen BM. Profiling of amyloid β peptide variants using SELDI ProteinChip arrays. Biotechniques 1999;27:1258–61.
11. von Eggeling E, Davies H, Lomas L, et al. Tissue-specific microdissection coupled with ProteinChip array technologies: Applications in cancer research. Biotechniques 2000;29:1066–70.
12. Wistuba II, Behrens C, Virmani AK, et al. High resolution chromosome 3p allelotyping of human lung cancer and preneoplastic/preinvasive bronchial epithelium reveals multiple, discontinuous sites of 3p allele loss and three regions of frequent breakpoints. Cancer Res 2000;60:1949–60.
13. Yaffe MB, Leparc GG, Lai J, Obata T, Volinia S, Cantley LC. A motif-based profile scanning approach for genome-wide prediction of signaling pathways. Nat Biotechnol 2001;19:348–53.
14. Feliciello A, Gottesman ME, Avvedimento EV. The biological functions of A-kinase anchor proteins. J Mol Biol 2001;308:99–114.
15. Herberg FW, Maleszka A, Eide T, Vossebein L, Tasken K. Analysis of A-kinase anchoring protein (AKAP) interaction with protein kinase A (PKA) regulatory subunits: PKA isoform specificity in AKAP binding. J Mol Biol 2000;298:329–39.
16. Maitra A, Wistuba II, Virmani AK, et al. Enrichment of epithelial cells for molecular studies. Nat Med 1999;5:459–63.
17. Baumeister W, Walz J, Zuhl F, Seemuller E. The proteasome: paradigm of a self-compartmentalizing protease. Cell 1998;92:367–80.
18. Ames JB, Tanaka T, Stryer L, Ikura M. Portrait of a myristoyl switch protein. Curr Opin Struct Biol 1996;6:432–8.
19. Ames JB, Ishima R, Tanaka T, Gordon JI, Stryer L, Ikura M. Molecular mechanics of calcium-myristoyl switches. Nature (Lond) 1997;389:198–202.
20. Resh MD. Fatty acylation of proteins: new insights into membrane targeting of myristoylated and palmitoylated proteins. Biochim Biophys Acta 1999;1451:1–16.
21. Templeton NS, Lasic DD, Frederik PM, Strey HH, Roberts DD, Pavlakis GN. Improved DNA: liposome complexes for increased systemic delivery and gene expression. Nat Biotechnol 1997;15:647–52.
22. Bhatnagar RS, Futterer K, Farazi TA, et al. Structure of N-myristoyltransferase with bound myristoylCoA and peptide substrate analogs. Nat Struct Biol 1998;5:1091–7.
23. Kamps MP, Buss JE, Sefton BM. Mutation of NH2-terminal glycine of p60src prevents both myristoylation and morphological transformation. Proc Natl Acad Sci USA 1985;82:4625–8.
24. Manenti S, Sorokine O, Van Dorsselaer A, Taniguchi H. Demyristoylation of myristoylated alanine-rich C kinase substrate. Biochem Soc Transact 1995;23:561–4.
25. Manenti S, Malecaze F, Chap H, Darbon JM. Overexpression of the myristoylated alanine-rich C kinase substrate in human choroidal melanoma cells affects cell proliferation. Cancer Res 1998;58:1429–34.
26. Song J, Hirschman J, Gunn K, Dohlman HG. Regulation of membrane and subunit interactions by N-myristoylation of a G protein alpha subunit in yeast. J Biol Chem 1996;271:20273–83.
27. Celeste A, Petersen S, Romanienko PJ, et al. Genomic instability in mice lacking histone H2AX. Science (Wash DC) 2002;296:922–7.
28. Cook DL, Gerber AN, Tapscott SJ. Modeling stochastic gene expression: Implications for haploinsufficiency. Proc Natl Acad Sci USA 1998;95:15641–6.
29. Dworkin J, Losick R. Differential gene expression governed by chromosomal spatial asymmetry. Cell 2001;107:339–46.
30. McLaughlin MEJ. Thinking beyond the tumor cell: Nf1 haploinsufficiency in the tumor environment. Cancer Cell 2002;1:408–10.
31. Seidman JG, Seidman C. Transcription factor haploinsufficiency: when half a loaf is not enough. J Clin Investig 2002;109:451–5.
32. Veitia RA. Exploring the etiology of haploinsufficiency. Bioessays 2002;24:175–84.
33. Zhu Y, Ghosh P, Charnay P, Burns DK, Parada LF. Neurofibromas in NF1: Schwann cell origin and role of tumor environment. Science (Wash DC) 2002;296:920–2.
34. Pihan GDS. Mutations and aneuploidy: co-conspirators in cancer? Cancer Cell 2003;4:89–94.

[CANCER RESEARCH 64, 5745–5752, August 15, 2004]

Synergistic Tumor Suppression by Coexpression of FHIT and p53 Coincides with FHIT-Mediated MDM2 Inactivation and p53 Stabilization in Human Non-Small Cell Lung Cancer Cells

Masahiko Nishizaki,[1] Ji-ichiro Sasaki,[1] Bingliang Fang,[1] Edward. N. Atkinson,[2] John D. Minna,[3] Jack A. Roth,[1] and Lin Ji[1]

Departments of [1]Thoracic & Cardiovascular Surgery and [2]Biomathematics, University of Texas M. D. Anderson Cancer Center, Houston, Texas, and [3]Department of Internal Medicine and Pharmacology, Hamon Center for Therapeutic Oncology Research, University of Texas Southwestern Medical Center, Dallas, Texas

ABSTRACT

Aberrations of the tumor suppressor genes *FHIT* and *p53* are frequently associated with a wide range of human cancers, including lung cancer. We studied the combined effects of FHIT and p53 proteins on tumor cell proliferation and apoptosis in human non-small cell lung carcinoma (NSCLC) cells *in vitro* and on tumor growth in animal models by adenoviral vector-mediated cotransfer of wild-type *FHIT* and *p53* genes. We found that the coexpression of FHIT and p53 synergistically inhibited tumor cell proliferation in NSCLC cells *in vitro* and suppressed the growth of human tumor xenografts in nude mice. Furthermore, we found that this synergistic inhibition of tumor cell growth corresponded with the FHIT-mediated inactivation of MDM2, which thereby blocked the association of MDM2 with p53, thus stabilizing the p53 protein. Our results therefore reveal a novel molecular mechanism consisting of FHIT-mediated tumor suppression and the interaction of FHIT with other cellular components in the pathways regulating p53 activity. These findings show that combination treatment with synergistic tumor-suppressing gene therapy such as Ad-*FHIT* and Ad-*p53* may be an effective therapeutic strategy for NSCLC and other cancers.

INTRODUCTION

The pathogenesis of lung cancer involves a multistep process of genetic and molecular changes. Genomic aberrations involving human chromosome 3p are the most frequent and earliest genetic events in lung tumorigenesis and may affect several tumor suppressor genes and oncogenes in this region (1). One such tumor suppressor gene is the *FHIT* gene that is located at 3p14.2 and spans the *FRA3B* fragile site, which is very vulnerable to environmental carcinogens and, in human cancer, is frequently involved in allele loss, genomic rearrangement, and cytogenetic abnormalities (2). Indeed, genomic alterations of the *FHIT* gene and resultant deficient expression of the FHIT protein have been associated with many types of human cancers, including those of the lung, breast, cervix, colon, pancreas, stomach, and kidney (2).

The *FHIT* gene encodes a protein composed of 147 amino acids and is a member of the histidine triad (HIT) nucleotide-binding protein superfamily (3). Several lines of experimental evidence, both *in vitro* and *in vivo*, have supported the tumor suppressor role of the *FHIT* gene. For example, the exogenous expression of FHIT protein in FHIT-deficient human cancer cells inhibited tumor cell proliferation *in vitro* (4, 5) and suppressed tumor growth and tumorigenicity *in vivo* (4, 6) by altering the cell cycle and inducing apoptosis. In addition, using an FHIT transgenic mouse model, Fong *et al.* (7) recently noted that the FHIT-heterozygous (+/−) mice developed multiple visceral and skin tumors similar to those seen in patients with Torre's syndrome, which is caused by a deficiency in a mismatch repair gene. Conversely, the reintroduction of the wild-type *FHIT* gene into the FHIT-deficient mice prevented tumor development (8). The molecular mechanism involved in the *FHIT*-mediated tumor-suppressing activities remains to be elucidated, however.

The tumor suppressor gene *p53*, on the other hand, is a well-established cellular gatekeeper that plays an important role in the regulation of numerous biological processes, including cell proliferation, cell cycle progression, apoptosis, and tumor surveillance (9). The *p53* gene is also the most frequently mutated gene in human cancers (10) with >50% of NSCLCs processing a mutation in this gene (11). Transfer of the wild-type *p53* gene, on the other hand, has proved effective in suppressing the proliferation of tumor cells bearing mutated *p53* as seen *in vitro*, in animal models, and in patients with cancer (12–15). However, because many cancer cells, including lung cancer cells, express wild-type *p53* and most tumors are also heterogeneous with respect to their *p53* status, *p53* gene transfer alone may be insufficient to suppress tumor cell growth because of the general resistance of the wild-type *p53*-expressing tumor cells to *p53* gene transfer (12, 14, 16).

Although the efficiency of p53 in preventing cell proliferation is a strong deterrent to malignant progression, the activity of p53 is tightly regulated by divergent extracellular and intracellular signals through the mechanisms that result in degradation, stabilization, or accumulation of p53 protein (9, 17). One protein that plays an essential role in the regulation of p53 is the MDM2 protein, which functions as a ubiquitin ligase for p53 (17–19). Multiple cellular pathways also exist in the regulation of MDM2 activity (17–19). One of the mechanisms that are potentially responsible for the resistance of wild-type p53-expressing tumors to *p53* gene transfer may be imposed via a negative feedback pathway of *p53* and MDM2 in which the introduction of exogenous p53 induces the overexpression of endogenous MDM2, which, in turn, results in rapid degradation of the p53 protein in the ubiquitin-proteasome system (20, 21).

We and others (4, 5) have studied the effects of FHIT and p53 on tumor cell proliferation and apoptosis in the context of diverse biological activities, especially the ability of FHIT to induce apoptosis and alter cell cycle kinetics in various types of cells and the apparent link of the *FHIT* genomic aberrations to the integrity of p53 function in lung tumorigenesis (22). In this study, we used the adenoviral vector-mediated cotransfer of *FHIT* and *p53* in NSCLC cells with a varying p53 status to evaluate the interaction and therapeutic potential of *FHIT* and *p53* gene coexpression by using isobologram modeling. We also sought to elucidate the molecular mechanism involved in the tumor suppression activities mediated by the interaction between

Received 1/20/04; revised 5/4/04; accepted 6/11/04.

Grant support: NIH P01 Grant CA78778-01A1, NIH Specialized Programs of Research Excellence 2P50-CA70970-04, gifts to the Division of Surgery from Tenneco and Exxon for the Core Laboratory Facility, University of Texas M. D. Anderson Cancer Center Support Core Grant CA 16672, a grant from the Tobacco Settlement Funds as appropriated by the Texas State Legislature, and a W. M. Keck Gene Therapy Career Development Grant.

The costs of publication of this article were defrayed in part by the payment of page charges. This article must therefore be hereby marked *advertisement* in accordance with 18 U.S.C. Section 1734 solely to indicate this fact.

Note: M. Nishizaki and J. Sasaki contributed equally to this work.

Requests for reprints: Lin Ji, Department of Thoracic and Cardiovascular Surgery, The University of Texas M. D. Anderson Cancer Center, Unit 445, 1515 Holcombe Boulevard, Houston, TX 77030. Phone: (713) 794-1443; Fax: (713) 794-4901; E-mail: ljj@mdanderson.org.

FHIT and p53 proteins *in vitro* and *in vivo*. We present here the first evidence that the coexpression of FHIT and p53 synergistically inhibited tumor cell proliferation in both p53-sensitive and p53-resistant NSCLC cell lines *in vitro* and suppressed the growth of p53-resistant tumor xenografts in nude mice. We also demonstrated that the synergism of the FHIT- and p53-mediated tumor-suppressing activity was associated with the FHIT-mediated inactivation of MDM2 and the subsequent stabilization of the p53 protein. Our results provide insight into the interaction of FHIT and p53 and the *FHIT*-mediated inhibition of tumor cell growth and regulation of p53 activity and suggest novel strategies for cancer gene therapy.

MATERIALS AND METHODS

Cell Lines and Cell Culture. Four human NSCLC cell lines, A549, H1299, H322, and H460, with a varied *p53* gene status of and deficiency of FHIT protein expression were used for both *in vitro* and *in vivo* experiments. The A549 line, which contains wild-type p53, was maintained in Ham's F-12 medium supplemented with 10% FCS. The H1299, H322, and H460 lines had an internal homozygous deletion of the *p53* gene, a mutated *p53* gene, and the wild-type *p53* gene, respectively, and were maintained in RPMI 1640 supplemented with 10% FCS and 5% glutamine. Normal human bronchial epithelial cells were obtained from Clonetics, Inc. (Walkersville, MD), and cultured in the medium supplied by the manufacturer according to the instructions provided. The normal human lung fibroblast line WI-38 and immortalized human bronchial epithelial cells were maintained in MEM Earle's BSS with 10% fetal bovine serum and 5% glutamine and used as normal cell control. All cells were incubated in a humidified incubator supplied with 5% carbon dioxide. All cell cultures were tested regularly for possible microplasma contamination.

Adenoviral and Plasmid Vectors. Recombinant adenoviral vectors Ad-*p53* and Ad-*FHIT*, which contain the wild-type *p53* gene and an *FHIT* gene, respectively, were used as gene therapy agents, and either Ad-*LacZ*, which contains a *β-galactosidase* gene, or Ad-*GFP* was used as a nonspecific negative control. Construction of these recombinant adenoviral vectors has been described previously (4). Viral stocks were prepared by the Vector Core Facility at The University of Texas M. D. Anderson Cancer Center (Houston, TX). Viral titers were determined by absorbance measurements (viral particles/ml) and plaque assays (plaque forming units/ml). Potential contamination of the viral preparations by a wild-type virus was monitored by PCR analysis. Expression plasmid vectors containing the cDNA of *FHIT*, *HDM2*, *LacZ*, and *GFP* genes were used to transfect NSCLC cells using a FuGENE 6 transfect reagent (Roche Molecular Biochemicals, Indianapolis, IN).

Immunofluorescence Staining. Cells were first cultured in chamber slides and treated with adenoviral vectors at various multiplicities of infection (MOI) for 24 h. Cells were then fixed with 4% paraformaldehyde in PBS (pH 7.4) for 30 min on ice. Cells were rinsed twice with PBS and permeabilized with 0.2% Triton X-100 for 10 min. For immunostaining, cells were incubated with rabbit anti-FHIT (Zymed Laboratories, South San Francisco, CA) and mouse anti-p53 or anti-MDM2 (Santa Cruz Biotechnology, Santa Cruz, CA) antibodies diluted in PBS containing 5% BSA for 1 h at room temperature. FITC-labeled antirabbit IgGs and rhodamine-labeled antimouse IgGs (Chemicon International, Temecula, CA) were diluted 1:200 in PBS, and the cells were incubated with the antibodies for 30 min. The nuclei were stained by 4′,6-diamidino-2-phenylindole and then examined under an Eclipse E400 fluorescence microscope (Nikon, Tokyo, Japan) equipped with a Sensys digital camera (Photometrics, Tucson, AZ) and Metamophore software (Universal Imaging Corp., Downingtown, PA).

Growth Inhibition and 2,3-Bis[2-methoxy-4-nitro-5-sulfophenyl]-2*H*-Tetrazolium-5-Carboxanilide Inner Salt Assay. Inhibition of tumor cell growth by adenoviral vector-mediated transfer of *FHIT* and *p53* genes was analyzed by quantitatively determining cell viability using an improved 2,3-bis[2-methoxy-4-nitro-5-sulfophenyl]-2*H*-tetrazolium-5-carboxanilide inner salt assay (Roche Molecular Biochemicals). PBS was used as a mock control and Ad-*LacZ* as a negative control. Briefly, cells were plated in 96-well microtiter plates at 1×10^3 cells/well in 100 μl of medium. One day after the cells were plated, 25-μl aliquots of medium containing adenoviral vectors at various MOI (viral particles/cell) were added. Cells were then incubated at 37°C in a humidified atmosphere under 5% CO_2. Four days after transduction, cell viability was quantified in a microplate reader (Model MRX; Dynatech Laboratories, Chantilly, VA) by a 2,3-bis[2-methoxy-4-nitro-5-sulfophenyl]-2*H*-tetrazolium-5-carboxanilide inner salt assay according to the manufacturer's instructions. The percentage of viable cells was calculated in terms of the absorbency in treated cells relative to the absorbency in untreated control cells. Experiments were repeated at least three times and triplicate samples were used for each treatment.

Isobologram Analysis of the Interaction of FHIT and p53. The effects of the coexpression of two tumor suppressor genes, *FHIT* and *p53*, on tumor cell growth in five human cell lines (WI-38, H1299, H460, H322, and A549) were analyzed quantitatively and statistically *in vitro* by the improved isobologram method of Steel and Peckham (23). The mathematical operation and statistical analysis methods have been described elsewhere (23, 24). The MOI for the cotransduction were based on the IC_{50} values determined from each individual vector in different cell lines (Table 1). An equal amount of viral particles from each of the two vectors in cotransduction experiment is used to bring the total viral particles to the same amount as those in a single vector transduction.

Apoptosis and Cell Cycle Kinetics Assay. Cells were transduced with adenoviral vectors at various MOI based on the ID_{50} values (Table 1). Seventy-two h after transduction, cells were collected, fixed in 4% paraformaldehyde, permeabilized with 70% ethanol, washed with PBS, and stained with propidium iodide solution containing 40 μg/ml propidium iodide and 10 μg/ml DNase-free RNase A. DNA fragmentation was analyzed by flow cytometry. The percentage of apoptotic cells was shown by the cells in the G_0-G_1 phase.

Immunoprecipitation, Immunodepletion, and Western Blot Analysis. For the preparation of crude cell lysates, cells were suspended in immunoprecipitation SDS-PAGE running buffer (radioimmunoprecipitation assay) containing 1% NP40, 0.5% sodium deoxycholate, 0.1% SDS, and a complete set of proteinase inhibitors (Roche Molecular Biochemicals) and lysed for 20 min at 4°C. Cell lysates were passed through a 25-gauge needle and briefly sonicated twice for 30 s each. Protein concentrations were determined using the Bio-Rad protein assay (Bio-Rad Laboratories, Hercules, CA). For the immunoprecipitation studies, cell lysates were precleared by incubation with 10 μl of protein A/G-agarose (Santa Cruz Biotechnology, Inc.) for 30 min at 4°C and then centrifugation. Each protein sample (500 μg) was incubated with its respective antibody at 4°C overnight, followed by incubation with 25 μl of A/G-agarose beads. After centrifugation, the resultant supernatant was saved as an immunodepleted fraction. The precipitated beads were then washed three times in radioimmunoprecipitation assay buffer and once in PBS. The bound proteins were solubilized by adding 25 μl of SDS-containing sample buffer. The crude cell lysates and the immunoprecipitated and immunodepleted samples were used in standard SDS-PAGE and Western blot analyses.

Quantitative Real-time Reverse Transcription-PCR (RT-PCR). The TaqMan probe and primers for the *MDM2* gene were designed using Primer-express software (Perkin-Elmer Applied Biosystems, Foster City, CA) and synthesized by the same manufacturer. The human genomic DNA or total RNAs were used as template standards, and the human β-actin or glyceraldehyde-3-phosphate dehydrogenase TaqMan probes and primers were used as their respective internal controls. Total RNAs were isolated from Ad-*FHIT*- and Ad-*p53*-transduced tumor cells using Trizol reagent (Life Technologies, Inc., Grand Island, NY), as instructed by the manufacturer, and RNA samples were treated with DNase (Life Technologies, Inc.). Real-time RT-PCR and the quantification of RT-PCR products were performed and the products analyzed using a TaqMan Gold RT-PCR Kit, an ABI Prism 7700 Sequence Detection System, and the appropriate software according to the manufacturer's instructions (Perkin-Elmer Applied Biosystems).

Efficacy of Combination Treatment with Ad-*FHIT* and Ad-*p53* in Animal Models. All animals were maintained and animal experiments performed according to NIH and institutional guidelines established for the Animal Core Facility at M. D. Anderson. The animals used in this study were female *Nu/nu* mice (6–8 weeks of age) that were purchased from Charles River Laboratories (Wilmington, MA). Before tumor cell inoculation, mice were subjected to 3.5 Gy of total body irradiation from a ^{137}Cs radiation source.

A549 cells were used to establish s.c. tumors in mice. Briefly, 1×10^6 cells were injected into the right flank of each mouse. When the average size of the xenograft tumors reached 5–8 mm in diameter, the mice were randomly divided into six treatment groups: PBS control; single treatments with Ad-

Table 1 *p53 status of NSCLC cell lines, ID_{50} values and combination effects of Ad-p53, Ad-FHIT, and Ad-LacZ*

Cell line	Histologic subtype	p53 status	ID_{50} value (MOI)			Combination effects		
			Ad-*p53*	Ad-*FHIT*	Ad-*LacZ*	Ad-*p53* + Ad-*FHIT*	Ad-*p53* + Ad-*LacZ*	Ad-*FHIT* + Ad-*LacZ*
H1299	LC	Null	120.7 ± 21.70	702.8 ± 49.16	3,669.0 ± 37.96	Synergy ($P = 0.0117$)	Additive	Additive
H322	AD	Mutant	2,608.6 ± 16.40	1,582.9 ± 30.04	8,907.7 ± 189.06	Synergy ($P = 0.0181$)	Additive	Additive
H460	LC	Wild-type	6,815.3 ± 72.31	4,932.4 ± 91.46	14,298.3 ± 446.02	Synergy ($P = 0.0051$)	Additive	Additive
A549	AD	Wild-type	3,052.8 ± 96.60	1,778.7 ± 149.57	9,273.4 ± 224.93	Synergy ($P = 0.0117$)	Additive	Additive
WI-38	NLF	Wild-type	7,920.24 ± 54.21	56,530.5 ± 250.38	UD	Additive	UD	UD

Abbreviations: MOI, multiplicity of infection, expressed as viral particles/cell; LC, large cell carcinoma; AD, adenocarcinoma; NLF, normal lung I fibroblast; UD, undetermined.

FHIT, Ad-*p53*, or Ad-*LacZ* vector alone; and combination treatment with Ad-*p53* + Ad-*FHIT* and Ad-*p53* + Ad-*LacZ*. Each treatment group contained eight mice, and experiments were repeated twice.

Mice were treated according to the following schedule: on day 0, each mouse was injected intratumorally with adenoviral vector (Ad-*p53*, Ad-*FHIT*, or Ad-*LacZ*) at a dose of 3×10^{10} viral particles/tumor in a volume of 0.2 ml. Ear tags were placed on the mice so that data obtained from individual animals could be traced. Tumor dimensions were measured three times/week using a digital caliper.

Statistical and Mathematical Analyses. Tumor volume was calculated using the equation V (mm^3) = $a \times b^2/2$, where a is the largest diameter, and b is the smallest diameter. Differences in tumor volumes between treatment groups were analyzed using the ANOVA test and statistical software. A difference was considered to be statistically significant when $P \leq 0.05$.

A mathematical model and a statistical method were developed to analyze the effects of combination treatments in our animal model according to the improved isobologram method of Steel and Peckham (23–25) Tumor volumes (V) were fitted with dose-response curves f_a(Da) for reagent A and f_b(Db) for reagent B by the following equations: $V = f_a$(Da) and $V = f_b$(Db). Then mode I, mode IIa, and mode IIb could be expressed as follows: $V_{\text{Mode I}} = f_a(D_a) \times f_b(D_b)$; $V_{\text{Mode IIa}} = fb[f_b^{-1}f_a(D_a) + D_b]$; and $V_{\text{Mode IIb}} = fa[f_a^{-1}f_b(D_b) + D_a]$. The range of additivity was defined as being between the maximum (V_{max}) and minimum (V_{min}) tumor volume among these three isoeffect volumes: $V_{\text{Mode I}}$, $V_{\text{Mode IIa}}$, and $V_{\text{Mode IIb}}$. When the observed tumor volume after combination treatment was between V_{max} (boundary between addition and antagonism) and V_{min} (boundary between addition and synergism), the treatment combination effect was regarded as additive. When the observed tumor volume after combination treatment was below V_{min} or above V_{max}, the effect was regarded as synergistic or antagonistic, respectively. The Wilcoxon signed rank test was used for statistical analysis, and $P < 0.05$ was taken to indicate a significant difference.

RESULTS

Coexpression of FHIT and p53 Inhibits NSCLC Cell Proliferation. The wild-type *FHIT* and *p53* genes were coexpressed in human NSCLC cells by recombinant adenoviral vector-mediated gene transfer to study the combined effects of FHIT and p53 proteins on tumor cell proliferation. The coexpression of the FHIT and p53 proteins was detected by immunofluorescence staining in H1299 and A549 cells cotransduced with Ad-*FHIT* and Ad-*p53* (Fig. 1*A*). In particular, the fluorescence images showed nuclear staining (4′,6-diamidino-2-phenylindole, blue) and cytoplasmic and nuclear staining for FHIT (FITC, green) and p53 (rhodamine, red) in H1299 cells (Fig. 1*A*, *a–d*) and A549 cells (Fig. 1*A*, *e–h*) 24 h after the cotransduction of Ad-*p53* and Ad-*FHIT*. Specifically, the coexpression of FHIT and p53 was seen in 97.6% of H1299 cells and 95.4% of A549 cells. χ^2 statistical analysis showed that these coincidences of the expression of both proteins in both types of cells were significant ($P < 0.001$), indicating that equivalent levels of expression of both the FHIT and p53 proteins could be achieved in transduced cells.

Next, the effect of FHIT and p53 expression on tumor cell proliferation was determined in four NSCLC cell lines by analyzing the relative viability of cells transduced by the Ad-*FHIT* and Ad-*p53* vectors alone or in combination: H1299 (*p53* null); H322 (mutant *p53*); H460 (wild-type *p53*); and A549 (wild-type *p53*) cells. The Ad-*LacZ* vector was used as a nonspecific control for gene transfer. Endogenous expression of the FHIT protein could not be detected in any of the cell lines.

The dose effect of each agent on tumor cell proliferation was then subjected to the median-effect equation to generate dose-response curves (24). The ID_{50} values (doses of adenoviral vectors that inhibited cell growth by 50%) were then determined on the basis of the resultant dose-response curves (Table 1). The responses of NSCLC cell lines to Ad-*p53* or Ad-*FHIT* varied from the most sensitive (low ID_{50}) to the most resistant (high ID_{50}) in the following orders of sensitivity: H1299 > H322 > A549 > H460 (Table 1). Although Ad-*LacZ* had a detectable inhibitory effect on cell proliferation, the effect was significantly less than that of Ad-*FHIT* or Ad-*p53*, and ID_{50} values of Ad-*LacZ* could be determined only at a very high dose (Table 1), supporting the specificity of FHIT- and p53-mediated tumor suppression activities.

The combined effects of FHIT and p53 on cell proliferation were evaluated by isobolograms generated (Fig. 1*B*) using averaged data from experiments done independently at least twice for all cell lines tested. Combination treatment with Ad-*FHIT* + Ad-*p53* exhibited a synergistic antiproliferative effect in all cancer cell lines tested independent of their *p53* status, whereas no synergistic effect was observed in normal human lung fibroblasts WI-38 cells (Fig. 1*B*). On the other hand, the combination of either Ad-*p53* + Ad-*LacZ* (Fig. 1*B*, *middle panels*) or Ad-*FHIT* + Ad-*LacZ* (Fig. 1*B*, *bottom panels*) showed no synergistic effects in any of the cancer cell lines. A nonparametric statistical analysis of the predicted data *versus* the observed data showed that the observed synergistic effects on tumor cell proliferation of Ad-*FHIT* + Ad-*p53* were statistically significant in all cancer cell lines (H1299, $P = 0.0117$; H322, $P = 0.0181$; H460, $P = 0.0051$; A549, $P = 0.0117$; Table 1).

Effects of Coexpression of FHIT and p53 on Apoptosis. One of the hallmark molecular events induced by tumor suppressors is apoptosis. To study the combined effects of FHIT and p53 on apoptosis, suboptimal doses (slightly lower than the ID_{50} values in each NSCLC line shown in Table 1) of Ad-*FHIT* and Ad-*p53* vectors were applied to each cancer cell line. For the combination treatment, the ratio of the MOI (viral particles/cell) of Ad-*FHIT* to Ad-*p53* was 500:50 in the H1299 cells and 2500:2500 in the H460, normal human bronchial epithelial, and WI-38 cells. For the single treatment, either Ad-*FHIT* or Ad-*p53*, an appropriate amount of Ad-*LacZ* vectors, was added to make the total viral particles equal to that of the combination treatment.

The apoptosis and cell-cycle kinetics in cells transduced with Ad-*FHIT* and Ad-*p53* were then analyzed by flow cytometry in conjunction with propidium iodide staining (Fig. 1*C*). The accumulation of cells in the sub-G_0-G_1 phase analyzed with propidium iodide staining was correlated with positive cells analyzed with terminal deoxynucleotidyl transferase-mediated nick end labeling staining by flow cytometry. A low level of apoptosis was observed in the H1299 and H460 cells transduced with Ad-*FHIT* alone at 72 h after posttranduction (Fig. 1*C*). An intermediate level was seen in the cells transduced with Ad-*p53* alone (Fig. 1*C*). However, a supra-additive

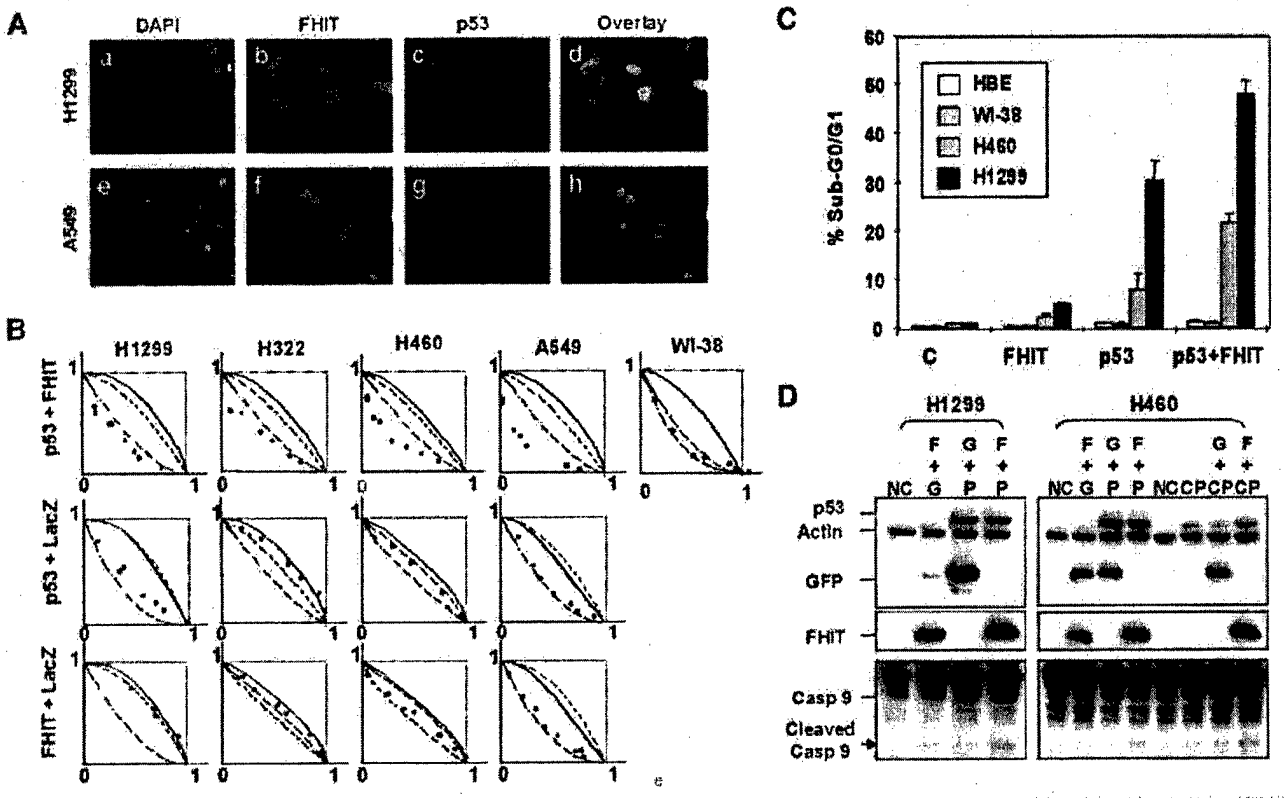

Fig. 1. Effects of coexpression of FHIT and p53 on the growth and apoptosis of NSCLC cells. *A*, immunofluorescence analysis of the expression of FHIT and p53 proteins in NSCLC cells cotransduced with Ad-*FHIT* and Ad-*p53* vectors. Immunofluorescence staining was performed on H1299 (*a–d*) and A549 (*e–h*) cells 24 h after transduction. Nuclei were stained by 4′,6-diamidino-2-phenylindole (DAPI; *blue*, *a* and *e*). Expression of FHIT proteins is shown in *green* (*b* and *f*), and expression of p53 proteins is shown in *red* (*c* and *g*). Immunofluorescence images were overlapped to confirm the coexpression of FHIT and p53 (*yellow*, *d* and *h*). *B*, evaluation of effects of coexpression of FHIT and p53 on the growth of NSCLC cells and normal lung fibroblasts (WI-38) shown by isobologram analysis at the ID_{50} level. The envelope of additivity in each isobologram is defined by three predicted isoeffect lines, and the observed data are plotted by ●. If the observed data are distributed inside, above, or below the envelope of additivity, the interaction is considered additive, antagonistic, or synergistic, respectively. The interaction of the gene therapy combination (Ad-p53 + Ad-FHIT, Ad-p53 + Ad-LacZ, and Ad-FHIT + Ad-LacZ) in each cell line is demonstrated by individual isobolograms. Statistical analysis was performed using the Wilcoxon signed rank test. $P \leq 0.05$ was considered significant (see "Materials and Methods"). *C*, the effect of overexpression of FHIT and p53 on apoptosis and cell cycle kinetics in Ad-*FHIT*- and Ad-*p53*-transduced NSCLC cells. DNA fragmentation and cell cycle kinetics in various NSCLC cells transduced with Ad-*FHIT* and Ad-*p53* alone or in combination were analyzed by flow cytometry in conjunction with propidium iodide staining. PBS was used as a control. The percentages of apoptotic cells are represented by G_0-G_1 cells in the sub-G_0-G_1 phase. *D*, Western blot analysis to assess FHIT-mediated p53 protein stabilization and caspase-9 activation. H1299 cells were cotransfected with Ad-*FHIT* and Ad-*p53* vectors for 72 h, and H460 cells were pretreated with 2 μM cisplatin for 24 h and then transduced with Ad-*FHIT* for 48 h. The cleaved caspase-9 products are indicated by an *arrow*. NC, negative control with PBS; F, Ad-*FHIT*; G, Ad-*GFP*; P, Ad-*p53*; and CP, cisplatin.

induction of apoptosis was seen in these same cell lines when they were cotransduced with Ad-*FHIT* and Ad-*p53*, but no significant enhancement of apoptosis was observed in normal cell lines cotransduced with Ad-*FHIT* and Ad-*p53* at the same viral doses and at the same time after transduction (Fig. 1*C*).

Consistent with the flow cytometry results, caspase-9 was also found to be activated in the H1299 and H460 cells transduced with either Ad-*FHIT* or Ad-*p53* alone or in combination, as shown by the cleavage products detected by Western blot analysis (Fig. 1*D*). In addition, caspase-9 was strongly activated in H460 cells (wild-type p53) in which the endogenous p53 was activated by cisplatin treatment followed by the transduction with Ad-*FHIT* (Fig. 1*D*, *Lane F+CP*) as compared with the effects in cells transduced with Ad-*GFP* (Fig. 1*D*, *Lane G+CP*). These results suggest that the observed synergism in the inhibition of tumor cell proliferation produced by the coexpression of FHIT and p53 is due to a synergistic induction of apoptosis.

Synergistic Inhibition of Tumor Growth by the Coadministration of Ad-*p53* and Ad-*FHIT* *in Vivo*. To determine whether the synergistic growth inhibition mediated by the cotransfer of the *FHIT* and *p53* genes observed *in vitro* could be reproduced *in vivo*, we evaluated the combined effects of FHIT and p53 overexpression on tumor growth by directly coadministering Ad-*FHIT* and Ad-*p53* vectors into human A549 s.c. xenografts in nude mice. Mice were divided into six treatment groups: four groups that received single treatment with PBS; Ad-*LacZ*, Ad-*p53*, or Ad-*FHIT* alone; and combinations of Ad-*p53* + Ad-*FHIT* or Ad-*p53* + Ad-*LacZ*. Each treatment group contained five to eight mice, and all experiments were repeated twice. The overall effects of treatments on tumor growth were analyzed by an ANOVA statistical method. Treatment with Ad-*p53* + Ad-*FHIT* significantly inhibited tumor growth in the A549 tumor model ($P < 0.05$) in comparison with the results seen in the other treatment and the control groups (Fig. 2*A*). We also analyzed whether there was a synergistic interaction between the combination treatment elements in these tumors using a modified isobologram method (see "Materials and Methods"). This showed that coadministration of Ad-*p53* and Ad-*FHIT* produced a significant synergistic inhibitory effect on tumor growth in the A549 tumor model ($P < 0.05$; Fig. 2*B*).

Stabilization of p53 Protein by FHIT Overexpression. To elucidate the molecular mechanisms responsible for the synergistic inhibitory effects of coexpression of FHIT and p53 on tumor growth, we studied their mutual effects on the accumulation and stability of the FHIT and p53 proteins themselves in Ad-*FHIT*- and Ad-*p53*-transduced NSCLC cells using Western blot analysis (Fig. 3, *A* and *B*). The overexpression of FHIT up-regulated the expression of endogenous wild-type p53 proteins >6-fold in Ad-*FHIT*-transduced H460 and

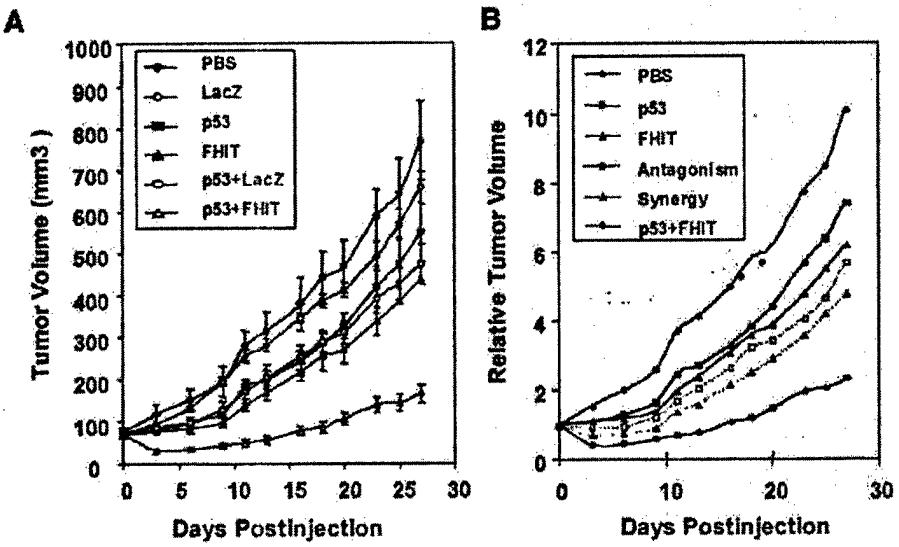

Fig. 2. Suppression of tumor growth by the coadministration of Ad-*p53* and Ad-*FHIT* vectors in human A549 xenografts in nude mice. *A*, effects on tumor growth. Results are reported as the mean ± SE. The tumors in the mice treated with the combination of Ad-*p53* + Ad-*FHIT* vectors were significantly smaller than those in the other groups ($P < 0.05$). *B*, analysis of synergism in tumors in which both Ad-*FHIT* and Ad-*p53* were administered. The combined effects of FHIT and p53 expression on tumor growth were analyzed using a modified isobologram method (see "Materials and Methods"). The predicted boundaries between the additive and antagonistic effects and between the additive and synergistic effects of combination treatments on tumor volumes are indicated by the *dashed line* with □ and the *dashed line* with △, respectively. Results are reported as the mean of relative tumor volumes. The inhibition of tumor growth by combination treatment with Ad-*p53* + Ad-*FHIT* is significantly synergistic ($P = 0.0033$).

A549 cells but not in the H322 cells with endogenous mutant p53 (Fig. 3*A*). A modest increase of exogenous p53 was also seen in Ad-*p53* and Ad-*FHIT* cotransduced cells, independent of the endogenous *p53* status in these cells (Fig. 3*B*). However, the level of the exogenous FHIT protein was not affected by either the endogenous or exogenous expression of p53 (Fig. 3*A*, *middle panels*), suggesting that the synergistic effect of the tumor suppressor genes may be due to FHIT-mediated up-regulation of the p53 protein but not the reverse.

To confirm that the increased level of p53 protein induced by FHIT is due to protein stabilization, we performed a protein synthesis inhibitor cyclohexamide-mediated pulse-chase Western blot analysis to monitor the endogenous p53 expression and protein turnover induced by pretreatment with cisplatin in the presence or absence of Ad-*FHIT*. In the absence of Ad-*FHIT*, the level of the p53 protein was dramatically reduced at 6 h and almost not detectable at 15 h after cyclohexamide treatment (Fig. 3*C*, PBS). By comparison, in the presence of exogenous Ad-*FHIT*, the endogenous p53 protein in these cells could still be detected even 24 h after cyclohexamide treatment (Fig. 3C, Ad-*FHIT*). These results indicate that expression of FHIT protein indeed stabilizes the p53 protein.

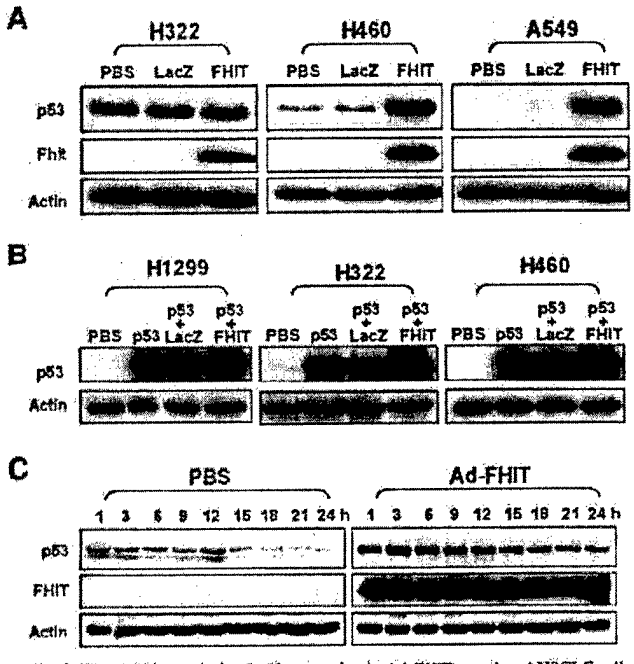

Fig. 3. Western blot analysis of p53 expression in Ad-*FHIT*-transduced NSCLC cells. The endogenous (*A*) and exogenous (*B*) expression of p53 proteins was probed by immunoblotting with a mouse monoclonal anti-p53 antibody. FHIT expression (*A*) was probed with rabbit anti-FHIT antibodies. *C*, effect of FHIT on endogenous p53 protein stability shown by cyclohexamide-mediated pulse-chase Western blot analysis. A549 cells were pretreated with 2 μM cisplatin at 24 h before 10 μM cyclohexamide with or without Ad-*FHIT* transduction. Cell extracts were then harvested at the indicated times.

Regulation of the *MDM2* by Coexpression of FHIT and p53. There are multiple pathways to stabilize p53 in response to different forms of stress. One of the key pathways is to inhibit MDM2-mediated p53 degradation by dissociating MDM2 from p53 (21, 26). To determine whether the enhanced stability of p53 is associated with the inactivated MDM2 in NSCLC cells cotransduced with Ad-*FHIT* and Ad-*p53*, we analyzed the expression of MDM2 proteins by Western blot analysis using a monoclonal MDM2 antibody (SMP-14; Santa Cruz Biotechnology, Inc.; Fig. 4*A*). We detected significantly decreased level of the 90-kDa MDM2 protein in the cells cotransduced with Ad-*FHIT* and Ad-*p53* in comparison with control cells treated with Ad-*p53* alone or with Ad-*p53* + Ad-*LacZ* (Fig. 4*A*) in all cell lines tested. Similar results were observed when MDM2 antibodies from different sources were used (N-20 from Santa Cruz Biotechnology, Inc., and IF2 from Oncogene, Cambridge, MA; data not shown).

To determine whether the reduction in the MDM2 protein was resulted from a transcriptional or posttranscriptional event, we analyzed *MDM2* mRNA transcription using a quantitative real-time RT-PCR in Ad-*FHIT*- and Ad-*p53*-transduced cells (Fig. 4*B*). Transcription of the *MDM2* mRNA was significantly up-regulated in both the Ad-*p53*-transduced and Ad-*FHIT* + Ad-*p53*-cotransduced cells but not in the cells transduced with Ad-*FHIT* alone (Fig. 4*B*). These results suggest that the overexpression of p53 activates *MDM2* at the transcriptional level through a feedback mechanism but that the FHIT-mediated regulation of MDM2 expression occurs at the posttranscriptional protein level.

To exclude the possibility that the adenoviral vector and p53 expression might have affected MDM2 expression, we analyzed the effect of FHIT expression on exogenous MDM2 expression in *p53*-null H1299 cells cotransfected with the *HDM2* and *FHIT* expressing

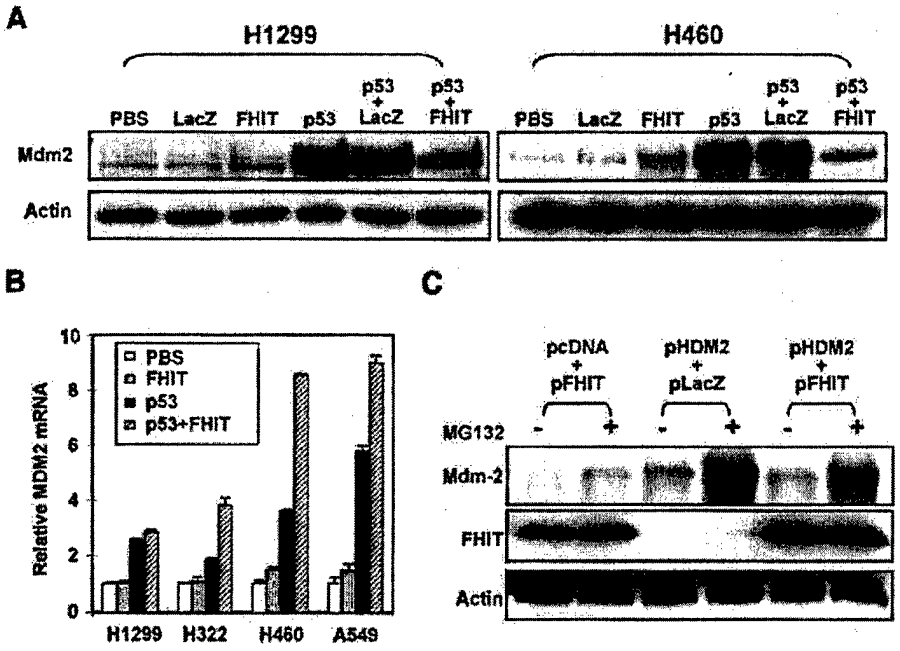

Fig. 4. Modulation of MDM2 expression in NSCLC cells transduced by *Ad-FHIT* and Ad-*p53*. *A*, Western blot analysis of the expression of MDM2 protein. Cells were transduced with *Ad-LacZ*, *Ad-FHIT*, or *Ad-p53* or cotransduced with Ad-*LacZ* + Ad-*p53* or Ad-*FHIT* + Ad-*p53* for 72 h. Cell extracts were analyzed by immunoblotting with a mouse anti-MDM2 monoclonal antibody. *B*, real-time RT-PCR analysis of MDM2 mRNA transcription. Total RNAs were isolated from cells transduced with Ad-*FHIT* or Ad-*p53* or cotransduced with Ad-*p53* + Ad-*FHIT* for 72 h. Real-time RT-PCR was performed with an MDM2 mRNA-specific TaqMan probe and primers on an ABI Prism 7700 Sequence Detection System, and PCR products were analyzed with the software the system was equipped with. *C*, effect of FHIT expression on exogenous MDM2 protein expression in H1299 cells cotransfected with the plasmid vectors pHDM2 and pFHIT. An empty backbone plasmid pcDNA was used as a control. Cells were preincubated with either DMSO or 5 μM MG132 for 3 h and then transfected with various combinations of plasmid vectors. Cells were harvested 48 h after transfection for the preparation of protein lysates.

plasmid vectors (*pHDM2* and *pFHIT*). H1299 cells cotransfected with *pHDM2* and *pLacZ* were used as the control. Consistent with the results obtained in the adenoviral vector-mediated *FHIT* gene transfer experiment (Fig. 4*A*), the level of exogenous MDM2 protein was also reduced in the cells cotransfected with *pHDM2* and *pFHIT* plasmids, compared with the levels in cells cotransfected with *pHDM2* and *pLacZ* (Fig. 4*C*). Furthermore, MDM2 proteins were clearly detected at a similar rate of recovery after treatment with a broad proteasome inhibitor, MG132, in all treatment groups (Fig. 4*C*), suggesting that the FHIT-mediated reduction in the MDM2 protein is independent of the proteasome degradation pathway.

Interruption of Association of MDM2 with p53 by FHIT. To further our understanding of the mechanism behind the observed stabilization of the p53 protein by FHIT, we investigated the interactions among the FHIT, MDM2 and p53 proteins in Ad-*FHIT*- and Ad-*p53*-transduced wild-type *p53*-bearing H460 and A549 cells using immunoprecipitation and Western blot analysis (Fig. 5). The FHIT protein was detected in MDM2-immunoprecipitated complexes in both H460 (Fig. 5*A*, *Lane 2*) and A549 (Fig. 5*A*, *Lane 6*) cells transduced with *FHIT*, indicating a direct interaction between the FHIT and MDM2 proteins. In addition, a significantly smaller amount of the FHIT/MDM2 complexes was observed in both H460 (Fig. 5*A*, *Lane 4*) and A549 (Fig. 5*A*, *Lane 8*) cells that were cotransduced with *Ad-FHIT* + *Ad-p53*. These results suggest that FHIT may cause degradation of MDM2 as implied by the reduced MDM2 levels in Ad-*FHIT* + Ad-*p53*-transduced cells (Fig. 4*A*) and that a large amount of p53 proteins may also interfere with the apparent FHIT-MDM2 interaction.

To determine whether the association of FHIT with MDM2 could interfere with the interaction of MDM2 with p53, we performed a MDM2 immunoprecipitation and MDM2 immunodepletion analysis followed by immunoblotting against p53 protein on denatured cell lysates from Ad-*FHIT*- and Ad-*p53*-transduced cells (Fig. 5*B*). We found that MDM2-bound p53 was detected in the MDM2-immunoprecipitated complexes in both H460 (Fig. 5*B*, *Lane 1*) and A549 (Fig. 5*B*, *Lane 3*) cells transduced with Ap-*p53*. However, the levels of MDM2-bound p53 protein were dramatically reduced in both H460 (Fig. 5*B*, *Lane 2*) and A549 (Fig. 5*B*, *Lane 4*) cells cotransduced with Ad-*FHIT* + Ad-*p53* vectors compared with the levels in cells transduced with Ad-*p53* alone. Furthermore, Western blot analysis of p53 proteins in MDM2-immunodepleted crude protein fractions showed that almost all of the p53 protein was associated with MDM2 in the absence of FHIT expression (Fig. 5*B*, *Lanes 5* and *7*), but the MDM2-p53 protein interaction was significantly interrupted by the presence of FHIT coexpression (Fig. 5*B*, *Lanes 6* and *8*). These results strongly suggest that the interaction of FHIT with MDM2 effectively blocks the association of MDM2 with p53, and this prevented the MDM2-mediated degradation thus enhancing the stability of p53 protein.

We also performed immunofluorescence image analysis of FHIT and MDM2 protein expression to study the interaction of these two proteins in living A549 cells in which endogenous p53 expression was induced by cisplatin and exogenous FHIT expression was induced by Ad-*FHIT* (Fig. 5*C*). In the Ad-*FHIT*-transduced cells (Fig. 5*C*, *a* and *b*), the FHIT protein was detected mainly in the cytosol (Fig. 5*C*, *a*), and the MDM2 protein was predominantly located in the nucleus (Fig. 5*C*, *b*). In untransduced cells (Fig. 5*C*, *b*), MDM2 protein expression could also be detected in the cytosol, but this was not seen in the FHIT-expressing cells (Fig. 5*C*, *b*). In addition, the fluorescence intensity of the MDM2 protein was reduced in nuclei in the FHIT-expressing cells compared with the intensity in the non-FHIT-expressing cells, indicating that a FHIT-mediated reduction in MDM2 protein expression and a FHIT-mediated interference in the association of MDM2 with p53 occurred in living cells.

DISCUSSION

In this study, we investigated the interaction of FHIT and p53 by recombinant adenoviral vector-mediated *FHIT* and *p53* tumor suppressor gene cotransfer in human NSCLCs *in vitro* and *in vivo*. We used improved isobologram modeling and statistical analysis to quantitatively evaluate the mutual effects of *FHIT* and *p53* coexpression on tumor cell proliferation *in vitro* and tumor growth in animal models and demonstrated that the coexpression of FHIT and p53 resulted in

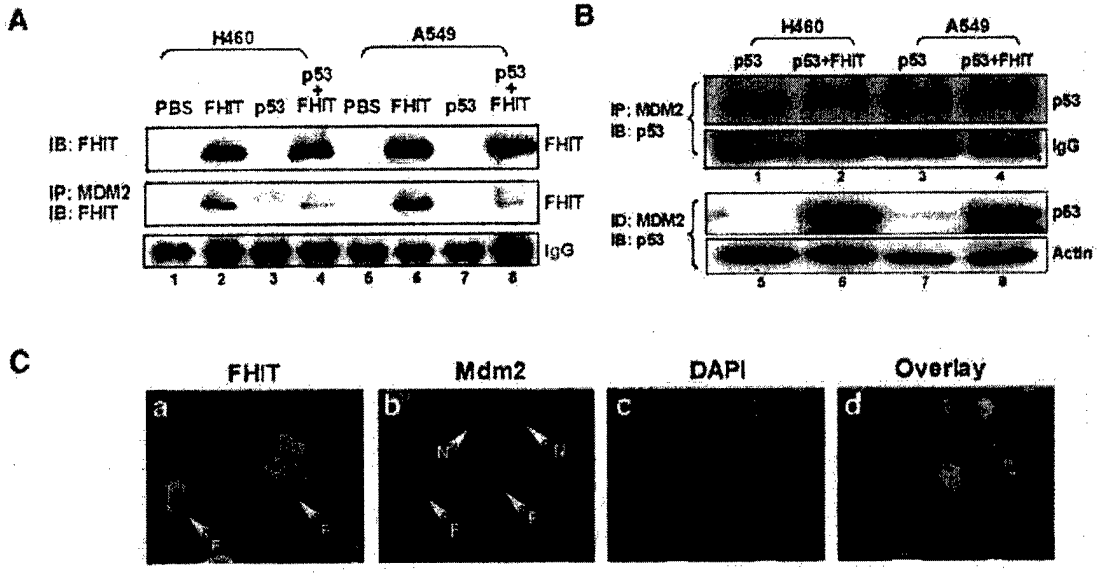

Fig. 5. Immunoprecipitation and immunoblot analysis for the interaction of FHIT, MDM2, and p53 proteins in NSCLC cells. *A*, interaction of FHIT with MDM2 proteins in the presence and absence of exogenous p53 protein expression in H460 and A549 cells. Cell extracts were prepared from cells transduced with Ad-*FHIT* or Ad-*p53* alone or in combination for 72 h. Cell extracts were immunoblotted (IB) with FHIT antibodies and then immunoprecipitated (IP) with a monoclonal MDM2 antibody followed by immunoblotting with polyclonal FHIT antibodies. *B*, effect of FHIT expression on the interaction of MDM2 with p53 proteins in H460 and A549 cells. Tumor cells were transduced with Ad-*p53* alone or cotransduced with Ad-*FHIT* + Ad-*p53* for 72 h. Cell extracts were IP with MDM2 or immunodepleted (ID) with MDM2 antibody followed by immunoblotting with the p53 antibody. *C*, immunofluorescence imaging analysis of the subcellular localization of FHIT and MDM2 proteins in A549 cells in which the endogenous expression of p53 was induced by cisplatin followed by transduction with Ad-*FHIT*. Immunofluorescence staining was performed 24 h after transduction. Expression of the FHIT proteins is shown in *green* (FITC) (*a*), MDM2 expression is shown in *red* (rhodamine) (*b*), and nuclei are shown in *blue* 4′,6-diamidino-2-phenylindole (DAPI) (*c*); an overlapped image is shown in *d*. The FHIT protein was mainly detected in cytosol, whereas the MDM2 protein was predominantly located in nuclei. The untransduced (N) and the Ad-*FHIT*-transduced (F) cells are indicated with *arrows*.

a significant synergistic inhibition in the growth of NSCLC cells both *in vitro* and *in vivo*.

There is increasing evidence that the inactivation of multiple tumor suppressor genes has a synergistic effect on tumor development and proliferation (22, 27). For example, >50% of NSCLCs have been found to carry *p53* mutations (11) and 50–70% of NSCLCs also have deficient *FHIT* gene expression (28, 29). In addition, several studies have demonstrated that an allelic imbalance within the *FHIT* locus frequently coexists with *p53* abnormalities and that this may be an early event in NSCLC pathogenesis (30, 31). From a clinical perspective, NSCLCs are highly resistant to conventional treatments such as surgery, radiotherapy, and chemotherapy (32). On the basis of these observations and known facts, combination treatment with synergistic tumor-suppressing gene therapy (in our case, adenoviral vector-mediated *FHIT* and *p53* gene cotransfer) may constitute a rational and effective strategy for the treatment of a wide range of both lung and other cancers.

The stability of p53 is the key to the maintenance of multiple cellular functions such as cell cycle arrest and apoptosis. The *p53* tumor suppressor gene is activated in response to diverse cellular stresses such as those inflicted by DNA-damaging agents and to oncogenic signals through mechanisms that result in the stabilization and accumulation of wild-type p53 protein (20, 33). Overexpression of FHIT protein up-regulated both the endogenous and exogenous wild-type p53 expression in NSCLC cells transduced by the Ad-*FHIT* vector alone or cotransduced by Ad-*FHIT* and Ad-*p53*. However, the latter results in synergistically enhanced tumor suppression and apoptotic activities, which may be a direct reflection of the FHIT-mediated stabilization of p53. This implicates an important molecular pathway in the regulation of FHIT-mediated tumor-suppressing activity. Although the sensitivity of tumor cells to the adenoviral vector-mediated *FHIT* transfer-induced growth inhibition was not significantly correlated with the *p53* gene status in the cells tested (4, 6), the activation of endogenous p53 in cells possessing wild-type *p53* by a chemotherapeutic agent such as cisplatin or the induction of the exogenous expression of *p53* in *p53*-null or mutant cells by a gene therapy agent such as Ad-*p53* could be used to enhance the therapeutic efficacy of Ad-*FHIT* in a wide range of tumor cells. For example, as shown in this study, in the H460 cells with wild-type *p53* pretreated with cisplatin and then transduced with Ad-*FHIT*, the expression of endogenous p53 was induced, the FHIT-mediated stabilization of the p53 protein was massively enhanced, and caspase-9 was activated (Fig. 1*D*). Of further relevance, the induction of apoptosis mediated by Ad-*p53* and Ad-*FHIT* also follows a different time course. That is, a peak apoptotic induction is seen for Ad-*p53* at ~48 h and for Ad-*FHIT* at ~96 h after transduction (33, 34). They also induce apoptosis via different pathways (35). These differences in therapeutic kinetics and molecular function may thus also contribute to the observed synergistic effect of combination treatment with Ad-*FHIT* and Ad-*p53* on both growth inhibition and apoptosis.

Structural and functional analysis of the MDM2 protein has revealed that MDM2 interacts directly with p53 in the NH_2-terminal domains (20, 36). As a result of this interaction, MDM2 directly blocks the transcription factor and a tumor suppressor activity of p53 (37) and targets p53 for degradation by proteolysis (33, 38). It has thus become clear that one way to stabilize and activate p53 in cells is by interrupting the interaction of MDM2 and p53 (39). Ways to do this are suggested by the fact that the activity of MDM2 is also regulated by covalent modifications and by noncovalent regulators, both of which can modulate the ability of MDM2 to bind p53 (19). In particular, two tumor suppressor proteins, human $p16^{Ink4A}$ and murine $p19^{Arf}$ (human $p14^{Arf}$), have been shown to bind to MDM2 and inhibit the MDM2-mediated degradation of p53 (40, 41). We observed a significant reduction of MDM2 proteins in cells cotransduced by Ad-*FHIT* and Ad-*p53* compared with those transduced by Ad-*p53* alone. We also noticed a significant reduction of MDM2-p53 complexes and detected the direct MDM2-FHIT interaction in those cells. These results suggest that the interaction of FHIT with MDM2 may

95th AACR Annual Me
March 27-31, 2004
Orange County Convention
Orlando, Florida

3796 Enhanced sensitivity of tumor cells to chemotherapeutic agents by activation of *fus1* tumor suppressor gene in lung cancer cells.

Jiichiro Sasaki, Futoshi Uno, John D. Minna, Jack A. Roth, Lin Ji.
UT. M.D. Anderson Cancer, Houston, TX and UT Southwestern Medical Center, Dallas, TX.

FUS1 is a novel tumor suppressor gene (TSG) identified in the human chromosome 3p21.3 region that is deleted in many cancers. We previously found that *FUS1* TSG was inactivated in many primary lung cancers and cancer-derived cell lines by either the loss of expression or the deficiency of the posttranslational myristoylation modification of the wild-type (wt)-Fus1 proteins. We also demonstrated that exogenous expression of the wt-*FUS1* by plasmid- or adenoviral vector-mediated gene transfer significantly inhibited tumor cell growth, induced apoptosis, and altered cell cycle kinetics in 3p21.3-deficient lung cancer cells *in vitro* and efficiently suppressed tumor growth and inhibited tumor progression and metastases in human lung cancer xenograft mouse models. Based on these pre-clinical investigations, a phase I clinical trial is now undertaking in advanced non-small cell lung cancer patients using systemic administration of DOTAP-cholesterol-complexed wt-*FUS1*-expressing plasmid DNA (*FUS1*-lipoplex). In this study, we explored the capability of the wt-*FUS1* gene product as a modulator of chemotherapeutic drugs for enhancing chemotherapeutic potency and overcoming drug resistance in lung cancer cells. We found that a transient expression of the wt-Fus1 protein in *FUS1*-expressing plasmid-transfected H1299 cells significantly enhanced the cisplatin-mediated inhibitory effect on tumor cell growth at a low-dose (1 micro molar) of cisplatin treatment. In addition, a stable expression of the wt-*FUS1* gene, which is under the control of a ponasterone A-inducible promoter, reduced more than 30% of IC_{50} values of both cisplatin and paclitaxel treatments in H1299 cells, even at a low level of induced Fus1 expression. However, the maximum stable expression of a functionally deficient mutant Fus1 protein (mt-Fus1) in a similar inducible system did not enhance the sensitivity of tumor cells to these drugs. Furthermore, a significant increase in apoptotic cell populations were detected in cells with the induced expression of the wt-Fus1 protein but not in those with induced expression of mt-Fus1, as shown by a FACS analysis with TUNEL reaction. These results suggest that the wt-Fus1 may play a critical role in modulating the sensitivity of tumor cells to the chemotherapeutic agents, especially, to DNA damaging agents such as cisplatin and that a combination treatment with the *FUS1*-lipoplex-mediated molecular therapy and the cisplatin or taxcel-based chemotherapy may be an efficient treatment strategy for lung cancer.

95th AACR Annual Me
March 27-31, 2004
Orange County Convention
Orlando, Florida

4821 Activation of apoptotic signaling pathway by direct interaction between tumor suppressor Fus1 and Apaf-1 proteins in lung cancer cells.

Futoshi Uno, Jiichiro Sasaki, Gitanjali Jayachandran, Kai Xu, John D. Minna, Jack A. Roth, Lin Ji. *The University of Texas M.D. Anderson Cancer Center, Houston, TX and The University of Texas Southwestern Medical Center, Dallas, TX.*

FUS1 is a novel tumor suppressor gene identified in a 120-kb overlapping homozygous-deletion region in human chromosome 3p21.3 in lung and breast cancers. We previously demonstrated that enforced expression of the wild-type (wt)-*FUS1* in 3p21.3-deficient non-small cell lung cancer (NSCLC) cells significantly suppressed tumor cell growth by induction of apoptosis and alteration of cell cycle kinetics *in vitro* and *in vivo*. However, the molecular mechanism and signaling pathway involved in the *FUS1*-mediated apoptosis remained unknown. In this study we aimed to identify the potential cellular targets of Fus1 protein to have an insight into the mechanism of Fus1 function. We performed immuno-precipitation (IP) analysis using anti-Fus1 antibodies with protein lysates prepared from Fus1-expressing plasmid-transfected NSCLC H1299 cells to analyze the Fus1-mediated protein-protein interactions. The potential cellular protein targets that directly interact with Fus1 protein were analyzed by SDS-PAGE of the IP complexes and further identified by peptide mapping of the trypsin-digested proteins in the complexes by a surface-enhanced laser desorption and ionization-mass spectrometry on a ProteinChip array. One of the potential Fus1-interacting proteins was predicted by peptide mapping as the apoptotic protease activation factor 1 (Apaf-1). This Fus1-Apaf1 interaction was further confirmed by IP and immuno-blot analysis using either anti-Fus1 or anti-Apaf1 antibodies, alternatively. We also observed that both the wt-Fus1 and a *N*-myristoylation-deficient mutant Fus1 (myr-mt-Fus1) protein but not the *C*-terminal-deletion (10-20 amino acids) mutants of Fus1 proteins could bind to Apaf-1 protein in H1299 transfectants. A computer-aided structural analysis predicted a PDZ domain in the *C*-termini of the both Fus1 and Apaf1 proteins, suggesting that the Fus1-Apaf-1 interaction might be mediated through these classic PDZ protein-protein interaction motifs. Using an immuno-fluorescence image analysis with Fus1 and Apaf1 antibodies, we detected that the Apaf1 proteins were co-localized with the wt-Fus1 proteins in their typical mitochondria and ER membrane locations but with the myr-mt-Fus1 proteins, which lost its membrane-attachment capability, everywhere in the cytoplasm in the wt-*FUS1* and myr-mt-*FUS1*-transfected H1299 cells, respectively. These results suggest that Fus1 protein may

Lipoplex Based Systemic Gene Therapy For Lung Cancer: Molecular Mechanisms, and Strategies To Suppress Lipoplex-Mediated Inflammatory Response.

Began Gopalan, Ph.D.[1], Isao Ito, M.D.[1], Cynthia D. Branch, B.S.[1], Clifton Stephens, D.V.M.[2], B. Neblyou Bekele, Ph.D.[3], Jack A. Roth, M.D.[1], and Rajagopal Ramesh, Ph.D.[1*]

[1]Department of Thoracic and Cardiovascular Surgery, [2]Department of Veterinary Medicine and Surgery, [3]Department of Biostatistics, The University of Texas M. D. Anderson Cancer Center, Houston, TX 77030.

*Address for Correspondence: Rajagopal Ramesh, Ph.D., Department of Thoracic and Cardiovascular Surgery, The University of Texas M. D. Anderson Cancer Center, 1515 Holcombe Blvd., Box 445, Houston, TX 77030 U.S.A. Phone: (713) 794-1479, Fax: (713) 794-4901; E-mail: rramesh@ mdanderson.org

Running Title. Suppression of lipoplex-mediated inflammatory response for systemic therapy

Keywords. Gene therapy, systemic, liposome, inflammation, Naproxen, cytokines

Abbreviations. DOTAP, Diethyl oleyl-1, 2-bis (oleoyloxy)-3-(trimethyl ammonio) propane; Chol, cholesterol; PGE_2, prostaglandin E_2; COX-2, cyclooxygenase; MAPK, mitogen activated protein kinase; TNF, tumor necrosis factor, IL, interleukin; NFκB, nuclear factor kappa-B; AP-1, activator protein-1.

Abstract

Cancer gene therapy for the treatment of lung cancer has shown promise in the laboratory and in Phase I/II clinical trials. However, it is currently limited to treating localized tumors due to host-immunity against the gene delivery vector and the transgene. Therefore, there is a tremendous effort to develop and test alternate gene delivery vectors that are efficient, non-immunogenic, and applicable for systemic therapy. One such gene delivery vehicle is the non-viral vector, DOTAP:cholesterol (DOTAP:Chol) liposome. Preclinical studies from our laboratory has shown that DOTAP:Chol. liposomes are effective gene delivery vectors that efficiently deliver tumor-suppressor genes to disseminated lung tumors when injected intravenously. Based on our findings we have recently initiated a Phase-I trial for systemic treatment of lung cancer using a novel tumor suppressor gene, *FUS1*. Although DOTAP:Chol. liposome complexed to DNA (lipoplex) are efficient vectors for systemic therapy, induction of an inflammatory response in a dose-dependent fashion has also been observed thereby limiting its use. A better understanding of the underlying mechanism for lipoplex-mediated inflammatory response will allow us to develop strategies to suppress inflammation and expand the therapeutic window in treating human cancer. In the present study we conducted experiments examining the mechanism of lipoplex-mediated inflammatory response in vitro and in vivo. We demonstrate that systemic administration of lipoplex induced multiple signaling molecules both in vitro and in vivo, that are associated with inflammation. Furthermore, use of small molecule inhibitors against the signaling molecules resulted in their suppression and thereby reduced inflammation without affecting transgene expression. Our results provide a rationale to use small molecule inhibitors to suppress lipoplex-mediated inflammation when administered systemically. Further development and testing will allow us to incorporate this strategy into future clinical trials that are based on systemic non-viral gene therapy.

Introduction

Lung cancer is one of the leading causes of death in the world (1). Despite recent advances in treatment strategies, drug resistance, loco-regional and distant failure and poor response to therapy contribute to a low overall 5-year survival rate for common epithelial cancers, including lung cancer (1). Therefore, novel forms of therapy are urgently needed. Gene transfer strategies with the tumor suppressor gene *p53* have shown clinical promise in Phase I/II trials for non-small cell lung cancer and head and neck squamous cell carcinoma (2-6). However, this strategy has been limited to loco-regional treatment because of adenovirus-mediated toxicity and immune responses associated with systemic delivery (7,8). An alternate to adenoviral vector system is to use non-viral gene delivery systems, which have been shown to be effective in delivering therapeutic genes to cancer sites when administered systemically (10-17). The advantage of using non-viral vector systems is that they are easy to manufacture and less immunogenic (18). Furthermore, it is feasible to develop non-viral vectors that target the tumor or tumor vasculature specifically. The best strategy one could envision for lung cancer treatment is a vehicle that systemically delivers a therapeutic agent to the primary tumor site and to distant metastatic sites without undue toxicity.

A non-viral liposomal vector that has been shown to efficiently deliver genes to the lungs when administered intravenously is the cationic DOTAP:cholesterol (DOTAP:Chol) liposome (10,11). Based on these reports we have tested DOTAP:Chol. liposome as a gene-delivery vehicle for treatment of lung cancer. Preclinical efficacy studies from our laboratory demonstrated intravenous injection of DOTAP:Chol.-DNA complex (lipoplex) in mice bearing experimental lung metastasis resulted in effective transgene expression in the tumors leading to a significant therapeutic effect (12,19). Furthermore, intravenous administration of lipoplexes resulted in

increased transgene expression in the lung tumors compared to the surrounding normal lung tissue that resulted in an increased therapeutic effect (20). Increased transgene expression in the tumors was due to increased and selective uptake of the lipoplex by the tumors in the lungs compared to the surrounding normal tissue (20). In a more recent study we have demonstrated the tumor suppressive effect of a novel 3p gene, *FUS1*, on disseminated lung tumors when injected intravenously (21, 22). These results suggest systemic delivery of therapeutic genes (*p53, Fhit, FUS1, mda-7*) to disseminated tumors is feasible using DOTAP:Chol. liposome. Based on our results, we have recently initiated a Phase-I clinical trial for systemic treatment of lung cancer using the *FUS1* tumor suppressor gene complexed with DOTAP:Chol. liposome.

Although DOTAP:Chol. liposome has been shown to be an effective systemic gene delivery vehicle, induction of an inflammatory response in a dose-dependent fashion has also been observed resulting in toxicity (Ramesh et al., unpublished data). Induction of inflammatory response following systemic administration of DOTAP:Chol.-DNA complex is neither surprising nor unique to the liposome composition. Induction of an inflammatory reponse has previously been reported using other non-viral liposomal vectors (23-29). Thus, the therapeutic window for DOTAP:Chol. liposome based systemic gene therapy for cancer will be limited. Therefore, a better understanding of the mechanism of lipoplex-mediated inflammatory response will enable us to develop strategies to overcome this limitation and thereby increase the therapeutic window to deliver higher doses of the therapeutic gene.

Recent studies have demonstrated immunostimulatory CpG motifs present in the plasmid DNA to play a major role in lipoplex-mediated inflammation. Reducing the number of CpG sequences in the plasmid DNA has been shown to reduce the inflammatory response and increase transgene

expression (30,31). Additional strategies tested to overcome the inflammatory response include the use of PCR-amplified DNA fragments instead of full-length pDNA (32) and the use of immunosuppressant (33). All of these strategies have shown improvements in reducing inflammation. However, they have not been able to completely suppress or eliminate the lipoplex-mediated inflammatory response. Furthermore, some of the strategies have not been feasible in a clinical setting. Therefore, additional strategies are warranted. A better understanding of the underlying mechanism for lipoplex-mediated inflammatory response will allow us to develop effective strategies to suppress inflammation and expand the therapeutic window in treating human cancer.

In the present study we conducted experiments examining the mechanism of lipoplex-mediated inflammatory response in vitro and in vivo. We demonstrate that systemic administration of lipoplex induced multiple signaling molecules both in vitro and in vivo that are associated with inflammation. Furthermore, use of small molecule inhibitors targeted against the signaling molecules resulted in their suppression and thereby reduced inflammation without affecting transgene expression. Our results provide a rationale to use small molecule inhibitors to suppress lipoplex-mediated inflammation when administered systemically. Further development and testing will allow us to incorporate this strategy into future clinical trials that are based on systemic non-viral gene therapy.

Materials and Methods

Materials. All lipids (DOTAP, Cholesterol) were purchased from Avanti Polar Lipids (Alabaster, AL). Naproxen for tissue culture experiments was purchased from Sigma Chemicals (St. Louis, MO). Clinical grade Naproxen for in vivo studies was purchased from Pharmacy at M. D.

Anderson Cancer Center (Houston, TX). U0126 and SB203580 were purchased from Calbiochem (San Diego, CA). Antibodies against phosphorylated p38MAPK, pJNK, p44/42MAPK, $pATF_2$, and pc-Jun were purchased from Cell Signaling (Cambridge, MA). Anti-COX-2 antibody was purchased from Cayman Chemicals (Ann Arbor, MI).

Cells, and culture methods. Human fibroblast (MRC-9) cell line was purchased from American Tissue Culture Collection (Rockville, MD). Cells were maintained in the appropriate medium as recommended by the supplier. Cells were regularly passaged and maintained at 37°C in humidified atmosphere with 5%CO_2.

Animals. Four – to six-week-old female C3H/Ncr mice (National Cancer Institute, Frederick, MD) used in the study were maintained in a pathogen-free environment and handled according to institutional guidelines established for animal care and use.

Preparation of lipoplex. Synthesis, and preparation of lipoplex carrying the *FUS1* gene was carried out as previously described (12). Freshly prepared lipoplex were used in each experiment described in the present study. Particle size analysis showed the lipoplex was 300-350 nm in size.

In vitro experiments. To determine the effect of DOTAP:Chol-*FUS1* complex on the activation of signaling molecules associated with inflammation, MRC-9 fibroblast cells were seeded in six-well plates (5 x 10^5 cells/well) and incubated overnight at 37°C and 5% CO_2. The following day, tissue culture medium was replaced with fresh medium and cells were either nor treated or treated with various concentrations of SB203580 (p38MAPK inhibitor; 10, and 30 μM), U0126 (p44/42 MAPK inhibitor; 10, 30 μM), or with Naproxen (COX-2 inhibitor; 0.5mM). Two-three hours after treatment,

cells were transfected with DOTAP:Chol-*FUS1* complex (2.5μg DNA) in 0.2% serum medium. Cells were harvested at different time-points (2h, 4h, 15h) after transfection, washed, and cell lysates prepared as previously described (12). Untransfected cells treated with PBS served as control in these experiments. Cell lysates were subjected to western blotting analysis and probed with various antibodies as previously described (19, 20). In all the experiments, β–actin was detected using anti-β-actin antibody (Sigma Chemicals, St. Louis, MO) as a measure of internal loading control.

To determine the effect of inhibitors on transgene expression, cells were transfected with a marker gene, luciferase (luc), complexed with DOTAP:Chol. liposome. All other experimental conditions were the same as described above. Luciferase expression was determined using the luciferase assay kit (Promega, Madison, WN) as previously described (19). Luciferase expression was expressed as relative light units per mg of protein (RLU/mg). Assays were performed in triplicates. Experiments were performed two times and the results represented as the average of two separate experiments.

Electrophoretic mobility shift assay (EMSA). MRC-9 cells were seeded in six well plates at 1.3 X 10^6 cells/well for EMSA. The following day cells were replaced with 0.2 % serum medium and then preincubated for 3 ½ hrs in the absence or presence of naproxen before the cells were transfected with lipoplex (2.5μg DNA). Cells were harvested at 2, 4 and 15h after transfection and nuclear extracts prepared. To the nuclear extracts (10 μg), DNA binding reaction mixture containing [γ-^{32}P]-ATP radiolabeled AP-1 oligonucleotide and 0.5 μg poly (dI-dC) were added and incubated at 25°C for 30 min in 5X gel shift binding buffer [20% glycerol, 5mM $MgCl_2$ 2.5mM EDTA, 2.5 mM DTT, 250mM NaCl, 50mM Tris-HCl (pH 7.5)]. The complexes were subsequently

resolved on 5% nondenaturing polyacrylamide gels in 0.5 X Tris-borate EDTA buffer for 1h 30min at 300 V. The bands were visualized by autoradiography.

PGE_2 production assay. Cells were seeded in 6-well plates (1-3 X 10^6 cells/well) and incubated at 37°C. Twenty-four hours later, the culture medium was replaced and replenished with fresh medium supplemented with 0.2% serum. Cells were then either not treated or treated with naproxen (0.5mM). At 3.5 h after treatment cells were transfected with DOTAP:Chol-*FUS1* complex (2.5μg DNA). The amount of PGE_2 secreted into the culture supernatant at various time (2h, 4h, and 15h) points was determined using the PGE_2 enzyme immunoassay (Cayman Chemicals, Ann Arbor, MI). Assay was performed according to manufacturer's protocol.

In vivo experiments. To determine the effect of intravenous administration of DOTAP:Chol-*FUS1* complex on inflammation and the potential use of inhibitors, in vivo experiments were conducted in immunocompetent female C3H mice. Mice were divided into three groups (n=5/group). Group 1 did not receive any treatment. Group 2 received a single dose of Naproxen (15 mg/Kg) orally 3h prior to intravenous injection of DOTAP:Chol-*FUS1* complex. Group 3 received intravenous injection of DOTAP:Chol-*FUS1* complex only. The amount of plasmid DNA injected was 100 μg. The rationale for selecting this dose was based on our previous results which showed that 100 μg of *FUS1* plasmid DNA to produce acute inflammation that was lethal producing 100% mortality (Began et al., unpublished data). The procedure for intravenous injections of liposome-DNA complex has previously been reported (12, 19, 20). At 2h, 4h, 6h and 15h after treatment with DOTAP:Chol-*FUS1* complex, animals were euthanized and blood and organs (lung, liver, spleen) collected. Blood samples were analyzed for mouse TNF-α by ELISA

(R&D Systems, MI). Tissue samples were analyzed for expression of inflammation-associated signaling molecules by western blotting (20).

Results

Lipoplex induces inflammation-associated signaling molecules in vitro. To test whether DOTAP:Chol-*FUS1* complex can induce inflammation-associated signaling molecules and whose expression can be suppressed by small molecule inhibitors, we first conducted in vitro experiments. Transfection of MRC-9 cells with DOTAP:Chol-*FUS1* complex resulted in a significant increase in the expression of p38MAPK, pJNK, p44/42MAPK, and its downstream substrates pATF-2, pc-Jun, and COX-2 compared to untreated control cells (Fig. 1). The activation of various inflammation-associated signaling molecules indicate the ability of DOTAP:Chol-*FUS1* complex to induce an inflammatory response.

Small molecule inhibitors suppress inflammation-associated signaling molecules induced by lipoplex. The ability of DOTAP:Chol-*FUS1* complex to induce inflammation -associated signaling molecules in vitro suggested its potential limitation in vivo. Therefore we tested the ability of small molecule inhibitors to inhibit inflammation-associated signaling molecules induced by lipoplex. For this purpose we tested inhibitors specifically targeted towards p38MAPK (SB 203580), p44/42 MAPK (U0126) or COX-2 inhibitor (Naproxen). Treatment of cells with various doses of SB 203580 prior to transfection with DOTAP:Chol-*FUS1* complex resulted in a marked suppression of p38 MAPK expression and its downstream substrates, pATF-2, pc-Jun, and COX-2 compared to cells that were only transfected with DOTAP:Chol-*FUS1* complex (Fig. 2A). The inhibitory effect was observed to be time-dependent and not dose-dependent. Baseline p38MAPK expression was observed in untreated control cells. Similarly, treatment of cells with U0126

resulted in a significant inhibition in p44/42 MAPK expression and its downstream substrates compared to cells that did not receive any treatment and cells that were transfected with DOTAP:Chol-*FUS1* complex only (Fig. 2B). The inhibitory activity exerted by U0126 was neither time-nor dose-dependent. p44/42MAPK expression levels was decreased more than the baseline expression seen in untreated control cells. These results suggest that p38MAPK and p44/42MAPK can be effectively inhibited using inhibitors targeted towards these molecules.

The effect of naproxen, a non-steroidal anti-inflammatory small molecule targeted to COX-2 was next investigated. Treatment of cells with naproxen prior to transfection with DOTAP:Chol-*FUS1* complex resulted in a significant inhibition of various MAPK that included p38MAPK, pJNK, and p44/42MAPK compared to cells that were transfected with DOTAP:Chol-*FUS1* complex only (Fig. 2C). The inhibitory effect on various MAPK correlated with decreased expression of their downstream substrates, pATF-2, pc-Jun and COX-2. Additionally the inhibitory effect on MAPK expression appeared to increase over time. Baseline expression of p38MAPK, pJNK, and p44/42MAPK was observed in untreated control cells. These results demonstrate that naproxen in addition to inhibiting COX-2 also inhibited all three kinase molecules that are associated with inflammation. Thus naproxen appears to function as a broad-spectrum inhibitor inhibiting multiple signaling molecules. Furthermore, based on its ability of to function as a broad-spectrum inhibitor we speculated that naproxen would be more effective than SB 203580 and U1026 in vivo. Hence, in all subsequent experiments we tested naproxen.

Lipoplex-mediated activation of AP-1 is inhibited by naproxen. Recent studies have demonstrated activation of p38MAPK by CpG containing DNA leads to the activation of transcription factor CREB/AP-1, that is an important mediator of inflammation (34). Presence of consensus AP-1 DNA binding site in the promoter region of several genes including COX-2 has

been reported (34). Based on these reports and ability of DOTAP:Chol-*FUS1* complex to induce COX-2 expression we speculated activation of AP-1 and that pretreatment with naproxen will result in reduced AP-1 DNA binding activity. Therefore to test this possibility, cells treated with DOTAP:Chol-*FUS1* complex in the presence or absence of naproxen were analyzed for AP-1 DNA binding activity by electro-mobility shift assay (EMSA). Untreated cells served as control in these experiments. Increased AP-1 activity was observed in DOTAP:Chol-*FUS1* transfected cells compared to untreated control cells (Fig. 3). In contrast, treatment with naproxen resulted in inhibition of AP-1 activity. Our data shows DOTAP:Chol-*FUS1* treatment results in activation of AP-1 that is inhibited by naproxen. Furthermore, AP-1 activation correlated with the activation of MAPK molecules that are upstream to these transcriptional factors. Correlation was also observed with the activation of COX-2 that is downstream of AP-1.

Lipoplex induced PGE_2 production is inhibited by naproxen. PGE_2 is a substrate for COX-2. Activation of COX-2 results in breakdown of PGE_2 into its metabolites that are potent inducers of inflammation (35, 36). Since naproxen inhibited lipoplex-induced COX-2 expression, we tested whether PGE_2 production is also inhibited. To test this possibility secreted PGE_2 levels were measured in the tissue culture medium growing cells that were transfected with DOTAP:Chol-*FUS1* complex in the presence or absence of naproxen. PGE_2 expression levels were determined by ELISA. As shown in Fig 4, treatment of cells with DOTAP:Chol-*FUS1* complex resulted in a time-dependent increase in the secreted PGE_2 levels (2000-4000 pg/ml) compared to the basal level in untreated control cells (10 pg/ml). However, pretreatment of cells with naproxen prior to transfection with DOTAP:Chol-*FUS1* complex resulted in a significant inhibition of PGE_2 (33-120 pg/ml; $P = < 0.001$). In fact the inhibition was almost complete starting from 2h after transfection. Similar results were also obtained from murine macrophage cell line (RAW 264.7; data not

shown). These results demonstrate the ability to naproxen to effectively inhibit both COX-2 expression and its substrate PGE_2 that are important mediators of inflammation.

Lipoplex-mediated transgene expression in not affected by naproxen. Although suppression of lipoplex-mediated signaling molecules was demonstrated, one question that remains unanswered are the effects of the inhibitors on transgene expression. The possibility that the inhibitors can also suppress transgene expression existed. Furthermore, previous studies have shown that lipoplex-mediated inflammatory cytokines inhibit transgene expression (37). Therefore we investigated the effect of naproxen treatment on transgene expression using luciferase as a marker gene. Luciferase expression was observed at 15h in both, cells that were transfected with DOTAP:Chol-*luc* complex containing naproxen and in cells that were transfected with DOTAP:Chol-luc and not treated with naproxen (Fig. 5; $P=< 0.001$). Furthermore, luciferase expression was greatly increased in naproxen treated cells compared to cells that were not treated with naproxen. No luciferase expression was observed in cells that were untreated (control) or treated with empty liposome. Enhanced transgene expression was also observed in lung tumor cells that were transfected with DOTAP:Chol-*luc* complex in the presence of naproxen (data not shown). Thus, naproxen treatment results in selective inhibition of signaling molecules associated with inflammation without affecting transgene expression.

Lipoplex-induced inflammatory response is suppressed by naproxen in vivo. Preliminary studies from our laboratory demonstrated showed that intravenous injection of DOTAP:Chol-*FUS1* complex resulted in the induction of an inflammatory response that was dose-dependent. Injection of 100 μg of *FUS1* plasmid DNA complexed to DOTAP:Chol. liposome resulted in acute inflammatory response resulting in 100% mortality (Began et al., unpublished data). Based these

observations we tested whether pretreatment of animals with naproxen prior to intravenous injection of a lethal dose of DOTAP:Chol-*FUS1* complex would suppress the acute inflammatory response. Suppression of inflammation by naproxen was determined by measuring TNF-α, a key mediator of inflammation (**38**), and by analyzing the lung tissues for the inflammation-associated signaling molecules at various (2h, 4h, 15h) time points after treatment.

Analysis for TNF-α in the blood of animals that were injected with DOTAP:Chol-F*US1* complex showed maximum TNF-α expression levels at 2h (873 pg/ml) and decreased over time (Fig. 6A; *P* = <0.04). In contrast, the TNF-α expression levels was reduced by half at 2h (411 pg/ml) in animals that were pretreated with naproxen prior to injection of DOTAP:Chol-*FUS1* complex. Reduced TNF-α in naproxen treated animals was also observed at all time points tested. These results showed that naproxen suppressed DOTAP:Chol-*FUS1* complex induced TNF-α.

We next tested for the expression of inflammation-associated signaling molecules in the lung tissues of mice that were either treated with naproxen or not treated with naproxen. As observed in our in vitro experiments, a marked activation of p38MAPK, pJNK, p44/42MAPK and their downstream substrates pATF2, pc-JUN, and COX-2 was observed in the lung of mice that were intravenously injected with DOTAP:Chol-*FUS1* complex compared to the lungs of control mice that did not receive any treatment (Fig. 6B). Activation of the signaling molecules was observed at all time points tested with maximum activation occurring at 2h that correlated with TNF-α production. However, activation of the various signaling molecules was markedly suppressed in the lungs of mice that were treated with naproxen prior to receiving DOTAP:Chol-*FUS1* complex. Suppression of activation of signaling molecules by naproxen was observed as early as 2h after DOTAP:Chol-*FUS1* complex treatment. The inhibitory activity of naproxen on the activation of signaling molecules correlated with its inhibitory activity on TNF-α. Our results show that naproxen

inhibits TNF-α production by inhibiting various signaling molecules that are associated with its induction.

Discussion

We have previously demonstrated DOTAP:Chol. liposomes to be an efficient systemic gene delivery vehicle that effectively delivers therapeutic genes (*p53, Fhit, FUS1, mda-7*) to primary and disseminated lung tumors in mice resulting in a therapeutic effect (12, 19, 20). Furthermore, we have recently shown that tumors in the lung selectively uptake DOTAP:Chol-DNA complexes compared to surrounding normal tissues resulting in increased transgene expression in the tumors (20). Based on the unique properties of DOTAP:Chol. liposome and the results obtained in our preclinical studies, we have recently initiated a Phase-I clinical trial for systemic treatment of lung cancer with the *FUS1* tumor suppressor gene. However preclinical toxicity studies from our laboratory revealed dose-limiting toxicity for DOTAP:Chol-*FUS1* complex (Ramesh et al., unpublished data). Toxicity was associated with the induction of an acute inflammatory response. Induction of an inflammatory response following intravenous administration of liposome-DNA complex is not surprising and is in agreement with previous reports from other laboratories (25-30). However, our results also suggested the potential limitation of DOTAP:Chol-DNA complexes for systemic therapy. Furthermore, it was also realized that the therapeutic window to observe a response in a clinical setting would be narrow. Thus if the doses required to achieve a therapeutic response were close or higher than the maximum tolerated dose (MTD) than it would not be possible to successfully treat patients and achieve a therapeutic response. We therefore explored strategies to overcome the existing limitation-induction of inflammatory response, thereby making DOTAP:Chol. liposome based systemic therapy feasible as well increasing the therapeutic window.

In order to overcome the existing limitation, we had to have a better understanding of the underlying mechanism responsible for lipoplex-mediated inflammatory response. A role for p38MAPK, p44/42MAPK, and JNK in inflammation has previously been demonstrated (39-41). Based on these reports we first examined for these inflammation-associated signaling molecules after lipoplex treatment. In vitro experiments showed lipoplex activated MAPK's (p38, p44/42), JNK, and their substrates that included pATF, and pc-Jun suggesting that these molecules may be participate in lipoplex-mediated inflammation.

Although activation of MAPK's and their substrates was observed, they alone do not directly contribute to inflammation. One molecule that is frequently activated by these kinases is COX-2 resulting in PGE_2 production. Activation of COX-2 by MAPK's and JNK has been shown to depend on the cell type, stimuli, and species. Furthermore, each MAPK has a different regulatory role in COX-2 gene transcription. In macrophages activated by human herpesvirus 6, JNK has been shown to play a critical regulatory role in human COX-2 gene transcription (42). Similarly, role for JNK in murine MC3T3-E1 osteogenic cells stimulated with TNF-α plus IL-1β has been reported (43). Requirement of both ERK and JNK for COX-2 promoter activity induced by IgE receptor aggregation has been shown in mast cells (44) while a role for ERK1/2 and p38 in regulating HSP60-induced COX-2 expression has been shown in macrophages and endothelial cells (45). Increased levels of COX-2 lead to production of PGE-2, a breakdown product of arachidonic acid. Elevated levels of COX-2, and PGE_2 have bee reported in inflammation and its associated disease process (46, 47). Similarly, the presence of CpG motifs in the plasmid DNA has been shown to induce COX-2 expression and prostaglandin production contributing to the development of airway inflammation (48). In the present study we showed activation of both COX-2 and PGE_2

production after lipoplex treatment suggesting it may play a role in lipoplex-mediated inflammation. However, the kinase (p38MAPK, p44/42MAPK, and JNK) activating COX-2 and PGE_2 production is not clear since all three kinases were activated. We are currently investigating the role of individual kinase in the lipoplex-mediated inflammatory response.

Activation of COX-2 by MAPK's including ERK, JNK and p38MAPK has been shown to be mediated by AP-1 (49). AP-1 is a potent transcriptional activation factor that can bind to the promoter region of several genes and activate their transcription. We therefore analyzed for AP-1 activation by EMSA. A significant activation of AP-1 was observed in lipoplex treated cells. Activation of AP-1 was observed as early as 2h that correlated with the activation of MAPK's and COX-2. Our results demonstrate that the molecular signaling pathway for lipoplex-mediated inflammatory response involves all three MAPKs (p38MAPK pJNK and ERK) leading to COX-2 and PGE-2 production via AP-1 activation. The possibility of NFκB involvement, another transcriptional factor, was also examined. However, activation of NFκB was not observed in lipoplex treated cells (data not shown). To our knowledge this is the first report detailing the pathways for lipoplex-mediated inflammatory response.

Now that we have identified the signaling molecules associated with inflammation, we next investigated the potential use of small molecule inhibitors targeted towards p38MAPK (SB 203580), p44/42MAPK (U0126), and COX-2 (naproxen) thereby suppressing inflammation. In vitro experiments demonstrated that each of the inhibitors was able to significantly and selectively suppress activation of the target molecule when cells were pretreated prior to treatment with lipoplex. Furthermore, inhibition of activation of the target molecules resulted in the suppression of COX-2 expression. Additionally, treatment with the inhibitors did not affect the transgene

expression. These exciting results raise the possibility of their potential use in suppressing lipoplex-mediated inflammation via inhibition of COX-2, a downstream target common to the MAPK's. However, their use is limited to in vitro situations unless they are proven to be effective in vivo.

We next investigated whether lipoplex-mediated activation of signaling molecules observed in vitro is also activated in vivo and can be inhibited by small molecule inhibitors. For this purpose mice that were either not treated or treated with an oral dose of naproxen were subsequently injected with a lethal dose of lipoplex and analyzed for suppression of inflammation at various levels. Analysis for TNF-α, a proinflammatory cytokine produced following systemic administration of lipoplex was significantly suppressed in naproxen treated animals compared to animals that did not receive naproxen treatment. Molecular analysis of lung tissues for activation of signaling molecules that were identified in our in vitro experiments demonstrated activation of all of the markers (p38MAPK, p44/42MAPK, JNK, COX-2) in lipoplex treated animals. However, activation of these molecules was significantly inhibited by naproxen akin to our in vitro results. The suppression of activation of these various inflammation-associated signaling molecules by naproxen resulted in 100% survival of animals receiving a lethal dose of lipoplex (Began et al., unpublished data). Furthermore, naproxen treatment did not inhibit FUS1 protein expression in vivo but rather slightly enhanced the expression suggesting the possibility for enhanced therapeutic effect (data not shown). The ability of naproxen to inhibit COX-2 expression is expected and not surprising, as previous studies have shown it to be a COX-2 inhibitor (50, 51). However, inhibition of MAPK's by naproxen observed in the present study was unexpected and surprising. Based on our results we speculate that naproxen in addition to its direct inhibitory activity on COX-2 also exerts its inhibitory activity on additional molecules such as MAPK's as shown in Figure 7. It will also be interesting to test whether combination of naproxen with lipoplex

carrying a tumor suppressor gene such as FUS1 will enhance the therapeutic effect. We are currently examining the mechanism by which naproxen inhibits MAPK's. Whatever the underlying mechanism of action by naproxen may be, our results clearly demonstrated that pretreatment of animals with naproxen prior to systemic administration of lipoplex results in suppression of lipoplex-mediated inflammation leading to animal survival.

In conclusion we have demonstrated the signaling mechanism and strategies to suppress lipoplex-mediated inflammatory response. Thus, use of small molecule inhibitors such as naproxen alone or in combination with other small molecule inhibitors prior to lipoplex based systemic therapy will be of clinical significance both in terms of suppressing toxicity as well increasing the therapeutic window. However, additional preclinical studies related to toxicity, dosing, and therapeutic efficacy are warranted prior to incorporation of this strategy in future Phase I/II clinical trials.

Acknowledgments

The authors thank Dr. Lin Ji (M.D. Anderson Cancer Center) for providing the FUS1 expressing plasmid vector; and Alma Vega for preparation of the manuscript. This work was supported in part by the Texas Higher Education Coordinating Board ATP/ARP Grant 003657-0078-2001 (R.R.), by a Career Development Award from The University of Texas M.D. Anderson Cancer Center SPORE in Lung Cancer P50-CA70907-5 (R.R.), by Public Health Service Grant P01CA78778-01A1 (J.A.R.), by the Texas Tobacco Settlement Fund, by the BESCT Lung Cancer Program Grant DAMD17-01-1-0689 (Project # 3), by the TARGET Lung Cancer Grant DAMD17-02-1-0706 (Project # 7), by the Institutional Research Grant (R.R.), by a Grant from the W. M. Keck Foundation (R.R.), by Cancer Center Support (CORE) Grant CA16672, grant, and by a sponsored research agreement with Introgen Therapeutics, Inc

References:

1. Greenlee, R. T., Murray, T., Bolden, S., Wingo, P. A. Cancer Statistics, 2000. *CA Cancer J. Clin. 50*, 7-33 (2000).

2. Roth, J. A., Nguyen, D., Lawrence, D. D., Kemp, B. L., Carrasco, C. H., Ferson, D. Z., Hong, W. K., Komaki, R., Lee, J. J., Nesbitt, J. C., Pisters, K. M. W., Putnam, J. B., Jr., Schea, R., Shin, D. M., Walsh, G. L., Dolormente, M. M., Han, C. I., Martin, F. D., Yen, N., Xu, K., Stephens, L. C., McDonnell, T. J., Mukhopadhyay, T., Cai, D. Retrovirus-mediated Wild-type p53 Gene Transfer to Tumors of Patients With Lung Cancer. *Nat.Med. 2*, 985-991 (1996).

3. Swisher, S. G., Roth, J. A., Nemunaitis, J., Lawrence, D. D., Kemp, B. L., Carrasco, C. H., Connors, D. G., el Naggar, A. K., Fossella, F., Glisson, B. S., Hong, W. K., Khuri, F. R., Kurie, J. M., Lee, J. J., Lee, J. S., Mack, M., Merritt, J. A., Nguyen, D. M., Nesbitt, J. C., Perez-Soler, R., Pisters, K. M. W., Putnam, J. B., Jr., Richli, W. R., Savin, M., Schrump, D. S., Shin, D. M., Shulkin, A., Walsh, G. L., Wait, J., Weill, D., Waugh, M. K. A. Adenovirus-mediated p53 Gene Transfer in Advanced Non-small Cell Lung Cancer. *J. Natl. Cancer Inst. 91*, 763-771 (1999).

4. Nemunaitis, J., Swisher, S. G., Timmons, T., Connors, D., Mack, M., Doerksen, L., Weill, D., Wait, J., Lawrence, D. D., Kemp, B. L., Fossella, F., Glisson, B. S., Hong, W. K., Khuri, F. R., Kurie, J. M., Lee, J. J., Lee, J. S., Nguyen, D. M., Nesbitt, J. C., Perez-Soler, R., Pisters, K. M. W., Putnam, J. B., Richli, W. R., Shin, D. M., Walsh, G. L., Merritt, J., Roth, J. A. Adenovirus-mediated p53 Gene

Transfer in Sequence with Cisplatin to Tumors of Patients with Non-small Cell Lung Cancer. *J. Clin. Oncol. 18*, 609-622 (2000).

5. Clayman, G. L., El-Naggar, A. K., Lippman, S. M., Henderson, Y. C., Frederick, M., Merritt, J. A., Zumstein, L. A., Timmons, T. M., Liu, T.-J., Ginsberg, L., Roth, J. A., Hong, W. K., Bruso, P., Goepfert, H. Adenovirus-mediated p53 Gene Transfer in Patients with Advanced Recurrent Head and Neck Squamous Cell Carcinoma. *J. Clin. Oncol. 16*, 2221-2232 (1998).

6. Swisher, S. G., Roth, J. A., Komaki, R., Gu, J., Lee, J. J., Hicks, M., Ro, J., Hong, W. K., Merritt, J. A., Ahrar, K., Atkinson, N., Correa, A. M., Dolormente, M., Drelling, L., El-Naggar, A. K., Fossella, F., Francisco, R., Glisson, B., Grammer, S., Herbst, R., Huaringa, A., Kemp, B., Khuri, F. R., Kurie, J. M., Liao, Z., McDonnell, T. J., Morice, R., Morello, F., Mosheim, M., Munden, R., Papadimitrakopoulou, V., Pisters, K. M. W., Putnam, J. B. Jr., Sarabia, A. J., Shelton, T., Stevens, C., Shin, D. M., Smythe, W. R., Vaporciyan, A., Walsh, G. L., Yin, M. Induction of p53 Regulated Genes and Tumor Regression in Lung Cancer Following Intratumoral Delivery of Adenoviral p53 (RPR/INGN 201) and Radiation Therapy. *Clin. Cancer Res. 9*, 93-101 (2003).

7. Marshall, E. Gene therapy death prompts review of adenovirus vector. *Science 286*, 2244-2245 (1999).

8. Kafri, T., Morgan, D., Krahl, T., Sarvetnick, N., Sherman, L., Verma, I. Cellular Immune Response to Adenoviral Vector Infected Cells does not Require de Novo Viral Gene Expression: Implications for Gene Therapy. *Proc. Natl. Acad. Sci. USA 95*, 11377-11382 (1998).

9. Liu, Y., Mounkes, L. C., Liggitt, H. D., Brown, C. S., Solodin, I., Heath, T. D., Debs, R. J. Factors Influencing the Efficiency of Cationic Liposome-mediated Intravenous Gene Delivery. *Nat. Biotechnol. 15*, 167-173 (1997).

10. Templeton, N. S., Lasic, D. D., Frederik, P. M., Strey, H. H., Roberts, D. D., Pavlakis, G. N. Improved DNA: Liposome Complexes for Increased Systemic Delivery and Gene Expression. *Nat. Biotechnol. 15*, 647-652 (1997).

11. Gaensler, K. M. L., Tu, G. H., Bruch, S., Liggitt, D., Lipshutz, G. S., Metkus, A., Harrison, M., Heath, T. D., Debs, R. J. Fetal Gene Transfer by Transuterine Injection of Cationic Liposome-DNA Complexes. *Nat. Biotechnol. 17*, 1188-1192 (1999).

12. Ramesh, R., Saeki, T., Templeton, N. S., Ji, L., Stephens, L. C., Ito, I., Wilson, D. R., Wu, Z., Branch, C. D., Minna, J. D., Roth, J. A. Successful Treatment of Primary and Disseminated Human Lung Cancers by Systemic Delivery of Tumor Suppressor Genes Using an Improved Liposome Vector. *Mol.Ther. 3*, 337-350 (2001).

13. Cristiano, R. J., Roth, J. A. Epidermal Growth Factor Mediated DNA Delivery into Lung Cancer Cells Via the Epidermal Growth Factor Receptor. *Cancer Gene Ther. 3*, 4-10 (1996).

14. Cristiano, R. J., Roth, J. A. Molecular Conjugates: A Targeted Gene Delivery Vector for Molecular Medicine. *J. Mol. Med. 73*, 479-486 (1995).

15. Densmore, C. L., Orson, F. M., Xu, B., Kinsey, B. M., Waldrep, J. C., Hua, P., Bhogal, B., Knight, V. Aerosol Delivery of Robust Polyethyleneimine-DNA Complexes for Gene Therapy and Genetic Immunization. *Mol. Ther. 1*, 180-188 (2000).

16. Lu, H., Zhang, Y., Roberts, D. D., Osborne, C. K., Templeton, N. S. Enhanced Gene Expression in Breast Cancer Cells in vitro and Tumors in vivo. *Mol. Ther. 6*, 783-792 (2002).

17. Shi, H. Y., Liang, R., Templeton, N. S., Zhang, M. Inhibition of Breast Tumor Progression by Systemic Delivery of the Maspin Gene in a Syngeneic Tumor Model. *Mol. Ther. 5,* 755-761 (2002).

18. Niidome, T., Huang, L. Gene Therapy Progress and Prospects: Nonviral Vectors. *Gene Ther. 9*, 1647-1652 (2002).

19. Ramesh, R., Ito, I., Miyahara, R., Saito, Y., Wu, Z., Mhashilkar, A.M., Wilson, D.R., Branch, C.D., Chada, S., Roth, J.A. Local and Systemic Inhibition of Lung Tumor Growth after Liposome Mediated mda-7/IL-24 Gene Delivery. *DNA and Cell Biol.* (in press).

20. Ito, I., Began, G., Mohiuddin, I., Saeki, T., Saito, Y., Branch, C.D., Stephens, L.C., Yen, N., Roth, J.A., Ramesh, R. Increased Uptake of Liposomal-DNA Complex by Lung Metastases Following Intravenous Administration. *Mol. Ther. 7*, 409-418 (2003).

21. Ito, I., Ji, L., Tanaka, F., Began, G., Cynthia, D.B., Kai, X., Atkinson E.N., Bekele B.N., Stephens C., Minna J.D., Roth J.A., Ramesh R. Liposomal Vector Mediated Delivery of the 3p *FUS1* Gene Demonstrates Potent Antitumor Activity Against Human Lung Cancer *in vivo.* (in press).

22. Uno, F., Sasaki, J, Nishizaki, M., Carboni, G., Xu, K., Atkinson, E.N., Kondo, M., Minna ,J.D, Roth, J.A., Ji, L. Myristoylation of the Fus1 Protein Is Required for Tumor Suppression in Human Lung Cancer Cells. *Cancer Res.. 64*, 2969-2976 (2004).

23. Whitmore, M., Li, S., Huang, L. LPD Lipopolyplex Initiates a Potent Cytokine Response and Inhibits Tumor Growth. *Gene Ther.* 6, 1867-1875 (1999).

24. Huang, L., Li, S. Liposomal Gene Delivery- a Complex Package. *Nat. Biotechnol.* 15, 620-621 (1997).

25. Li, S., Wu, S.P., Whitmore, M., Loeffert, E.J., Wang, L., Watkins, S.C., Pitt, B.R., Huang, L. Effect of Immune Response on Gene Transfer to the Lung Via Systemic Administration of Cationic Lipidic Vectors. *Am. J. Physiol. 276*, L796-L804 (1999).

26. Freimark, B.D., Blezinger, H.P., Florack, V.J., Nordstrom, J.L., Long, S.D., Deshpande, D.S., Nochumson, S., Petrak, K.L. Cationic Lipids Enhance Cytokine and Cell Influx Levels in the Lung Following Administration of Plasmid-cationic Lipid Complexes. *J. Immunol. 160*, 4580-4586 (1998).

27. Tousignant, J. D., Zhao, H., Yew, N.S., Cheng, S.H., Eastman, S.J., Scheule, R.K. DNA sequences in cationic lipid: pDNA-mediated systemic toxicities. *Hum.Gene Ther, 14*; 203-214 (2003).

28. Dow, S.W., Fradkin, L.G., Liggitt, D.H., Willson, A.P., Heath, T.D., Potter, T.A. Lipid-DNA Complexes Induce Potent Activation of Innate Immune Responses and Antitumor Activity when Administered Intravenously. *J. Immunol. 163*, 1552-1561 (1999).

29. Scheule, R.K., St George, J.A., Bagley, R.G., Marshall, J., Kaplan, J.M., Akita, G.Y., Wang, K.X., Lee, E.R., Harris, D.J., Jiang, C., Yew, N.S., Smith, A.E., Cheng, S.H. Basis of Pulmonary Toxicity Associated with Cationic Lipid-mediated Gene Transfer to the Mammalian Lung. *Hum. Gene Ther. 8*, 689-707 (1997).

30. Yew, N.S., Zhao, H., Wu, I.H., Song, A., Tousignant, J.D., Przybylska, M., Cheng, S.H. Reduced Inflammatory Response to Plasmid DNA Vectors by Elimination and Inhibition of Immunostimulatory CpG Motifs. *Mol. Ther. 1*, 255-262 (2000).

31. Yew, N. S., Zhao, H., Wu, I.H., Song, A., Tousignant, J.D., Przybylska, M., Cheng, S.H. CpG-depleted Plasmid DNA Vectors with Enhanced Safety and Long-term Gene Expression in vivo. *Mol. Ther. 5*, 731-738 (2000).

32. Hofman, C.R., Dileo, J.P., Li, Z., Li, S., Huang, L. Efficient *in vivo* Gene Transfer by PCR Fragment with Reduced Inflammatory Activity. *Gene Ther. 8*, 71-74 (2001).

33. Tan, Y., Li, S., Pitt, B. R., Huang, L. The Inhibitory Role of CpG Immunostimulatory Motifs in Cationic Lipid Vector-Mediated Transgene Expression *in vivo. Hum. Gene Ther. 10*, 2153-2161 (1999).

34. Yeo, S.J., Gravis D., Yoon J.G., Yi A.K. Myeloid Differentiation Factor 88-dependent Transcriptional Regulation of Cyclooxygenase-2 Expression by CpG DNA: ROLE OF NF-κB AND p38. *J. Biol. Chem. 278*, 22563-22573 (2003).

35. DeWitt, D. L. Prostaglandin Endoperoxidase Synthase: Regulation of Enzyme Expression. *Biochem. Biophys. Acta. 1083*, 121-134 (1991).

36. Ghosh, D.K, Misukonis, M.A., Reich, C., Pisetsky, D.S., Weinberg, J.B. Host Response to Infection: the Role of CpG DNA in Induction of Cyclooxygenase 2 and Nitric Oxide Synthase 2 in Murine Macrophages. *Infect. Immun. 69*, 7703-7710 (2001).

37. Batttz J.E., Zou Y., Korfhagen T.R. Inhibitory Effects of Tumor Necrosis Factor-α on Cationic Lipid-Mediated Gene Delivery to Airway Cells in vitro. *Biochim. Biophys. Acta. 1535*, 100-109 (2001).

38. Palladino M.A., Bahja, F.R., Theodorakis E.A., Moldawer, L.L. Anti-TNF-α Therapies: The Next Generation. *Nat. Rev. Drug Dis.*. 2, 736-746 (2003)

39. Kumar, S., Boehm, J., Lee, J.C. P38 MAPKinases:Key Signalling Molecules as Therapeutic Targets for Inflammatory Diseases. *Nat. Rev. Drug Dis.* 2, 717-726 (2003).

40. Manning. A.M., Davis R.J. Targeting JNK for Therapeutic Benefit: From Junk to Gold. *Nat. Rev. Drug Dis.* 2, 554-565 (2003).

41. Lai, W.C, Zhou, M., Shankavaram, U., Peng, G., Wahl LM. Differential regulation of lipopolysaccharide-induced monocyte matrix metalloproteinase (MMP)-1 and MMP-9 by p38 and extracellular signal-regulated kinase 1/2 mitogen-activated protein kinases. *J. Immunol. 170*, 6244-9 (2003).

42. Janelle, M.-E., Gravel, A., Gosselin, J., Tremblay, M.J, Flamand, L. Activation of Monocyte Cyclooxygenase-2 Gene Expression by Human Herpesvirus 6. Role for cyclic AMP-response element-binding protein and activator protein-1. *J. Biol. Chem.* 277, 30665-30674 (2002)

43. Wadleigh, D. J., Herschman, H.R. Transcriptional Regulation of the Cyclooxygenase-2 Gene by Diverse Ligands in Murine Osteoblasts. *Biochem. Biophys. Res. Comm. 264*, 865-870 (2000).

44. Reddy, S.T., Wadleigh, D. J., Herschman, H.R. Transcriptional Regulation of the Cyclooxygenase-2 Gene in Activated Mast Cells. *J. Biol. Chem. 275*, 3107-3113 (2000).

45. Billack, B., Heck, D.E., Mariano, T.M., Gardner, C.R., Sur, R., Laskin, D.L., Laskin, J. D. Induction of Cyclooxygenase-2 by Heat Shock Protein 60 in Macrophages and Endothelial cells. *Am. J. Physiol. 283*, C1267-C1277 (2002).

46. Turini, M.E., DuBois, R.N. Cyclooxygenase-2: A Therapeutic Target. *Annual Review of Medicine. 53*, 35-57 (2002).

47. FitzGerald, G.A. COX-2 and beyond: Approaches to Prostaglandin Inhibition in Human Disease. *Nature Reviews Drug Discovery.* 2, 879 - 890 (2003).

48. Chen, Y., Zhang, J., Moore, S. A., Ballas, Z.K., Portanova, J.P., Krieg, A.. M., Berg, D. J. CpG DNA Induces Cyclooxygenase-2 Expression and Prostaglandin Production. *Int. Immunol. 13*, 1013-1020 (2001).

49. Kang, G., Kong, P.J., Yuh, Y.J., Lim, S.Y., Yim, S.V., Chun, W., Kim, S.S. Curcumin suppresses lipopolysaccharide-induced cyclooxygenase-2 expression by inhibiting activator protein 1 and nuclear factor kappab bindings in BV2 microglial cells. *J Pharmacol Sci. 94*; 325-328 (2004).

50. Barrios-Rodiles Miriam., Keller K., Belley A., Chadee K. Nonsteroidal Antiinflammatory Drugs Inhibit Cyclooxygenase-2 Enzyme Activity but Not mRNA Expression in Human Macrophages. *Biochim. Biophys. Res. Comm.* 225, 896-900 (1996).

51. Zyglewska, T., Sanduja, R., Ohashi, K., Loose-Mitchell, D.S., Sanduja, S.K., Wu, K. K. Inhibition of Endothelial Cell Prostaglandin H Synthase Gene Expression by Naproxen. *Biochim. Biophys. Acta. 1131*, 78-82 (1992).

Figure Legends

Figure 1. **Lipoplex-mediated induction of inflammation associated signaling molecules.** MRC-9 cells were transfected with empty liposome, naked plasmid DNA or DOTAP:Chol-*FUS1* complex and analyzed for inflammation associated signaling molecules by western blotting at 2h and 4 h after transfection. Cells that did not receive any treatment served as negative control. β-actin was detected as internal loading controls. The expression levels were determined by densitometery and the values determined with control value arbitrarily set to 1.

Figure 2. **Suppression of lipoplex induced inflammation-associated signaling molecules by small molecule inhibitors.** Cells pretreated with various concentrations of ***A***, p38MAPK inhibitor, SB 203580; ***B***, p44/42MAPK inhibitor, U0126; and ***C***, COX-2 inhibitor, naproxen were transfected with DOTAP:Chol-*FUS1* complex. At 2h and 4h after transfection cells were harvested and analyzed for signaling molecules by western blot analysis. β-actin was detected as internal loading controls. The expression levels were determined by densitometery and the values determined with control value arbitrarily set to 1.

Figure 3. **Lipoplex-mediated activation of AP-1 is inhibited by naproxen** MRC-9 fibroblast cells were not treated or treated with naproxen (0.5 mM) prior to transfection with DOTAP:Chol-*FUS1* complex. Cells not receiving any treatment served as control. At 2h after transfection cells were harvested, nuclear extracts prepared, and AP-1 binding activity using consensus oligonucleotide probe was determined by EMSA. Untreated cells served as control in these experiments.

Figure 4. **Inhibition of lipoplex induced PGE_2 production by naproxen.** Cells were either not treated or treated with naproxen (0.5 mM) prior to transfection with lipoplex (2.5 μg DNA). Tissue culture supernatant was collected at various time points and analyzed for PGE_2 concentration using a PGE_2 enzyme immunoassay kit. A significantly inhibition in PGE_2 levels were observed in naproxen treated cells compared to cells that were not treated with naproxen. Naproxen inhibited PGE_2 levels at all time points tested. Data is represented as the average of triplicate wells. Bars denote standard error.

Figure 5. **Naproxen does not affect transgene expression.** Cells were either not treated or treated with naproxen prior to transfection with DOTAP:Chol-*luc* complex. At 2h, 4h, and 15h after transfection cell

lysates were prepared and assayed for luciferase activity. Luciferase activity was observed in both naproxen treated and untreated cells. However, a slight increase in luciferase activity was observed in naproxen treated cells. Luciferase activity was expressed as relative light units per milligram of protein (RLU/mg protein). Results are represented as the average triplicates. Error bar denotes standard error.

Figure 6. **Lipoplex induced inflammatory response is inhibited by naproxen in vivo.** Mice were divided into three groups and treated as follows: Group 1 received no treatment and served as control; Group 2 received an intravenous injection of DOTAP:Chol-*FUS1* complex; Group 3 received an oral dose of naproxen (15mg/Kg) 3h prior to receiving an intravenous injection of DOTAP:Chol-*FUS1* complex. Animals were euthanized at various time points and analyzed for TNF-α in the blood and signaling molecules in lung tissues. ***A***, lipoplex-mediated TNF-α expression was markedly suppressed in Group 3 mice compared to TNF-α expression in Group 2 mice. Baseline TNF-α levels were observed in Group 1 mice. Bars denote standard error. ***B***, inhibition of various inflammation-associated signaling molecules was observed in the lungs of Group 3 mice compared to the lungs from Group 2 mice. Baseline expression levels of the signaling molecules were observed in the lungs of Group 1 mice. The expression levels were

determined by densitometery and the values determined with control value arbitrarily set to 1.

Figure 7. **Schematic representation of the inflammation-associated signaling pathways induced by lipoplex and potential targets for naproxen**. Intravenous injection of lipoplex results in activation of the various signaling molecules leading to the activation of COX-2 that breaks down arachidonic acid into PGE_2 metabolites. Production of PGE_2 metabolites leads to inflammation. However, naproxen inhibits PGE_2 production by inhibiting COX-2. Additional potential inhibitory targets for naproxen include the MAPK's, NFκB, and AP-1.

Fig. 1

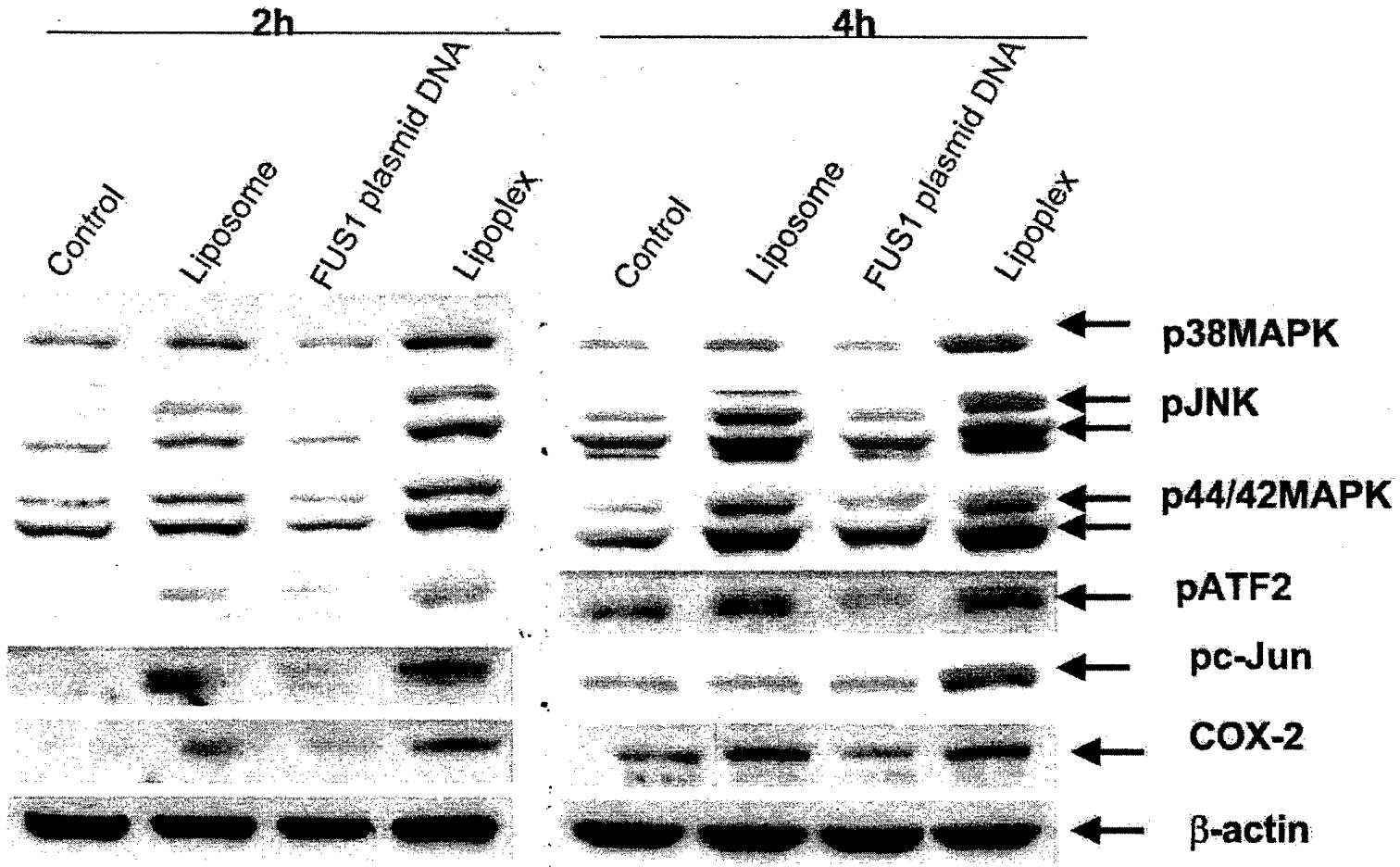

p38MAPK	1.0	1.2	0.6	1.5	1.0	1.4	0.8	2.1
pJNK	1.0	1.1	0.9	1.4	1.0	1.4	1.1	1.6
P44/42MAPK	1.0	1.0	0.7	1.3	1.0	1.4	1.3	1.8
pATF2	1.0	1.1	0.9	1.3	1.0	1.0	1.2	1.8
Pc-Jun	1.0	1.0	0.9	1.1	1.0	1.2	0.8	1.5
COX-2	1.0	1.1	0.8	1.3	1.0	1.1	1.0	1.7

Fig. 2A

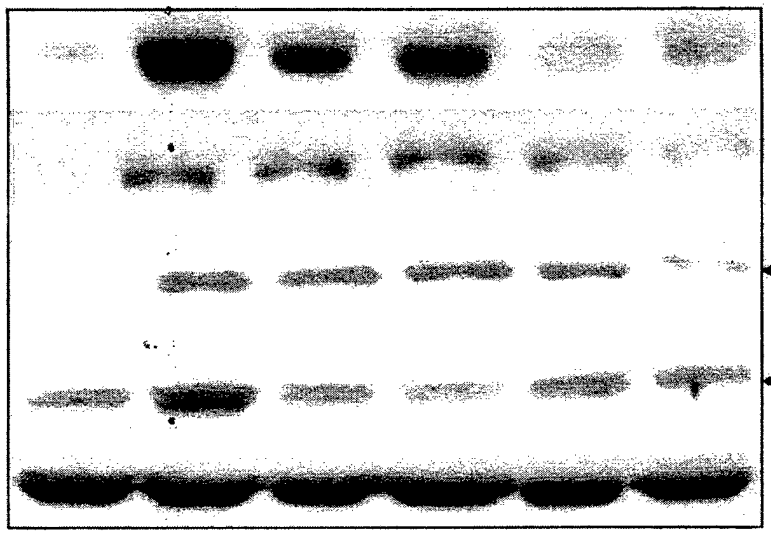

P38MAPK	1	3.6	2.37	2.6	1.4	1.8
pATF2	1	5.6	5.1	5.2	3.6	2.0
pcJun	1	7.7	7.4	7.3	5.9	3.9
COX-2	1	1.8	1.0	0.9	1.2	1.0

Fig. 2B

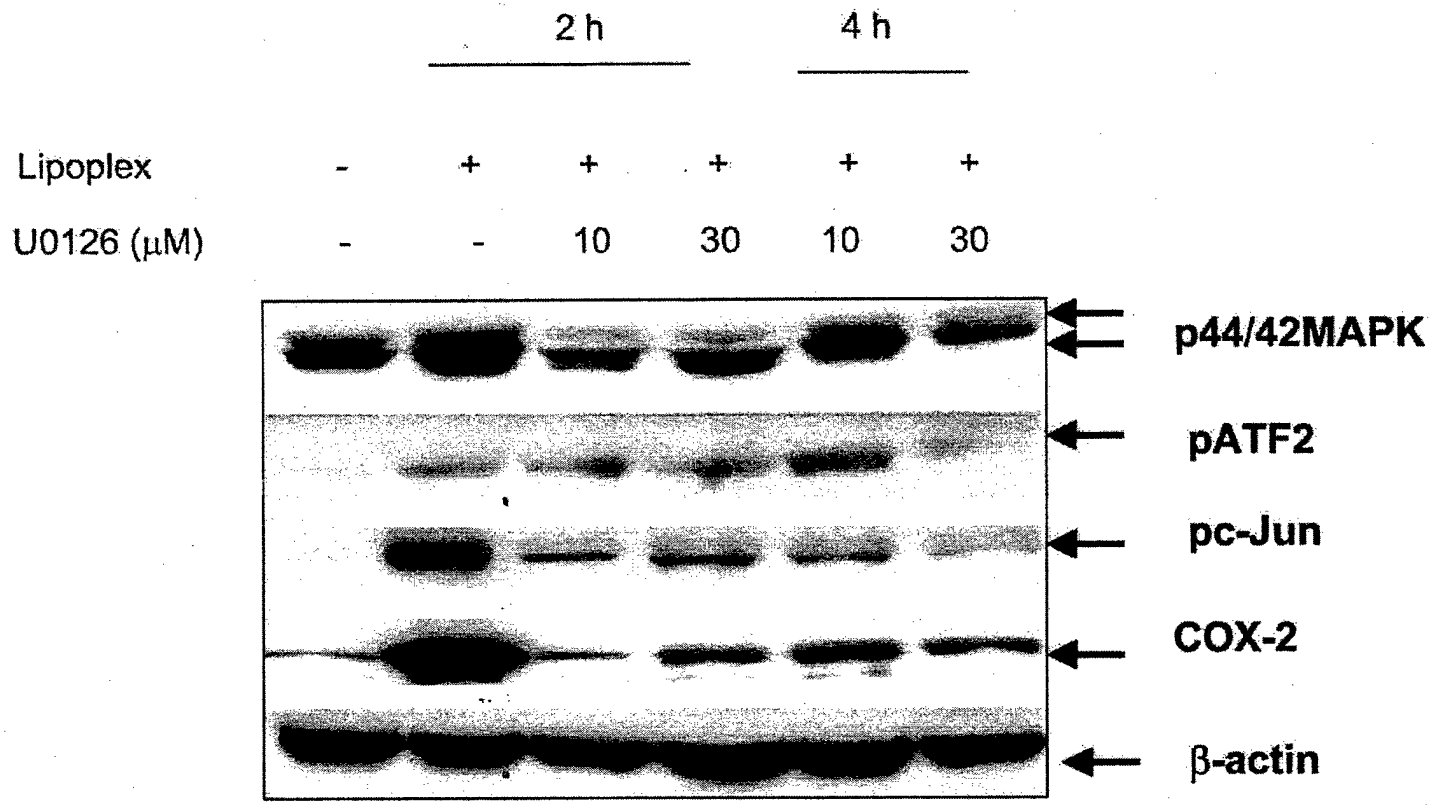

p44/42MAPK	1	1.1	0.9	1.0	1.0	1.0
pATF2	1	2.9	3.7	4.1	3.7	2.5
pcJun	1	4.8	2.3	2.7	2.3	1.8
COX-2	1	12.8	3.1	3.2	4.9	2.5

Fig. 2C

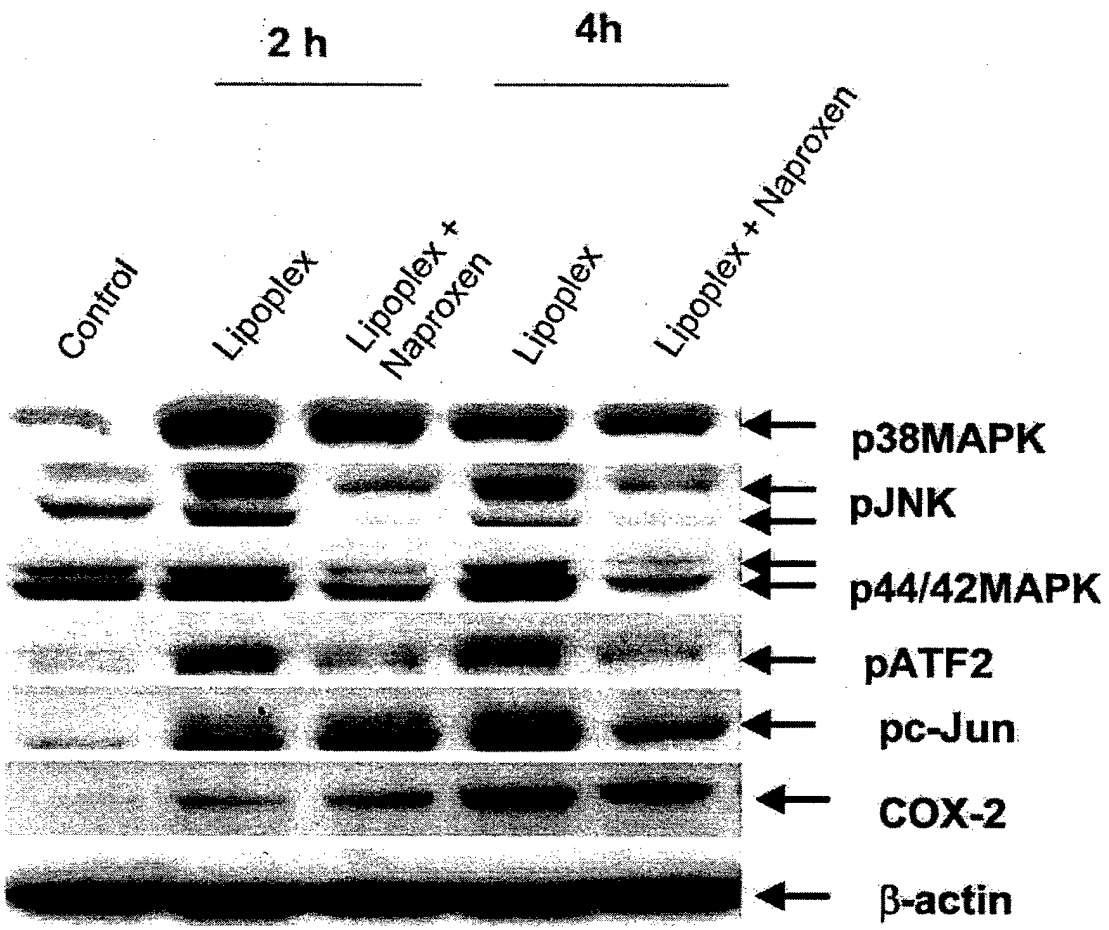

p38 MAPK	1.0	3.5	3.1	2.5	2.0
pJNK	1.0	4.3	1.5	3.9	1.7
P44/42MAPK	1.0	1.4	0.6	1.1	0.5
pATF2	1.0	2.1	1.3	2.1	1.0
pcJun	1.0	3.3	3.6	4.3	2.4
COX-2	1.0	2.4	2.9	4.1	3.5

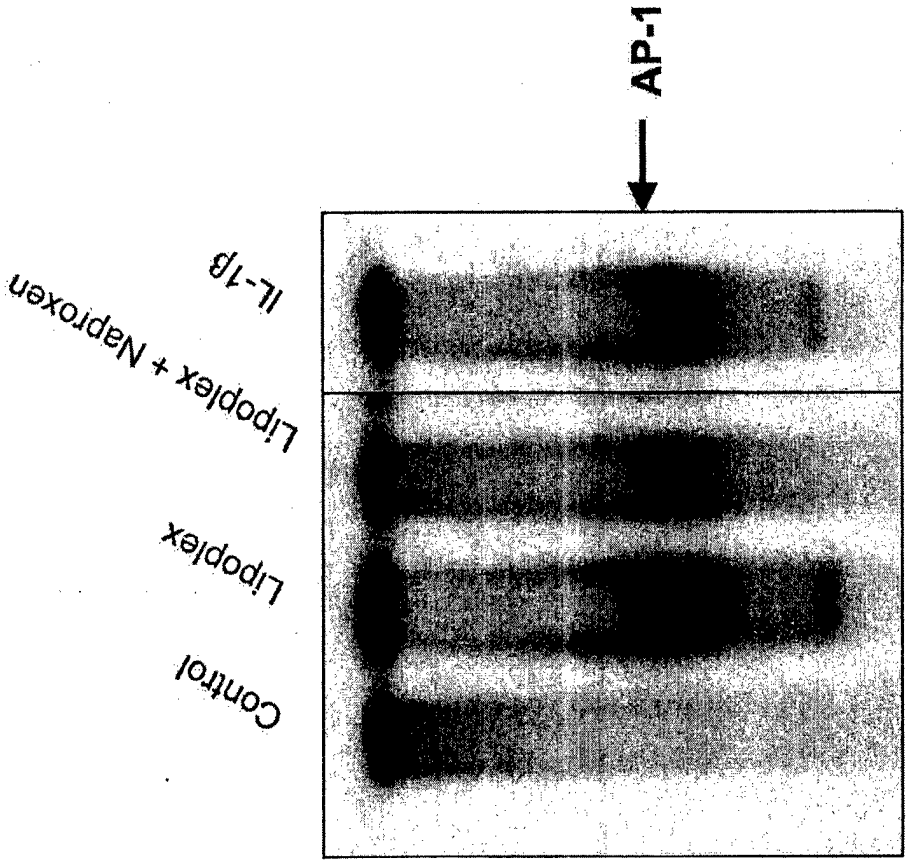

Fig. 3

Fig. 4

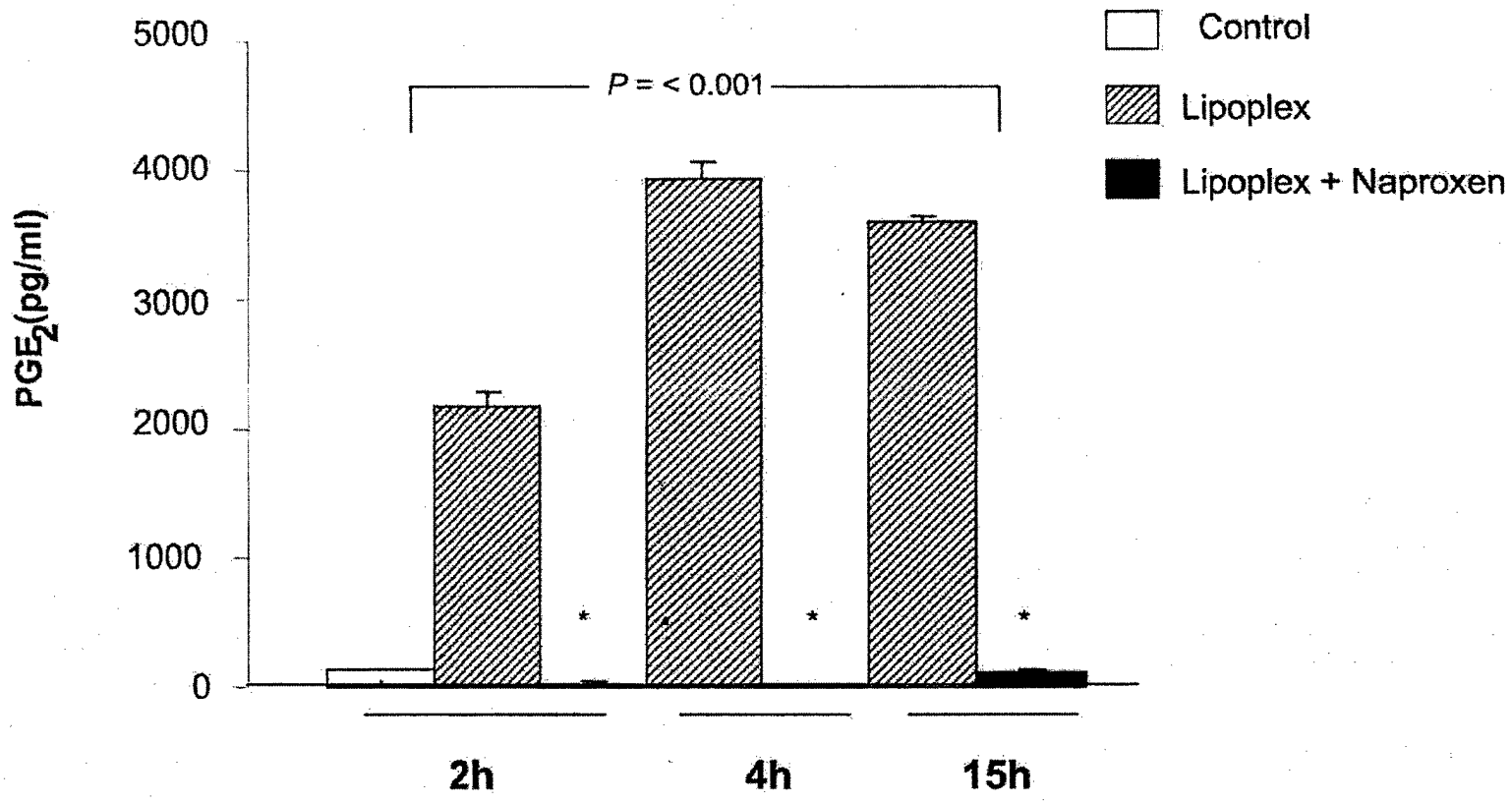
5000
4000
3000
2000
1000
0
PGE2(pg/ml)
P = < 0.001
Control
Lipoplex
Lipoplex + Naproxen
*
*
*
*
2h
4h
15h

Fig. 5

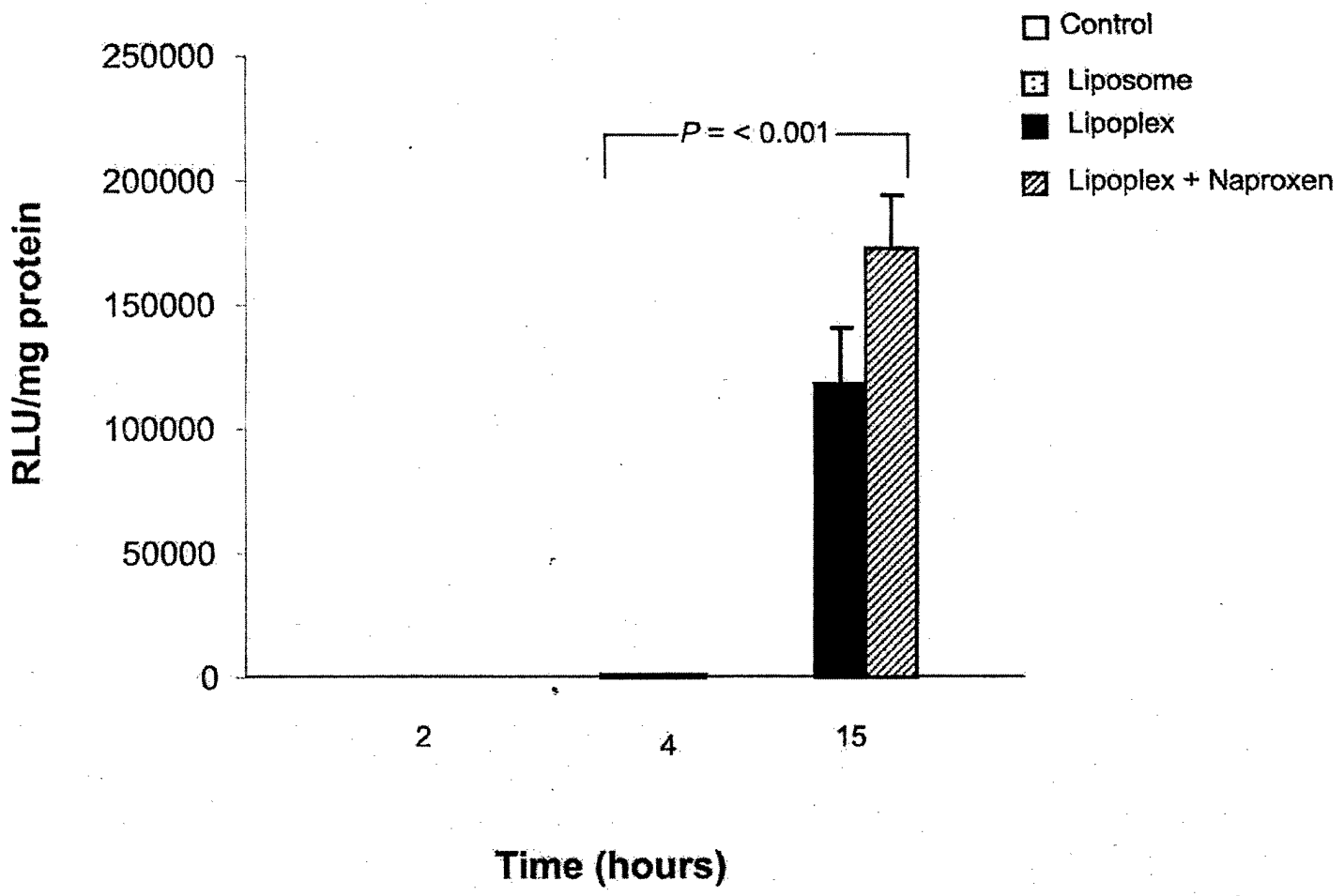
Control
Liposome
Lipoplex
Lipoplex + Naproxen
P = < 0.001
250000
200000
150000
100000
50000
0
RLU/mg protein
2
4
15
Time (hours)

Fig. 6A

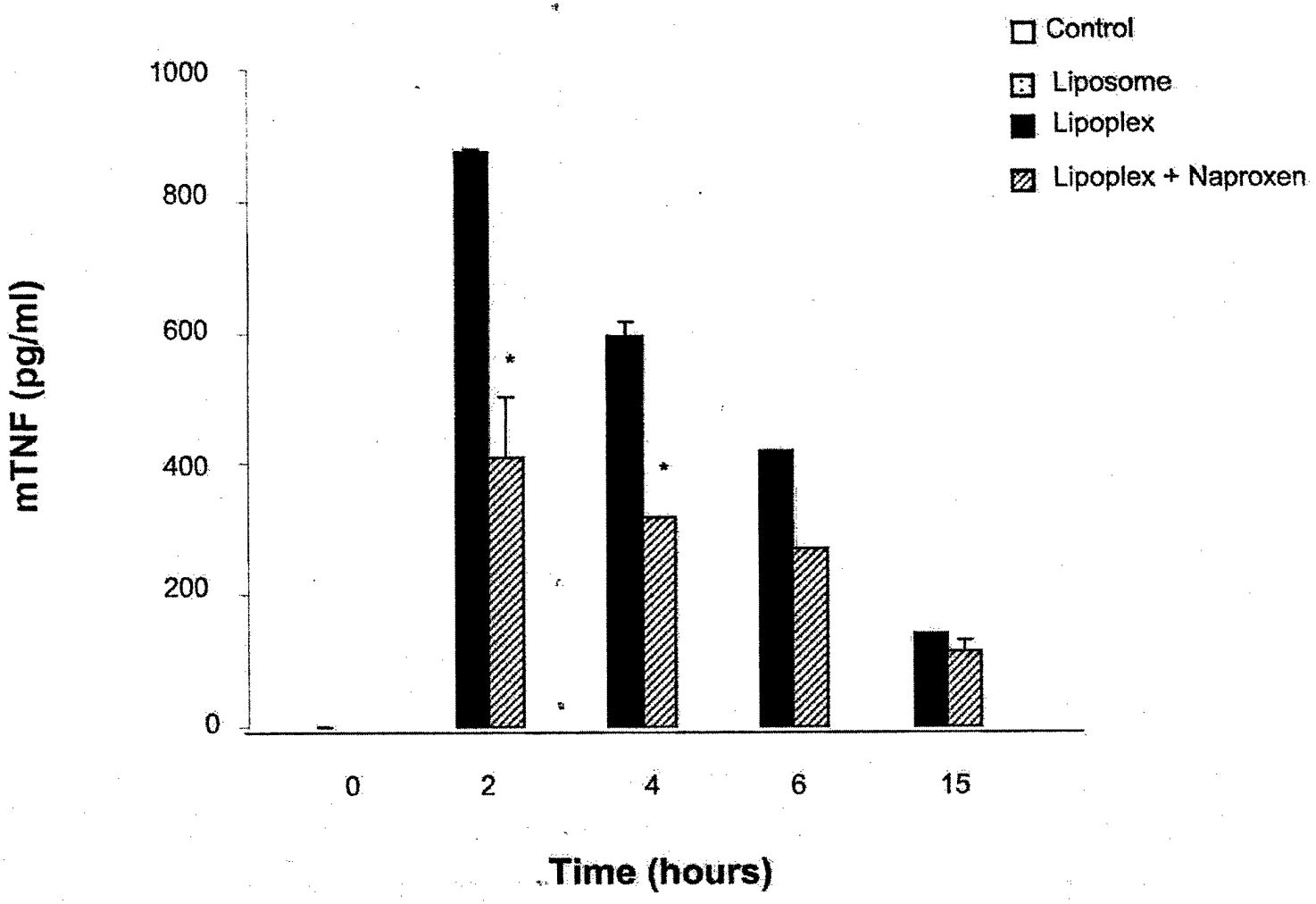
Control
Liposome
Lipoplex
Lipoplex + Naproxen
mTNF (pg/ml)
1000
800
600
400
200
0
*
*
0
2
4
6
15
Time (hours)

Fig. 6B

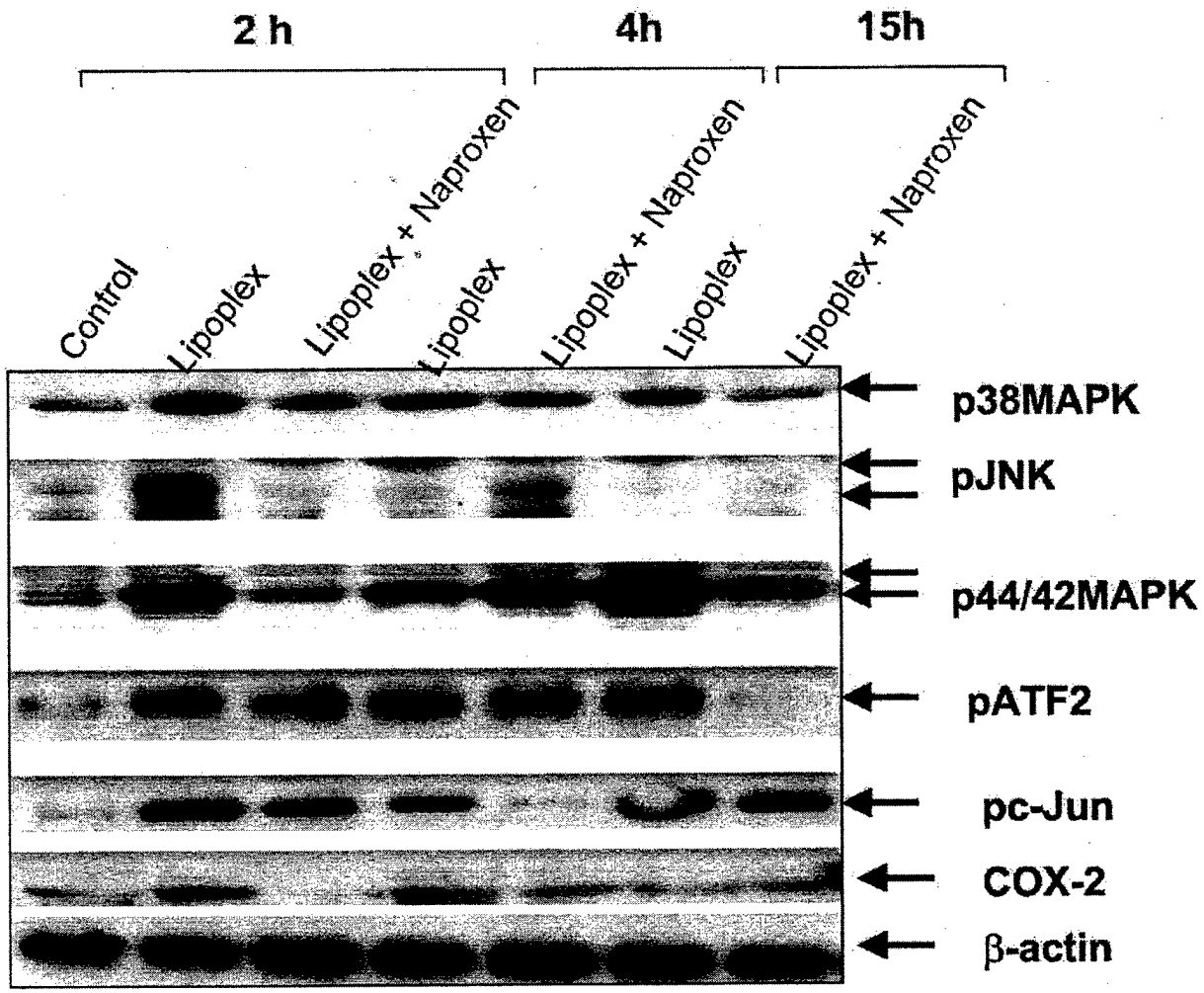

P38MAPK	1.0	1.7	1.2	1.3	1.1	1.1	1.0
pJNK	1.0	1.9	0.8	1.0	1.5	0.9	1.3
P44/42MAPK	1.0	1.9	0.9	1.6	2.2	2.6	1.8
pATF2	1.0	1.4	1.2	1.3	1.3	1.5	0.9
pcJun	1.0	5.8	3.8	2.8	0.7	4.2	4.6
COX-2	1.0	1.6	0.5	1.7	1.0	0.9	1.4

Fig. 7

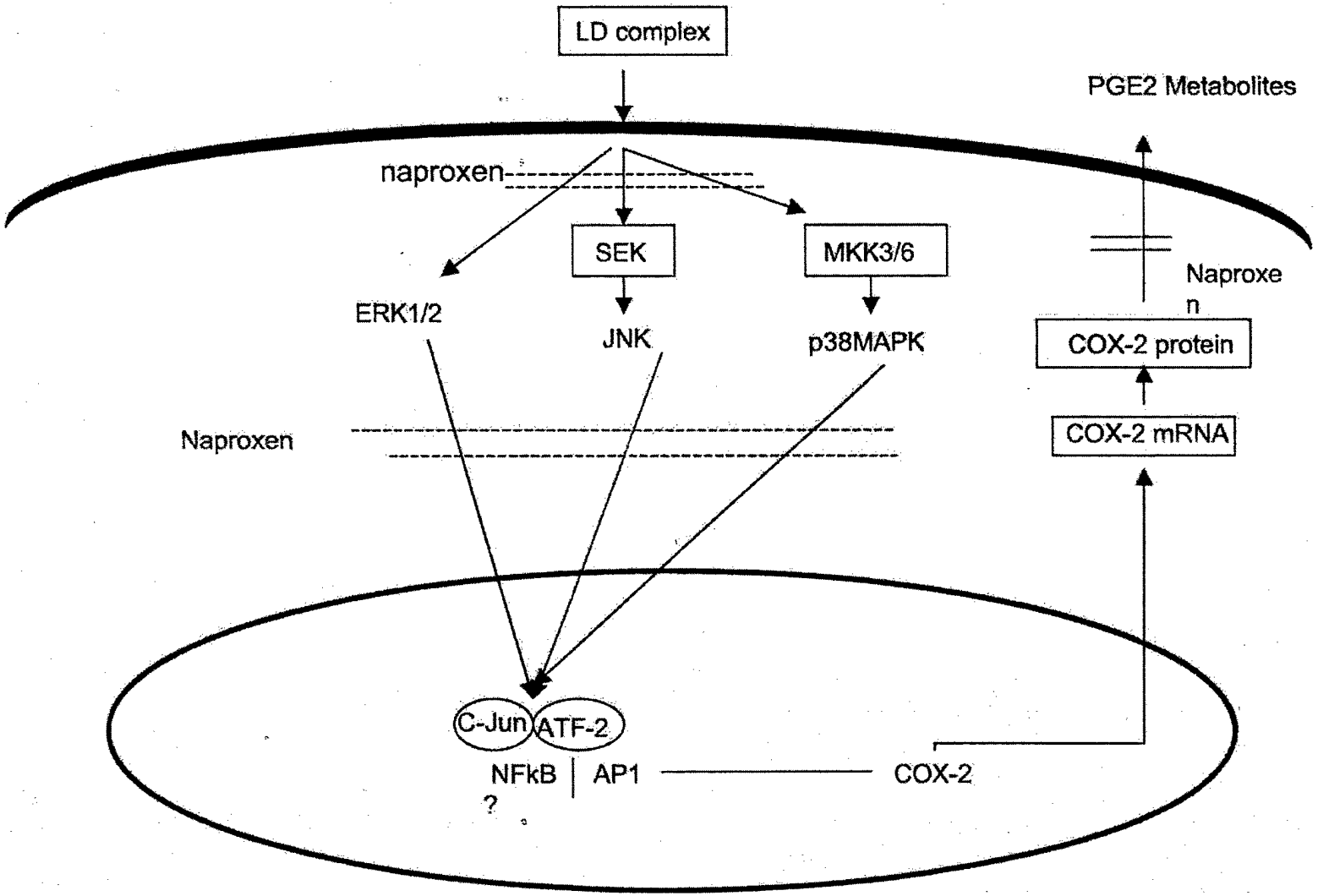
LD complex
PGE2 Metabolites
naproxen
SEK
MKK3/6
ERK1/2
JNK
p38MAPK
Naproxe
n
COX-2 protein
COX-2 mRNA
Naproxen
C-Jun
ATF-2
NFkB
?
AP1
COX-2

Development of an Orthotopic Model to Study the Biology and Therapy of Primary Human Lung Cancer in Nude Mice

Amir Onn,[1,2] Takeshi Isobe,[2] Satoshi Itasaka,[2,3] Wenjuan Wu,[2] Michael S. O'Reilly,[2,3] Waun Ki Hong,[1] Isaiah J. Fidler,[2] and Roy S. Herbst[1,2]

Departments of [1]Thoracic/Head and Neck Medical Oncology, [2]Cancer Biology, and [3]Radiation Oncology, The University of Texas M. D. Anderson Cancer Center, Houston, Texas

ABSTRACT

Purpose: **This study was conducted to develop biologically relevant animal models of human lung cancer that are reproducible, inexpensive, and easy to perform.**

Experimental Design: **Human lung adenocarcinoma (PC14PE6), bronchioloalveolar carcinoma (NCI-H358), squamous cell carcinoma (NCI-H226), poorly differentiated non-small cell lung cancer (NCI-H1299 and A549), or small cell lung cancer (NCI-H69) cells in Matrigel were injected percutaneously into the left lungs of nude mice. The growth pattern of the different lung cancer tumors was studied. For PC14PE6 and NCI-H358, the growth pattern in the subcutis and the response to paclitaxel were also studied.**

Results: **As is observed for human primary lung cancer, tumors formed from a single focus of disease and progressed to a widespread and fatal thoracic process characterized by diffuse dissemination of lung cancer in both lungs and metastasis to intra- and extrathoracic lymph nodes. When the lung cancer cell lines were implanted s.c., systemic therapy with paclitaxel induced tumor regression. However, only a limited therapeutic response to paclitaxel was observed when the same cells were implanted orthotopically into the lung. Immunohistochemical analysis of tumor tissue revealed increased expression of the proangiogenic factors interleukin 8, basic fibroblast growth factor, and vascular endothelial growth factor/vascular permeability factor.**

Conclusions: **Our orthotopic models of human lung cancer confirm the "seed and soil" concept and likely provide more clinically relevant systems for the study of both non-small cell lung cancer and small cell lung cancer biology, and for characterizing novel therapeutic strategies.**

INTRODUCTION

Lung cancer is a major health problem worldwide, and the leading cause of cancer related death for both men and women in the United States with an annual mortality rate that exceeds breast, prostate, and colorectal cancers combined (1). In most cases, lung cancer patients are diagnosed with advanced inoperable disease, and the only therapeutic option is systemic chemotherapy. Unfortunately, recent studies have concluded that conventional therapies may have reached a ceiling of clinical impact as evidenced by the 5-year survival for NSCLC[4] and SCLC, which remains at 14% and 5%, respectively (2). Clearly, a new approach to the therapy of lung cancer is mandatory. Because organ microenvironment influences the phenotype of tumor cells, as originally enunciated by Pagets' "seed and soil" theory (3) and confirmed by others (4–6), the identification of novel therapeutics depends on the availability of biologically relevant *in vivo* models (7).

NSCLC represents 80% of all lung cancer cases, and most research focuses on this subtype, including the development of several orthotopic models of human NSCLC in rodents. These models include implantation of human cancerous tissue obtained surgically (8) and the injection of tumor cells into the rodent airways (9–11), pleural cavity (12, 13), or lung parenchyma after skin incision (14) or thoracotomy (15–17). In contrast, only two reports describe the use of orthotopic models to study SCLC, which comprises 20% of all lung cancer cases (5, 12). Despite their availability, orthotopic models of human lung cancer are not widely used, and most of the research and development of novel therapeutics for lung cancer still relies upon s.c. tumor models, which are potentially less clinically relevant.

In this article, we describe the development of orthotopic models for different primary human lung cancers in athymic nude mice. We have developed models of each of the most common lung cancer histological types including adenocarcinoma, squamous cell, bronchioloalveolar, and small cell. For each tumor type, lesions develop after direct injection of a tumor cell suspension into the thorax of the mouse, making it a reproducible technique to study either NSCLC or SCLC human tumors. The present model recapitulates the local and regional growth pattern seen in lung cancer patients, *i.e.*, from a solitary

Received 5/13/03; revised 7/15/03; accepted 7/21/03.

Grant support: Supported in part by an M. D. Anderson Cancer Center Physician Scientist Program Award (R. S. H.), an ASCO Cancer Development Award (R. S. H.), a NIH grant for Specialized Program of Research Excellence (SPORE) in Lung Cancer (P50 CA70907, to R. S. H.), a grant from the Department of Defense (DAMD 17-02-1-0706, to W. K. H.), and an award from the CRH Foundation (R. S. H.). The costs of publication of this article were defrayed in part by the payment of page charges. This article must therefore be hereby marked *advertisement* in accordance with 18 U.S.C. Section 1734 solely to indicate this fact.

Requests for reprints: Roy S. Herbst, MD, PhD, The University of Texas M. D. Anderson Cancer Center, 1515 Holcombe Boulevard, Unit 432, Houston, Texas 77030. Phone: (713) 792-6363; Fax: (713) 796-8655; E-mail: rherbst@mdanderson.org.

[4] The abbreviations used are: NSCLC, non-small cell lung cancer; SCLC, small cell lung cancer; i.t., intrathoracic; FBS, fetal bovine serum; GFP, green fluorescent protein; IHC, immunohistochemistry; bFGF, basic fibroblast growth factor; VEGF, vascular endothelial growth factor; IL, interleukin; VPF, vascular permeability factor.

nodule to a diffuse thoracic disease involving both lungs and the lymph nodes. Furthermore, in contrast to tumors growing s.c., tumors in the lung are less susceptible to treatment with paclitaxel, suggesting that orthotopic models are more relevant to evaluate chemotherapeutics and other therapies for human lung cancer.

MATERIALS AND METHODS

Cell Lines and Tissue Culture Conditions. Six human lung cancer cell lines were studied. NCI-H358 (bronchioloalveolar carcinoma), NCI-H1299 and A549 (poorly differentiated NSCLC), and NCI-H69 (SCLC) were obtained from the American Type Culture Collection (Manassas, VA). PC14PE6 was selected from human adenocarcinoma cell line PC14 to produce pleural effusion when injected into mice (18, 19). NCI-H226 (lung squamous cell carcinoma) was the gift of Dr. John D. Minna, University of Texas Southwestern Medical Center (Dallas, TX; Ref. 20). B16BL6 melanoma cells (21–23) were initially used to determine the feasibility of the orthotopic injection procedure. Floating aggregates of NCI-H69, floating and adherent monolayer cultures of PC14PE6, and adherent monolayer cultures of other cell lines were incubated at 37°C in 5% CO_2-95% air. NCI-H358 was cultured in RPMI 1640 supplemented with 10% FBS, L-glutamine, and penicillin-streptomycin. NCI-H69 cells were cultured in Dulbecco's modified MEM supplemented with 10% FCS and penicillin-streptomycin. All of the other cell lines were cultured in Eagle's MEM supplemented with 10% FBS, sodium pyruvate, nonessential amino acids, L-glutamine, 2-fold vitamin solution, and penicillin-streptomycin mixture (CMEM; Flow Laboratories, Rockville, MD). All of the tumor cell cultures were free of *Mycoplasma*, and the following pathogenic murine viruses: retrovirus type 3, pneumonia virus, K virus, Theiler's encephalitis virus, Sendai virus, minute virus, mouse adenovirus, mouse hepatitis virus, lymphocytic choriomeningitis virus, ectromelia virus, and lactate dehydrogenase virus (assayed by Microbiological Associates, Bethesda, MD).

Animals and Animal Care. Male athymic nude mice (NCr-nu) and C57BL/6 mice were purchased from the Animal Production Area of the National Cancer Institute-Frederick Cancer Research and Development Center (Frederick, MD). The mice were housed and maintained in specific pathogen-free conditions in facilities approved by the American Association for Accreditation of Laboratory Animal Care, and in accordance with current regulations and standards of the United States Department of Agriculture, United States Department of Health and Human Services, and the NIH. The mice were used in accordance with institutional guidelines when they were 6–10 weeks old.

Matrigel and Preparation of Cell Suspension for i.t. Injection. Matrigel is a basement membrane matrix preparation extracted from Engelbreth-Holm-Swarm mouse sarcoma (Becton Dickinson & Co., San Jose, CA; Refs. 14, 16, 17). For all of the experiments a stock solution of 500 μg Matrigel in 1 ml PBS using a dilution factor of approximately ×30 according to compound concentration was used. Cell suspensions for thoracic injections were prepared of equal volumes of cells in PBS and Matrigel stock, giving final dilution factor of approximately ×60. Matrigel was thawed on ice to avoid gel formation, which can rapidly occur at room temperature or above. In accordance with the manufacturer's instructions, all of the cell line suspensions, syringes, and needles were kept on ice before injections. To prepare suspensions of tumor cells in Matrigel, adherent tumor cells were harvested from subconfluent cultures by a brief exposure to 0.25% trypsin and 0.02% EDTA. Trypsinization was stopped with medium containing 10% serum, and the cells were washed once in serum-free medium and resuspended in PBS. Floating cells were collected after centrifugation. Trypan blue staining was used to assess cell viability, and only single-cell suspensions of >90% viability were used for the injections. Both Matrigel matrix and growth factor-reduced Matrigel matrix were used.

i.t. Injection. Mice anesthetized with sodium pentobarbital (50 mg/kg body weight) were placed in the right lateral decubitus position. One-ml tuberculin syringes (Becton Dickinson) with 30-gauge hypodermic needles were used to inject the cell inoculum percutaneously into the left lateral thorax, at the lateral dorsal axillary line, ~1.5 cm above the lower rib line just below the inferior border of the scapula. The needle was quickly advanced 5–7 mm into the thorax and was quickly removed after the injection of cell suspension. After tumor injection, the mouse was turned to the left lateral decubitus position. Animals were observed for 45–60 min until fully recovered.

s.c. Flank Injection. For s.c. flank injections, unanesthetized mice underwent s.c. injection of cells suspended in a volume of 100 μl HBSS (Sigma Chemicals Co., St. Louis, MO) directly into the flank using 1-ml tuberculin syringes (Becton Dickinson) with 30-gauge hypodermic needles. For chemotherapy experiments, mice were injected with tumor cells in 150 μl PBS with Matrigel. The cell suspension was prepared as described above for i.t. injection. Mice were then examined daily for evidence of tumor development.

***In Vivo* Selection of Cell Lines for Increased Tumorigenicity.** Using the i.t. injection technique described above, NCI-H226 cells were injected into the lungs of nude mice. The mice were killed when moribund, and the largest thoracic tumors were harvested by aseptic techniques, dissociated mechanically using pipetting, and placed into culture for three to five passages (24). The cells were then reinjected into the lungs of nude mice.

***In Vitro* Selection for Increased Tumorigenicity: Growth in Semisolid Agarose.** NCI-H69 *in vitro* selection for increased invasive properties *in vivo* was accomplished using agarose, as described previously (25, 26). Briefly, agarose (Sigma Chemical Co.) was dissolved in distilled water and autoclaved. Base layers of Eagle's MEM with tryptose phosphate broth, 10% FBS, and 0.6% agarose were set in six-well plastic dishes. Over this bottom layer, a second layer of medium containing agarose and a suspension of 1×10^5 single tumor cells was laid. The concentration of agarose in the top layer was 0.9%. After the top layer gelled, 1–2 ml of CMEM medium with 10% FBS was added. Colonies formed from single cells were harvested and expanded by growth as monolayer cultures for *in vivo* injection.

GFP Transfection Protocol. For GFP transfection, cultures of PC14PE6 and NCI-H358 at 70% confluency were transfected with PEGFPC1 plasmid (Clontech Laboratories Inc.,

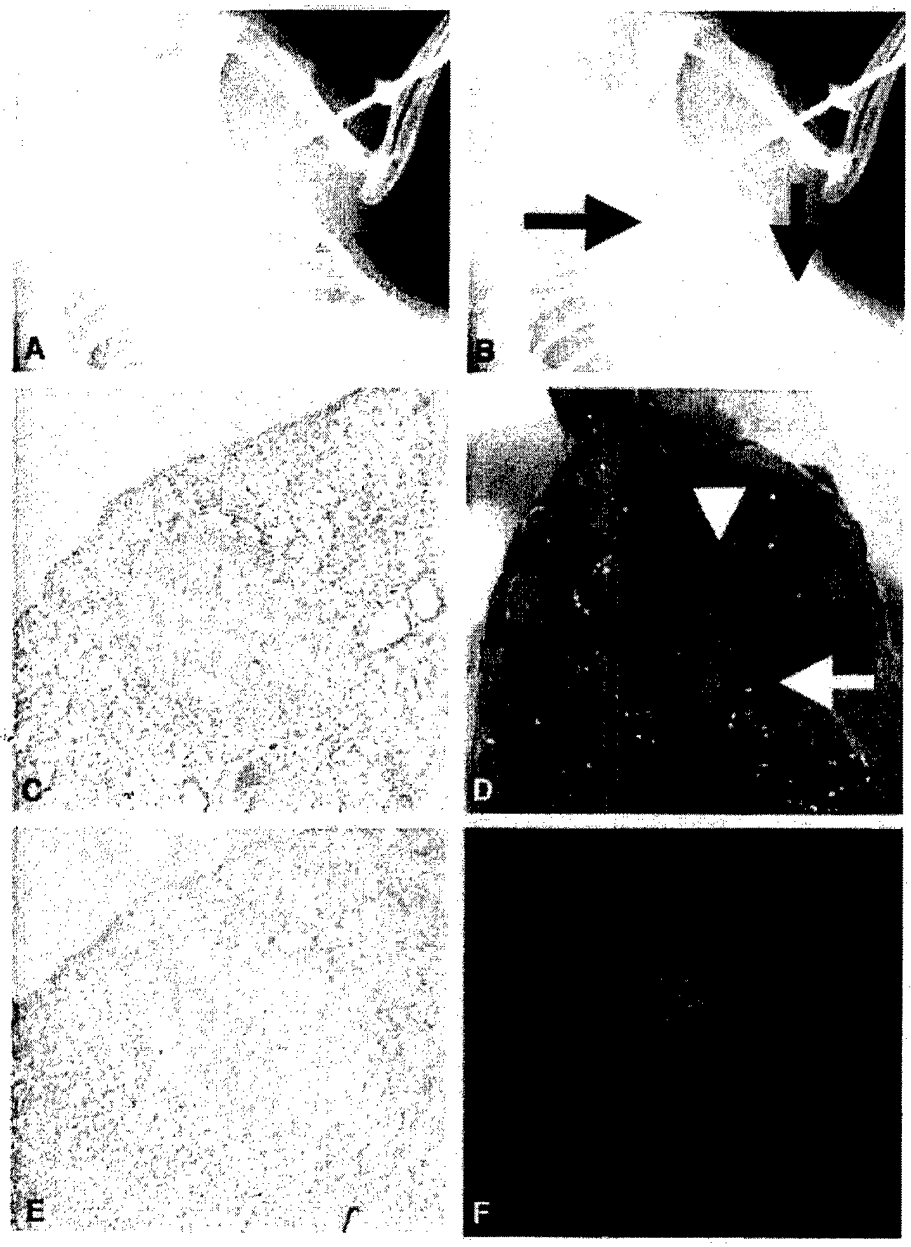

Fig. 1 *A*, to demonstrate fluid spreading after injection into the thorax, a 27.5-gauge needle was inserted into the left lung of a nude mouse (Faxitron X-ray image). *B*, the image was taken immediately after an injection of 75 μl of iohexol (omnipaque), an iodinated contrast agent. The fluid blunted the tip of the needle in the lung parenchyma and accumulated in the pleura according to gravity forces (*arrows*). *C*, the solitary nodules surrounded by a normal lung developed several days after injection of tumor cells with Matrigel, which anchored them and prevented cell suspension spread. PC14PE6 (*adenocarcinoma*) tumor, 9 days after tumor implantation. *D*, diffuse thoracic disease involving the injected site, the contralateral lung, and lymph nodes. Note the heart (arrowhead) and the small portion of the lung (*arrow*). *E*, IHC staining revealed that lung cancer in this system expressed bFGF from an early stage of disease. *F*, to study the sequence of metastasis we transfected two cell lines with GFP. The lesion is a microscopic left lung tumor on day 4 after injection of PC14PE6 cells with Matrigel. At this time, we found metastasis in the regional lymph nodes and the right lung.

Palo Alto, CA) using FuGene VI transfection reagents (Roche Molecular Biochemicals, Indianapolis, IN) according to the manufacturer's protocol. After 48 h, the cells were harvested by a 0.25% trypsin-0.02% EDTA solution and placed at a ratio of 1:15 into selective medium containing 800 μg/ml G418 (Life Technologies, Inc., Gaithersburg, MD) and plated. Neomycin-resistant clones were isolated with cloning cylinders by trypsin-EDTA. For *in vivo* studies, clones with high-intensity GFP fluorescence and stability were pooled. PC14PE6 cells (0.5×10^6) or NCI-H358 cells (1×10^6) in Matrigel were injected into the lungs of 10 mice. The mice (2/group) were killed at sequential time points thereafter.

Chemotherapy Studies. Therapeutic effects of paclitaxel were determined using NCI-H358 tumors implanted i.t. (1×10^6 cells in 75 μl) or s.c. (2.5×10^6 cells in 150 μl), or for PC14PE6 i.t. tumors (0.5×10^6 cells in 75 μl) or s.c. (1.5×10^6 cells in 150 μl). All of the cell suspensions were prepared in Matrigel. Four experiments were carried out with NCI-H358 i.t. tumors: one with s.c. tumors, one with PC14PE6 i.t, and two s.c. In all of the experiments, mice were randomized on day 7

Table 1 Production of thoracic tumors

Titration of human NSCLC and SCLC cell lines was conducted to determine the best number of cells needed to repeatedly produce orthotopic thoracic tumors in nude mice. Cells were injected in Matrigel into the left lung, as described in the text. Tumors metastasized to thoracic lymph nodes and the contralateral lung.

Cell line	Histology	Cell number	Tumor development	Survival (days)	Rt. lung metastases/ Lymph node metastases
PC14PE6	Adenocarcinoma[a]	0.5×10^6	10/10	26–30	+/+
		1×10^6	10/10	18–23	+/+
		2×10^6	10/10	14–18	+/+
NCI-H358	Bronchioloalveolar carcinoma	0.5×10^6	8/10	70–80	+/+
		1×10^6	9/10	56–63	+/+
		2×10^6	10/10	42–49	+/+
NCI-H226	Squamous	1.5×10^{6a}	10/10	63–70	+/+
		2×10^6	6/10	3.5–4 mo	+/+
NCI-H1299	Poorly diff NSCLC	1×10^6	10/10	32–40	+/+
A549	Poorly diff NSCLC	1×10^6	10/10	50–60	+/+
NCI-H69	SCLC	1.5×10^{6c}	9/10	50–56	+/+
		2×10^6	1/20	up to 4 mo	−/−

[a] PC14PE6 tumors were associated with pleural effusion. The amount of effusion collected was inversely related to number of cells injected as described in "Results."

[b] NCI-H226 cells were selected three cycles *in vivo* in the lung to improve tumor uptake and shorten survival time.

[c] NCI-H69 cells were selected on agarose for a more tumorigenic clone.

after tumor implantation to a control arm (i.p. 200 μl PBS/single dose/week) or a treatment arm [i.p. 200 μl paclitaxel, dosages ranged from 100–200 μg (4–8 mg/kg)/single dose/week]. For each of the cell lines, the experiment was terminated when i.t. control mice became moribund. Thus, all of the i.t. and s.c. mice for a particular cell line had the same number of chemotherapy cycles and, simultaneously, they were killed, autopsied, and tumor tissues were harvested.

Necropsy, Tissue Preparation, and IHC Staining. Mice were killed with a lethal dose of sodium pentobarbital (100 mg/kg body weight). Subsequent to a laparotomy, the thoracic cavity was inspected through the diaphragm for evidence of pleural effusion. Any pleural effusion was collected, and the thoracic organs were then removed enblock, including all of the lymph nodes and tumors. After dissection and removal of the heart, the lung and tumor mass were washed in cold PBS and weighed. Other visceral organs were removed and inspected for presence of metastases. Subcutis tumors were removed, washed in PBS, and weighed. For IHC and H&E staining procedures, one part of the tumor was fixed in formalin and embedded in paraffin, and another part was embedded in OCT compound (Miles, Inc., Elkhart, IN), rapidly frozen in liquid nitrogen, and stored in −80°C. IHC determination of bFGF, VEGF/VPF, and IL-8 were performed as described previously (27).

Microscopy and Imaging. For studies of tumor cells transfected with GFP, a Leica (model MZ FLIII) fluorescence dissecting stereomicroscope was used to visualize fluorescent metastases. The microscope was equipped with a 100-W, mercury vapor lamp power source and fitted with a GFP filter set. Images were processed using Image Pro Plus (version 4.0; Media Cybernetics, L.P., Silver Spring, MD) and Adobe Photoshop (version 5.5; Adobe Systems Inc., San Jose, CA). Digitalized imaging was performed using Faxitron specimen radiography system model MX-20 (Faxitron X-Ray Corp., Wheeling, IL). Energy was set to 26 kV, time to 10 s.

RESULTS

Formation of Lung Tumors. In the initial set of experiments, we determined the volume of tumor cell inoculum necessary to produce lung lesions without leading to immediate toxicity. For this purpose we used the highly metastatic B16BL6 melanoma cells, which were implanted into the lungs of syngeneic C57BL/6 mice. We selected the injection volume of 75 μl Matrigel containing suspended tumor cells. The necessity of Matrigel as an anchor to tumor cells, to avoid diffuse spread in the thorax, is demonstrated in Fig. 1, *A* and *B*. Injection of tumor cells in saline resulted in spread according to gravity forces, whereas injection of tumor cells with Matrigel formed a solitary lesion as an initial focus of disease. Four NSCLC cell lines (PC14PE6, NCI-H1299, NCI-H358, and A549) suspended in Matrigel were injected into the left lung and produced solitary lesions that progressed to diffuse thoracic disease.

The characteristics of tumor development and metastasis for the various human lung cancer cell lines are summarized in Table 1. The adenocarcinoma (PC14PE6) was the most rapidly growing tumor. Typically, 9 days after injection, solitary lesions could be detected in sections of lung (Fig. 1*C*). Diffuse thoracic growth (Fig. 1*D*) lead to death by 2.5–4.5 weeks after injection, depending on the number of cells injected. At the time of death, lymph node metastasis (bilateral axilla and neck) was evident. An inverse ratio was found between the number of tumor cells injected and production of pleural effusion. The injection of 0.5×10^6 cells yielded 8 lung nodules sized 1–2 mm with 0.8 ml bloody pleural effusion. The injection of 1×10^6 cells produced larger tumors that occupied 80% of the thorax with 0.2 ml bloody pleural effusion, and the injection of 2×10^6 cells produced rapid death from extensive tumor with no pleural effusion. In all of the cases, the formation of pleural effusion was associated with pleural seeding by tumor cells. NCI-H12999 (poorly differentiated NSCLC) also produced rapidly growing tumors, and the mice died with diffuse disease 5 weeks

Table 2 Paclitaxel therapy of bronchioloalveolar (NCI-H358) and adenocarcinoma (PC14PE6) i.t. and s.c. tumors

Cells were implanted orthotopically in the lungs or subcutis as described in the text. In all experiments, paclitaxel therapy began on day 7 after tumor implantation. For each of the cell lines, the experiment was terminated when i.t. control mice became moribund. More pronounced effect was noticed in the subcutis tumor in comparison to the thoracic tumors, suggesting that paclitaxel had limited effect on the thoracic tumors in this system.

	Control			Paclitaxel		
		Lung and tumor weight (g)			Lung and tumor weight (g)	
	Incidence[a]	Median	Range	Incidence	Median	Range
Bronchioalveolar thoracic tumors						
Study 1	10/10	0.307	0.219–0.515	10/10	0.266	0.192–0.342
Study 2	9/9	0.319	0.256–1.240	10/10	0.271	0.229–0.305
Study 3	9/9	0.345	0.266–1.313	9/9	0.215	0.171–0.338
Study 4[b]	9/9	0.340	0.190–0.399	8/9	0.248	0.180–0.329
Bronchioalveolar subcutis tumors						
Study 1[c]	5/5	0.412	0.225–0.662	5/5	0.085	0.025–0.220
Adenocarcinoma thoracic tumors						
Study 1	5/5	0.320	0.298–0.350	5/5	0.231	0.192–0.300
Adenocarcinoma subcutis tumors						
Study 1[c]	5/5	0.550	0.380–0.850	5/5	0.098	0.015–0.320
Study 2[c,d]	5/5	1.728	0.950–1.950	5/5	0.542	0.132–1.700

[a] Number of positive mice/number of mice survived the experiment.
[b] Paclitaxel dosage was 200 μg/mouse/week in all experiments except study 4 of NCI-H358 thoracic tumors in which it was 100 μg/mouse week.
[c] Tumor weight only reported.
[d] In the PC14PE6 subcutis experiments, 1.5×10^6 cells were injected in the first study and 2×10^6 cells in the second study.

after injection. NCI-H358 (bronchioloalveolar carcinoma) cells produced tumors with an intermediate growth rate as compared with the other cell lines that were studied. Solitary nodules were found 2 weeks after injection of 1×10^6 cells, and mice died of progressive disease 8–9 weeks later. A549 (poorly differentiated NSCLC) cells formed slow-growing tumors leading to cachexia characterized by wasting of the interscapular muscles. None of the mice studied became cyanotic, and mice were killed on the development of labored mouth breathing.

Tumorigenicity in Orthotopic and Ectopic Organs. Two human NSCLC cell lines suspended in saline or Matrigel were injected s.c. into the right flank of 5 mice/group. The rate of tumor development was similar in all of the mice. NCI-H358 cells developed s.c. tumors in 80% of mice injected with 2.5×10^6 cells, whereas 100% of mice injected i.t. with 2×10^6 cells developed lung tumors. PC14PE6 cells produced s.c. tumors in 80% of mice injected with 1×10^6 cells, whereas all of the mice injected i.t. with 0.5×10^6 cells developed lung tumors. Thoracic tumors were fatal in all of the mice, whereas s.c. tumors were not associated with mortality when tumors reached maximal permissible size.

Serial *in Vivo* Passages for Selection of Cells with Increased Tumorigenicity. The squamous cell carcinoma cell line NCI-H226 produced slow-growing tumors with no pleural effusion. Injection of 0.5×10^6 or 1×10^6 cells did not form visible tumors up to 4 months after tumor implantation. Six of 10 mice injected i.t. with 2×10^6 cells developed a thoracic tumor and became moribund 3.5–4 months after tumor injection. The largest tumors were harvested and established *in vitro*. Viable cells were harvested and reinjected into the lungs of nude mice. After three such selection cycles, a cell line with an increased tumorigenicity was isolated (Table 1).

***In Vitro* Agarose Selection Enhanced the *in Vivo* Tumorigenicity of NCI-H69 Cells.** The injection of human SCLC NCI-H69 (0.5×10^6, 1×10^6, and 2×10^6 cells) into the lungs of nude mice did not form tumors. In 1 mouse injected i.t. with 2×10^6 cells, a 2-mm tumor was found 12 weeks after injection. To enhance the invasive potential of the parental NCI-H69 cell line, a method of *in vitro* selection using anchorage-independent growth of cells in agarose (25, 26) was used. The selection process was twice repeated using higher concentrations of top layer agarose from 0.9% to 1.2% (Table 1). After two cycles of selection in agarose, tumor cells formed lung tumors in all of the mice injected i.t.

Lung and Lymphatic Metastasis of NSCLC Tumor Cells After i.t. Injection. To study tumor progression and metastasis, adenocarcinoma (PC14PE6) and bronchioloalveolar carcinoma (NCI-H358) cells were transfected with GFP. Ten mice were injected with either 0.5×10^6 or 1×10^6 cells in Matrigel, into the left lung as described above. Two mice were killed at 4–7-day intervals. All of the mice injected developed microscopic tumors identified by fluorescence microscopy (Fig. 1*F*). PC14PE6 progressed to mediastinal lymph nodes and spread to the right lung on day 4 after tumor implantation. In NCI-H358 tumors, lymph node and right lung lesions were detected on day 28 after injection.

Chemotherapy Study. We studied the effect of paclitaxel on NCI-H358 (bronchioloalveolar carcinoma) and PC14PE6 (adenocarcinoma) tumors, growing in the lungs or the subcutis. In all of the experiments, therapy began on day 7 after tumor inoculation. We conducted several experiments using 100 or 200 μg (4 or 8 mg/kg)/dose paclitaxel. Therapy was administered for up to five cycles or until control mice became moribund. Mice injected with NCI-H358 were treated for five cycles and killed 7.5–9 weeks after tumor injection. Mice injected with PC14PE6 cells, a more aggres-

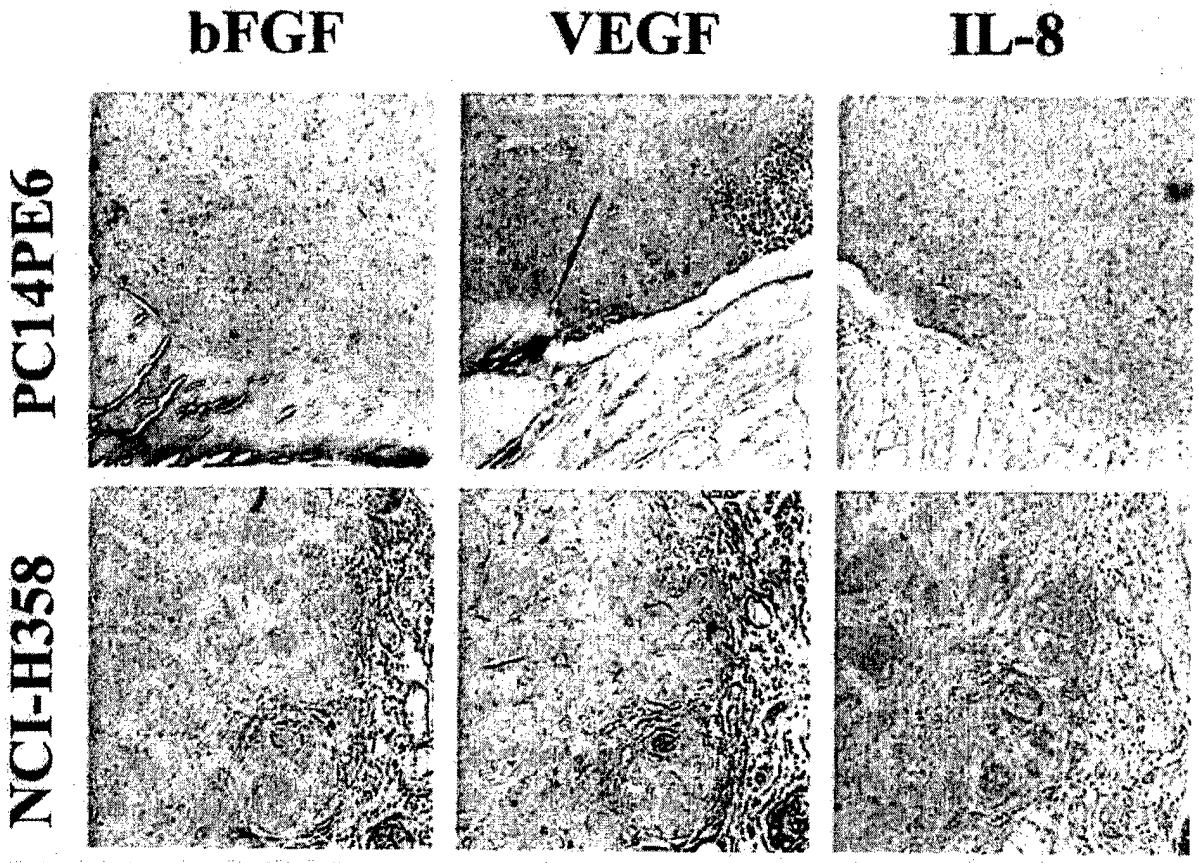

Fig. 2 IHC staining for bFGF, VEGF/VPF, and IL-8 of PC14PE6 and NCI-H358 orthotopic tumors. Although all of the factors were expressed by the two tumors, VEGF/VPF expression was prominent in PC14PE6 tumor, an adenocarcinoma that produces pleural effusion.

sive cell line, were treated for four cycles and were killed 4 weeks after tumor implantation. Control mice in the s.c. injected groups did not have evidence of morbidity at the end of the experiment. All of the mice in all of the groups tolerated therapy well, as assessed by similar median body weights in control *versus* treatment groups (data not shown). The results of all of these experiments suggest that whereas paclitaxel is efficacious in controlling tumor growth in the lungs, it is much more effective for treating s.c. tumors (Table 2). The treatment results of the thoracic tumors did not vary significantly when using 100 or 200 μg/dose paclitaxel. Similarly, the drug effect did not change significantly when by 7.5 or 9 weeks after tumor implantation.

Immunohistochemical Analysis of Thoracic Tumors. Thoracic tumors were examined for expression of several proangiogenic factors including bFGF, IL-8, and VEGF/VPF. These factors were expressed at an early stage of tumor progression, as noted by positive staining for bFGF in PC14PE6 tumors on day 9 after injection (Fig. 1*E*). A differential pattern of expression for each growth factor was noted between the different types of lung cancer. The pleural effusion producing adenocarcinoma (PC14PE6) tumors expressed higher levels of VEGF/VPF as compared with IL-8 and bFGF. These three factors were also expressed by the bronchioloalveolar tumors (NCI-H358), although to similar degree (Fig. 2). The NCI-H358 tumor had low expression of E-cadherin and high expression of matrix metalloproteinase 2 (data not shown).

DISCUSSION

We have developed reliable and reproducible orthotopic nude mouse models of lung cancer in a stepwise fashion. First, we verified the feasibility of thoracic injection and the development of regional metastasis using the pigmented B16BL6 melanoma cell line in syngeneic mice. Next, four different human lung tumor lines were injected into the lung of nude mice: PC14PE6, a pleural effusion producing adenocarcinoma, NCI-H358 bronchioloalveolar carcinoma, and NCI-H1299 and A549 poorly differentiated NSCLC lines. Two additional tumor lines developed tumors after selection for more aggressive and invasive clones: NCI-H226 squamous cell carcinoma was selected *in vivo* in the lung using our model, and NCI-H69 small cell lung carcinoma was selected on agarose *in vitro*. For each of the lung cancer cell lines studied, tumors formed as a single focus at the site of injection into the lung. Tumors then grew progressively within the injected lung and spread to regional and

extrathoracic lymph nodes, and the contralateral lung. The pattern of spread of lung cancer within the thorax is similar to that observed clinically in patients with lung cancer, suggesting that the model is clinically relevant. The absence of clinically apparent distant metastasis is most likely due to the aggressive pattern of locoregional spread of cancer cells with mice dying of diffuse thoracic disease before development of significant distant metastasis. To overcome this potential limitation, complementary models of metastatic disease (*i.e.*, brain, liver, and bone models) are now being developed for each of the lung cancer types.

This model validates the orthotopic principle that tumor cells grow better in their tissue of origin and that more clinically relevant studies can be performed using the orthotopic site of tumor growth. The importance of orthotopic models to study the biology and therapy of cancer had been demonstrated for other neoplasms (4, 7). Chen *et al.* (28) studied the interaction between NSCLC tumors and macrophages in surgical specimens and in cell lines, and found that the importance of tumor cell and microenvironment interaction holds also for the lung. They suggested that this interaction up-regulated the expression of IL-8 by the tumor. Furthermore, high-density infiltration of tumor by macrophages was correlated with increased tumor angiogenesis and adverse outcome in NSCLC patients. Moreover, our model closely resembles human lung cancer in its partial response to chemotherapy. Although treated mice had shown a reduction in tumor burden in response to paclitaxel (as assessed by lung and tumor weight), a more dramatic response was noted in s.c. tumors. This effect of paclitaxel on s.c. implanted tumors may in part explain the difficulty with the translation into a clinical reality of dramatic responses to therapy that have been observed for anticancer agents in preclinical studies that rely solely on s.c. tumor xenografts (6). Therefore, it may be prudent to first screen novel anticancer agents in s.c. tumor models and to then screen active agents in orthotopic models before the initiation of clinical trials.

To date, several orthotopic rodent models have been developed to study human lung cancer. Different techniques have been used to introduce tumors including intrabronchial implantation of a tumor cell inoculum (9–11) with resultant tumor formation in the center of the thorax in 35–95% of animals. However, intrabronchial techniques necessitated irradiation and tracheostomy or laryngoscopy and were associated with operative mortality of >5%. Alternatively, intrapleural implantation of a tumor cell inoculum without Matrigel has been used (12, 13), which resulted in the development of extrathoracic tumors and an operative mortality of 5–10%. Tumors can also be implanted in the lung parenchyma after skin incision (14) or thoracotomy and surgical exploration of the pleura (15–17). The skin incision model was associated with low operative mortality yet was much more time consuming and laborious, whereas the thoracotomy model was associated with mortality of about 5%. Another common technique used surgical human cancerous specimens, which were implanted into the lungs (8). However, in this system the number of tumor cells varies between surgical specimens. To date, none of these models had been widely accepted, and most research is still done using s.c. models.

The models of lung cancer that we describe complement those that have been developed previously and may overcome some of the limitations associated with them. We have developed orthotopic models of each of the common types of lung cancer, which should lead to an improved understanding of the influence of tumor histology on response to existing and emerging therapies. The techniques needed for our models are reproducible, can be performed quickly (*i.e.*, each mouse can be injected in under 15 s), and are easily taught. It is associated with virtually no procedure related animal mortality. Whereas pneumothorax may occur, as shown in 3 of 10 treated mice studied with X-ray imaging (Faxitron; data not shown), death within 72 h of the thorax puncture is <1%. Matrigel is used to provide a reproducible anchor, which fixes the tumor cells to the site of injection and avoid cell dispersion. In most experiments we used growth factor-reduced Matrigel. It contains limited amounts of growth factors, which are additionally diluted in the process of cell suspension preparation. Overall tumor cell implantation with its addition results in a reproducible tumor size, which enables therapeutic experiments as demonstrated with paclitaxel as well as study of tumor biology and metastasis.

Of special interest is the expression of proangiogenic factors by the implanted lung tumors. The significance of bFGF, VEGF/VPF, and IL-8 in human NSCLC had been studied extensively, and their expression had been shown to correlate with poor outcome in human lung cancer patients (29). These factors are important for tumor progression and the formation of the angiogenic phenotype from an early stage disease. In our model of lung adenocarcinoma, bFGF was expressed by early and locally advanced human lesions in the lungs of nude mice. These data are consistent with what has been observed in the clinic, because bFGF was shown to play a key role in human lung cancer progression (30) and was expressed even in small tumors (≤2 cm) growth (31). Taken together, the data suggest that it may be prudent to target bFGF for lung adenocarcinoma using anti-bFGF therapies such as low dose-daily IFN (32). In our model of bronchioloalveolar carcinoma (NCI-H358), tumors were found to have low expression of E-cadherin (associated with cell-to-cell cohesion and adhesion) and high expression of matrix metalloproteinase 2 (associated with invasion). This proportion had been found to correlate with increased human lung cancer tumor aggressiveness (33), which substantiates the metastatic behavior of this tumor. Interestingly, VEGF/VPF expression was higher in lung adenocarcinomas (PC14PE6) than for other lung cancer histologies, which may be related to production of pleural effusion by PC14PE6 tumors. Indeed, Senger *et al.* (34) had identified this molecule by its ability to induce vascular leaking and named it vascular permeability factor. Yano *et al.* (19) had found the relation between VEGF/VPF and PC14PE6 tumors in a metastatic tumor and, as far as we know, our finding is the first in an orthotopic model.

In summary, we have developed *in vivo* models of primary lung cancer for both human NSCLC and human SCLC, which are reproducible, well tolerated, feasible, and straightforward to perform. These lung cancer models closely mimic the patterns observed for the natural progression of primary lung cancer from a single nodule to disseminated disease, and enables study of novel therapeutics and better understanding of lung cancer metastasis.

ACKNOWLEDGMENTS

We thank Bich Tran for her assistance in the preparation of this manuscript.

REFERENCES

1. Jemal, A., Murray, T., Samuels, A., Ghafoor, A., Ward, E., and Thun, M. J. Cancer statistics, 2003. CA. Cancer J. Clin., *53:* 5–26, 2003.

2. Carney, D. N. Lung cancer–time to move on from chemotherapy. N. Engl. J. Med., *346:* 126–128, 2002.

3. Paget, S. The distribution of secondary growths in cancer of the breast. 1889. Cancer Metastasis Rev., *8:* 98–101, 1989.

4. Wilmanns, C., Fan, D., O'Brian, C. A., Bucana, C. D., and Fidler, I. J. Orthotopic and ectopic organ environments differentially influence the sensitivity of murine colon carcinoma cells to doxorubicin and 5-fluorouracil. Int. J. Cancer, *52:* 98–104, 1992.

5. Kuo, T. H., Kubota, T., Watanabe, M., Furukawa, T., Kase, S., Tanino, H., Saikawa, Y., Ishibiki, K., Kitajima, M., and Hoffman, R. M. Site-specific chemosensitivity of human small-cell lung carcinoma growing orthotopically compared to subcutaneously in SCID mice: The importance of orthotopic models to obtain relevant drug evaluation data. Anticancer Res., *13:* 627–630, 1993.

6. Killion, J. J., Radinsky, R., and Fidler, I. J. Orthotopic models are necessary to predict therapy of transplantable tumors in mice. Cancer Metastasis Rev., *17:* 279–284, 1998.

7. Fidler, I. J. Critical factors in the biology of human cancer metastasis: Twenty-eighth G. H. A. Clowes memorial award lecture. Cancer Res., *50:* 6130–6138, 1990.

8. Hoffman, R. M. Orthotopic metastatic mouse models for anticancer drug discovery and evaluation: a bridge to the clinic. Investig. New Drugs, *17:* 343–359, 1999.

9. McLemore, T. L., Liu, M. C., Blacker, P. C., Gregg, M., Alley, M. C., Abbott, B. J., Shoemaker, R. H., Bohlman, M. E., Litterst, C. C., and Hubbard, W. C. Novel intrapulmonary model for orthotopic propagation of human lung cancers in athymic nude mice. Cancer Res., *47:* 5132–5140, 1987.

10. Howard, R. B., Chu, H., Zeligman, B. E., Marcell, T., Bunn, P. A., McLemore, T. L., Mulvin, D. W., Cowen, M. E., and Johnston, M. R. Irradiated nude rat model for orthotopic human lung cancers. Cancer Res., *51:* 3274–3280, 1991.

11. Hastings, R. H., Burton, D. W., Quintana, R. A., Biederman, E., Gujral, A., and Deftos, L. J. Parathyroid hormone-related protein regulates the growth of orthotopic human lung tumors in athymic mice. Cancer (Phila.), *92:* 1402–1410, 2001.

12. McLemore, T. L., Eggleston, J. C., Shoemaker, R. H., Abbott, B. J., Bohlman, M. E., Liu, M. C., Fine, D. L., Mayo, J. G., and Boyd, M. R. Comparison of intrapulmonary, percutaneous intrathoracic, and subcutaneous models for the propagation of human pulmonary and nonpulmonary cancer cell lines in athymic nude mice. Cancer Res., *48:* 2880–2886, 1988.

13. Kraus-Berthier, L., Jan, M., Guilbaud, N., Naze, M., Pierre, A., and Atassi, G. Histology and sensitivity to anticancer drugs of two human non-small cell lung carcinomas implanted in the pleural cavity of nude mice. Clin. Cancer Res., *6:* 297–304, 2000.

14. Doki, Y., Murakami, K., Yamaura, T., Sugiyama, S., Misaki, T., and Saiki, I. Mediastinal lymph node metastasis model by orthotopic intrapulmonary implantation of Lewis lung carcinoma cells in mice. Br. J. Cancer, *79:* 1121–1126, 1999.

15. Wang, H. Y., Ross, H. M., Ng, B., and Burt, M. E. Establishment of an experimental intrapulmonary tumor nodule model. Ann. Thorac. Surg., *64:* 216–219, 1997.

16. Miyoshi, T., Kondo, K., Ishikura, H., Kinoshita, H., Matsumori, Y., and Monden, Y. SCID mouse lymphogenous metastatic model of human lung cancer constructed using orthotopic inoculation of cancer cells. Anticancer Res., *20:* 161–163, 2000.

17. Boehle, A. S., Dohrmann, P., Leuschner, I., Kalthoff, H., and Henne-Bruns, D. An improved orthotopic xenotransplant procedure for human lung cancer in SCID bg mice. Ann. Thorac. Surg., *69:* 1010–1015, 2000.

18. Yano, S., Nokihara, H., Hanibuchi, M., Parajuli, P., Shinohara, T., Kawano, T., and Sone, S. Model of malignant pleural effusion of human lung adenocarcinoma in SCID mice. Oncol. Res., *9:* 573–579, 1997.

19. Yano, S., Herbst, R. S., Shinohara, H., Knighton, B., Bucana, C. D., Killion, J. J., Wood, J., and Fidler, I. J. Treatment for malignant pleural effusion of human lung adenocarcinoma by inhibition of vascular endothelial growth factor receptor tyrosine kinase phosphorylation. Clin. Cancer Res., *6:* 957–965, 2000.

20. Levitt, M. L., Gazdar, A. F., Oie, H. K., Schuller, H., and Thacher, S. M. Cross-linked envelope-related markers for squamous differentiation in human lung cancer cell lines. Cancer Res., *50:* 120–128, 1990.

21. Fidler, I. J. Selection of successive tumour lines for metastasis. Nat. New Biol., *242:* 148–149, 1973.

22. Nicolson, G. L., Brunson, K. W., and Fidler, I. J. Specificity of arrest, survival, and growth of selected metastatic variant cell lines. Cancer Res., *38:* 4105–4111, 1978.

23. Fidler, I. J. Rationale and methods for the use of nude mice to study the biology and therapy of human cancer metastasis. Cancer Metastasis Rev., *5:* 29–49, 1986.

24. Myers, J. N., Holsinger, F. C., Jasser, S. A., Bekele, B. N., and Fidler, I. J. An orthotopic nude mouse model of oral tongue squamous cell carcinoma. Clin. Cancer Res., *8:* 293–298, 2002.

25. Cifone, M. A., and Fidler, I. J. Correlation of patterns of anchorage-independent growth with *in vivo* behavior of cells from a murine fibrosarcoma. Proc. Natl. Acad. Sci. USA, *77:* 1039–1043, 1980.

26. Li, L., Price, J. E., Fan, D., Zhang, R. D., Bucana, C. D., and Fidler, I. J. Correlation of growth capacity of human tumor cells in hard agarose with their *in vivo* proliferative capacity at specific metastatic sites. J. Natl. Cancer Inst., *81:* 1406–1412, 1989.

27. Baker, C. H., Solorzano, C. C., and Fidler, I. J. Blockade of vascular endothelial growth factor receptor and epidermal growth factor receptor signaling for therapy of metastatic human pancreatic cancer. Cancer Res., *62:* 1996–2003, 2002.

28. Chen, J. J., Yao, P. L., Yuan, A., Hong, T. M., Shun, C. T., Kuo, M. L., Lee, Y. C., and Yang, P. C. Up-regulation of tumor interleukin-8 expression by infiltrating macrophages: its correlation with tumor angiogenesis and patient survival in non-small cell lung cancer. Clin. Cancer. Res., *9:* 729–737, 2003.

29. Onn, A., and Herbst, R. S. Angiogenesis, metastasis, and lung cancer: An overview. *In:* B. Driscoll (ed.), Molecular Pathology Methods and Review 1, pp. 329–348. Totowa: Humana Press, 2002.

30. Volm, M., Koomagi, R., Mattern, J., and Stammler, G. Angiogenic growth factors and their receptors in non-small cell lung carcinomas and their relationships to drug response *in vitro*. Anticancer Res., *17:* 99–103, 1997.

31. Ito, H., Oshita, F., Kameda, Y., Suzuki, R., Ikehara, M., Arai, H., Mitsuda, A., Saito, H., Yamada, K., Noda, K., and Nakayama, H. Expression of vascular endothelial growth factor and basic fibroblast growth factor in small adenocarcinomas. Oncol. Rep., *9:* 119–123, 2002.

32. Slaton, J. W., Perrotte, P., Inoue, K., Dinney, C. P., and Fidler, I. J. Interferon-α-mediated down-regulation of angiogenesis-related genes and therapy of bladder cancer are dependent on optimization of biological dose and schedule. Clin. Cancer Res., *5:* 2726–2734, 1999.

33. Herbst, R. S., Yano, S., Kuniyasu, H., Khuri, F. R., Bucana, C. D., Guo, F., Liu, D., Kemp, B., Lee, J. J., Hong, W. K., and Fidler, I. J. Differential expression of E-cadherin and type IV collagenase genes predicts outcome in patients with stage I non-small cell lung carcinoma. Clin. Cancer Res., *6:* 790–797, 2000.

34. Senger, D. R., Galli, S. J., Dvorak, A. M., Perruzzi, C. A., Harvey, V. S., and Dvorak, H. F. Tumor cells secrete a vascular permeability factor that promotes accumulation of ascites fluid. Science (Wash. DC), *219:* 983–985, 1983.